

**Simplified Models of Vehicle Impact for Injury
Mitigation**

Presented By

Edward Brell

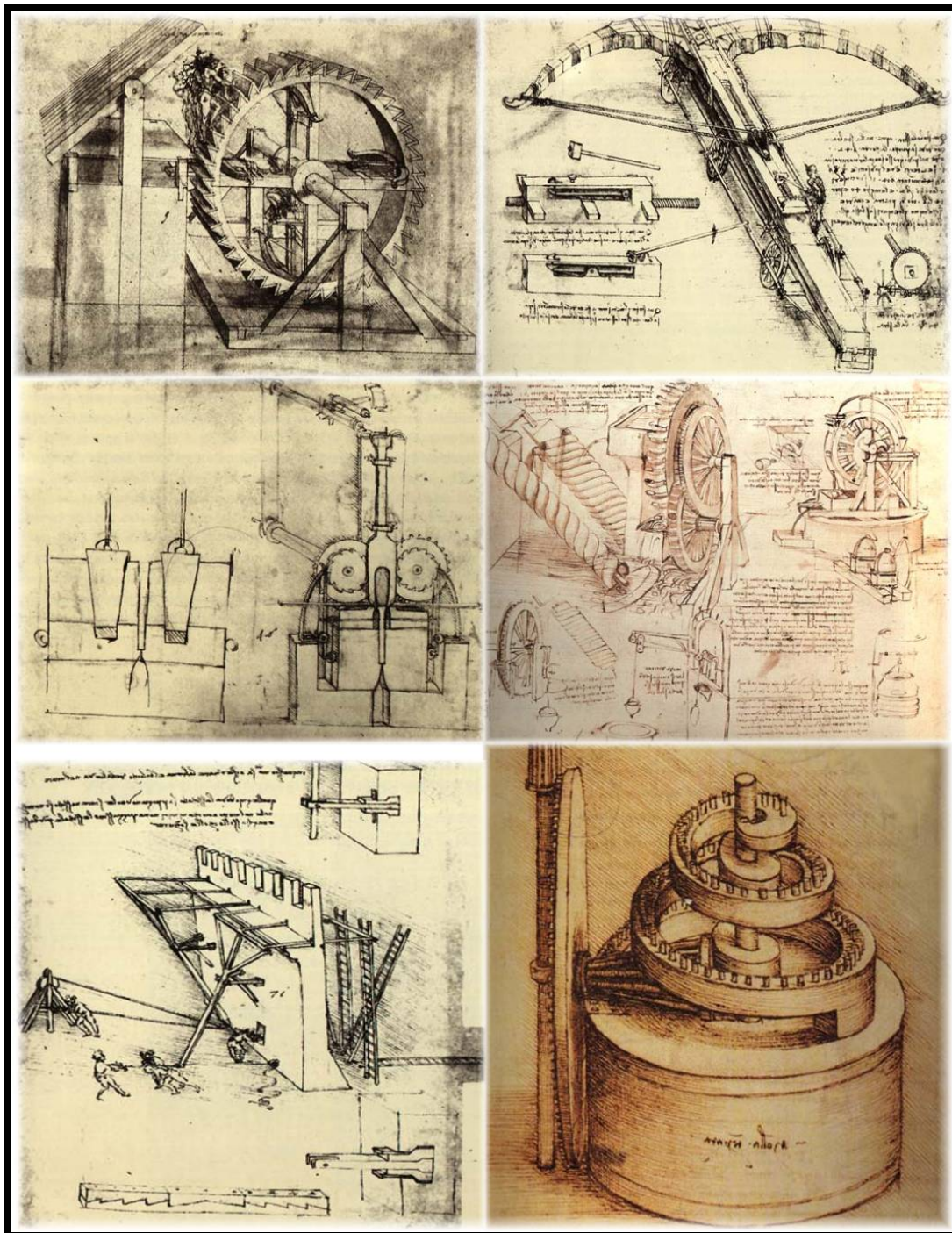
Submitted for the degree of

Doctor of Philosophy

School of Urban Development

Queensland University of Technology

26 January, 2005



“Simplicity is the ultimate sophistication.”

Leonardo da Vinci
(born 1452, died 1519)

Declaration

The work contained in this thesis has not been previously submitted for a degree or diploma at any other higher education institution. To the best of my knowledge and belief, the thesis contains no material previously published or written by another person except where due reference is made.

The experiments in this thesis constitute work carried out by the candidate unless otherwise stated. The thesis complies with the stipulations set out for the degree of Doctor of Philosophy by the Queensland University of Technology.

Signature: _____

Date: _____

Edward Brell¹

School of Urban Development

Queensland University of Technology

Brisbane

Australia

¹ © E.W. Brell 2004

Table of Contents

Acknowledgments	i
Publications.....	iii
Publications arising from the research.....	iii
Other publications	iii
Thesis abstract.....	iv
Notations	vi
1. GENERAL INTRODUCTION	1-1
1.1 Background	1-1
1.1.1 Modelling.....	1-2
1.1.2 Vehicle Mass	1-3
1.1.3 General	1-4
1.2 Aims and Objectives	1-6
1.3 Approach and Scope	1-7
2. INJURY RISK CRITERIA.....	2-13
2.1 Introduction.....	2-13
2.2 Mechanics of Injury	2-13
2.3 Human Tolerance to Impact.....	2-18
2.4 Proximity	2-22
2.5 Body Part Uncoupling.....	2-27
2.6 Vehicle Acceleration as Injury Objective	2-29
2.7 Effect of Proximity in Approach and Coupling Phases.....	2-31
2.7.1 Introduction.....	2-31
2.7.2 Injury Determined in the Approach Phase.....	2-31
2.7.3 Injury Determined in the Coupling Phase.....	2-33
2.7.4 Conclusion	2-39
2.8 Validity of Classic Ride-Down Model.....	2-40
2.8.1 Example of Blunt Injury by ‘Hammering’.....	2-43
2.9 Injury Risk Measure for This Study.....	2-45
2.9.1 What is Injury Risk?.....	2-45
2.9.2 Engineering Link to Statistical Injury Risk	2-48
2.10 Conclusion	2-49

3.	QUALITY OF CRUMPLE ZONE.....	2-50
3.1	Introduction.....	3-51
3.2	What Is Stiffness?	3-51
3.2.1	<i>Single Crash Stiffness</i>	3-55
3.2.2	<i>Spectrum Stiffness</i>	3-55
3.2.3	<i>Aggregate Stiffness</i>	3-55
3.2.4	<i>Instant Stiffness</i>	3-55
3.3	Physical Influences on Structural Stiffness.....	3-56
3.4	Mechanisms Influencing Stiffness	3-60
3.4.1	<i>Stretching</i>	3-60
3.4.2	<i>Column Wrinkling</i>	3-60
3.4.3	<i>Plastic Hinges</i>	3-61
3.4.4	<i>Crushing</i>	3-63
3.5	State Of The Art.....	3-63
3.6	Optimum Pulse Shape.....	3-68
3.7	CONCLUSION.....	3-71
4.	REPRESENTING VEHICLE RESPONSE.....	4-73
4.1	Introduction.....	4-73
4.2	NHTSA Linear Stiffness Parameter.....	4-75
4.3	Using Reluctance as a Stiffness Metric.....	4-78
4.4	Mass-Spring Analogy	4-81
4.5	Fidelity of Linear Spring Analogy with Test Data.....	4-83
4.6	Velocity-Displacement Interaction Curve.....	4-85
4.7	Progression of the Occupant Cell at the Micro Level.	4-87
4.7.1	<i>Instantaneous Reluctance</i>	4-87
4.7.2	<i>Instantaneous Stiffness</i>	4-87
4.7.3	<i>Specific Impedance</i>	4-92
4.8	Adding Rebound.....	4-96
4.9	Conclusion	4-98
5.	VEHICLE RESPONSE TO VARYING CONDITIONS.....	5-99
5.1	Introduction.....	5-99
5.2	Spectrum Stiffness	5-99
5.3	Spectrum of Initial Velocities	5-100
5.3.1	<i>Predicting Reluctance – Variations in Velocity</i>	5-102
5.4	Vehicle Mass Variation.....	5-104
5.4.1	<i>Introduction</i>	5-104
5.4.2	<i>Simulation</i>	5-105
5.4.3	<i>Mass Softening in Real Tests</i>	5-110

5.4.4	<i>Implications of Mass Softening</i>	5-111
5.4.5	<i>Predicting Reluctance – Variations in Mass</i>	5-112
5.5	Conclusion	5-116
6.	ACHIEVING AN INJURY REPRESENTATIVE PULSE	6-117
6.1	Introduction.....	6-117
6.2	Injury Fidelity Compared with Vehicle Motion Fidelity	6-118
6.2.1	<i>Optimized Reluctance for a Proximity Range</i>	6-119
6.2.2	<i>Haversine</i>	6-120
6.3	Conclusion	6-126
7.	INJURY PREDICTION MODEL DEVELOPMENT	7-127
7.1	Introduction.....	7-127
7.1.1	<i>Injury Reluctance</i>	7-129
7.1.2	<i>Prediction for Different Velocity</i>	7-131
7.1.3	<i>Accounting for Rebound</i>	7-135
7.1.4	<i>Accounting for Vehicle Load Variations</i>	7-137
7.2	Conclusion	7-140
7.2.1	<i>Compliance Legislation</i>	7-140
7.2.2	<i>Fitment of Appurtenances</i>	7-140
7.2.3	<i>Accident Repair</i>	7-141
7.2.4	<i>Litigation Support</i>	7-141
7.3	Example 1 –Production Vehicle vs ULSAB Injury Performance.	7-142
7.3.1	<i>Introduction</i>	7-142
7.3.2	<i>Published Vehicle Acceleration</i>	7-142
7.3.3	<i>Velocity Decay of Comparison Vehicles</i>	7-143
7.3.4	<i>Injury Risk Comparison</i>	7-144
7.3.5	<i>Conclusion</i>	7-145
7.4	Example 2 – Safety Implications of Seatbelt Slack.	7-146
7.4.1	<i>Introduction</i>	7-146
7.4.2	<i>Problem Statement</i>	7-146
7.4.3	<i>Solution</i>	7-147
7.4.4	<i>Conclusion</i>	7-149
8.	INERTIAL STRESS	7-150
8.1	Introduction.....	8-151
8.2	Strain Progression	8-152
8.3	Finite Element Analysis	8-154
8.4	Impact Experiments	8-160
8.4.1	<i>Elastic Waves from Collinear Impact</i>	8-160
8.4.2	<i>In-line Momentum Trap</i>	8-163

8.4.3	<i>Right-Angled Momentum Trap</i>	8-164
8.4.4	<i>Velocity of Strain Propagation</i>	8-165
8.4.5	<i>Directional Nature of Strain Disturbance</i>	8-167
8.4.6	<i>Vectorial Nature of Strain Disturbance</i>	8-169
8.4.7	<i>Inelastic Waves</i>	8-175
8.5	Evidence in Vehicle Reluctance	8-181
8.6	Evidence at the Component Level	8-182
8.7	Summary	8-187
9.	VEHICLE REBOUND	8-188
9.1	Introduction.....	9-189
9.2	How Mass and Velocity Affects Models	9-191
9.3	Conclusion	9-196
10.	REBOUND IN THE FLEET.....	10-197
10.1	Introduction.....	10-197
10.2	Mass Influence on Rebound.....	10-198
10.3	Specific Energy Absorption	10-199
10.4	Velocity Influence on Rebound	10-204
10.5	Rebound Prediction Example.....	10-207
10.6	Conclusion	10-208
10.7	Discussion.....	10-209
11.	MASS & STIFFNESS TRENDS IN FLEET	10-212
11.1	Introduction.....	11-213
11.2	Errant Trends	11-214
11.3	Vehicle Mass Trend	11-218
11.4	Demographic Reluctance Trend.....	11-219
11.4.1	<i>Injury Implications of Trend</i>	11-221
12.	CONCLUSION	12-223
12.1	The Essence	12-223
12.2	Summary of Contributions.....	12-225
12.3	Further Research	12-227
12.4	Recommendations.....	12-228
13.	References.....	13-229

Figures

Figure 2-1: Four events in blunt injury.	2-15
Figure 2-2: Four vehicle events comprising a crash.....	2-15
Figure 2-3: Occupant interaction with vehicle interior.	2-16
Figure 2-4: Definition of body part velocity differential and ride-down.....	2-17
Figure 2-5: Photographic traces of dummy motion. (redrawn from Hendler, O'Rourke et al. (1974)).....	2-24
Figure 2-6: Proximity graphically defined.....	2-24
Figure 2-7: Pre-crash distance.....	2-25
Figure 2-8: Velocity and displacement integrations from rear seat and dashpanel accelerometer data from Nissan Test No 4215.	2-26
Figure 2-9: Brain stem injury.....	2-27
Figure 2-10: Whip velocity defined.	2-28
Figure 2-11: Sketch to highlight the statistical nature of body parts and independence to main body part statistics.	2-28
Figure 2-12: Example of maximum injury risk at zero vehicle deceleration.	2-30
Figure 2-13: Holden & Falcon velocity-time graphs from dash acceleration.	2-32
Figure 2-14: Holden & Falcon velocity-time graphs showing equal proximity.....	2-32
Figure 2-15: Holden & Falcon body part contact velocity vs. proximity.....	2-33
Figure 2-16: Driver dummy contact point on airbag.....	2-35
Figure 2-17: Passenger dummy head contact point on dummy and dash.....	2-36
Figure 2-18: Approximate locus of passenger dummy head.....	2-36
Figure 2-19: Velocity integrations for dash and heads of dummies.....	2-37
Figure 2-20: Timing of passenger's head resultant acceleration peaks with peak seatbelt load and gradient change of velocity.....	2-38
Figure 2-21: Chest velocity decay in Honda and Holden showing approach phase shaded.....	2-40
Figure 2-22: Mechanical analogue of model for Runge-Kutta simulation.....	2-41
Figure 2-23: Torso in seatbelt with varying stiffness and slack adjustment showing stiff cushion with 50 mm proximity and soft cushion with 150 mm (for presentation clarity).....	2-41
Figure 2-24: Head impact on windscreen despite airbag deployment.....	2-42
Figure 2-25: 50 mm proximity study showing the multiple impact nature of "ride-down".	2-43
Figure 2-26: 200 mm proximity study showing body part contact force distribution.....	2-43

Figure 2-27: Plot of average contact force for four proximity cases.....	2-44
Figure 2-28: Fatal, non-fatal dividing line from Prasad and Mertz (1985)	2-45
Figure 2-29: Risk of injury by seriousness Prasad and Mertz (1985)	2-47
Figure 2-30: Correlation of HIC with Maximum Abbreviated Injury Scale (MAIS) (Shojaati (2003)).	2-47
Figure 3-1: Visualization elastic/plastic crumple zone as elastic using two springs giving three spring rates.	3-53
Figure 3-2: Macro-micro visualization of stiffness concepts.	3-54
Figure 3-3: Velocity sensitive structure (Deshpande and Fleck (2000)).	3-57
Figure 3-4: Photograph of chassis rail near firewall showing impact weakening convolutions.....	3-58
Figure 3-5: Photograph of front of chassis rail with localizing convolutions.	3-58
Figure 3-6: Cross-section of chassis rail showing lower strengthening channel.....	3-59
Figure 3-7: Examples of both chassis stiffening and softening by addition of reinforcement strut and initiation creases.	3-59
Figure 3-8: Example of local wrinkling in response to a localizing initiator.	3-61
Figure 3-9: Effect of crush initiators on early force.....	3-61
Figure 3-10: Underside photographs of chassis rail of 2003 Chevrolet Siverado before and after full frontal rigid barrier NCAP Test No 4472 at 56.3 km/h.	3-62
Figure 3-11: Crash speed and frequency distribution.....	3-65
Figure 3-12: Comparison of hypothetical pulses (Sparke and Tomas (1994)).....	3-65
Figure 3-13: Motozawa and Kamei (2000a) ideal crash pulse.....	3-66
Figure 3-14: Progressive collapse mechanism from Motozawa, Tsuruta et al. (2003a) timed sequentially from A to C.	3-67
Figure 3-15: Relative barrier force inferred from occupant cell acceleration from NCAP Test #4936 Chrysler Town & Country 2005 Model & NCAP Test #4985 Chevrolet Equinox 2005 Model	3-68
Figure 3-16: Normalized velocity-time curves having identical areas under curves but mirrored between blue and red dots.	3-69
Figure 3-17: Concept of equal proximity – unequal time for early and late trough normalized velocity profiles.....	3-70
Figure 3-18: Normalized contact velocity-proximity curves derived from the example in Figure 3-16.	3-70
Figure 4-1: Comparison of acceleration test data from Toyota Landcruiser ANCAP Test #B8057 with equation derived from NHTSA linear stiffness parameter.....	4-76
Figure 4-2: Comparison of velocity test data from Toyota Landcruiser ANCAP Test #B8057 with equation derived from NHTSA linear stiffness parameter.	4-76

Figure 4-3: Comparison of positional test data from Toyota Landcruiser ANCAP Test #B8057 with equation derived from NHTSA linear stiffness parameter.	4-77
Figure 4-4: Sketch of linear motor redrawn from Otten, Vries et al. (1997).....	4-78
Figure 4-5: Normalized force for varying circular frequencies.....	4-79
Figure 4-6: Normalized displacement for varying circular frequencies.	4-80
Figure 4-7: Parametric plot of normalized transient force vs. normalized transient displacement.....	4-80
Figure 4-8: Mass on coil compression spring, showing one spring loaded and another identical spring unloaded to illustrate stiffness independence of mass.	4-82
Figure 4-9: Visualization of surge velocity in linear elastic springs.	4-82
Figure 4-10: Falcon ANCAP test #8055 compared with cosine using reluctance derived from test limit conditions of initial velocity and dynamic crush.	4-83
Figure 4-11: Falcon ANCAP test #8055 compared with cosine using reluctance derived from best-fit of data.	4-84
Figure 4-12: System curves drawn for two initial velocities for the same spring.	4-85
Figure 4-13: Elastic spring depicted in time and space illustrating the parametric nature of the system curve.	4-86
Figure 4-14: Honda Accord system curves (Red curves are equivalent linear elastic system curves)	4-86
Figure 4-15: Slope in spatial domain reflecting slopes in transient domain.....	4-87
Figure 4-16: Instantaneous stiffness of system curve compared with test data.	4-88
Figure 4-17: Velocity from cosine based on peak conditions.	4-88
Figure 4-18: Velocity from cosine based on reluctance giving coincident intersection with the x-axis.	4-89
Figure 4-19: Test data for Honda Accord compared with time normalized cosine equivalents.....	4-90
Figure 4-20: Instantaneous stiffness for Honda Accords compared with linear elastic spring equivalents on normalized time.	4-91
Figure 4-21: Comparison of time-based instant stiffness and position-based impedance.....	4-93
Figure 4-22: Impedance for Honda Accords compared with linear elastic spring equivalents on normalized positions.....	4-94
Figure 4-23: Impedance for Honda Accords linear elastic spring equivalents for normalized positions showing apparent absence of speed influence.	4-95
Figure 4-24: NCAP test data for 2005 Model Ford Escape Test #4952 with cosine reluctance based on limit conditions ($V = 15.6 \text{ m/s}$ & $X = 0.611 \text{ m}$).....	4-96
Figure 4-25: Rebound cosine curve added to ingoing cosine curve.....	4-97
Figure 4-26: NCAP Test #4952 Ford Escape with rebound equation and occupant head velocity from test data.	4-97

Figure 5-1: Three Hondas in full frontal rigid barrier crash tests graphed initial impact velocity vs. dynamic crush in spectrum setting. Dashed line projects to y-intercept.....	5-100
Figure 5-2: Reluctances calculated for 1998 Honda Accord for a range of initial velocities.....	5-101
Figure 5-3: Extrapolation errors using origin rays on Crash3 line.	5-102
Figure 5-4: Maximum prediction error from extrapolation of a single data point for 1998 Honda Accord.....	5-103
Figure 5-5: Schematic of one dimensional lumped parameter model.	5-105
Figure 5-6 Transient position for occupant cell mass variations on Ford Explorer Test #2256 at test speed 47.3 km/h.	5-107
Figure 5-7 Reluctance change for occupant cell mass variations on Ford Explorer Test #2256 at test speed 47.3 km/h. (Data points trended).....	5-108
Figure 5-8: Reluctances for mass changes in simulation of eight crash tests.....	5-109
Figure 5-9: Photographs of 1980 Ford Courier after 48 km/h rigid barrier impact. Upper vehicle weight 1427 kg – lower vehicle weight 1982 kg.....	5-110
Figure 5-10: Injury risk for 1987 Hyundai Excel GLS Test #1092 40 km/h with 75kg deleted from test mass compared with 300kg added to test mass	5-112
Figure 5-11: Visualization of linear elastic system under mass variation.....	5-113
Figure 5-12: Extrapolation errors using linear elastic spring stiffness ray showing Crash3 line for reference.....	5-113
Figure 6-1: Definition of cosine-based injury equations.....	6-118
Figure 6-2: Comparison of contact velocities from test data of Falcon ANCAP #8055 using reluctance from NHTSA linear spring parameter.....	6-118
Figure 6-3: Comparison of contact velocities from test data of Falcon ANCAP #8055 using reluctance from best-fit improvement.	6-119
Figure 6-4: Comparison of contact velocity from test data of Falcon ANCAP #8055 with optimized reluctance to suit statistical distribution.....	6-120
Figure 6-5: Plot of versine, haversine & cosine.	6-121
Figure 6-6: Plot of cosine and phase-displaced versine & haversine.....	6-122
Figure 6-7: Plot of phased displaced haversine with rebound added.	6-122
Figure 6-8: Linear elastic spring and haversine system curves compared with test data system curve for Honda Accord Test #2712	6-123
Figure 6-9: Derivation sketch of injury haversine equations.	6-123
Figure 6-10: Typical parametric plot of normalized velocity and proximity.	6-124
Figure 6-11: Contact velocity – proximity study for Falcon Test #8055.....	6-125
Figure 6-12: Contact velocity proximity study for Holden #7030 using haversine.	6-125

Figure 7-1: Visualization of hypothesis to be tested.	7-127
Figure 7-2: Comparison of contact velocity at various proximities. (Initial impact velocity including rebound = 18 m/s) (Reluctances (Ω) shown as $w = 15$, $w = 20$ and $w = 25$).....	7-130
Figure 7-3: Determination of injury reluctance for Honda Accord Test #2836 by trial and error.	7-131
Figure 7-4: Error incurred by use of different reluctances (Ω) shown as $w=13$ to $w=15$	7-132
Figure 7-5: Prediction of injury and comparison with test data from Honda Accord Test #2712.....	7-133
Figure 7-6: Variation from test data trying different reluctance values.	7-134
Figure 7-7: 1990 Ford Taurus injury test data used to derive reluctance.	7-136
Figure 7-8: 1990 Ford Taurus injury values predicted from Test # 1385 and compared with test data from Test #1403.....	7-136
Figure 7-9: Simulated velocity decay curves for 1987 Toyota Celica from Test #1100 adding 300 kg and subtracting 75 kg from test mass.....	7-138
Figure 7-10: Injury values for simulated and mathematical models.	7-138
Figure 7-11: Predicted injury values from mathematical model.	7-139
Figure 7-12: Vectorized copy of published ULSAB average car acceleration.....	7-142
Figure 7-13: Accelerometer data for occupant cell Nissan NCAP Test #4215	7-143
Figure 7-14: Velocity decay for ULSAB and Nissan vehicles.....	7-144
Figure 7-15: Injury risk comparison of ULSAB Vehicle with 2002 Nissan Altima.	7-145
Figure 7-16: Fifth percentile female in 2001 Dodge Caravan (pix mirrored to simulate Australian conditions).....	7-146
Figure 7-17: Velocity-time curves for 2001 Dodge Caravan.	7-147
Figure 7-18: Manual-fit of 2001 Dodge Caravan crash test data	7-148
Figure 7-19: Predicted contact velocity compared with test data.....	7-148
Figure 7-20: Predicted contact velocity for 2001 Dodge Caravan at 56 km/h (from 40 km/h).....	7-149
Figure 8-1: Typical accelerometer readings of left and right B-pillar undergoing crash-induced impulses.	8-153
Figure 8-2: Progressive skeleton of ULSAB vehicle from cosmetic to structure.....	8-155
Figure 8-3: Terminology for ULSAB vehicle components.....	8-156
Figure 8-4: Non-linear finite element analysis of ULSAB vehicle under conditions of NCAP crash test showing also time-corresponding occupant cell velocity.	8-157
Figure 8-5: Idealization of impact load path replacing upper rail and dash rail with two impact bars and reflection plane.....	8-158

Figure 8-6: Lagrange Diagram showing pulse progression and separation point.	8-160
Figure 8-7: Stress Pulse in Bar.....	8-161
Figure 8-8: Exaggerated Effect of Impact.....	8-161
Figure 8-9: Wave Direction	8-162
Figure 8-10: Pulse Length for Different Impact Severity	8-162
Figure 8-11: Wave Shape Visualization.....	8-162
Figure 8-12: A Simple Momentum Trap Experiment.....	8-163
Figure 8-13: Sketch of Right-Angled Momentum Trap.....	8-164
Figure 8-14: Photo of oscilloscope measuring real-time distal face velocity (mm/s)	8-166
Figure 8-15: Interferometer output of distal end velocity (mm/s) against time (s)	8-166
Figure 8-16: Schematic of impact gun prior to firing	8-167
Figure 8-17: Apparatus for testing the directional nature of elastic waves.	8-168
Figure 8-18: Cut-away section of apparatus showing tube bellling at each end.	8-168
Figure 8-19: Plan view of oblique impact apparatus.....	8-170
Figure 8-20: Schematic of oblique impact apparatus.	8-170
Figure 8-21: Schematic of oblique impact apparatus (with side-guide removed).....	8-171
Figure 8-22: Schematic of oblique impact apparatus with tube cut-away at distal end showing distal piston and hydraulic oil.....	8-172
Figure 8-23: Schematic of oblique impact apparatus with tube cut-away at impact end showing piston and hydraulic oil as well as support glide plate minimizing interaction with table.	8-172
Figure 8-24: Photograph of lead ball after impact with side guide fitted. (LHS is in-line ball, RHS is distal ball.).....	8-173
Figure 8-25: Photograph of lead ball after impact with side guide removed. (LHS is in-line ball, RHS is distal ball.).....	8-173
Figure 8-26: Stress-strain diagram for low-carbon steel showing mechanical work done (per unit volume) as areas under curves comparing elastic (dark grey) with inelastic energy (light grey) areas.	8-175
Figure 8-27: Collinear Impact of Long Bar.....	8-176
Figure 8-28: Unloading Elastic Wave – Lagrange Diagram	8-177
Figure 8-29: Schematic of Shot after Firing at Abutment.....	8-178
Figure 8-30: Location Diagram of Shot onto Abutment	8-179
Figure 8-31: Location Diagram for Collinear Rods	8-180

Figure 8-32: Reluctances for Honda tests #2712, #2836 & # 3807 for linearly extrapolated velocities over and under test velocities (from Figure 5-1).	8-181
Figure 8-33: Chassis horn for Toyota Echo shown cut away.....	8-183
Figure 8-34: Combined left and right load cell force in barrier approximately in-line with chassis horns showing velocity of occupant cell and approximate trend of velocity and force decay for Model 2001 Toyota Echo Test #3806.	8-184
Figure 8-35: Combined left and right load cell force in barrier approximately in-line with chassis horns showing velocity of occupant cell and approximate trend of velocity and force decay for Model 2003 Mini Cooper Test #4273.	8-184
Figure 8-36: Combined left and right load cell force in barrier approximately in-line with chassis horns showing velocity of occupant cell and approximate trend of velocity and force decay for Model 2003 Chevrolet Silverado Test #4472.....	8-185
Figure 8-37: Combined left and right load cell force in barrier approximately in-line with chassis horns showing velocity of occupant cell and approximate trend of velocity and force decay for Model 2001 Ford F150 Test #3902.	8-185
Figure 8-38: Combined left and right load cell force in barrier approximately in-line with chassis horns showing velocity of occupant cell and approximate trend of velocity and force decay for Model 2002 Isuzu Rodeo Test #4241.....	8-186
Figure 9-1: Theoretical models to explain formation of rebound.....	9-190
Figure 9-2: Inertial stress model showing reduction in rebound impulse with increase in velocity	9-192
Figure 9-3: Proportional model showing increase in rebound impulse with increase in velocity.	9-192
Figure 9-4: Models for rebound formation under conditions of increased velocity.	9-193
Figure 9-5: Models for rebound formation under conditions of increased mass.....	9-193
Figure 9-6: Increased rebound velocity prediction for mass and velocity effects.	9-193
Figure 9-7: Fraction of normalized velocity concept.	9-194
Figure 9-8: Discernment sensitivity of controlling effect varying velocity.....	9-194
Figure 9-9: Mass influence sensitivity on rebound formation.....	9-195
Figure 9-10: Mass effect comparing proportional model rebound increase over inertial stress model varying velocity fraction (0 denotes low velocity and 1 denotes high velocity crashes)	9-196
Figure 10-1: Coefficient of restitution for 161 vehicles from Smith and Tsongos (1986) data.....	10-198
Figure 10-2: 1987 Hyundai Excel GLS Test #1092 40 km/h with 75kg deleted from test mass compared with 300kg added to test mass to compare rebound.....	10-198
Figure 10-3: Comparison of coefficient of restitution of older to new NCAP cars (N=41 for 2003 models & N=32 for early models) linear regression lines to highlight trends.	10-199
Figure 10-4: Best power curve-fit to data from Table 24.....	10-205

Figure 10-5: Velocity-time graph for 1998 Nissan Altima full frontal rigid barrier tests #2858 & #2744.....	10-207
Figure 10-6: Velocity-time curves for 2003 Toyota Matrix highlighting rapid relative velocity change of engine to occupant cell from 39 km/h difference to 11 km/h difference in 10 milliseconds.....	10-210
Figure 11-1: 558 NCAP tests mass-crush plot with trend line.....	11-214
Figure 11-2: 558 NCAP tests mass-stiffness plot with trend line.....	11-215
Figure 11-3: NHTSA crash tests mass-stiffness plots for 1622 vehicles.....	11-215
Figure 11-4: Demographic relationship of wheelbase and vehicle mass.....	11-216
Figure 11-5: NCAP cars linear regression analysis of average linear stiffness in year of test.....	11-217
Figure 11-6: 1622 NHTSA test results for stiffness by year of test.....	11-217
Figure 11-7: NCAP cars linear regression analysis of average vehicle mass in year of test.....	11-218
Figure 11-8: 1622 NHTSA test results for stiffness by year of test.....	11-219
Figure 11-9: NCAP cars stiffness by reluctance metric.....	11-220
Figure 11-10: 1622 NHTSA test results for reluctance by year of test.....	11-220
Figure 11-11: Injury risk for 1979 model cars compared with 1997 model cars.....	11-222

Tables

Table 1: Abbreviations/Terminology.....	vi
Table 2: Symbols.....	vi
Table 3: List of main crash evaluation techniques in use.....	1-10
Table 4: Overview of study perspectives with summary implications.....	1-11
Table 5: Curve-fitting parameters to Wayne State Equation.....	2-21
Table 6: HIC summary of ANCAP test B9001.....	2-35
Table 7: Threat to life according to the Abbreviated Injury Scale.Shojaati (2003).....	2-46
Table 8: Comparison of reluctance units with NHTSA stiffness parameter units.....	4-81
Table 9: Fidelity of reluctance to best sinusoidal fit of data.....	4-84
Table 10: 1998 Honda Accord full frontal rigid barrier test details.....	4-89
Table 11: Input file for simulation of 1996 Ford Explorer 47.3 km/h.....	5-106

Table 12: Results of simulations of Ford Explorer Test #2256 with varying masses.	5-107
Table 13: Effect of mass on reluctance in 1980 Ford Courier.....	5-111
Table 14: Ford Explorer Test #2256 prediction of reluctance for lower vehicle mass.....	5-114
Table 15: Prediction of reluctance using occupant cell mass.....	5-115
Table 16: Range of variation from test data summarizing Figure 7-6.....	7-133
Table 17: Prediction of injury reluctance for lower vehicle mass.	7-137
Table 18: ULSAB vehicle millisecond event report (ULSAB (1998)).....	8-159
Table 19: Measurements of lead balls after impact.....	8-173
Table 20: Specific energy absorption for 1983 sample of cars.	10-201
Table 21: Specific energy absorption for modern cars.....	10-201
Table 22: Specific energy absorption values for oldest NCAP tests.....	10-202
Table 23: Specific energy absorption values for most recent NCAP tests.....	10-203
Table 24: Rigid barrier full frontal tests used to show velocity influence on restitution.....	10-204
Table 25: Results of rebound equation compared with literature.....	10-206
Table 26: Results of individual curve-fit of specific energy absorption and velocity giving individual vehicle coefficients of restitution.....	10-206
Table 27: Predicted rebound values for 1998 Nissan Altima.	10-208
Table 28: Table of 558 NCAP tests showing first and last four tests.....	11-213
Table 29: Table of 1622 NHTSA tests showing first and last four tests.	11-214

Acknowledgments

The first half of the work was performed at the University of Queensland and the remainder at Queensland University of Technology. The change in university coincided with a change in focus for the project.

I thank my academic committee at QUT for seeing the value of the project and for teaching (amongst many other things) that to complete, rationalization is as important as creation. Faith, encouragement as well as honest feedback, invisible but indispensable elements in the fabric of this thesis, were amply supplied by the committee. The tedium of reading draft after draft, patiently without murmur, did not go unnoticed:

Thank you,

- Professor David Thambiratnam,
- Professor Rod Troutbeck.

Research work often has ‘dry gullies’ where unfruitful areas are explored. Early work seems to attract more dry gullies than towards the end.

Thanks for being there during the main dry gully period.

- Dr. Martin Veidt,
- Dr. Bill Daniel,
- Mr. Rodney Vaughan (the late).

"You see things and say 'Why?', but I dream things that never were and say 'Why not?'"
George Bernard Shaw

I especially thank my academic committees past and present for never quenching the “why not?” in my endeavours.

Thanks also to Professor Tomasz Wierzbicki, Director of Impact and Crashworthiness Laboratory, Massachusetts Institute of Technology and Dr Falk Zeidler Head of Accident Research Daimler Chrysler, Sindelfingen Germany, for taking the time to commentate manuscripts, so important in refocussing of early endeavours.

My appreciation also goes to Colin Jackson from Crashlab who helped make sense of the crash test signals. Encouragement came from Chris Coxson, Chairman of ANCAP by word and deed, the latter in the form of crash test results, giving the work an Australian flavour.

To the many who encouraged and who were not acknowledged here, please know that your kind words formed enabling building blocks for this project.

Finally, thanks go to my wife Diana, who never faltered in her support. Her faith was fuel for the entire project duration.

To my children...

Jam 'n Axe
(Jasmine and Alexander)

Publications

Publications arising from the research

- **Influence of Deceleration Profiles on Occupant Velocity Differential and Injury Potential**
E. Brell, M. Veidt & W. Daniel
International Journal of Crashworthiness. Volume 6, Issue 4, 2001.
- **A New Analysis and Visualisation Tool for Vehicle Crush Data**
E. Brell and M. Veidt
International Journal of Crashworthiness Conference Proceedings ICrash2002
- **On Quality of Crumple Zones**
Edward Brell, David Thambiratnam & Rod Troutbeck
Physical Infrastructure Centre Conference 2002 Queensland University of Technology
- **Modified Crash Pulse and Injury – a clear link.**
E. Brell, M. Veidt and W. Daniel
Feature Article – Accident Reconstruction Network, February 2001.

Other publications

- **Materials Choices for Frangible Structural Elements**
E. Brell and C. Slattery
International Journal of Crashworthiness Conference Proceedings ICrash2002
- **Train Crashworthiness and its Impact on Society**
Edward Brell, Gerard Van Erp and Chris Snook
Australian Journal of Mechanical Engineering, ME25 No2 Institution of Engineers, Australia

Thesis abstract

The following hypothesis is tested by the research:

A single crash test contains information that can be used to predict vehicle response accounting for different crash conditions such as vehicle mass and initial velocity and thus can be used to predict the effect on occupant injury risk for varying occupant positions within a vehicle

It is established that the response of the crumple zone is influential in the level of injury risk. The metric for such response in common use is the NHTSA linear stiffness parameter. This parameter is used to show that stiffness increases with vehicle mass in a demographic setting. However, by comparing vehicle mass trends over 28 years of crash testing with similar trends in stiffness, a mass influence in the stiffness increase is implicated. This influence is supported by the introduction of a mass-independent stiffness metric, called reluctance, which shows a lesser increase in mass-independent stiffness over the 28 years.

The idea that stiffness should increase with vehicle mass runs counter to intuition and is tested by comparing two identical vehicles in crash tests where one of the vehicles carries an extra 555kg. The idea is further tested by simulation using a multiple mass-spring model on vehicles, varying mass and impact velocity. Using the reluctance stiffness metric it was concluded that increased vehicle mass decreases stiffness, confirming intuition.

Using the injury risk metric of contact velocity differential between occupant and interior of the vehicle it is shown that increased vehicle mass reduces injury. This has important implications for the industry where a marginal performer in a compliance crash test needs only to increase production vehicle mass to reduce injury levels to the statutory injury reference values. A fleet study presents evidence of increasing average vehicle mass.

The study observes that blunt injury generally commences prior to vehicle rebound and continues well into rebound. Recognizing vehicle rebound to be influential in almost all blunt injury led to analysis of the fleet for improvement to this injury parameter. Using specific energy absorption as criterion, 18 modern cars were compared with 19 cars 15-17 years older at compliance test velocities. No improvement was discerned. Similarly, two baskets of cars (n=41 modern & n=32 older) tested at NCAP speeds separated by nominally 20 years failed to show improvement in rebound velocity. The implications for this study of the rebound findings was to ensure that the model presented was capable of representing injury into the rebound phase of the crash. To assist in this, a rebound formulation to reflect varying initial velocity was determined to be a linear function, studying 7 models of vehicles involved in 20 crashes at nominally 40, 48 & 56 km/h crash speeds.

Occupant position within a vehicle is identified as an important variable in injury determination. Vehicle crash tests require seating positions to be set to mid-track adjustment. This discriminates against vehicles having more “legroom” while appearing to be fair, using seating adjustment as the determinant. An empirical mathematical model is proposed permitting crash test results to be extended to investigate the effects of varying occupant positions thus eliminating the legroom anomaly. In addition to the varying occupant position facility, the mathematical model can easily accommodate changes in vehicle mass and varying impact velocity showing fidelity with test data.

The model is used to show that injury risk in the National Fleet has not improved over an 18-year period of crash testing.

Notations

Table 1: Abbreviations/Terminology

Term	Meaning
ANCAP	Australian New Car Assessment Program
ATD	Anthropomorphic Test Device (Crash Dummy)
EuroNCAP	European New Car Assessment Program
National Fleet	All passenger vehicles within a National boundary. (Generic intent but usually USA due to convenient availability of crash data)
NCAP	New Car Assessment Program
NHTSA	National Highway and Traffic Safety Administration
OOPS	Out Of Position Setting (Airbags)
SISAME	Structural Impact Simulation And Model Extraction
ULSAB	Ultra Light Steel Auto Body
CRASH3	Linear formulation to estimate impact velocity from crumple zone crush distance.
IARV's	Injury Assessment Reference Values

Table 2: Symbols

Symbols	Meaning
w	Used for ω where software lacks Greek typefacing facility.
ω	Reluctance
Ω	Reluctance used in haversine equations.
V	Velocity.
V_i	Initial Impact Velocity.
V_R	Rebound velocity.
c	Coefficient of restitution.

1. GENERAL INTRODUCTION

1.1 Background

The coroner presiding over Britain's first road fatality in 1896 said: "This must never happen again". About twenty-five million died on the World's roads since then. Faith (1997)

The most recent U.N. statistics show that almost 1.2 million people were killed on the World's roads in 1998. By 2020, road accidents will be the world's third leading cause of death, just behind heart disease. Over 42000 people died on US roads in 2002 Evans (2003) That equates to a death every 12 minutes. The human cost of pain and suffering is inestimable, especially when injury is included. Hyder (2002). Mineta and Martin (2002) report an annual US cost of \$US230 billion or \$820 per person living in the US.

The cost of road crashes in Australia in 1996 has been conservatively estimated at \$15 billion in 1996 dollar values. (Ferguson, Johnson Amoako et al. (2000). Road crashes impose a substantial financial and personal burden on the community as a whole and in Australia, net road safety gains have plateaued since 1997. (Porter (2002)

Smith (2000) suggests that there are no more silver bullets, alluding to such major safety items as seatbelts and airbags. He continues, that improvements on our current level of safety will be progressively more costly and harder to achieve, bringing into some focus the need to simplify assessment of crash data to produce reduction of injury, the essence of the present study.

The first crash test in history was performed by General Motors in 1936, evaluation consisting of exterior observation of the crush. Dubois, Chou et al. (2004) The Ford Motor Company is reported to have crash tested its first vehicle in 1954 Autonews (2003) Kallina, Scheunert et al. (1999) report on the first crash test by Mercedes Benz occurring in 1959, showing pictures of both the test and the letter of patent granted for the crumple zone concept. Since then thousands of crash tests have been performed around the world to demonstrate the efficacy of injury mitigation measures. Yet crash tests cannot determine injury risks at velocities other than test velocities. This makes comparative results arbitrary given that some vehicles perform better at higher speeds and other vehicles perform better at lower speeds.

Similarly, crash tests cannot determine injury risks for varying occupant size and seating preferences for any condition other than test conditions. This limitation is overcome by performing multiple crash tests. This expensive option still only determines for the as-tested conditions, e.g. 5th percentile female and 95th percentile male and not for the intermediate

anthropomorphic proportions. Such limitations of crash tests are acknowledged by Beuse (2002) who reported greater injury risk for the 5th percentile female as compared to the 50th male injury profile.

To overcome these limitations, crash tests are supplemented by modelling. The upper class of modelling include computer software such as MADYMO (Mathematical Dynamic Model) to model rigid multibody kinematics and dynamics to assess occupant injuries, e.g. Deshpande, Gunasekar et al. (1999). MADYMO requires input of joint stiffness, in turn determined from finite element analysis of key structural elements comprising the crumple zone. Such software is expensive both in terms of acquisition cost and computational running expense, requiring hundreds of hours of computation time even on today's supercomputers. (Marzougui, Kan et al. (1996). Whilst producing excellent results, the so-called 'black box' technique to some extent insulates the user from the basic mechanics of the crash event.

1.1.1 Modelling

The simplest model in use is an analogy of a mass-spring oscillator. It has great value in aiding the understanding of the crash interaction with occupants. However, the analogy has been criticized for inherent inaccuracies ostensibly for the lack of coincidence of the crash pulse peak and peak force in the spring. Such criticism achieves validity through the injury link with vehicle acceleration implicit in the head injury criterion. It is to be shown that maximum injury can result at a time when there is no vehicle acceleration.

The mass-spring analogy is exploited in this study using a pseudo-spring stiffness to represent resultant injury as if a spring were present to provide the equivalent motion characteristics. This is used to improve fidelity of injury reporting with test data permitting essential proximity studies to be performed. This is a contribution by the author and the general concept is extended to apply to a narrow range of statistically significant proximities improving fidelity even further.

The important principle exploited by the author in the mass-spring analogy and the prime model is to use a pseudo spring stiffness that reports injury accurately rather than focus on vehicle kinematics where the two are in conflict.

The usefulness of mass-spring analogy can be extended to other velocities by the application of the Crash3 Algorithm in common use in accident reconstruction, for example Turner (1998). The linearity provisions of this algorithm are applied to the prime model as well.

1.1.2 Vehicle Mass

Vehicle mass is a considerable issue in passive safety. It has long been known that if a car is heavier, it reduces risk to its driver, but increases risk to other drivers. (Evans (2004a) The overall fleet effect of this was determined by Hertz (1997) showing that an extra 100 pound (45 kg) would increase fatalities by 1.1%. Evans (2001a), in lamenting the lack of empirical data on mass variation, observed that crashes had varying occupancy. This enabled him to conclude that adding a passenger reduces a driver's frontal crash fatality risk by 7.5%, but increases the risk to the other driver by 8.1% providing considerable insight into the role of mass in a crash.

Whilst his conclusions as reported are most useful for fleet-wide decisions, they are essentially momentum considerations and do not reflect what additional mass imposes at the crumple zone level. Information at the crumple zone level is needed for vehicle structure decisions.

Response to additional mass at this level and influence on injury appears to have little or no coverage in the literature. Research in this area by physical testing would require multiple crash testing varying mass for each test; an expensive option.

Fortunately this limitation is overcome by the application of public domain software that is dynamically calibrated typically over two crash tests. The software models the crumple zone as multiple masses connected to linear and non-linear springs. Such a model requires extraction of participating masses, eg wheel-sets, engine, etc. as well as connecting elements stiffness from crash test data. Once extracted, the one-dimensional lumped parameter model can be conveniently used in conjunction with lower end computer software and hardware. This modelling software is used to demonstrate the reduced injury effect of additional mass on crumple rate. This is a contribution by the author.

A limitation on the usefulness of this software is that considerable practitioner skill is needed to manipulate crash test data to perform parameter extraction. (Mentzer (2001). A contribution of the present work is to provide techniques that require a lesser degree of skill. The technique justifies pro-rata methods to linearly scale stiffness with mass increase. The procedure permits simple modelling to be applied to changing vehicle loadings as might be found with varying vehicle occupancy.

Whilst a simple and effective model may not be the next 'silver bullet', the need for such a model permitting convenient optimization of injury reduction measures across all strata of velocity, vehicle mass and occupant position is manifest. To test this need, and as a contribution of this study, the National fleet is studied for trends in these important areas:

1. Vehicle rebound. This important contributor to injury is shown in this study to have remained stagnant over the period studied. In the many details provided by NHTSA on crash tests, vehicle rebound is not reported in the public domain database.
2. Vehicle mass. Vehicle mass is shown to have increased over the period studied.
3. Crumple zone stiffness. A mass independent stiffness metric shows an increase in stiffness over the period studied.

All have significant implications in injury and the efficacy of the crash testing legislation specifying testing procedures. Opportunities for extending crash test results to other conditions encountered in the normal use of a vehicle are explored.

1.1.3 General

In the forefront of general injury reduction is the airbag. The airbag provides more than just featherbedding at the internal impact point, it also reduces the occupant stroking distance before dangerous velocity differentials between the occupant and his² surrounds build. In an OOPS³ situation where the occupant is too close, the velocity differentials can be higher than normal, the deploying airbag membrane being the rapidly approaching internal impact surface. So successful has the airbag been that there is risk in trivialising other injury risk reduction measures. Extremity body parts, while not usually fatal, are often debilitating and account for a significant societal cost in terms of lost wages and medical bills, etc. Similarly, seatbelt injuries do not often kill but are also mitigated by an optimised crash pulse. The prime model proposed by this study facilitates consideration of injury of extremity body parts as well.

A pulse by definition implies a time element. However, a crash pulse can be legitimately defined in many ways including parametrically as velocity decay at any point of crush. Here the time element is acting as the background parameter. To avoid ambiguity, the term crash pulse is used usually to mean transient velocity decay of the occupant cell unless explicitly stated or obvious by the context.

A crash pulse can be changed either by design prior to manufacture or by fitment of an appurtenance such as an energy absorbing bumper or bull bar. There is a community need to assess the result of such fitment to assist a range of decision-making from legislature on one end of the spectrum to personal buying decisions at the other end. The difficulty in arriving

² No Gender connotation intended, male used as representative of both genders.

³ Acronym for Out Of Position Setting

at a black and white picture representing choice is that what is beneficial at one crash speed may be detrimental at another. Decisions thus become a compromise where the 'greatest good' becomes the optimisation goal. A prime example is the legislated crash test requiring fixed occupant positions within the vehicle and fixed dummy proportions often the 50th percentile male. The crash pulse result may favour the prescribed parameters and remain silent on changes of dummy size and position. Similarly, it may favour conditions at the tested speed and give no indication what the results may be at a higher or lower crash speed. If all of speeds, occupant position and size including vehicle mass need to be varied, the complexity increases manifold. Thus the value of simple modelling techniques comes into focus. Adding a partner vehicle to the crash test specification makes modelling an imperative considering the costs associated with vehicle-to-vehicle crash tests.

The motor industry is on an upward spiral of increasing mass and stiffness. It is shown that additional mass helps in the compliance process. However, additional mass also increases injury risk for the other driver. The increasing popularity of large 4WD⁴ vehicles witnesses the “bigger is better” philosophy. Additional mass requires additional strength. This can be achieved by using high strength materials. High strength materials increase crush stiffness affecting compliance. The compliance problem can be solved by additional mass, so completing a cycle in this spiral.

By identifying the interacting role of vehicle mass and structural stiffness in the compliance process, the compliance process itself is identified as the agent responsible for the state of the fleet. This recognition leads to recommendations to legislation changes that limit maximum mass-stiffness ratios and prescribe maximum ratios of crash energy conversion to rebound velocity.

⁴ Abbreviation for four wheel drive vehicle.

1.2 Aims and Objectives

The central aim of this study is to test the following hypothesis:

A single crash test contains information that can be used to predict vehicle response accounting for different crash conditions such as vehicle mass and initial velocity and thus can be used to predict the effect on occupant injury risk for varying occupant positions within a vehicle

The overall expected outcome of the study is to improve vehicle design and reduce the societal cost of motor vehicle crashes and crash testing. Specific objectives are to investigate and understand the causes of motor vehicle induced injury. This study is to encompass the various strata of cause and effect and how they relate to each other, from the empowering legislation for crash tests to the internal collision of the occupant. The reduction of injury sought in the overriding aim of the study is expected to be found in these causes.

To enable assessment of the success of injury reduction measures, an objective of the study is to winnow extant injury criteria for a universal measure that bypasses the peculiarities and individual sensitivities of body-part-specific criteria.

Such a broad spectrum injury measure is necessary to determine what crumple zone response profile is ideal, the other objective of the study. Once an ideal crumple zone profile is identified, it is an objective to study those causal factors that might shape this profile. The causal factors range from quasi-static behaviour of structural members in the crumple load paths to progression of strain disturbance of the impact by wave motion in the structural material.

For convenience and relevance to injury a crumple zone response is typically presented as occupant cell response. Such a response, when derived from a crash test is data intensive. The sheer volume of data alone makes the process of broad spectrum injury assessment time consuming. To enable study of conditions not represented by crash tests efficiently and effectively it is an objective of this study to represent crash test data mathematically permitting reliable extrapolation of crash data to variations of conditions, as follows:

- Vehicle mass.
- Initial impact velocity.
- Relative occupant position.

It is an objective of the study to identify endemic responses of crumple zones that exacerbate injury and attempt to ascribe societal cause via crash test regimes. If such a societal link can be established legislative reform can effectively address the issue.

1.3 Approach and Scope

The thesis is arranged into two informal parts. The first part addresses substantially the objective to test the hypothesis. Chapter 7 marks the end of the first part while the remainder of the thesis focuses more on the wider issues of the aims and objectives.

The aims and objectives cover a wide area ranging from an instantaneous view of a crash progressing to overall perspectives of the National Fleet. Because of this a single literature review is not presented. Instead, literature is reviewed topically throughout the thesis.

In the world of crashes, there are frontal, offset frontal, rear and side impact conditions. In addition, a motor vehicle crash can have a number of collision partners, among which are trees, roadside furniture and other vehicles. Impact can occur centrally and collinear or oblique. Because the model proposed in this study extends into the rebound phase of the crash, there may be scope for the model to represent vehicle response in other than frontal crashes as well.

In a typical vehicle to vehicle crash there may be a mass imbalance and a crumple zone stiffness imbalance. In this wide field of possibilities the scope needs to be limited to permit examination to the detail required, yet allow timely completion of the project.

The study then is aimed at the more common crashes and crash velocities. Given that in the crash statistics there is a predominance of frontal crashes, the scope is thus limited to frontal collinear central impact at impact velocities within a nominal 20% of compliance and NCAP test speeds. The proposed model validation is thus limited to full frontal rigid barrier impact.

Australia has abandoned the full frontal fixed barrier crash test in favour of the offset deformable type. Older Australian vehicle tests are used to provide some local relevance. The more modern crashes are sourced from the USA database of crash tests.

There are two types of tests that predominate namely the compliance test at 48 km/h (30 mph) and NCAP tests at 56 km/h (35 mph). Tests at other speeds are sourced as available.

A prime endeavour of the study is to establish early, criteria by which a crumple zone performance is to be judged. A number of common criteria are considered and shortcomings discussed in Chapter 2. The choice is made for contact velocity of the particular body part under study. A link between contact velocity and injury risk is established and contact

velocity is assigned to be representative of injury risk. Proximity is defined in terms of intrusion and incursion. A study is presented in Chapter 2 that emphasizes the discrete nature of proximity where a small increase can have a large consequence and vice versa, depending on the circumstances. A further study in this chapter shows that an increase in proximity has a non-linear effect on contact force.

“Ride-down” is a recurring injury reduction goal in the literature. It purports to align velocities of occupant and vehicle for a gentler approach to stop. In a presentation of an injury model, a contribution by the author, it is shown that “ride-down” is a matching of body deceleration with vehicle deceleration. It is shown that alignment of velocities occurs only on hard impact surfaces and exists in the form of multiple body part impact. A much more common occurrence is internal impact commenced during the vehicle ingoing phase and separating some time after vehicle separation from the barrier. A long body part coupling phase has implications extending to the rebound phase of the vehicle. For this important reason, development of the prime model includes rebound.

Chapter 3 expands the concept of stiffness of the crumple zone beyond the extant literature to include variations in velocity, mass as well as stiffness at an instant in time. Structural stiffness is discussed in terms of contributing factors including, *inter alia*, component strength, stiffness sensitivity to changing velocity and failure initiators in the main crash load bearing members. The literature position on what is an ideal crumple zone profile concludes this chapter.

Discussions in Chapter 4 are confined to occupant cell response. Focus is entirely on vehicle response leaving injury consideration for later chapters. It is shown in this chapter that reasonable fidelity with test data can be achieved from a cosine curve for transient velocity and transient position. The term reluctance is introduced in this chapter as a stiffness metric to reflect velocity decay more appropriately. It also adds distance to the force association attached to the stiffness semantic. This is important as the concept moves further away from the mass-spring analogy.

Chapter 4 introduces the system curve, a parametric velocity displacement curve, leading into the subject of instantaneous response of the occupant cell. This instant concept leads to the introduction of impedance, a concept that is foundational to models explaining rebound formation presented much later. To show feasibility that sine-cosine curves can be phased and joined to represent the full response of the occupant cell including rebound, an equation is presented, finalizing this chapter. The addition of rebound in the equation for the phased sine-cosine curves merely serves to underscore the elegance of the prime model presented later.

Chapter 5 deals with crumple zone stiffness (occupant cell reluctance) for varying conditions of vehicle mass and initial impact velocity.

The idea that stiffness should respond to variations in mass is alien to the mass-spring analogy. It is shown in Chapter 5 that crumple zone stiffness varies with velocity and mass, signposting the limit of the analogy. In the early parts of this chapter the term stiffness is retained only to maintain consistency with literature terminology. As the chapter progresses the use of the stiffness term diminishes being replaced by the reluctance term. Chapter 5 introduces the concept of mass softening and its role in the statutory compliance process.

Prior to Chapter 6 the focus was to present models aiming for fidelity with test data in respect of vehicle motion. In Chapter 6 and beyond, models seek to improve fidelity with differential motion of occupant with occupant cell. The importance of this idea is emphasized by an example of an early force peak compared with a late force peak but of equal impulse. It demonstrates quality of crash pulse and defends pulse improvement endeavours.

Heading towards achieving a better model to represent injury response, the cosine model was optimized to give fidelity to injury for proximities of body parts as statistically distributed. This chapter concludes with an introduction to the phased haversine (in the form of \cos^2) as a suitable mathematical model to be developed further subsequently.

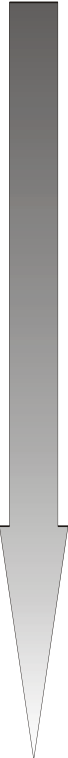
The phased haversine or just haversine is the “engine” of the prime model which is further developed in Chapter 7. It is applied to varying conditions of both velocity and vehicle mass with considerable success. Final development of the model is deferred until Chapter 0 to accommodate the need for injury reluctance not from test data but from boundary conditions as determined by fleet information. This was to permit presentation of important fleet relevant factors first.

The position of the prime model in relation to the literature is summarized in Table 3.

Chapter 7 marks the formal acquittal of the hypothesis test as outlined in the abstract to this thesis. However, the mandate of the aims and objectives provides opportunity to explore further. The hypothesis is thus considered in a wider context, one that includes influences and ramifications in the fleet detail to the fleet aggregate. The full gambit of such perspectives is summarized in Table 4.

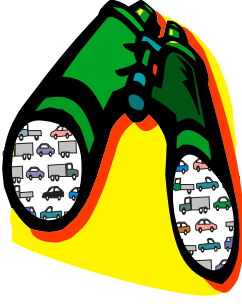


The mesoscopic view was summarized in some detail above. The macroscopic and microscopic view will now be summarized in more detail below Table 4.

Table 3: List of main crash evaluation techniques in use.

<u>ABSTRACTION FROM REAL WORLD CRASH</u>	METHODOLOGY	COMMENT
<p style="text-align: center;">LESS ABSTRACT</p>  <p style="text-align: center;">MORE ABSTRACT</p>	REAL WORLD CRASH	Occupants range in size and position within vehicle. Initial impact velocity varies. Until crash recorders are fitted routinely, vital crash signals are lost.
	BARRIER CRASH	Only 1 initial impact velocity can be chosen per crash. Dummies are fixed size and position in vehicle.
	FINITE ELEMENT MODELLING	Requires laborious discretization of each participating structural component. Computation expense is high requiring top end computing power and long run times.
	LUMPED MASS MODELS WITH JOINT RESTRAINTS	This sort of analysis is typically performed with MADYMO ⁵ software. Model development and computation expense is high.
	MULTIPLE MASS SPRING MODELS	Occupant cell, motor, wheels, etc. are represented as lumped masses and interconnecting structural items as springs. This system including method of participating mass extraction is available as SISAME
	REPRESENTATION OF CRUMPLE ZONE BY NON-LINEAR SPRING	Mooi and Huibers (1998) from the TNO Crash Laboratory (the principals of MADYMO) proposed a two-stage spring to represent the crumple zone.
	GAP & SPRING MODEL	Probably the earliest study on occupant was the gap + spring model by Emori (1970)
PRESENT RESEARCH		The crumple zone is represented by a stiffness model where stiffness is determined by fidelity to injury risk also permitting mass and velocity variations.

⁵ MADYMO is a general-purpose program with integrated multibody and finite element (FE) techniques.

Table 4: Overview of study perspectives with summary implications.

LEVEL OF VIEW INTIMACY	MACRO-VIEW	MESO-VIEW	MICRO-VIEW
DESCRIPTION OF VIEW LEVEL	 <p>VIEW OF THE FLEET AT LARGE</p>	 <p>VIEW OF SINGLE CRASH CONDITIONS</p>	 <p>VIEW AT THE COMPONENT AND INSTANT LEVEL</p>
STATE OF THE ART	<ol style="list-style-type: none"> 1. Linear stiffness parameter 2. Rigidity (Note 1) 	<ol style="list-style-type: none"> 1. Cosine model of transient velocity 	<ol style="list-style-type: none"> 1. Component energy absorption
CONCEPTS DEVELOPED	<ol style="list-style-type: none"> 1. Reluctance from boundary conditions (initial velocity & final crush) 2. Specific energy absorption 	<ol style="list-style-type: none"> 1. Reluctance from injury fidelity 2. System curve of velocity vs. displacement 3. Haversine model 	<ol style="list-style-type: none"> 1. Impedance 2. Theoretical rebound formation models <ul style="list-style-type: none"> • Proportional • Inertial stress
CONCEPTS APPLIED	<p>Fleet trends of:</p> <ul style="list-style-type: none"> • Mass • Stiffness • Rebound 	<p>Injury risk, varying::</p> <ul style="list-style-type: none"> • Mass • Velocity • Rebound • Proximity 	<p>Better understanding of rebound formation</p>
IMPLICATIONS	<ol style="list-style-type: none"> 1. Assessment of effectiveness of crash testing regime 2. Reduction of injury 	<ol style="list-style-type: none"> 1. Better prediction for other crash conditions 2. Reduction in numbers of crash tests needed 3. Injury reduction. 	<ol style="list-style-type: none"> 1. Rebound velocity reduction 2. Better choice of component materials 3. Better crumple zone design 4. Injury reduction

Note 1: Kahane (2003) defines frontal rigidity as the slope of the force-deflection profile for the nominal first 150 mm of crush.

The microscopic view is applied in Chapters 0 & 0. The results of a public domain finite element analysis are reviewed to establish the existence of inertial stress remote from the impact point. In this way strain progression by wave fronts is demonstrated. This is supported by a series of experiments performed for the present study to increase understanding of the wave phenomena. The work in Chapter 0 on inertial stress formed the basis of one theoretical model of rebound formation. The inertial stress model was compared with another theoretical model of rebound formation, the proportional model.

A subsequent chapter sought support for either theoretical model from test data. Since rebound is heavily implicated in injury, a trend in the fleet was regarded as an important indicator to the success of crash testing in general. A trend was extracted over a number of years of crash test data by the author such that clear conclusions could be drawn.

Increased vehicle mass was implicated in reducing injury risk in earlier chapters. If it could be shown that aggregate fleet mass was on the increase then an indication of the self-feeding mass-stiffness cycle suggested earlier would retain some credibility.

Similarly, if stiffness were on the increase the cycle would be more strongly supported. It was shown that the literature method of assessing stiffness by the linear stiffness parameter was invalid in an environment of increasing mass, since increasing mass increases the parameter value in direct proportion. The reluctance method of representing stiffness showed a mass-independent minimum increase in stiffness as a contribution by the author.

The derivation of injury reluctance was confined to crash test data for a single vehicle comprising a velocity decay curve in each case. To extract injury reluctance in this way for a fleet-wide study would require undertaking well beyond scope. However, useful data from the public domain includes initial velocity and crush. The prime model to acquit the hypothesis test established earlier thus needed to be refined to be amenable to available fleet data. This refinement was added in Chapter 0 where an injury trend was presented for the period spanning 1979 to 1997.

A concluding chapter summarized the contributions and implications of the findings and makes recommendations for further study as well recommends changes in the crash testing regime.

2. INJURY RISK CRITERIA

2.1 Introduction

The ultimate measure of crashworthiness must be expressed in terms of the resulting injury risk exposure of the occupants and their survival prospects. Injury risk needs to be considered in context of human tolerance to impact. (McHenry and Miller (1970) Injury risk also needs reflection of modal patterns of the fleet at large. For example, there would be no point in optimizing a crash pulse feature that reduces injury at a speed of 200km/h, a speed clearly unrepresentative of population habits.

A criterion is developed in this chapter that permits evaluation of crash pulse performance at nominated ranges. It will be noted that the recurring causal element in the injury correlations to follow is velocity differential. The use of body part velocity differential with the internal impact surface as injury criteria will be justified in this chapter. These criteria are indirect risk assessment criteria as they are derived from the motion of the vehicle. (Troutbeck, Barker et al. (2001)

The basic motivation for this chapter is to support the axiom that a reduced velocity differential on impact of a body part will produce less injury overall.

Having established crash pulse efficacy criteria, this chapter then presents nominal application of the criteria in studies by the author to examine the validity of the classic “ride-down” model in modern vehicles. In addition, the inadequacy of industry practice of mid-seating ATD⁶ dummy positioning is highlighted.

2.2 Mechanics of Injury

In a vehicular collision there are three basic impacts:

1. Primary Impact - (the vehicular collision)
2. Secondary Impact - (body or body part collision with the vehicle interior)
3. Tertiary Impact - (organ collision within the body)

These collisions are always sequenced as shown above. For example, a tertiary impact is not feasible until after the secondary collision has commenced. Similarly, a secondary impact

⁶ ATD- Acronym for Anthropomorphic Test Device.

cannot start before a vehicle impact. Tertiary impact includes organ impact within the body as well as the "third collision" when soft tissue is crushed by the decelerating skeletal structure inside the body. Viano and Lau (1990) as quoted by Evans (2001a) Chapter 9. Tertiary impact is beyond the scope of this study being essentially a study in biomechanics. This section is limited to the interaction of the secondary impact.

Dale (2003) defines impact with the vehicle interior succinctly:

“Mechanism of injury is the exchange of forces that results in an injury to the patient(s). In an auto accident, the mechanism of injury is the process by which forces are exchanged between the auto and what it struck, the patient and the interior, and the various tissues and organs as they collide with each other within the body.”

To understand injury, it can be helpful to distinguish between blunt injury and penetrating injury. Penetrating injury occurs when a relatively sharp object penetrates the skin's surface and enters the underlying tissues.

Blunt injury occurs when the skin surface is struck with a flat, dull, rounded, or unpointed object. As a result, sprains and strains of tendon-ligamentous attachments are commonly seen. Extensive contusions caused by blunt trauma may be so severe as to cause vascular compromise. Blunt injury directly over bone may also cause fracture⁷.

Trauma from penetrating objects is typically apparent while blunt injury may lack symptoms. (Rouhana (1993) While penetrating injury appears impossible to characterize in the motor vehicle context, significant advances have been made to understand blunt injury. Even so, the task of relating vehicle kinematics with tissue response is complex and difficult. To illustrate the complexity, Melvin, Lighthall et al. (1993) is quoted as an example. They report six mechanisms implicated in brain injury of which three can be caused by non-impact mechanisms (inertial linear and rotational acceleration of the brain).

These and other factors together with varying human capacity for blunt trauma make the task of relating vehicle response to injury extremely complex.

The National Trauma Data Bank (US) report that blunt injury is the most common form of injury, both in general terms and applying to motor vehicles specifically.

⁷ <http://nsweb.nursingspectrum.com/ce/ce100.htm>

Blunt injury, now just injury, is caused by the interaction of particular portions of the human anatomy, called a body part with the interior of the occupant cell. This interaction is captured cinematographically in cartoon caricature in Figure 2-1.

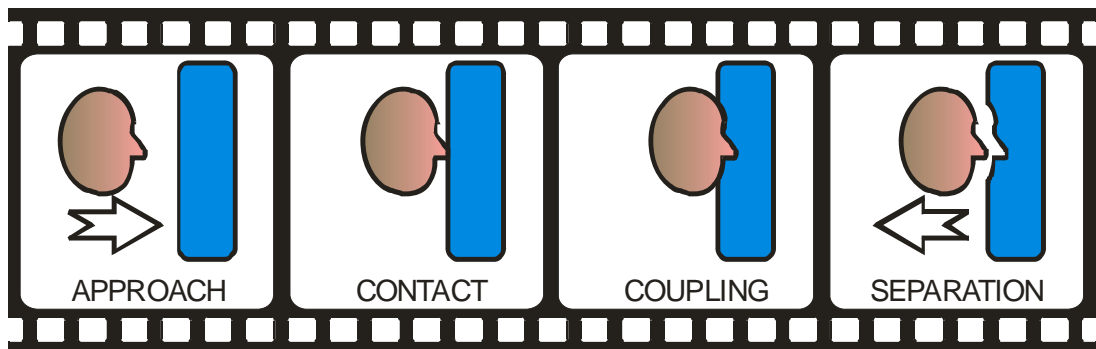


Figure 2-1: Four events in blunt injury.

The approach to the interior surface is a phase having its beginning the commencement instant of occupant cell deceleration. This phase ends with a time node where first contact is made. This is followed by another phase, the coupling phase, (Faidy (1995), during which the velocity differential is equalized. Halfway through this phase the body part “bottoms out”. Still part of the coupling phase, the body part rebounds from the surface. Separation is an event that marks the end of the coupling phase.

These events occur during the velocity decay of the occupant cell and beyond in certain cases. Similar events are occurring at the occupant cell as shown in Figure 2-2.

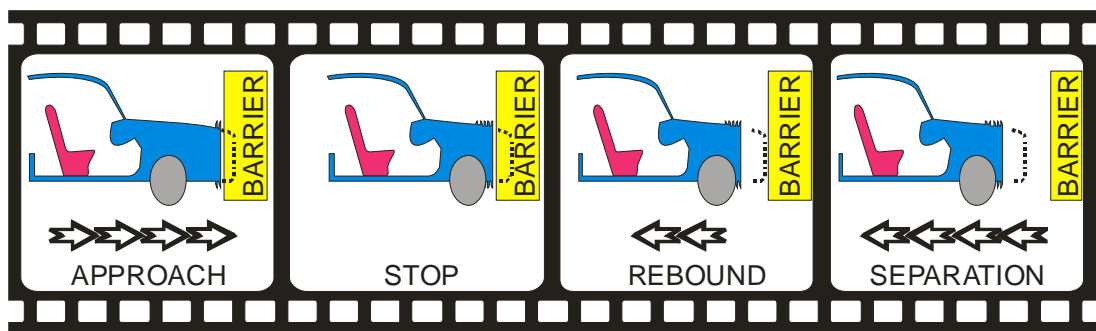


Figure 2-2: Four vehicle events comprising a crash.

The first event is a phase marked by first signs of occupant deceleration. This phase ends at a time node marked *STOP* in Figure 2-2. At this instant, the occupant cell mass has converted all kinetic energy into both mechanical work done and strain energy. The residual strain energy reverses the occupant cell direction into the next phase, rebound. This phase continues until contact with the barrier (or collision partner) ceases.

The process of the vehicle events and injury events is idealized Figure 2-3. The occupant is assumed to be in free flight as per the flail space model. (Ross, Sicking et al. (1993a) The vehicle velocity decay curve is a nominal cosine curve leading into a small radius curve to represent rebound velocity.

The icons from Figure 2-1 are reused to maintain a graphic link. It will be noted that the upper icons have arrows to denote a time node while the lower icons are set on a phase to denote the time-consuming character of the phases.

Once impact has occurred, deceleration of the body part becomes a function of the impact surface stiffness, the body part stiffness (e.g. skin, hair and clothing) and any superposition of ground acceleration from occupant compartment deceleration adjusted for rate of intrusion.

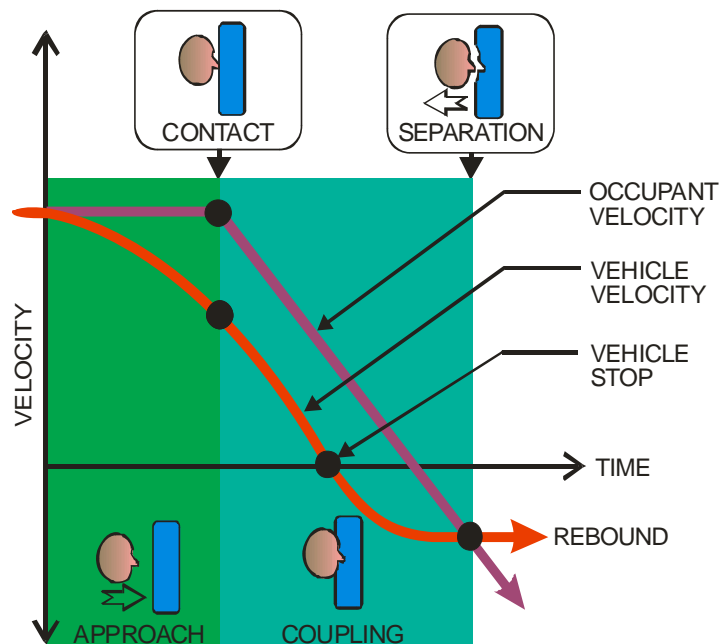


Figure 2-3: Occupant interaction with vehicle interior.

At its most basic level, the mechanical process of injury involves forces on human body parts, e.g. leg, thorax, etc. These forces are the result of a reduction in kinetic energy in the body part by the process of mechanical work done. Forces are either directly measured as for example in dummy necks and femurs or inferred by other measures such as head deceleration or chest compression measurement.

These forces (or derivative measures) are typically compared with the capacity of the body parts to withstand these forces. This capacity is expressed as a reference value that sometimes masks the mechanical-work-done nature of injury for example head injury

criterion (HIC) and neck injury criterion (Nij). On other injury, the reference value is more direct as for example in chest compression which is expressed in millimetres.

Present injury criteria have been established for a variety of body parts. Selection of criteria has been influenced, in the main, by the uniqueness of each body part response characteristics. A numeric assignment to these characteristics purports to be a threshold between acceptability and unacceptability, in each case a lesser number is better. The typical criteria values listed below are often referred to as injury assessment reference values (IARV's). These are mandated in the US by Part 572--Federal Motor Vehicle Safety Standards.

The forces on body parts result from contact with the interior of the vehicle. If the contact surface is soft the coupling period is long. If the contact surface is hard the coupling period is short. The velocity at which an occupant impacts the interior surface is called body part velocity differential, often referred to as contact velocity in this thesis. This velocity differential is shown on the graph of Figure 2-4

A condition of "ridedown" acceleration occurs when the coupling phase is short allowing the body part velocity to align with vehicle velocity. When a body part is in contact with its surface it is able to withstand much greater deceleration. (Kato and Nakahama (1982))

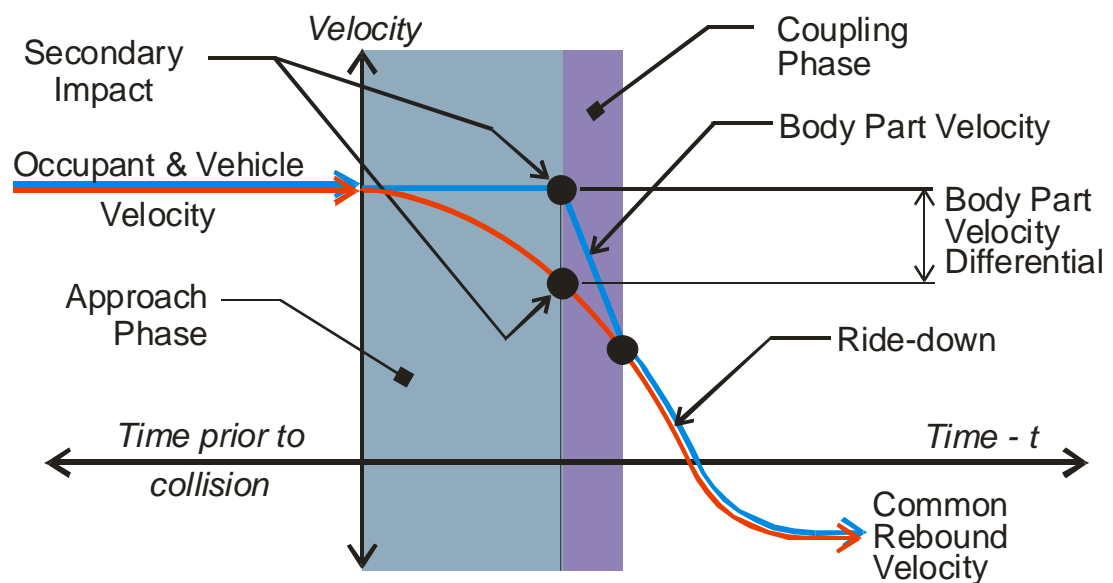


Figure 2-4: Definition of body part velocity differential and ride-down.

Injury can only occur in the coupling phase with a velocity differential precursor from the approach phase. It is noteworthy that opportunity exists in both the approach and coupling phase to improve the crash pulse.

2.3 Human Tolerance to Impact

The capacity for survival of an injury impulse varies greatly in individuals. Occupant age, state of health, gender, stature and weight are some of the variables impacting on the survival prospects of a participant in a crash. (Nahum, Siegel et al. (1970)

Human tolerance to impact has been widely studied, injury having been assessed against:

- Pressure – eg Hodgson and Patrick (1968)
- Velocity – eg Kroell, Pope et al. (1981), Roberts and Compton (1993)
- Energy – eg Atkinson, Benny et al. (1999)
- Compression – eg Ridella and Viano (1990)
- Maximum force – eg Kroell, Schneider et al. (1974)
- Acceleration – eg Gurdjian and Lissner (1964)
- Average dynamic acceleration pulse sustained by the passenger compartment. (Jawad (2002)

Ideally, level of injury should reflect the biomechanics of the specific body part to achieve an absolute measure. However this involves a significant complexity over a very short exposure time and the result may not be useful for crash pulse assessment. An example is the celebrated Head Injury Criterion (HIC). HIC does not correlate well with head injury (Viano (1988). Newman (1980) regards the concept of HIC invalid, there being no kinematic support for the theory. Even if it did correlate well, the comparison is still relative to HIC=1000 being an arbitrary dividing line between fatal and non-fatal derived from the controversial Wayne State Tolerance Curve (SAE-J885 (1986). Since a pulse progression is continuous, a fatal/non-fatal dichotomy is of no value in the injury reduction continuum.

Since the HIC enjoys legislative imprimatur there is some value in reviewing its genesis.

The Head Injury Criterion has for a long time been litmus for determining efficacy of injury reduction measures. The strength of its position in gauging injury in the industry surrogates for the difficulties with injury criteria generally, hence its expanded treatise here.

The HIC is surrounded by considerable controversy. Its failure to improve crash pulses and its general obsolescence in relation to the airbag's success brings continued use into question. A presentation later in this chapter of an ANCAP⁸ test result that showed head

⁸ Acronym for Australian New Car Assessment Program

injury severity HIC⁹ nominally the same for a driver position equipped with airbag as for front passenger position without airbag is presented to emphasize the HIC's weakness to correlate injury with crash pulse response.

Bir (2001) credits Professor H.R. Lissner (engineering) and Dr. E.S. Gurdjian (neurosurgeon) as having conducted the first head injury experiments as early as 1939. She informs that with pressure gauges located in temporal and posterior regions and an accelerometer centred on the occiput, dry human skulls and embalmed cadaver heads were dropped onto metallic and padded surfaces.

Head injury is the cause of 50% of all automotive-related fatalities. Even with the airbag; there are still many sources of head injury within the vehicle, including the windshield supports and the roof rail. King, Yang et al.) Head injury is a complex event with many variables. In addressing this issue, Wayne State University developed a finite element (FEA) model of such complexity that it takes the computer processor unit of a J-90 Cray computer with 4 parallel processors 32 hours for a 15 millisecond simulation.

The FEA model is used to simulate a variety of impacts to different parts of the head. There are hopes that this model will assist in replacing the HIC described by King, Yang et al. (2005) as a "rudimentary tolerance level" to assess injury risk. Being based on the Wayne State Tolerance Curve (WSTC) which was published about 40 years ago it was described as "theoretically only valid for head impacts against rigid surfaces... and cannot account for brain injury caused by rotation of the head."

Newman (1980) concluded that since no general kinematic correlation can be developed (for the HIC), the HIC concept is invalid. Attempts to develop relationships between head injury Abbreviated Injury Scale (AIS) and HIC, were shown to substantiate his views.

Gadd (1966) noted that long-time pulse duration (beyond 50 ms) tended toward an asymptote at a fixed g level.

Hodgson and Thomas (1972) showed that time durations in excess of 15 ms could be regarded as long duration exposure: "Evidence is mounting that the entire concussion tolerance curve may not exist and that only impact against relatively stiff surfaces producing short rise time are critical." Legislation followed requiring crash testers to report the 15 ms time slice as well.

The difference between the Japan Head Tolerance Curve and the WSTC was identified as negligible between the 1-10 ms range. Melvin, Lighthall et al. (1993)

⁹ Acronym for Head Injury Criterion

Cavanaugh (2000) quoted others that the HIC could be interpreted as a measure of the rate of change of specific kinetic energy imparted to the head. He also credited Prasad and Mertz (1985) with recommending that the HIC duration be limited to 15 ms or less, the time duration, $t_2 - t_1$ being controversial. Initially it was restricted to head contact other than to the belt system. Later, it was changed to include any pulse duration, whether there was head contact or not. Field data shows little evidence of brain injury in the absence of head contact, confirming intuition. Current US legislation, FMVSS 208 limits the search for maximum HIC to 36 ms. with the death/life threshold $HIC_{36} = 1000$ for a 50th percentile male.

Newman, Shewchenko et al. (2000) propose a new hypothesis that the threshold for head injury will be exceeded if the rate of change of kinetic energy of the head exceeds some limiting value. They propose a functional relation, which includes all six degrees of motion and directional sensitivity characteristics, relating the rate of change of kinetic energy to the probability of head injury. The maximum value that the function achieves during impact is the maximum power input to the head and serves as an index by which the probability of head injury might be assessed.

Gadd (1966) first approximated the WST curve with an empirical expression for which the slope of the Wayne State curve when plotted in log-log coordinates was approximately -2.5 . Hence the exponent 2.5 that appears in the equation below:

$$a_{AVE}^{2.5} = 1000 \quad [2-1]$$

Where a_{AVE} is average acceleration.

Versace (1971) experimented with constants and exponents for Equation [2-1] and commented as shown in the table below. The table further emphasizes the inadequacy of the HIC, as different curve-fitting parameters were tested for suitability.

It is noted from the table that the exponent 1.9 performed well up to 12 ms into the impact. The numeric proximity to the kinetic energy exponent 2 is noteworthy.

Table 5: Curve-fitting parameters to Wayne State Equation.

CONSTANT	EXPONENT	COMMENT
1000	2.5	Above WSTC beyond 2 ms. Goes through a reference point of about 23 g @ 400 ms
3780	2.9	Only slightly above WSTC beyond 4 ms. Also goes through the same reference point.
9580	3.2	Extremely tight fit to WSTC from WSTC. Also goes through the same reference point.
30.8	1.9	Extremely tight fit to WSTC from WSTC for less than 12 ms then diverges.

For some unknown reason he did not propose an exponent of 2.0 which has “engineering significance” as pointed out by Newman, Shewchenko et al. (2000):

$$a_{AVE}^{2.0} = 6737 \quad [2-2]$$

Equation [2-2] can be rewritten exposing its power-based character:

$$\frac{(V_1 - V_2)^2}{T} = 6737 \quad [2-3]$$

The two velocities in Equation [2-3] account for the head velocity change and so account for the head kinetic energy change. The ratio with T , reveals the character of Equation [2-3], unit energy/time, representing units of power.

Newman, Shewchenko et al. (2000) observe that Equation [3] is a better fit to WSTC than Equation [1] between 5 and 30 ms. This, together with the more appropriate kinematic basis gives appeal to Equation [3].

Because the HIC enjoys legislative imprimatur and because the legislative motivation is ostensibly to improve crashworthiness, it is not unreasonable to expect a valid causal relation in addition to good correlation with test data. Because of this and other factors mentioned, the HIC is not used in this work. Also, no attempt is made in this thesis to distinguish between capacities of human body parts for injury. Other injury criteria currently in use are causally close to injury of the body part represented but causally remote to the crash pulse. This is because of the many insulating variables such as pre-crash stroking distance, impact cushion properties and tolerance for injury.

2.4 Proximity

The role of proximity in injury causation is well published even if the exact terminology differs. For example Lau, Capp et al. (1991) refers to proximity as “initial spacing”. This section reviews the literature and defines proximity more precisely, distinguishing between pre-crash distance, intrusion and incursion.

The idea of occupant proximity to an internal collision object is extended to include any occupant body part. Seat belt slack, ankle distance to brake pedal and neck extension are all occupant proximities within the meaning of this concept. Each body part can thus be shown to have its own unique secondary impact velocity for a given vehicle deceleration profile. Since secondary impact velocity is the engineering variable directly linked to injury, the risk of injury can thus be compared for various crumple profiles. Proximity is a variable in this study but varies once only per crash. Proximal displacement or position varies as the crash progresses.

Atkinson, Benny et al. (1999) referring to proximity as pre-crash distance found:

“That the risk of knee injury was most sensitive to the IP (Instrument Panel) stiffness, crash pulse, delta-V (body part velocity differential), and the pre-crash distance between the knee and IP. (Parentheses notes added, IP is abbreviation for instrument panel)

Flyte (1998) in studying the anthropomorphic characteristics of drivers and their position writes:

“The interaction between the occupant and the safety system is critically dependent on the size of the occupant and their proximity to the steering wheel.”

In context, the safety systems included seatbelts, airbags and by inference, cushioning. A broader interpretation would see the steering wheel reference merely a geographic reference point indicative of other internal impact points as well.

Parkin, Mackay et al. (1993) found that crash test seating positions did not necessarily match with real-world seating as measured with video recording of drivers passing by. They report a 5th percentile female actually sits up to 92 mm further forward than used by crash tests.

Manary, Flanagan et al. (1998) propose a seating accommodation model to predict driver proximity based on steering wheel outstand and seating angle.

Chabert, Ghannouchi et al. (1998) used modern techniques (mag resonance etc) to characterize seated proportions.

Happee, Haaster et al. (1998) point out the need to take into account proportions of the population other than height.

Husher, Noble et al. (1995) report:

“For many years, crash testing performed for the U.S. Department of Transportation National Highway Traffic Safety Administration (NHTSA) has been used to analyse and study trends in the measured Anthropomorphic Test Device (ATD) test responses in 48 kph (FMVSS 208) and 56 kph (NCAP) frontal barrier crash tests. Although many variables must be controlled in these tests, the initial seated position of the dummy has been found to significantly affect the measured dummy parameters (head acceleration, chest acceleration, femur loads). ...”

The driver and proximity are important given that the driver is the minimum and certain occupant. Driver seating position is determined by a number of factors that are absent on passenger seating generally and in taxis specifically. For example, it is obvious that the driver’s leg must reach the pedals. Even for a short trip a seating adjustment becomes necessary for safety and perception of safety. Most trips in taxis are short. A short trip in a taxi does not ordinarily attract a forward seating adjustment. (Brell, Thambiratnam et al. (2002c).

Wilson (1969) made the observation that even in the early days with hard internal impact surfaces, knee-to-dash injuries were not a serious injury-producing event. It is entirely appropriate that as the prime causes of death and injury are mitigated to an acceptable measure, that focus is redirected to the lesser serious events. Head injury has for years been the litmus indicator of injury generally. With the developing success of the airbag this litmus can no longer be relied upon for optimization procedures. Since proximity is a significant parameter in injury and since it can be conveniently be decoupled from other causal effects, knee-to-dash is offered as a reference indicator of relative position of occupant. It has the added benefit of being a measure completely independent of anthropomorphic distributions in the population since it can be measured directly at source. In taxis, occupant proximity is largely controlled by the seating position set by the driver or the last person to occupy the front seat.

Proximity testing in NHTSA (1997) involves OOP¹⁰ rather than a “proximity study” involving a crash pulse interaction with body parts. Hendler, O'Rourke et al. (1974) studied head and body positions during a crash sequence using high-speed photographic techniques. Figure 2-5 is redrawn from this study.

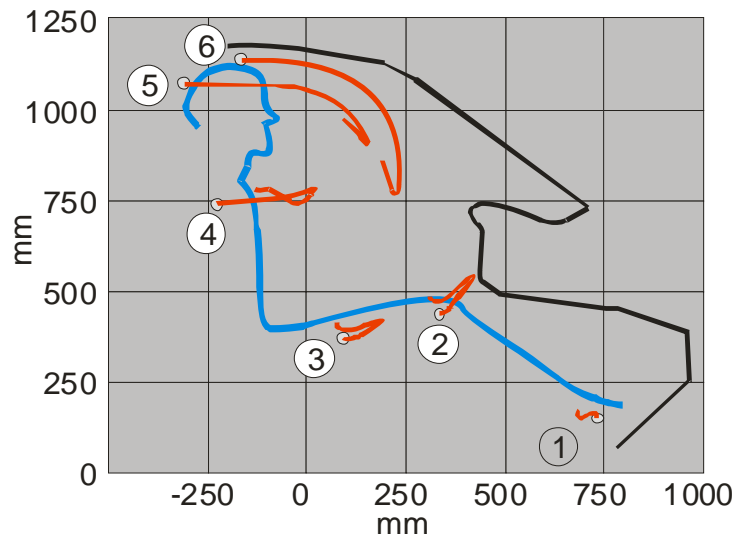


**Figure 2-5: Photographic traces of dummy motion.
(redrawn from Hendler, O'Rourke et al. (1974))**

Traces 5 and 6 in Figure 2-5 confirm the whip action shown in Figure 2-10.

Proximity is defined in Figure 2-6. Attention is drawn to the arithmetic difference between proximity and pre-crash distance, being the intrusion distance.

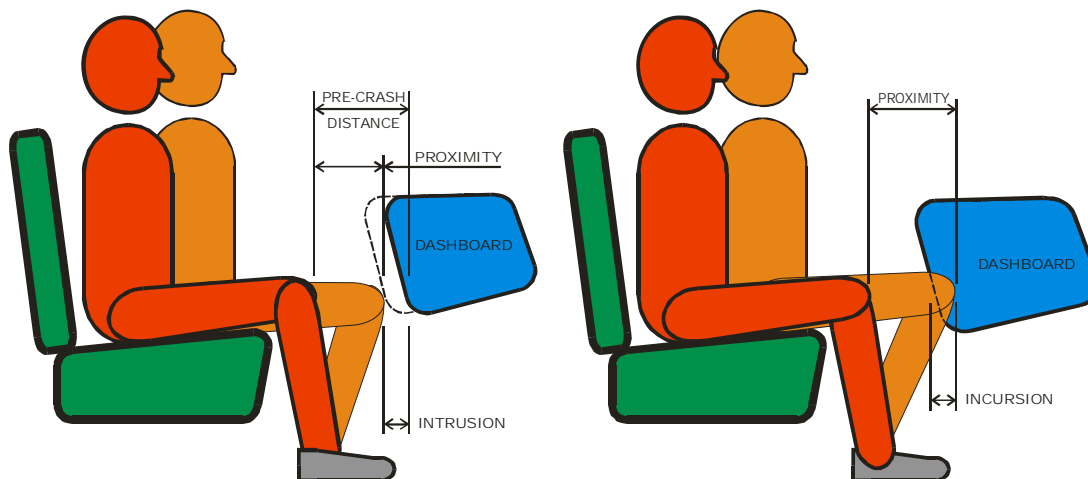


Figure 2-6: Proximity graphically defined.

¹⁰ Acronym for Out Of Position (in relation to airbag deployment)

Intrusion occurs when an internal impact surface shifts from its original position relative to stable points within the vehicle, e.g. rear seat. Intrusion can occur prior to internal impact and also during internal impact. In the latter case the rate of intrusion exacerbates injury.

Intrusion is not necessarily detrimental as it can reduce proximity and cause ride-down to commence earlier. One of the functions of an airbag that appears unpublished is reduction of proximity by intrusion (airbag deployment).

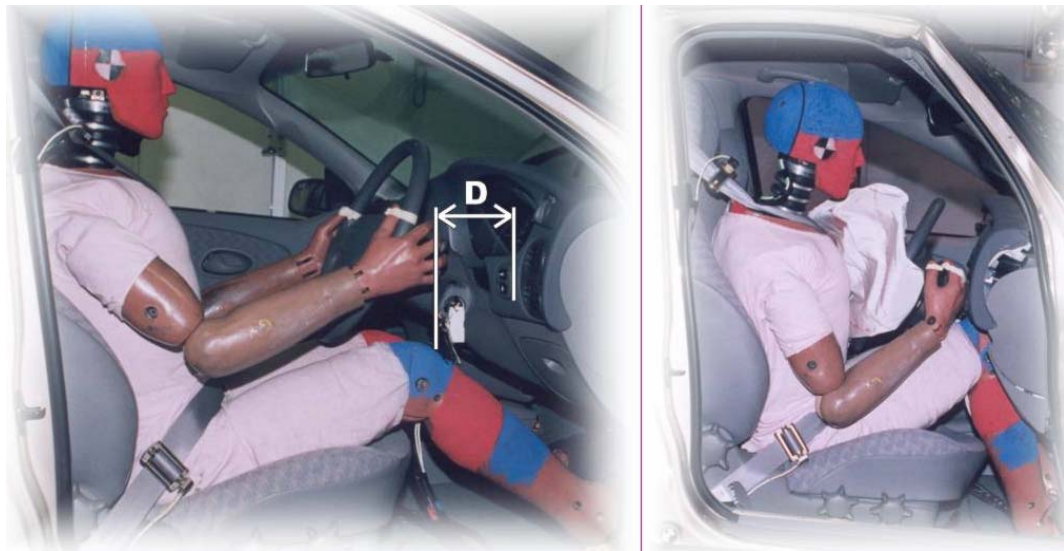


Figure 2-7: Pre-crash distance

Figure 2-7 shows a dummy in position on the left with a pre-crash dimension D . There appears considerable incursion (opposite directional sense to intrusion, see right-hand side of Figure 2-6 for definition) on the right-hand photo during the crash indicating a case where proximity is greater than the pre-crash distance.

If intrusion has ceased at the point of internal impact, the amount of intrusion merely reduces the stroking distance (proximity) of the body part. Under most circumstances a reduced stroking distance can reduce injury. For example, pyrotechnic seat belt tighteners reduce seatbelt slack to permit early restraint, so reducing velocity differential build-up between body and seatbelt.

If intrusion continues throughout the crash, there is risk of injury being exacerbated by the amount of intrusion velocity. There can be significant differences in velocity between different measuring points on the vehicle. Differences between dashboard and rear seat velocity decay are strongly evident in Figure 2-8.

Velocity history affects the ultimate proximity of the body part. Accordingly, the injury effects of intrusion are ideally determined from a proximity/contact velocity study. Examples of such studies appear later in this thesis.

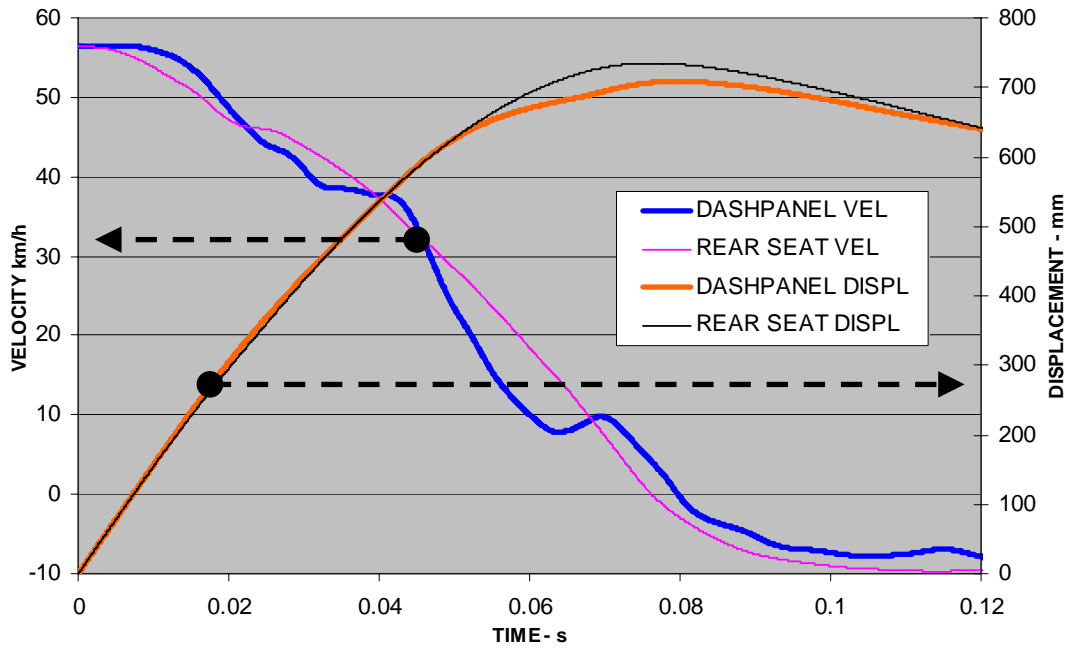


Figure 2-8: Velocity and displacement integrations from rear seat and dashpanel accelerometer data from Nissan Test No 4215.

2.5 Body Part Uncoupling

In the literature, body parts are routinely uncoupled notionally from the body. Because the resistance to motion of the body part up to the point of restraint is small, the body part is regarded as being in free flight. The basis for body part uncoupling stems from the so-called flail space model. (Ross, Sickling et al. (1993a)

During the progression of a crash there may be interaction of the body part with the vehicle interior which may assist in equalizing velocity differentials. Such interaction may take the form of friction of torso with the seat topography or, at the other extreme, multiple impacts. The effects of friction are to some extent counteracted by whip action (for definition refer Figure 2-10.

The uncoupling idea is easier to visualize for ankle injury and knee to dash contact, even seatbelt take-up. However, it can also include, for example, injuries like, brain stem injury where head is uncoupled and velocity differential builds until the neck offers restraint creating tensile stress in the brain stem. This is shown in caricature in Figure 2-9.

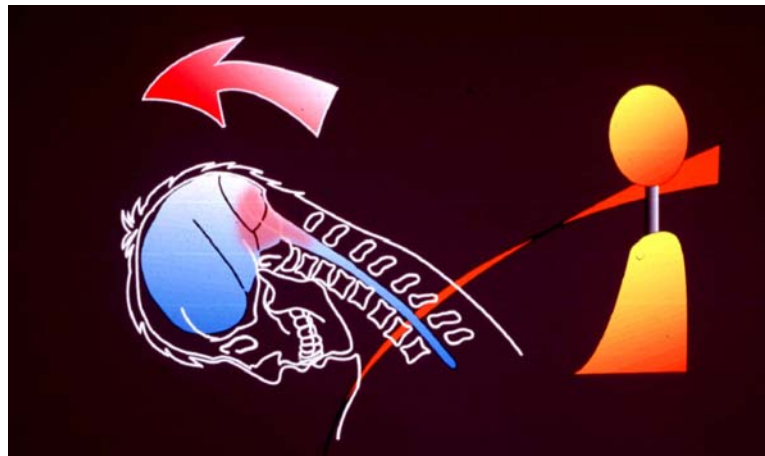


Figure 2-9: Brain stem injury.¹¹

“The most frequent source of severe neck injury was ... non-contact injuries” report McLean, Fildes et al. (1997)

Backaitis, Hicks et al. (1995) studied the clearance dimensions (proximities) to see if a relationship existed between dummy response and such dimensions. They noted there was a large dispersion between the proximities of dummy body parts when seated in the prescribed mid-seat position. They recommended that dummy placement should be influenced by real-world seating preferences.

¹¹ Picture used with permission from Dr AC Croft

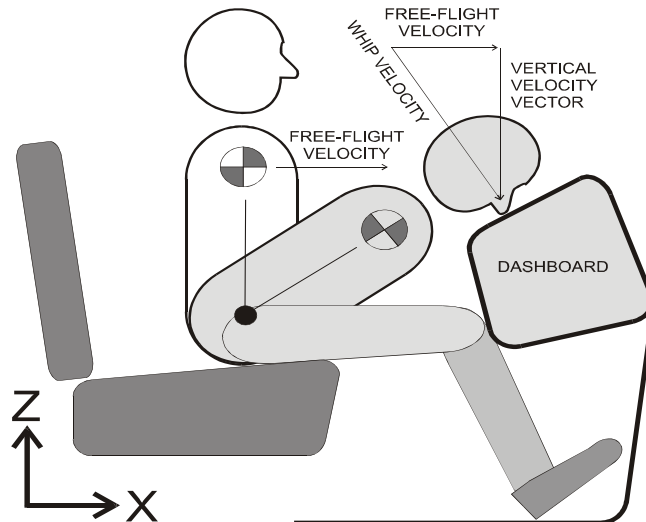


Figure 2-10: Whip velocity defined.

Crash test specifications call for a 50% anthropomorphic male dummy to be seated in mid-track position. This has the effect of appearing to level the ‘playing field’ an essential element in the overall crash testing program. However, this does not reflect the following:

1. So-called leg-room is equated with luxury. A luxury car will have greater proximities than a compact. The legislation discriminates against the luxury car even though the luxury car crash pulse may be superior.
2. A 50th percentile dummy appears to represent 50% of the male population. Anthropomorphic proportions are not entirely linked to the percentile. Each body member has its own distribution. A short person may have long legs and a tall person may have short legs. This anomaly in the average male proportions is interpreted in context of pre-crash distance as a statistical distribution issue of femur (upper leg) length in Figure 2-11.

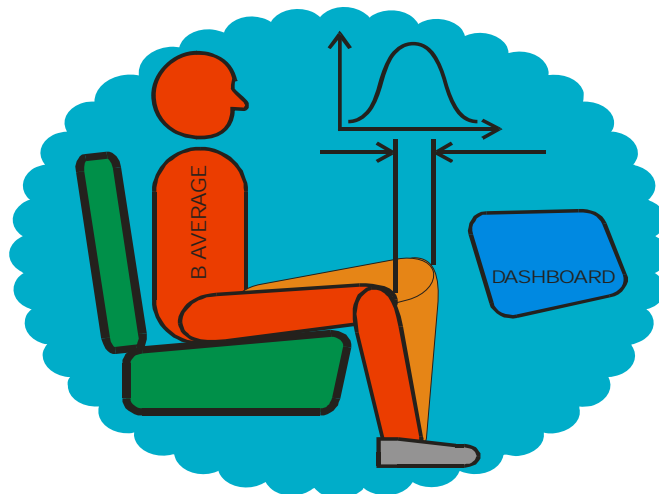


Figure 2-11: Sketch to highlight the statistical nature of body parts and independence to main body part statistics.

2.6 Vehicle Acceleration as Injury Objective

Vehicle acceleration is conveniently available from test data thus making it a prime contender as a metric for injury risk assessment. The purpose of this section is to highlight the inadequacy of vehicle acceleration as a measure of injury risk. This is achieved by demonstrating a common case where injury risk is highest and vehicle acceleration is zero. Vehicle acceleration can thus be eliminated as a metric for injury reduction measures.

It is not uncommon in the literature to find vehicle acceleration equated with injury levels. It will be shown in this section that the worst injury scenario can occur when there is no vehicle acceleration at all. For example, Ignatovich, Diaz et al. (2000) in using a lattice arrangement to represent the frontal part of a car remark:

"There are critical performance criteria to consider for different types of impacts. In a front impact test, for example, the critical performance measure is the acceleration at the driver's position..."

Similarly, Motozawa and Kamei (2000a) aim to reduce vehicle deceleration as an objective function to reduce injury. No mechanism is offered by the authors as to how vehicle acceleration might affect injury outcome.

The worst injury scenario is shown in Figure 2-12 where the occupant's proximity causes the maximum contact velocity of initial impact velocity plus rebound velocity. Coupling is omitted for presentation clarity.

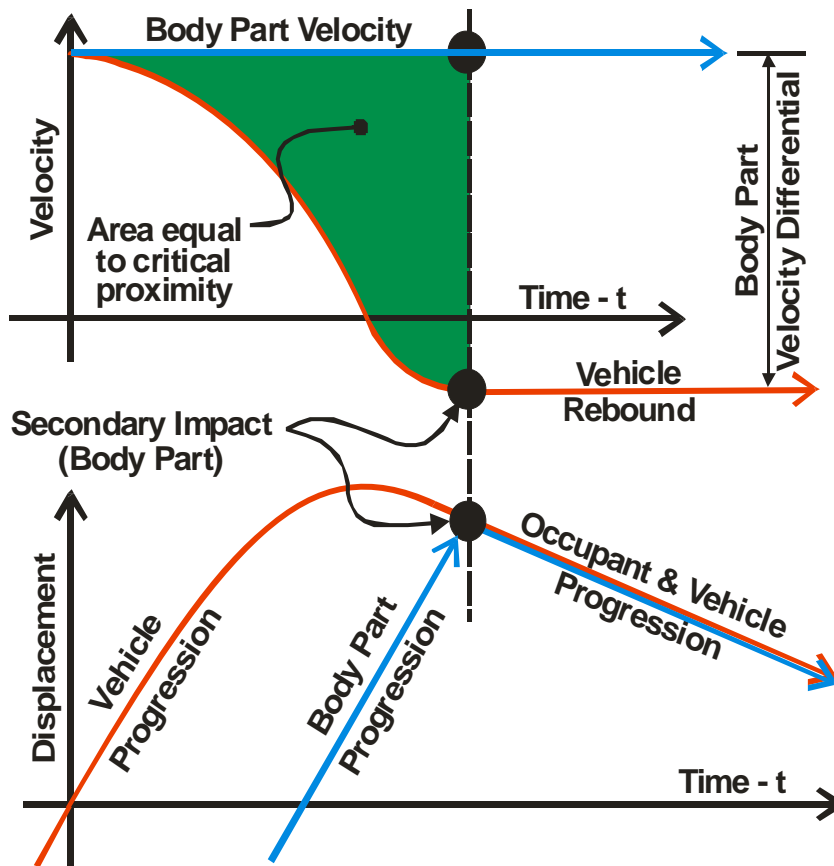


Figure 2-12: Example of maximum injury risk at zero vehicle deceleration.

In view of the above, vehicle acceleration without a proximity study is an inadequate predictor of injury. As a mere note, above the critical proximity injury cannot increase.

2.7 Effect of Proximity in Approach and Coupling Phases

2.7.1 Introduction

Choi and Lee (1999) advocating computer modelling, recognize limitations of current design practice using crash dummies, as follows:

- a. • *dummy designs are not based on recent biomechanical knowledge*
- b. • *dummies are designed for durability: they cannot fracture*
- c. • *limited body sizes and no muscle activity*
- d. • *limited capabilities for variations in positioning*
- e. • *injury criteria are not based on tissue failure*
- f. • *reduction in the need for tests with biological human body surrogates*

Their findings are posted in full to preserve the overall context. The effect of their point “(d) *limited capabilities for variations in positioning*” is confirmed here by the following:

1. Comparing contact velocities, varying proximities, for two similar six cylinder Australian sedans in ANCAP tests. Focus is on approach phase.
2. Comparing a vehicle driver protected by an airbag and a passenger without an airbag in an Australian 4WD ANCAP test. Focus is on coupling phase.

Since this whole thesis is based on improvement to injury risk by optimization of crumple zone performance in the approach phase, it is to be shown that it is important not to ignore the coupling phase where the injury actually occurs.

The motivation for this section is to demonstrate the importance of proximity in both phases.

2.7.2 Injury Determined in the Approach Phase

The end of the approach phase marks the beginning of injury. The relative injury risks, as measured by contact velocity, of the 1998 ANCAP Holden and Falcon Test Numbers #3030 and #8055 respectively are to be considered. The acceleration traces measured at the dash are used to derive velocity decay curves by integration, as shown in Figure 2-13.

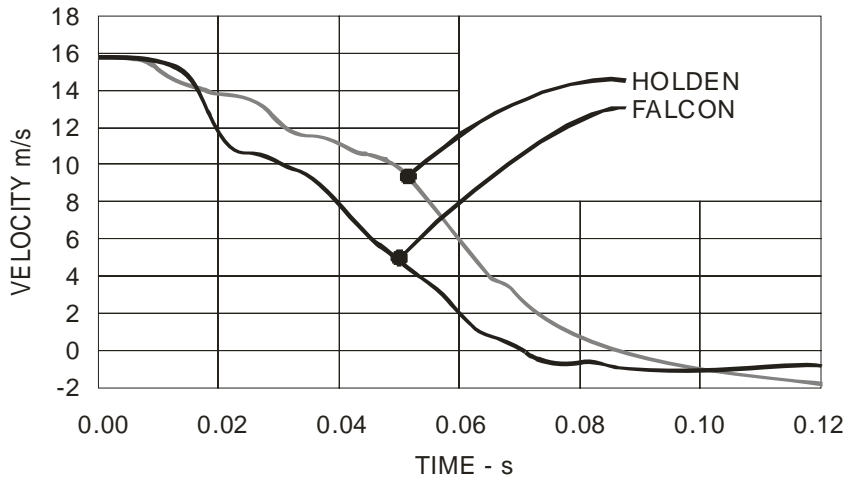


Figure 2-13: Holden & Falcon velocity-time graphs from dash acceleration.

The area above the velocity decay curves but below the free-flight curves represent body part proximity, as shown Figure 2-14:

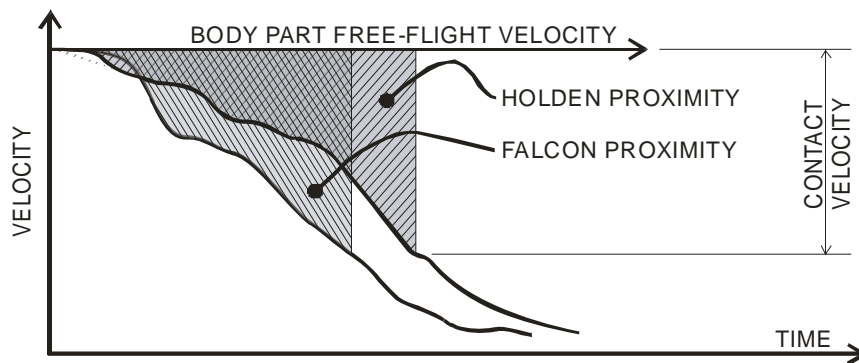


Figure 2-14: Holden & Falcon velocity-time graphs showing equal proximity.

The two hatched areas are equal in size. It so happens that contact velocities are also equal in Figure 2-14.

The areas are varied by time increments and the contact velocities recorded. Figure 2-15 is a plot of proximity so determined against the corresponding contact velocity.

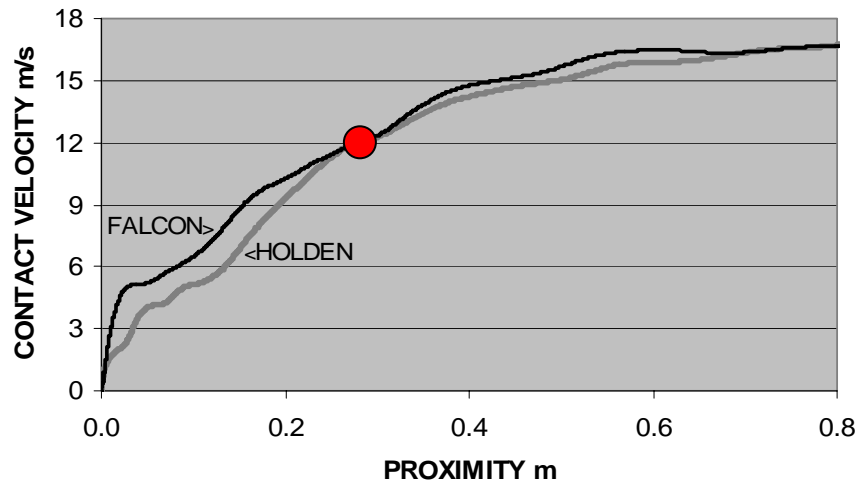


Figure 2-15: Holden & Falcon body part contact velocity vs. proximity.

The red lens centre in Figure 2-15 corresponds with the two different times shown in Figure 2-14.

Taking contact velocity as indicative of injury risk, Figure 2-15 shows the Holden to be the better performer, considering the following:

- The Holden shows an improvement of injury risk over the Falcon for body part proximities up to 0.26 m from the dash.
- The injury risk is indifferent at the red spot.
- The Holden shows an improvement of injury risk over the Falcon above the red spot.
- The injury risk is indifferent above proximities 0.7 m.

It is worth noting that the Holden was awarded 1 ANCAP star while the Falcon received two stars (five stars is best) highlighting the inadequacy of the ANCAP system of rating to assess crash pulse performance.

2.7.3 Injury Determined in the Coupling Phase

In an earlier section it was shown that proximity can vary on account of variations in body part proportions and seating adjustment preferences. Here an example is given where vehicle internal dimension were influential in reducing injury. This supports the idea that the practice mid-seating adjustment in crash test specification can be grossly misleading.

It emphasizes the need to encompass the whole of seating/anthropometric combinations possible in the vehicle under test, seeding into subsequent chapters on modelling methodology as important supplements to crash testing.

Restraint in the occupant cell causes injury. Management of restraint forces reduces injury. Reduction of restraint forces to below the body part injury threshold eliminates injury. Restraint is best applied where the human body is capable of large forces. Proximity can dictate to what body part the forces are applied. This is argued below. The value of airbags is that they spread the restraint over more body parts reducing individual body part forces. In conjunction with seatbelts they are aptly named Supplementary Restraint Systems (SRS). Air bags also serve to reduce body part proximity causing commencement of the coupling phase earlier. This comes at a cost to the occupant in terms of relatively minor injuries consisting of erythema, abrasions, and contusions to the face, anterior neck, or upper chest as the air bag membrane closes the proximity space at speeds in excess of 300 km/h. Hearing loss, tinnitus and / or disequilibrium are typical otologic symptoms of air bag deployment. McFeely, Bojrab et al. (1998)

Evans (2004b) is critical of airbags on the basis of cost-benefit estimating a 3:1 ratio. In this section there is scope to support his argument. It could also be used to add more doubt to the value of the HIC to report injury risk faithfully. Neither is intended here. The motivation is to focus attention on the value of supplementary restraints such as seatbelts in a proximity space that might permit flail without internal impact except for coupling with the seatbelt. A luxury car with a long wheelbase could provide the amount of space.

ANCAP Test N0 B9001 is presented here for a 1998 4WD Nissan Patrol as a contribution by the author. The ANCAP test is important because the occupants are subjected to the same crash pulse, one side of the vehicle equipped with airbag and the other side is without airbag. The current trend to fit vehicles with a proliferation of airbags makes the absence of an airbag on the passenger front seating position rare. In addition, the test series was the last (Australian) of the full frontal fixed barrier crash tests prior to adoption of the Euro-NCAP protocols by Australia as part of the international harmonization program. (As a result of this program the full frontal crash test is replaced by an offset test.)

This taken together with the knowledge from Griffiths, Paine et al. (1999.) that a full frontal test is severe on restraint systems further emphasizes the importance of the particular test.

Details of the test are disseminated here. The calculated HIC values are shown in the table below for both the 36 ms integration time and the 15 ms time.

Table 6: HIC summary of ANCAP test B9001.

HIC BASIS	DRIVER DUMMY	PASSENGER DUMMY
HIC ₃₆	834	890
HIC ₁₅	569	402

It will be noted that the 15 ms HIC was lower for the passenger without airbag than the driver with airbag. Both dummies were primarily restrained by a seatbelt. There were no remarks in the report to allude to any ‘bottoming out’ of the drivers head. Both dummies were covered with disclosing paint to highlight the impact points. The driver dummy appeared to couple with the airbag normal to the airbag membrane as can be seen in Figure 2-16:



Figure 2-16: Driver dummy contact point on airbag.

The passenger dummy impacted the dash panel with the crown of his head. Figure 2-17 shows the two mating points of dummy head and dash encircled with a joining line. The disclosing paint shows text-book contact of knees to dash.



Figure 2-17: Passenger dummy head contact point on dummy and dash.

The locus of the passenger dummy's head can be seen by the approximate overlay (dotted lines) in Figure 2-18. The purpose for showing this locus is to draw attention to the whip velocity of the head at impact with the dashboard. Since the dash travels nominally horizontal while the head velocity approaches the dash at an angle, a complex collision results.

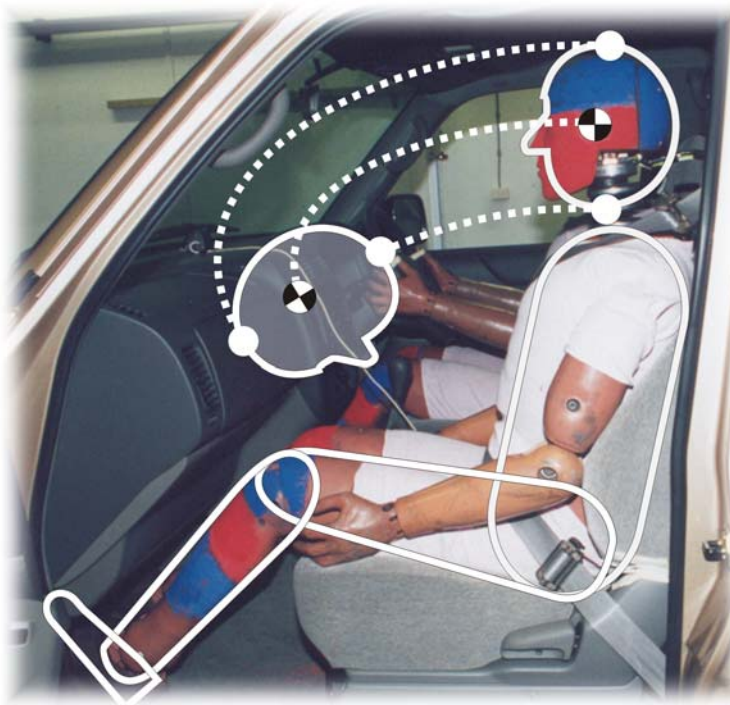


Figure 2-18: Approximate locus of passenger dummy head.

Whip velocity occurs when a body part is hinged at one end and the other end is nominally free to rotate at the lap. In the example in Figure 2-10, the free-flight velocity (velocity in x-direction) applies to the centre of mass of the rotating head and torso. The free-flight velocity of the head is then greater due to lever amplification.

The top of the passenger's head strikes the flat of the dashboard. Figure 2-19 reflects this by taking the resultant of velocities in the x-direction (forward) and z-direction (vertical).

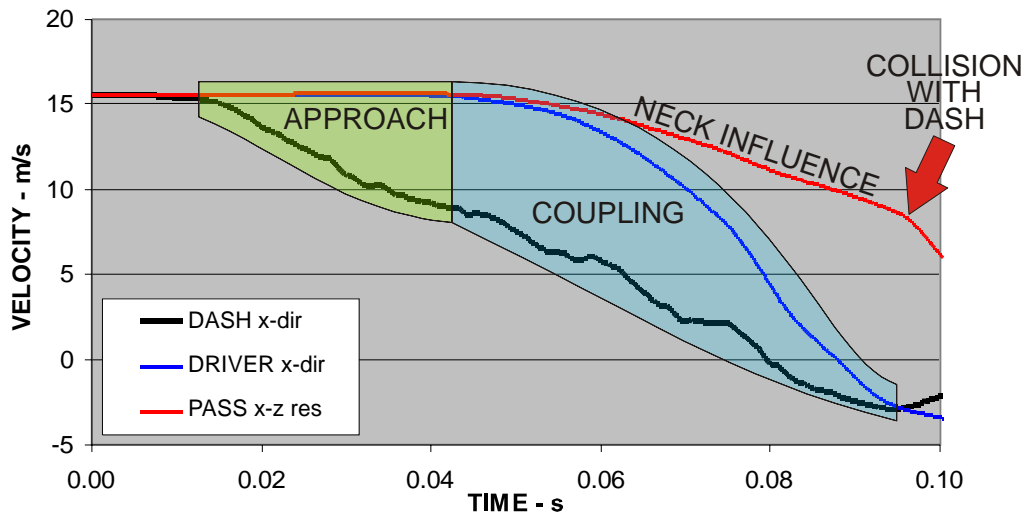


Figure 2-19: Velocity integrations for dash and heads of dummies.

Figure 2-19 shows velocity decay of the dashboard, driver’s head (in the forward direction) and passenger’s head resultant from horizontal and vertical velocity vectors. The green lens marks the approach phase while the blue lens marks the airbag coupling of the driver’s head. The red arrow marks a rapid change of gradient. The gradient change corresponds with the second peak in Figure 2-20. The passenger head velocity is extrapolated and shown dotted to emphasize the gradient change.

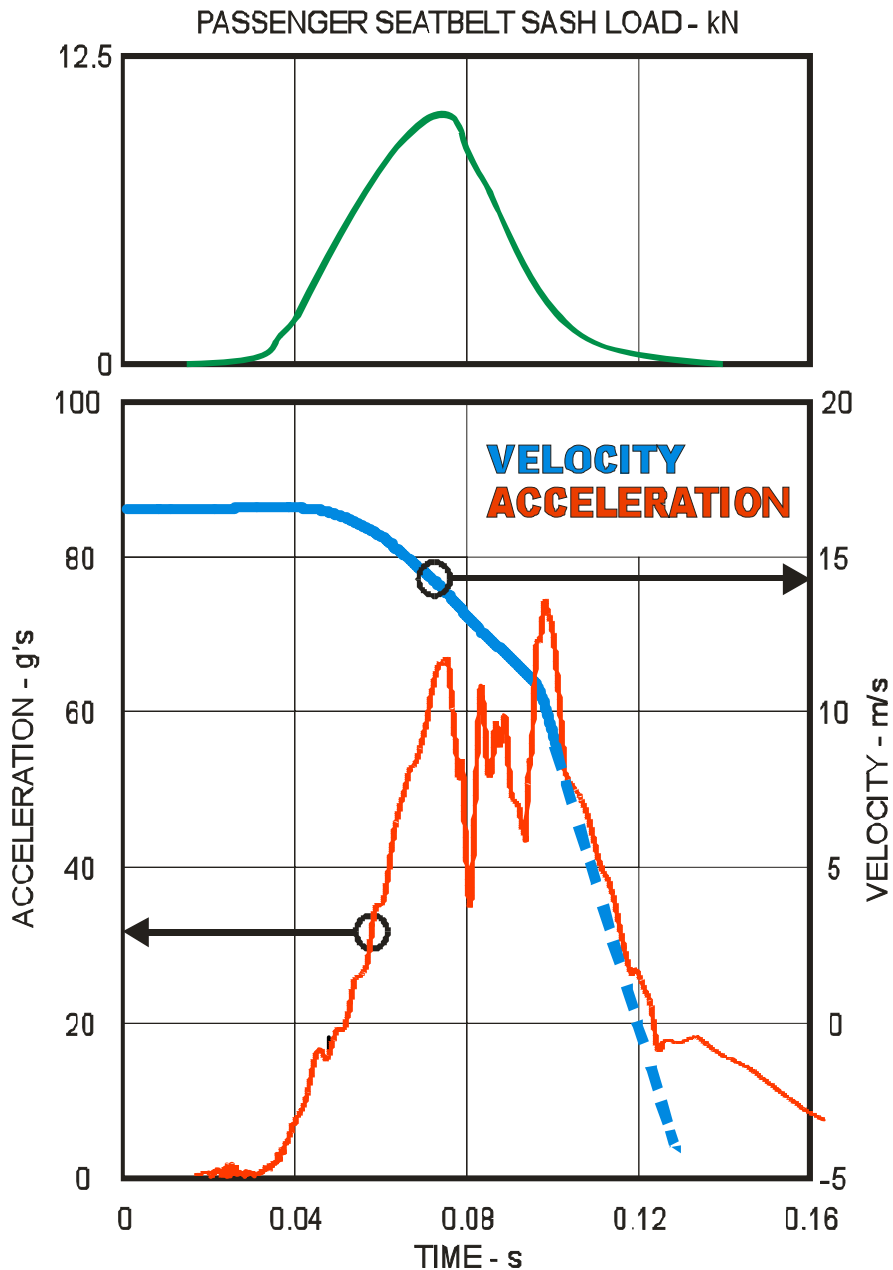


Figure 2-20: Timing of passenger's head resultant acceleration peaks with peak seatbelt load and gradient change of velocity.

There are two peaks in the passenger head acceleration profile. The first acceleration peak in Figure 2-20 corresponds with the seatbelt sash peak load. The driver head acceleration is almost identical up to the first peak (60Hz filter) of the passengers but continues to rise to 80 g's at 0.08 s. Being a single fulgurant peak, the acceleration affects the HIC₁₅ value and helps explain the variation in HIC values in Table 6. The second peak timing corresponds with the passenger's peak compressive neck load confirming the timing of the head impact with the dash cushion.

What has been described are the conditions resulting from mid track seating position. A reduction in proximity would have seen lesser seatbelt load in favour of a greater HIC. Conversely, an increase in general proximity by adjusting the seat further from the dash would have caused a lesser HIC and a greater seatbelt load. This highlights the sensitivity of seating adjustment generally but also in determining the load sharing between head impact and seatbelt coupling in this specific test.

If then, a manufacturer offers more legroom, a highly valued feature of luxury cars, two things may result:

1. The body part may impact at a later point in the crash sequence where injury is more severe (i.e. where body part contact velocity is equal to initial velocity plus rebound velocity.).
2. The body part may be entirely restrained by the seatbelt and so miss the internal impact surface altogether. (In such a situation head injury is non-feasible in the conventional mechanism since head coupling with dashboard does not take place)

2.7.4 Conclusion

The study has shown that injury risk can vary significantly depending on proximity of a body part (e.g. head, chest etc) to an internal impact point (e.g. dash, windscreen, etc.). It has been shown how by altering proximity, occupant restraint can shift from one restraining device to another and influence significantly the injury outcome. The result of such action is not continuous but discrete. A percentage reduction in proximity does not necessarily equate with a proportionate change in injury risk. Modelling of injury risk should take into account the possibility of different restraints dominating the sequence.

2.8 Validity of Classic Ride-Down Model

The purpose of this section is to show that ride-down is a feature of stiff impact surfaces. Stiff surfaces give rise to multiple impacts. This is a contribution of the study.

The validity of the classic ride-down model was assessed. It was found that the velocities of the body part and internal impact surfaces did not always equalize prior to rebound but carried through to a point in time beyond the onset of rebound. An example of this is shown for two ANCAP vehicles, a Honda and Holden, both 4WD in Figure 2-15. Here rebound commenced before 0.07 s and the coupling phase did not finish much later in both vehicles.

Proximity was shaded green and can be seen to be approximately equal. The outer curve shaded red represents front seat passenger chest velocity: The classical ride-down expected was absent. The coupling phase was sustained well past the vehicle rebound point.

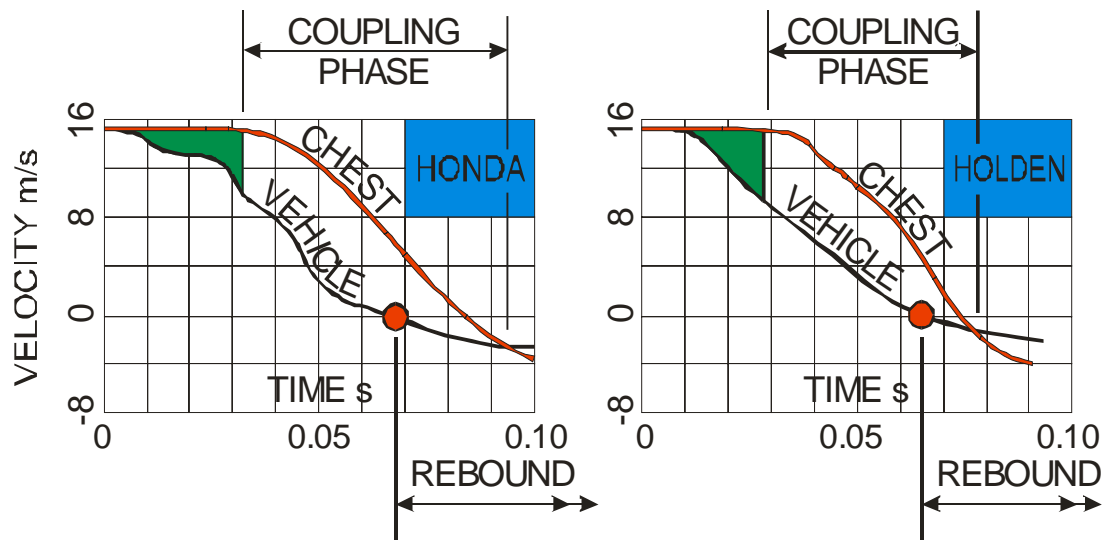


Figure 2-21: Chest velocity decay in Honda and Holden showing approach phase shaded.

The length of coupling phase beyond the vehicle rebound point is commonly found in test data and results from soft internal impact surfaces. To demonstrate this, a torso was modelled by the author in a Runge-Kutta simulation¹² using a cosine to represent the vehicles in Figure 2-15. Cushion stiffness and proximity were varied to give a range. Rebound was nominally set at 2.0 m/s truncating the sinusoidal action of the mechanical analogue shown in Figure 2-22.

¹² Using software Workingmodel 2D by Knowledge Revolution Inc.

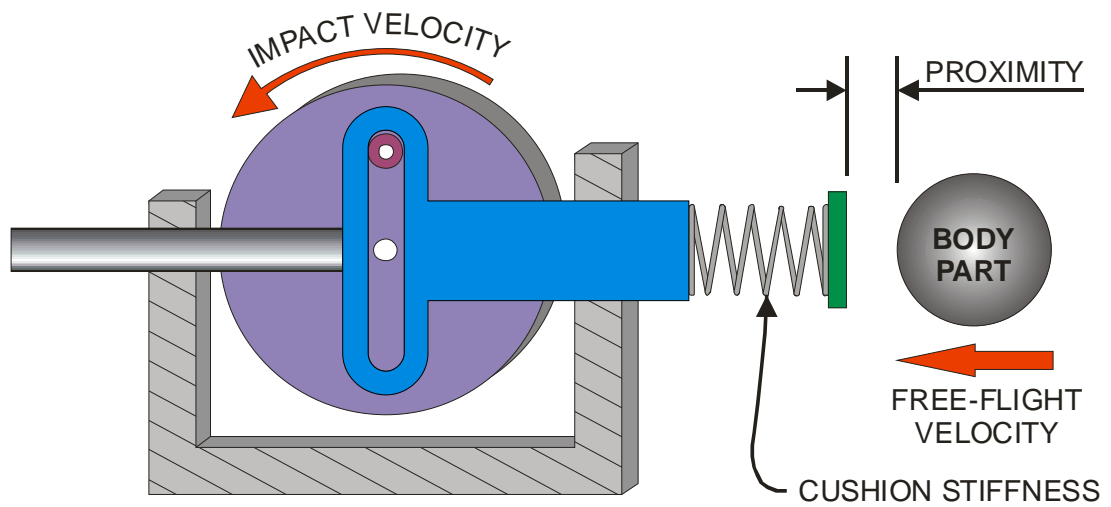


Figure 2-22: Mechanical analogue of model for Runge-Kutta simulation.

The results of varying proximity (seatbelt slack) and cushion stiffness is shown in Figure 2-23.

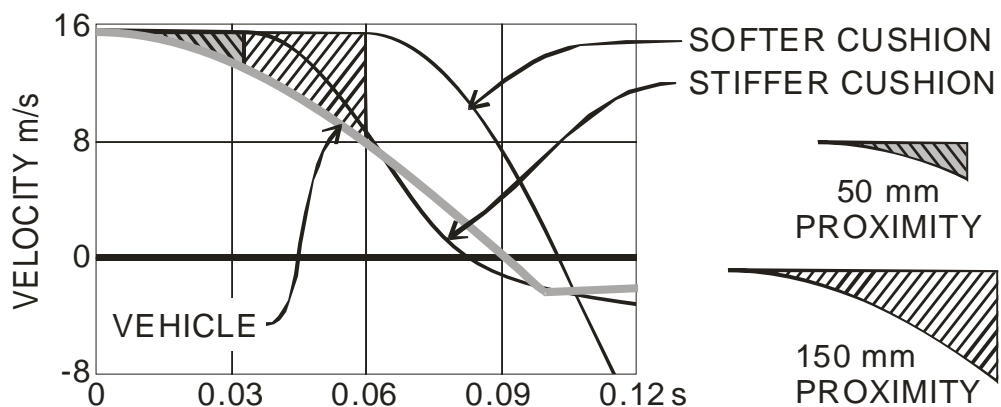


Figure 2-23: Torso in seatbelt with varying stiffness and slack adjustment showing stiff cushion with 50 mm proximity and soft cushion with 150 mm (for presentation clarity).

The slack adjustments corresponded to a proximity ranging from 50 mm to 150 mm. The overall stiffness (linear) of the seatbelt was varied from 70,000 N/m to 250,000 N/m. Contrary to expectations, it is the stiffer cushion which gives the torso ride-down. The softer cushion was more in keeping with the actuals of Figure 2-15.

It was found that when the internal impact surface is hard, multiple internal impacts occur. Little is known of the effects of the ‘hammering’ phenomenon¹³ on injury. It is beyond the scope of this study. Notwithstanding, a hammering example follows to illustrate the concept.

There is a paucity of biomechanical studies on multiple impact injury criteria. However Ray, Sferco et al. (2001) abstract:

”Much analysis of accident data and most crash tests focus on single impacts. However, in reality, multiple impacts account for a large proportion of serious injury accidents and are expected to become a larger proportion as countermeasures, developed primarily for single mode impacts, take effect. It is proposed that multiple impacts should be considered separately since consideration of their characteristics may have implications for occupant protection.”

To limit the effect of hard surfaces, US Federal motor vehicle safety standard (FMVSS) 201 stipulates that tests have to be conducted on the upper interior of vehicles to estimate the head injury criteria. (Kamarajan, Rajagopalan et al. (1999)

Accordingly, there is a trend to introduce soft and padded impact surfaces in a vehicle interior. Notwithstanding, hard impact (high combined spring rate) is still feasible within a vehicle interior as shown Figure 2-24, a photograph showing an enlarged inset of impact of a driver’s head with the windscreen in a mechanism caricaturized by the icon.



Figure 2-24: Head impact on windscreen despite airbag deployment.

¹³ Terminology coined here.

2.8.1 Example of Blunt Injury by ‘Hammering’

A theoretical example is presented here as a contribution by the author to show that ride-down is the result of hard impact surfaces.

The vehicle model used in Figure 2-23 is reused except the body part mass of 5kg is used to represent shoe, foot, ankle and part tibia against a hard object such as a brake pedal. The idea of combining skin, flesh and object cushioning follows Vilenius and Ryan (1996). The combined spring rate used for the study below is a nominal 1,000,000 N/m. The model was run for 50 mm to 200 mm proximity in steps of 50 mm. The 50 mm proximity shows the multiple impact nature of ride-down in Figure 2-25 while the 200 mm proximity in Figure 2-26 does not exhibit ride-down

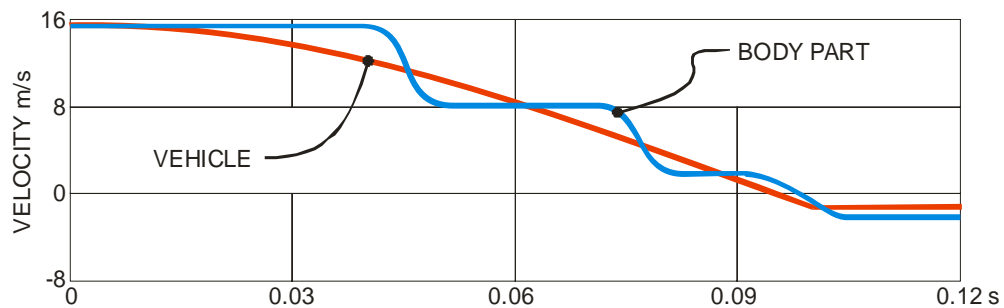


Figure 2-25: 50 mm proximity study showing the multiple impact nature of “ride-down”.

Figure 2-26 shows the same vehicle model as previous but with the body part proximity of 200 mm. The contact forces were extracted on a time basis and superimposed on the graphs to show the timing and peak occurring when the body part velocity is equal to the vehicle velocity.

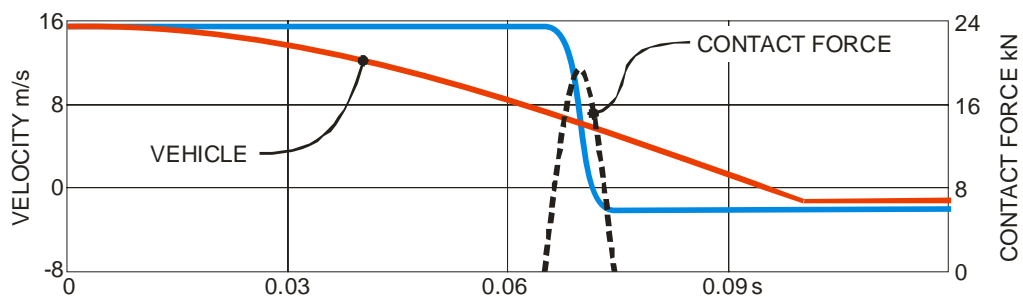


Figure 2-26: 200 mm proximity study showing body part contact force distribution.

The peak velocities and timing for the other cases of proximities were extracted and posted to a spreadsheet for further processing. The laws of conservation of momentum were applied to derive an average force. Average force is thought to be more representative of injury than peak force, following Zeidler, Schreier et al. (1997). Average contact forces for the four proximity cases are posted to Figure 2-27.

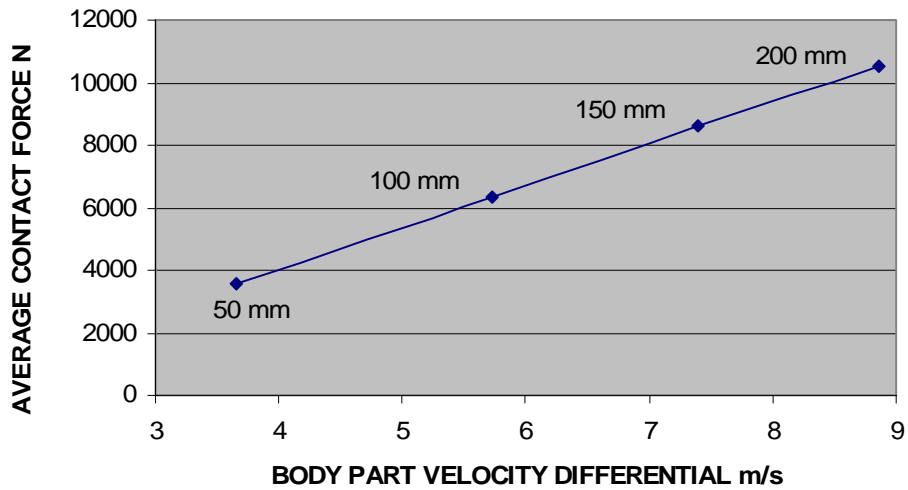


Figure 2-27: Plot of average contact force for four proximity cases.

It can be seen from Figure 2-27 that there is an expected linear relationship between body part velocity differential and contact force following Newton's second law.

However, on a wider note, it is observed in Figure 2-27 that a pro-rata increase in proximity does not have a corresponding increase in contact force, highlighting the non-linear relationship of proximity with contact force and injury.

2.9 Injury Risk Measure for This Study

2.9.1 *What is Injury Risk?*

A number of criteria have been presented earlier in general use to assess occupant injury risk. Theoretical Head Impact Velocity (THIV), Post-Impact Head Deceleration (PHD) and the Acceleration Severity Index (ASI) have been adopted by the European Committee for Standardization as measures of occupant risks.

However injury risk is more complex than merely exposure to velocity and deceleration. Injury results from violent exchanges of energy. Injury risk can be defined as a likelihood of injury or death occurring from such energy exchanges. Identical exchanges of energy can have different injury outcomes dependant on many factors. Some influencing factors in injury not related to impact energy are listed below:

1. Specific body part injured. Some body parts are more susceptible to injury due to inherent sensitivity, eg brain injury.
2. Angle of impact. Sagittal impact (in line with vehicle motion) produces less injury than templar (side-on).
3. Age, general health and fitness of patient.
4. Immediacy and quality of treatment. (Joksch (2000) P27).

Head injury criterion once again provides a convenient metric to discuss the complexity of the topical issue. A meaningful statistical dividing line between fatal and non-fatal with respect to head injury taking into account the above influencing factors and more, is graphed below:

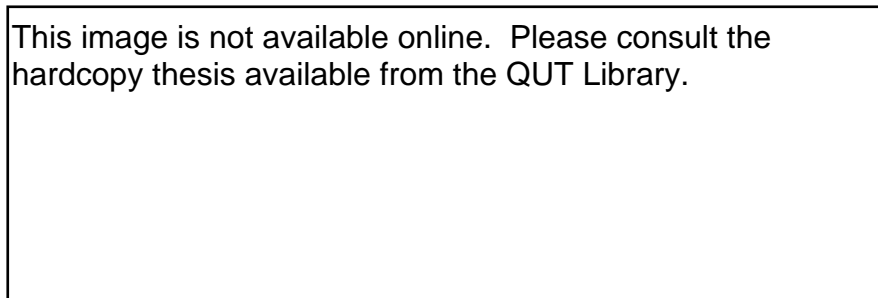


Figure 2-28: Fatal, non-fatal dividing line from Prasad and Mertz (1985)

The risk in Figure 2-28 can also be viewed by level of injury scaled according to the Maximum Abbreviated Injury Scale (MAIS). The MAIS is of significant value to the medical profession for triaging purposes (battle field prioritizing) as well as other purposes. The abbreviated injury scale is ranked from 1 to 6 according to the level of threat to life. In the present context maximum scale is appropriate since, for example, a broken leg would not rank in the assessment if the patient had impressed skull fracture.

Table 7: Threat to life according to the Abbreviated Injury Scale. Shojaati (2003)

<p>This table is not available online. Please consult the hardcopy thesis from the QUT Library.</p>

The statistical risk that an injury from 1 to 5 may occur produces left and right skew about a normal distribution for MAIS3. This is shown in Figure 2-29. (A score of MAIS6 produces Figure 2-28).

This image is not available online. Please consult the hardcopy thesis available from the QUT Library.

Figure 2-29: Risk of injury by seriousness Prasad and Mertz (1985)

Injury risk above has progressed from a number representing HIC to a number representing injury seriousness. To close the loop MAIS was correlated to HIC by Shojaati (2003) shown as a curve in Figure 2-30.

This image is not available online. Please consult the hardcopy thesis available from the QUT Library.

Figure 2-30: Correlation of HIC with Maximum Abbreviated Injury Scale (MAIS) (Shojaati (2003)).

2.9.2 Engineering Link to Statistical Injury Risk

The link from injury seriousness (MAIS) to a measurable engineering entity that is useful in directing crumple zone changes is provided by Figure 2-30. However, the path is convoluted and because of the uncertainties of the many variables involved at every step, becomes doubtful overall. This path is summarized below for exemplar HIC:

1. A body part undergoes a change in velocity and a number is awarded. The number represents deceleration of the body part (in the example an occupant's head).
2. From the acceleration another number is calculated, this time representing the HIC.
3. This number (HIC) is entered into the graph of Figure 2-30 to obtain another number. This time the number represents a rank in injury seriousness. (MAIS).
4. This number must now be interpreted by reference to Table 7 to be meaningful in terms of injury seriousness.

None of these numbers are easily integrated into crash pulse assessments. Occupant cell motion is conveniently available from tests. However, it was shown in previous chapters that vehicle acceleration as an injury criterion has deficiencies. This results from softer internal cushioning causing body part coupling to occur later in the crash sequence where little or no vehicle acceleration is occurring. Depending on body part proximity, coupling can occur after all significant vehicle acceleration has ceased. Injury risk is at its greatest in this phase while vehicle acceleration injury risk reports zero for this phase.

Except in the unusual case of perfect ride-down, body part coupling will always be preceded by a velocity differential between the body part and the imminent impact surface. The bigger the velocity differential the greater the injury, whether young or old, sagittal impact or oblique. Reduced body part velocity differential benefits all occupants irrespective of proximity.

Contact velocity, referred to body part velocity differential earlier, correlates easier with occupant cell motion. Injury risk would more appropriately be correlated to the square of the contact velocity to achieve a linear comparison and reflect the kinetic energy implicated in the injury process. It was thought that the mere comparison between contact velocity to be sufficient distinction to be meaningful. Accordingly, contact velocity is chosen to represent comparative injury risk, following many authors and most recently, Sala and Wang (2003).

Ross, Sicking et al. (1993a) provide a preferred occupant impact velocity of 3 m/s and a maximum occupant impact velocity of 5 m/s. These limits are helpful in this thesis to gauge order of merit. However, in the comparative approach of this thesis, less is better.

2.10 Conclusion

In this chapter contact velocity or velocity differential of a body part with its internal impact surface at the point of internal impact was developed as the injury criterion for this thesis. Proximity distance was more accurately defined than offered by the literature taking into account intrusion of the internal surface and incursion of the body part into the cushion.

The much-vaunted literature “ride-down” of occupant with the vehicle was critically examined as a contribution of this study. The classical ride-down was identified with hard impact surfaces not found to any extent on modern vehicles. A modern version of ride-down is proposed as occupant alignment of acceleration rather than with velocity.

Studies by the author in support of this study found that body part coupling extended in time to vehicle rebound. The implications are that vehicle rebound affects injury even when occupants are close to the internal impact surface. By contrast, the classical ride-down assumption states that coupling is complete prior to rebound. This has the effect of elevating the importance of vehicle rebound.

As a contribution by the author, this study notes that vehicle acceleration as used in the literature as an injury criterion is flawed since it was shown that the highest level of injury can occur when there is no vehicle acceleration. (See Figure 2-12).

BLANK

3. QUALITY OF CRUMPLE ZONE

3.1 Introduction

This chapter presents a brief study of the crumple zone and its components to better understand what comprises a crumple zone and how its elements influence stiffness. Quality of crumple zone is proposed in terms of ability to reduce injury. It will be shown that energy absorption is no guarantee of injury improvement and that it matters when in the crash sequence energy is absorbed.

A crumple zone is a structure with multiple load paths. It is also multiply loaded as the crash progresses. This occurs while heavy objects within the crumple zone impose load on structure between the crash interface and the object. Heavy objects such as the engine and wheelset 'bounce' into and out from the crash interface a number of times during the progression of the crash.

Crumple zone response can be measured as force at the barrier or crash interface, or inferred from occupant cell motion. Quality of crumple zone response is gauged by reduced contact velocity of occupant.

3.2 What Is Stiffness?

Stiffness in general engineering terms is defined as the resistance of a body to deformation upon the application of an external stimulus or load.

The NHTSA (1996) dichotomize a crash pulse into stiff and soft ostensibly for conceptual convenience, as follows:

“A crash pulse is the graph or picture of how quickly the vehicle occupant compartment is decelerating at different times during a crash.

- *Stiff crash pulses. In crashes with stiff pulses, the occupant compartment decelerates very abruptly. An example of a crash with a stiff pulse would be a full head-on crash of a vehicle into a like vehicle. The perpendicular rigid barrier crash test produces a stiff crash pulse.*
- *Soft crash pulses. In crashes with soft pulses, the occupant compartment decelerates less abruptly, compared to crashes with hard pulses. An example of a crash with a soft pulse would be the crash of a vehicle into sand-filled barrels such as those seen at toll booths or at the leading edge of a concrete median barrier. The offset*

deformable barrier crash test and the 30 degree oblique rigid barrier crash test produce soft crash pulses.

In crashes involving comparable reductions in velocity, an unrestrained occupant would hit the vehicle interior (i.e., steering wheel, instrument panel and windshield) at a much higher speed in a crash with a stiff pulse than in a crash with a soft pulse.”

An overall softer pulse then, is associated with reduced injury and vice versa.

Verma, Lange et al. (2003) in context of test barrier influence on front stiffness writes:

“The term ‘stiffness’ is used to indicate the peak forces that are generated and it is therefore different from the definition of linear definition of stiffness (force per unit deflection).”

Kahane (2003) prefers the term rigidity defined as:

“The average slope of the force-deflection profile maintained for at least 150 millimetres during the vehicle’s initial crush in an NCAP frontal impact with the barrier.”

In engineering terms, *stiffness* is the ability of a structure to resist a deformation. It is commonly considered within its elastic (structure returns to its original form) range of behaviour. A high-speed automotive crash is highly non-elastic with permanent deformation of the crumple zone. (Park, Hackney et al. (1999). The elastic/plastic process is visualized as two springs in Figure 3-1 in three stages:

1. Take-up – The bumper, radiator are crushed. This is equivalent to the foremost coil compressing to the second coil.
2. Stroking – Chassis rails wrinkle and buckle. The linear spring analogy breaks down and some licence is taken to represent loosely the constant force.
3. Densification – Structural elements are crushed. The coils here are touching and act as a solid with a great increase in stiffness.

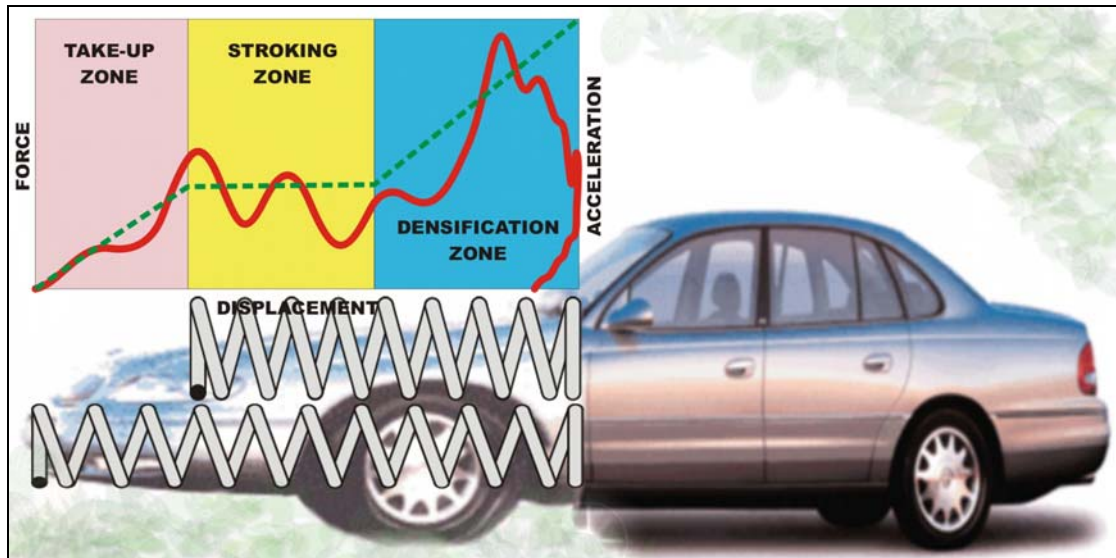


Figure 3-1: Visualization elastic/plastic crumple zone as elastic using two springs giving three spring rates.

The acceleration/displacement curve in Figure 3-1 is drawn parametrically from accelerometer output graphed against its double integral (displacement) with time as the parameter. The source was ANCAP¹⁴ Test #7030 Holden Commodore VT Full Frontal 56.3 km/h.

Whether the y-axes are force or acceleration is merely a scale change by the operation of Newton's second law ($F=ma$). The participating mass in this idealization is to the right of the springs rather than vehicle mass.

It is not uncommon to find a piecewise linear representation of the graph as a force-deflection curve (shown dotted in Figure 3-1) in the literature. E.g. Mooi and Huibers (1998) The area under the curves (full and dotted lines) equal mechanical work done equivalent to the kinetic energy just prior to impact.

The idea of spring representation is an oversimplification of the actual crash event. It is to be contra-distinguished with theory presented in Chapter 0 where impact forces not only retard the occupant cell where it joins to the crumple zone, but also from the rear and other parts of the vehicle wherever strain disturbances initiated by the crash reflect.

¹⁴ ANCAP - Australian New Car Assessment Program.

Stiffness is disserted in this thesis as follows:

1. Single crash stiffness specified by:
 - Structural stiffness
 - NHTSA linea stiffness parameter.
 - Mechanical reluctance.
2. Spectrum stiffness specified by:
 - Stiffness of vehicle responding to changes in initial impact velocity.
 - Stiffness of vehicle responding to changes in vehicle mass.
3. Aggregate stiffness specified by:
 - Stiffness trends of vehicle fleet.
 - Demographic reluctance.
4. Transient stiffness specified by:
 - Instantaneous stiffness.
 - Mechanical impedance.

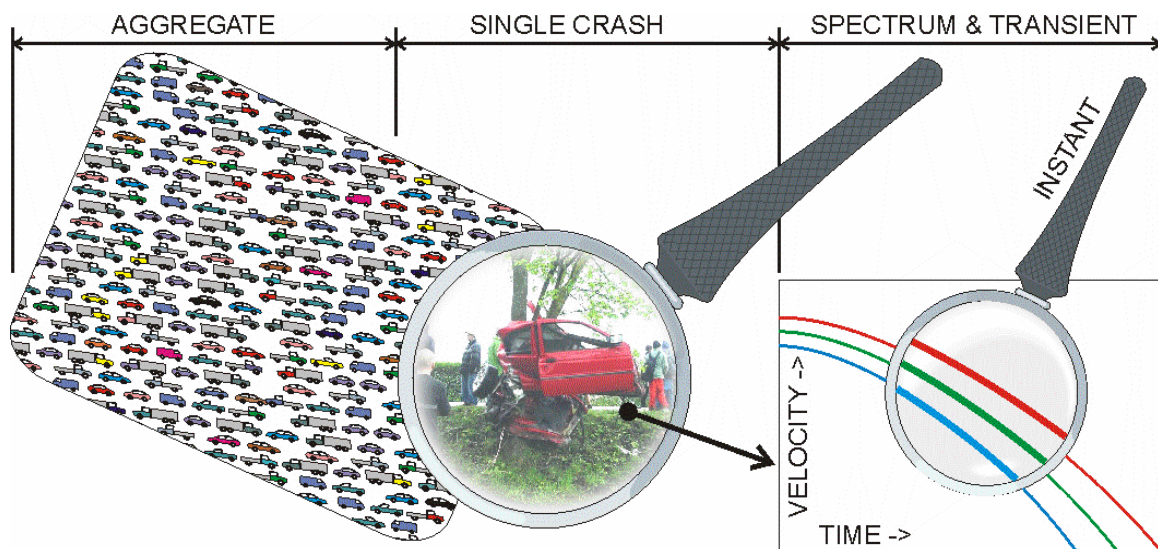


Figure 3-2: Macro-micro visualization of stiffness concepts.

Because of the dissipative nature of the crumple zone, the above stiffness concepts are adaptations of stiffness analogous to linear elastic behaviour. The concepts as outlined above and detailed below are a contribution of this study.

3.2.1 Single Crash Stiffness

Stiffness reflecting the events of a single crash can be described by the NHTSA linear stiffness parameter. The units of this parameter are identical to structural stiffness expressed in N/m. The mass used in determining the parameter is vehicle mass.

Stiffness can also be expressed as a resistance to motion. The term applied here to resistance to motion is reluctance being momentum change per metre of dynamic crush. The derivation of reluctance is treated separately under its own heading. It is a contribution of this work.

3.2.2 Spectrum Stiffness

Crashes occur under a wide variety of conditions. Notable among the variations are initial velocity and vehicle mass. The concept of spectrum stiffness accounts for the plethora of variations by a single crash response algorithm. Spectrum stiffness then, relates to the vehicle stiffness under varying conditions of velocity and mass. Spectrum stiffness considers resistance to motion of the occupant cell mass rather than complete vehicle mass. Accordingly, it is more appropriately termed reluctance in accordance with the previous definition. The stiffness term is retained here for consistency.

Relative spectrum stiffness is how the occupant cell motion compares with motion of an equivalent linear spring.

3.2.3 Aggregate Stiffness

A national fleet is comprised of many different makes and models. Crash incidents occur in a wide variety of combinations and speeds. This and other factors add considerable complexity to the assessment of success or failure of measures to improve the crumple zones. Nevertheless, such feedback is indispensable to improving fleet crashworthiness. A concept of aggregate stiffness across a given year across vehicles tested in the year is presented in this study to highlight trends in mass and stiffness increase.

The NHTSA linear stiffness parameter is used as the metric for this study.

3.2.4 Instant Stiffness

During progression of a single crash, the rate of velocity decay varies as does the rate of crush. Instantaneous stiffness is a comparison of the two rates. Relative instantaneous stiffness is a comparison of instantaneous stiffness with instantaneous stiffness of a linear spring.

3.3 Physical Influences on Structural Stiffness

An inexhaustive, annotated list of effects that may influence the structural stiffness of a crumple zone appears below:

- Metal thickness of chassis outstands. As the mass of vehicles increases, there is need to strengthen the chassis. Against a physical limit of overall cross-section in the tight constraints of engine bay packaging, thickness increase of chassis member wall is a resort. Extra thickness in chassis walls require a greater buckling force under conditions of longitudinal impact and so increase structural stiffness.
- Additional stiffeners. The more members in a parallel load path, the greater the structural stiffness. An example of a member in a parallel load path is given in Figure 3-7 showing a reinforcement strut.
- Failure initiators or localizers. These help in the management of the crash load. A gross columnar failure absorbs energy only at the buckling knees. Failure initiators avoid gross buckling and thereby promote local wrinkling. Local wrinkling, in aggregate, absorbs more energy and gives rise to the desired flat stroking response shown in Figure 3-1. In the example in Figure 3-4, the initiation creases ostensibly help minimize occupant cell intrusion by the chassis member. Another example of localised buckling is given in Figure 3-8.
- Cross supports or diagonal bracing shorten the column length and avoid gross column buckling. A long buckling column offers very little resistance to the crash force once the column eccentricity has reached significance. Cross supports are by this mechanism a measure to stiffen the crumple zone.
- Mechanical impedance. Impedance is a material property that can help localize plastic action. The higher the impedance, the more localization of plastic strain. Mismatching material impedance can have the effect of initiation of plastic action at the mismatch juncture. This results in softening the crash pulse.
- High strength materials. A tear in a structural member in the crash load path offers little resistance to the crash force and largely renders the component unfit for crumple duty. High strength materials can have a comparatively lower fracture strength. A tear in a strut is thus a softening measure. High yield strength materials also raise the crash stiffness by increasing the plastic working level at the higher yield point of the material.

- High strain rate materials. Some materials exhibit an elevation of yield and ultimate strength under conditions of high strain rates. As length of structural member is a significant determinant in strain rate, this effect is thought to manifest in the shorter components of the crumple zone. Even so, great claims are made for this material property by the steel industry as being an agent for greater energy absorption. (Simunovic, Shaw et al. (2000). Since strain rate effect is a strengthening event it increases vehicle stiffness as found by Mahadevan, Liang et al. (2000)
- Thin-walled beam members in vehicle structures generally function as main load carrying members, serving functionally as beam or beam-column. The cross sections of thin walled beam members are the major sections to be analysed in the design process of vehicle structures. In the design of structural components for crash resistance, it is desirable to allow for various levels of plastic deformation. Allowing the structure to deform plastically enables it to absorb more of the energy imposed by the impact loading. (Barone, Kamal et al. (1981) To gain an appreciation of some of these members, some photographs are posted below.
- Velocity sensitive arrangement of compression members increases initial force. This was shown by Deshpande and Fleck (2000) in the context of aluminium foam. It is exploited in a practical way by Motozawa, Tsuruta et al. (2003a) to achieve a initial high force crush profile. The general idea is embodied in Figure 3-3 where Type 2 rises to a fulgurant force peak in response to velocity. The motivation for holding velocity constant is to highlight differences between the type of structure.

This image is not available online. Please consult the hardcopy thesis available from the QUT Library.

Figure 3-3: Velocity sensitive structure (Deshpande and Fleck (2000)).



Figure 3-4: Photograph of chassis rail near firewall showing impact weakening convolutions.

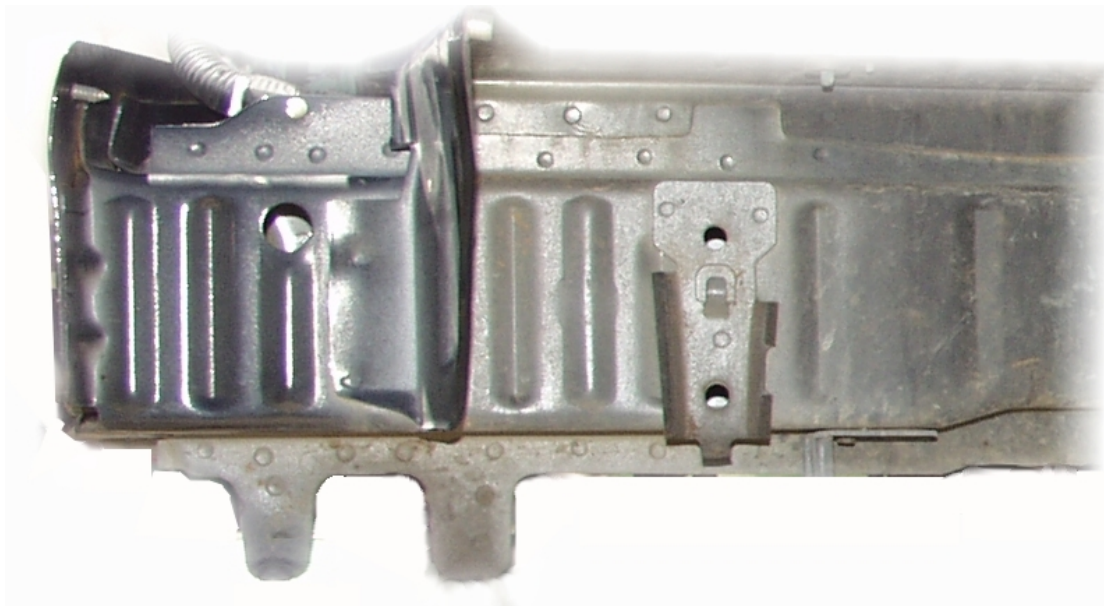


Figure 3-5: Photograph of front of chassis rail with localizing convolutions.



Figure 3-6: Cross-section of chassis rail showing lower strengthening channel.

Figure 3-7 is a photograph of a Holden Ute¹⁵ chassis at the firewall.

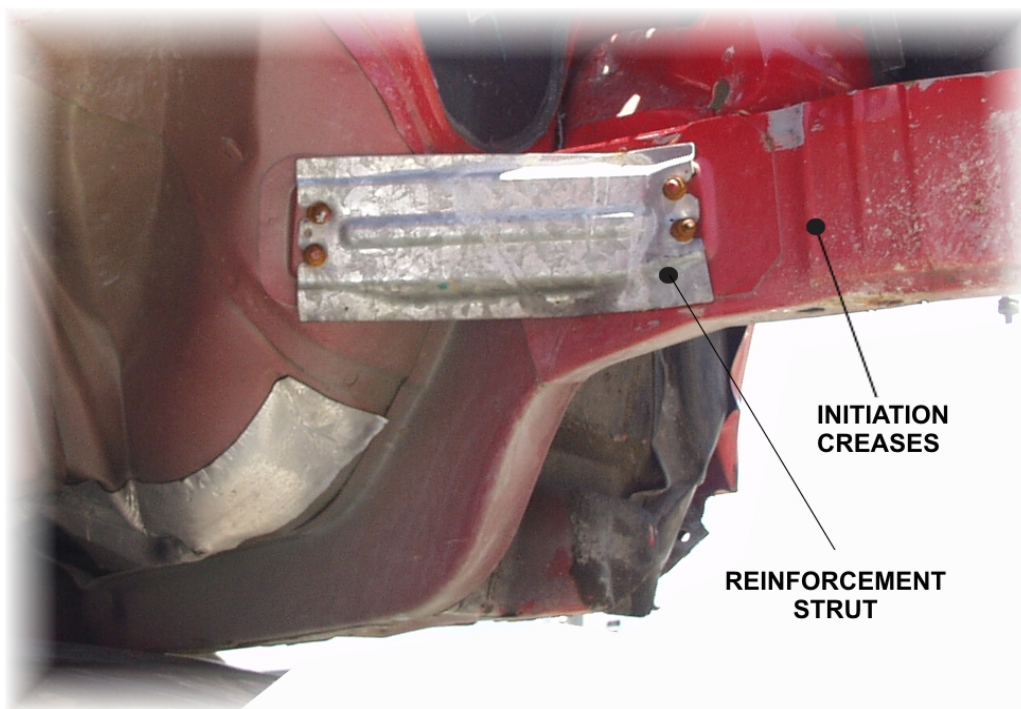


Figure 3-7: Examples of both chassis stiffening and softening by addition of reinforcement strut and initiation creases.

¹⁵ The word *Ute* is an abbreviation of the Australian term *Utility* being a styleside vehicle.

3.4 Mechanisms Influencing Stiffness

Energy is absorbed by many different mechanisms of shear, tension and compression. There is value in characterizing some mechanisms that occur during a frontal crash into their main categories:

1. Stretching
2. Column wrinkling
3. Plastic hinges
4. Crushing

3.4.1 Stretching

In the different mode shapes of the structure some members of the crumple zone can impact many times. The result of differential motion of the crumple zone members can result in tensile loads within the structure. These tensile loads manifest as stretching either elastically or plastic.

Tensile strain absorbs significant energy only if volume of material affords resilience. A non-resilient member tears quickly. A torn member absorbs no further energy.

3.4.2 Column Wrinkling

Column wrinkling of the main structural members being the horns can occur in response to built-in failure initiators as shown in Figure 3-6. Wrinkling can also occur in response to material impedance or stress locking. Stress locking is reserved for future study while material impedance receives some treatment later in this thesis.

Figure 3-8 is a plan view example of local wrinkling of a chassis member in response to frontal crash forces. Wrinkling initiators alter the crumple zone profile by denying the structural member the initial fulgurant force peak. This is visualized in Figure 3-9 redrawn from AISI (2002). The resultant early peak in the crumple zone profile has implications in injury as published by Brell, Veidt et al. (2001b) resulting from the current research.



Figure 3-8: Example of local wrinkling in response to a localizing initiator.

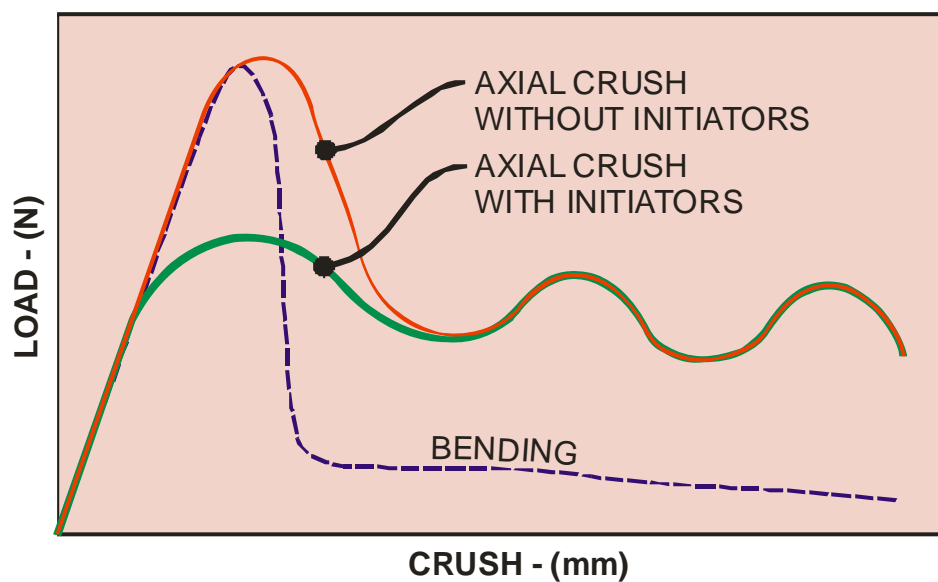


Figure 3-9: Effect of crush initiators on early force.

3.4.3 Plastic Hinges

A plastic hinge for these purposes refers to a local part of a beam that is partially or fully yielded at a cross-section. Any member exhibiting bending action qualifies, for example, an eccentrically loaded column.

No distinction is made for these purposes between a partial or fully formed plastic hinge since a partial hinge is likely to form fully with the progression of the crush.

When a column fails by knee action, the plastic hinge so produced is associated with other plastic hinge action. If there is sideways shift, there are at least two knees. If there is no sideways shift there is a minimum of three knees affected by column failure by the plastic hinge mode.

An example of knee action formed in two places in a chassis rail is shown before the crash in the upper picture of Figure 3-10 and after the crash at the arrow in the lower picture.

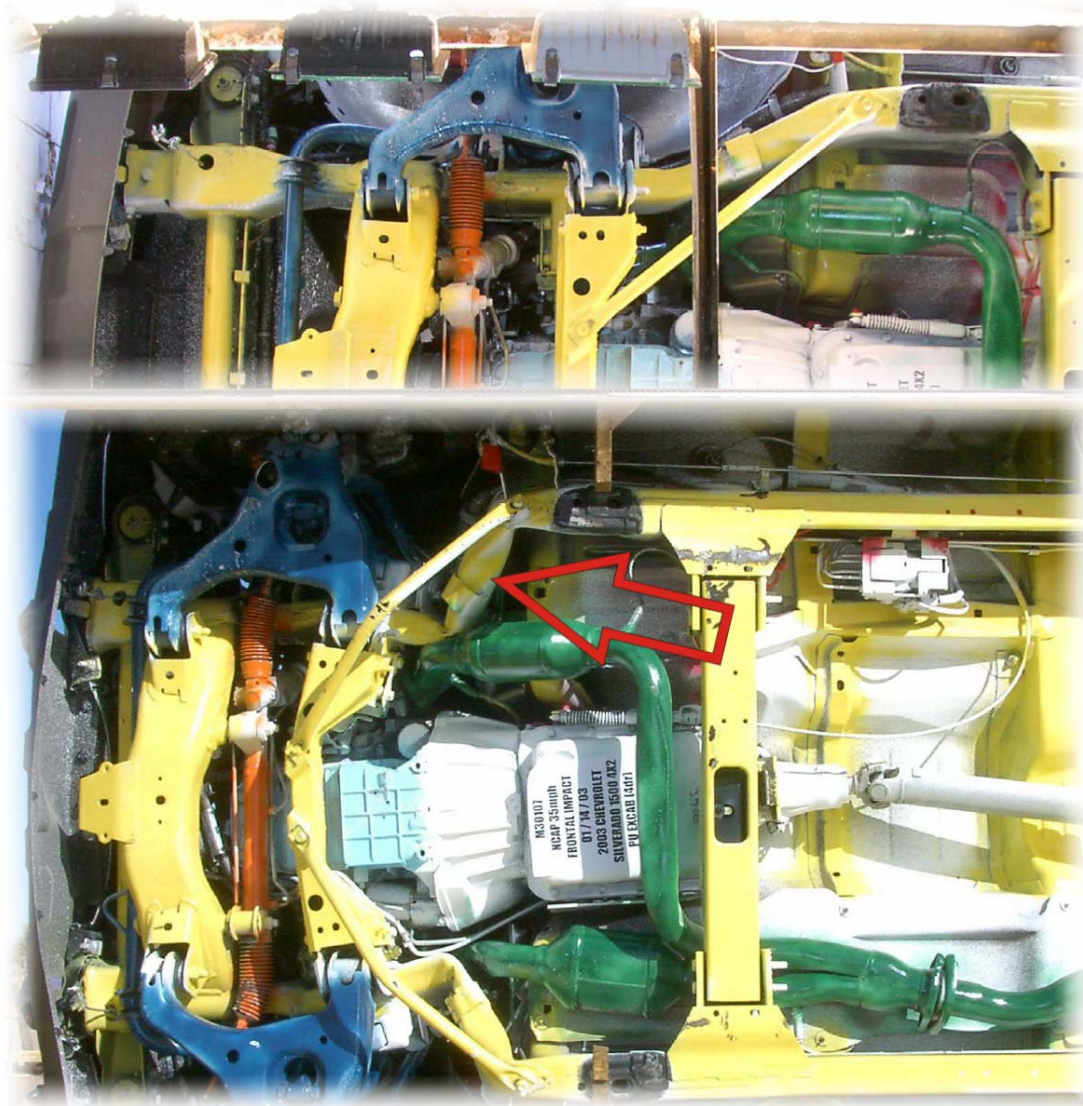


Figure 3-10: Underside photographs of chassis rail of 2003 Chevrolet Siverado before and after full frontal rigid barrier NCAP Test No 4472 at 56.3 km/h.

3.4.4 Crushing

Crushing occurs when a member is interspersed between two stiffer members. It is distinguished from wrinkling by its unpredictability. When column knee action has run its full gambit, the members are then subjected to crushing if the kinetic energy ahead of the members has not been converted.

3.5 State Of The Art

The structural elements of a crumple zone undergo large inelastic strains. A crumple zone can be regarded as the sacrificial front end of the vehicle to protect the occupant cell from damaging forces. In relative terms, the occupant cell is expected to be stiffer. In the dynamic view of a crash event there may be inertial localization which dissipates the crash kinetic energy prior to influence on occupant cell velocity.

During the progression of a crash it would be wrong to assume that heavy members such as engine and cross member come to rest at the barrier while other areas crumple. High speed film discloses a ‘bouncing’ away from the barrier of the engine and to a lesser visible extent other heavy parts. The crumple zone structure adapts to the particular vibrational mode shape current for the instant of viewing. This is also evident when velocity traces for, say, engine and occupant cell are compared. A general explanation of a crash event is offered by

“In general, the deceleration-time history is a superposition of a spectrum of frequencies representing the instrumentation noises, elastic-plastic vibrations, structural collapse, and engine/accessories interactions as they impact one another.”

There are many studies that optimize crumple zone components on the basis of specific energy absorption. E.g. Santosa (1999), Singace (1999), Witteman and R.F.C.Kriens (1999b), Makmood and Fileta (2004). This maximises energy absorption for reduced mass of structural member. This follows a world-wide quest for reduced vehicle mass pursuing the benefits of fuel-efficient transportation without sacrifice to safety. (Vaughn and Martin (2000)

There are factors in the quality of a crumple zone that lie outside of the scope of this thesis. Examples are cost reduction of accident repairs, reduction of panel damage, etc. A big heavy bull bar (frontal protection device) may improve a crumple zone by reducing panel

damage but possibly at a cost to other objectives such as reduction in aggressivity, injury reduction, etc.

Wood (1992) writes the ideal energy absorber for frontal collisions is “one which crumples in a predictable manner without significant variation during crushing.”

For this thesis, there is only one criterion by which to assess the quality of a crumple zone, ie. How it reduces injury for the participants to a crash. There are many intermediate steps that are important analysis objectives. For example, a popular objective in the literature is increasing the amount of energy absorbed. To retain overall direction, it is essential that each intermediate step remains on a means-end hierarchy. If then, increasing energy absorption is not a means to achieve injury reduction, there is risk of the result being irrelevant. It will be shown later in this chapter that undue focus on energy absorption can distort the goal of injury reduction.

Energy absorption as an injury mitigation element achieves relevance only if body part proximity is large enough to make rebound a factor. No study could be found that distinguishes between capacitive energy and mechanical work done during the impact phase preceding rebound. Such a distinction remains for future study. The existence and quantum of energy absorption is certainly important in terms of reducing rebound velocity, a subject to be considered more fully later in this thesis.

Kinetic energy is dissipated in a crash by noise, heat and most importantly, by mechanical work done. The latter is achieved by friction and mostly, by plastic deformation. The proportion of energy available as plastic work done compared to elastic work done is quite large in steel.

An early occupant –car model was used to predict occupant dynamic and kinematic response to changes in the load carrying capacity of structural elements. (Thompson (1968)). His ‘occupant’ consisted of three masses, head, torso and leg. The crash pulse was idealized to a truncated triangular pulse. The injury level was gauged as maximum deceleration. No attempt was made to observe any variation in body part deceleration on account of differing proximity within the occupant cell, although recommendations for secondary collisions were offered as refinements.

Moore (1970) used a spring kinematic model to determine an optimum waveform to minimize head injury.

In optimizing crash pulses, Sparke and Tomas (1994) uses hypothetical examples of stiff soft and optimized pulses at three vehicle impact speeds, 30, 45 and 55 km/h. The choice of speeds reflect a significant coverage of the crash frequency distribution sourced from Roberts and Compton (1993) in Figure 3-11:

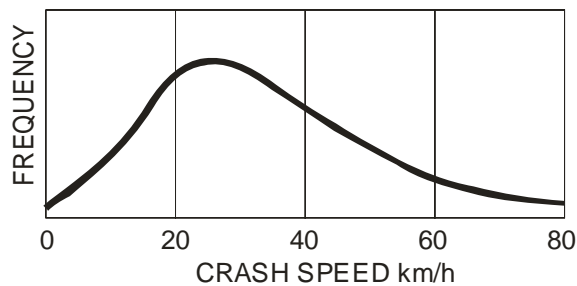


Figure 3-11: Crash speed and frequency distribution.

The crash pulses are redrawn for 55km/h only for reasons of clarity in presentation in Figure 3-12. The optimized pulse is shown as a gentle rise, peaking towards the end of the crash sequence. It will be shown that this profile does not produce optimum injury results.

This image is not available online. Please consult the hardcopy thesis available from the QUT Library.

Figure 3-12: Comparison of hypothetical pulses (Sparke and Tomas (1994)).

The choice of full frontal optimization was made by Sparke and Tomas (1994) to concord with the reported frequency of 60% representing all serious and fatal injuries resulting from frontal crashes.

To measure injury risk, a computer model determined thoracic viscous criterion which showed an improvement in the optimized pulse for the three speeds considered. The Sparke and Tomas (1994) study is important for this thesis as it represents an early optimization attempt to modify a crash pulse to improve injury risk.

In contrast, Yang, Tho et al. (1999) used maximum energy absorption as their objective function.

The optimized shape in Figure 3-12 should be contradistinguished with Motozawa and Kamei (2000a) who propose an optimized shape that exhibits an early high acceleration followed by a plateau. Their optimization goal was reduction of acceleration during a time when body part contact occurs most frequently. This is shown as stage 3 in the graph smoothed and redrawn from Motozawa and Kamei (2000a). The Y-axis is rescaled to acceleration from the original force scale, by the operation of Newtons 2nd law.

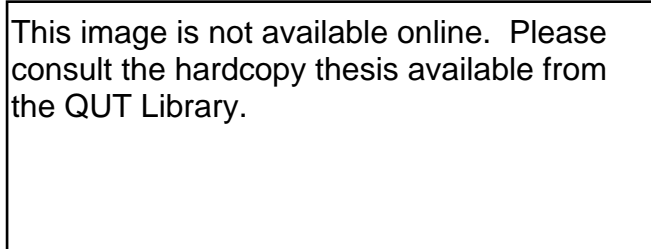


Figure 3-13: Motozawa and Kamei (2000a) ideal crash pulse.

To achieve the profile Motozawa, Tsuruta et al. (2003b) explored a progressive collapse mechanism confirming the value of the profile in Figure 3-13. The general idea to have a low-acceleration time phase is embodied in the mechanism of Figure 3-14.

Frei, Kaeser et al. (1999) also recognized the value of an early peak force followed by a lower plateau in the design of their elbow-shaped chassis outstands.

This image is not available online. Please consult the hardcopy thesis from the QUT Library.

Figure 3-14: Progressive collapse mechanism from Motozawa, Tsuruta et al. (2003a) timed sequentially from A to C.

The Sparke and Tomas (1994) study proposes a gentle initial impulse while the Motozawa and Kamei (2000a) proposes an initial aggressive impulse. These opposing positions were examined by Brell, Veidt et al. (2001b) who showed in a closed form analysis that an initially aggressive impulse has a beneficial effect on injury reduction.

An initially aggressive pulse in practice is feasible since an elbowed column offers less resistance than immediately after impact. Conversely, an initially soft pulse is enabled by failure initiators as shown in Figure 3-4, Figure 3-5 and Figure 3-8.

Inertial stress acting in concert with strain rate localization is proposed as a plausible explanation for an initially aggressive pulse prior to major columnar collapse.

A pyrotechnic device that triggers midway through the crash pulse deferring deceleration for later to emulate the curve in Figure 3-13 is proposed by Brell, Thambiratnam et al. (2002c)

3.6 Optimum Pulse Shape

The purpose of this section is to show that quality of crumple zone with respect to injury risk exists. Implications are that more energy absorption is not necessarily better. In the example that follows energy is held constant while injury risk is monitored for mirrored, same magnitude impulse.

The theoretical ideal crash pulse has been known since 1970. Moore (1970) writes: "The optimum waveform has a characteristic high-G, initial peak value followed by a lower, constant level deceleration." This is also shown analytically by Brell, Veidt et al. (2001b) that a high deceleration at the right time can improve injury risk. The existence of an optimum pulse was shown analytically by a one-dimensionally lumped mass gap model by Motozawa, Tsuruta et al. (2003a) Motozawa, Tsuruta et al. (2003b)

The benefits in terms of reduced injury resulting from high early stiffness are to be presented here. An example follows with two impulses identical in magnitude and ending at the same reference time. One impulse exhibits an early peak while the other impulse exhibits a later peak. The reduction in velocity as a result of either impulse is the same at the reference point in time according to impulse-momentum arguments.

It will be shown here that it is important in terms of injury results whether the force is applied early or late in the sequence. Actual impulses are not shown in the example; however, typical early and non-early peaks are sourced from recent NCAP tests and graphed to Figure 3-15 to show that the presence or absence of early peaks is a common phenomenon.

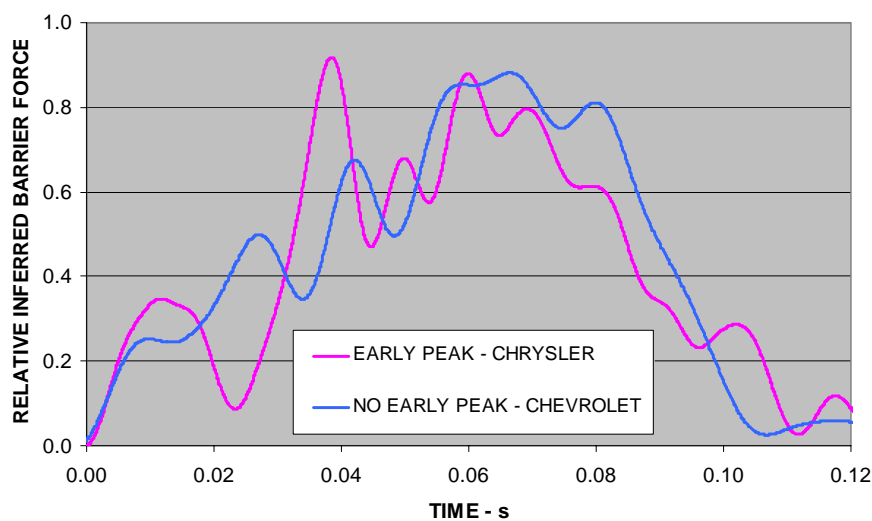


Figure 3-15: Relative barrier force inferred from occupant cell acceleration from NCAP Test #4936 Chrysler Town & Country 2005 Model & NCAP Test #4985 Chevrolet Equinox 2005 Model

The example was carefully arranged to ensure that the curves between the red and blue dots are mirrored about a common centre line giving an early trough in velocity and a late trough after the curves intersect midway between the dots in Figure 3-16. This ensured that the overall area under the two curves remained identical.

Figure 3-16 then shows that the early peak impulse causes a corresponding early trough in velocity and a more gentle reduction of velocity for the late impulse peak. Similarly, the late peak impulse a late velocity trough and a more gentle reduction in velocity for the early peak impulse in the final comparison sequence.

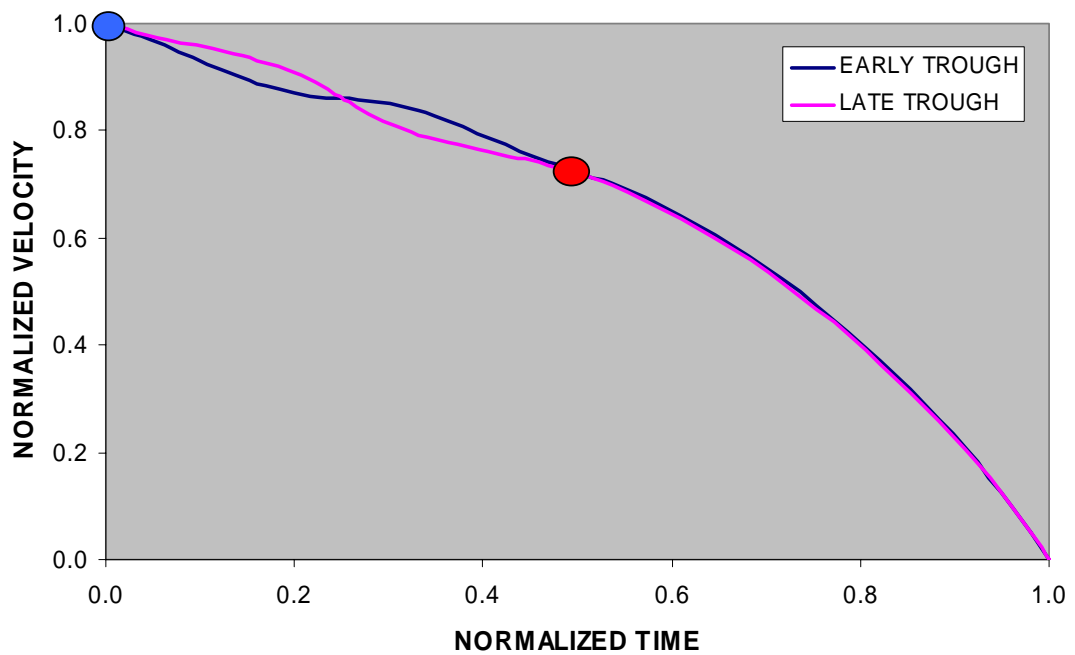


Figure 3-16: Normalized velocity-time curves having identical areas under curves but mirrored between blue and red dots.

Using procedure previously explained the area above the curves is determined by integration and the corresponding contact velocity determined for the time step. The idea of equal proximity but unequal time is graphed for a normalized proximity of 0.03 corresponding to the equal areas depicted in Figure 3-17.

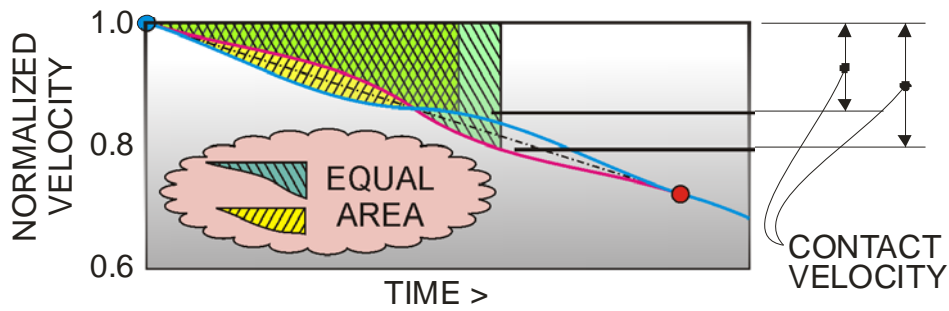


Figure 3-17: Concept of equal proximity – unequal time for early and late trough normalized velocity profiles.

Normalized contact velocity is determined by subtracting normalized velocity from 1.0 at each time step. The results are graphed in Figure 3-18.

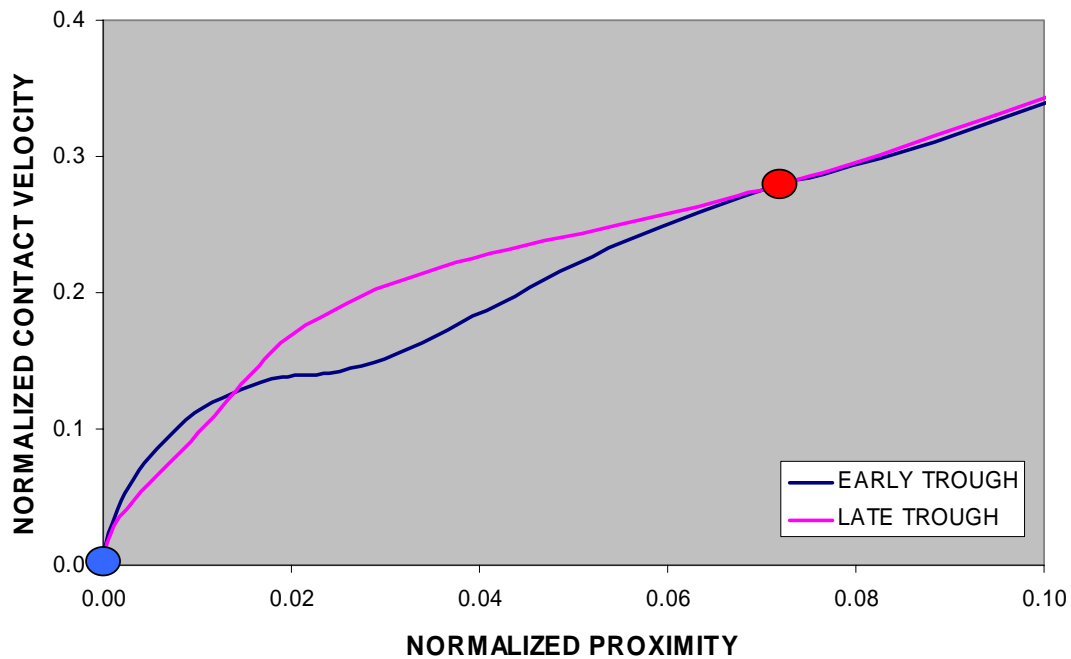


Figure 3-18: Normalized contact velocity-proximity curves derived from the example in Figure 3-16.

The positions of the dots in Figure 3-18 correspond with Figure 3-16. The red dot marks the point where contact velocity returns to being equal for the remainder of the sequence and corresponds with the red dot reference time in Figure 3-16.

Although the exemplar impulses were the same the injury result was significantly different as can be seen in Figure 3-18

The result of the example here is consistent with the mathematical argument presented as part of this research in Brell, Veidt et al. (2001b) for two identical area triangular impulses which were mirrored in time.

It was shown that different injury risk results can manifest from identical applied impulse. It follows that kinetic energy absorption can produce different injury results depending on where and when the energy is absorbed in the crash sequence.

3.7 CONCLUSION

An overview has been presented of the influencing factors that affect crumple zone response. Stiffness of crumple zone has been offered from a number of vantage points including time, space and demography. The resulting insight is a contribution by the author. A further contribution is made by showing that the phasing of energy absorption in the crash sequence is important in injury reduction. This has implications for instantaneous stiffness, a contribution of this study to be presented later.

Contrary to the optimized crash pulse being proposed in the literature as a gentle rising pulse with time, an early stiffness was shown to be beneficial in reducing injury. (Ref Figure 3-17) This contribution has implications for failure initiator in the main load bearing members ahead of the firewall.

These localizing initiators, while preventing gross columnar collapse and reduce firewall intrusion, have the capacity to deny the crumple zone of its initial force peak to decelerate the occupant cell early in the sequence when typically no body part has made contact.

Accordingly, a trade-off between the benefits and alternatives is recommended in the continued use of the localizing initiators.

A contribution of this chapter is found in better understanding of the physical influences and the mechanisms active in a crumple zone during a crash. This understanding underpins the practical aspects of a crumple zone to lead into the theoretical and analogous representations of the crumple zone in subsequent chapters.

BLANK

4. REPRESENTING VEHICLE RESPONSE

4.1 Introduction

The purpose of this chapter is to introduce a number of stiffness metrics, among which are the linear stiffness parameter, reluctance, instantaneous stiffness and impedance. Reluctance is used throughout this thesis in the mathematical representation of occupant cell motion. Instantaneous stiffness and impedance are a precursor to rebound formation models presented later in the thesis. Their early introduction here is motivated by perceived value of grouping vehicle response.

A suitable facility to represent crash data will permit exploration of conditions not provided by the crash data set such as injury risk at varying body part proximities.

A single crash test data set is typically comprised of two columns of numbers, one being an accelerometer reading and the other elapsed time from the crash start. With the incremental time at say, a tenth of a millisecond, more than 1000 data co-ordinates are common for a typical working range in a set. (The data typically precedes the crash start and is captured well beyond the working range). Integration and other data manipulation that may be needed to extend crash data to other analysis are feasible in modern software.

In considering the need to represent a crash in any other form than the original data elements, the value of an analogous representation is questioned. Some notes appear below addressing this question:

1. Whilst handling the volume of data is feasible in modern computers, it is neither convenient nor efficient.
2. An analogous framework based on the laws of physics permits cause to be explored and validated.
3. There is comparative value in arriving at a single value to represent the crash data set.
4. Extrapolation and interpolation of conditions outside of test conditions is enabled by the use of representative equations.
5. Even phenomenologically derived equations without causal foundations can have predictive qualities. For example, Lim (1972) using polynomials to represent crash data could effectively interpolate between upper and lower crash conditions.

The literature offers a number of ways to represent vehicle response to a crash among which idealized pulses can be found. Chou (2004) lists a number of hypothetical pulses in common use:

- Half-sine, haversine, cosine
- Triangular
- Equivalent square wave

Being pulses, it could be argued their positions are closer to the physics of the crash event. However, taking some lead from Lim (1972) on his phenomenologically derived polynomials; the crash event can be explained by any equation that gives fidelity results. Such an equation can represent transient acceleration as a pulse or simply represent either transient velocity or transient position direct. Thus the lack of fidelity at the acceleration/pulse level is then not so important if fidelity is achieved at the velocity level when velocity is under scrutiny. This principle gives rise to a pseudo-stiffness selected “as if it were so” to give a certain result either as transient velocity or in later chapters, as injury. Although the various stiffness based metrics used in this thesis are of the pseudo-stiffness type, the prefix is curtailed for convenience.

There are many variations of stiffness ranging from structural stiffness to an arbitrarily assigned metric of rigidity (see P3-52 for definition) in the literature. In addition, there are the stiffness metrics foreshadowed in the previous chapter. All find value in their specific applications. However, it becomes essential that if test data is to be extended in analogy or other representative form that it be explained fully complete with limits of validity if it purports to represent cause.

In the assessment of the fidelity of such a system, test data is used. If there is great variability in the test data the quality of the system of prediction suffers. Notwithstanding, test data is the only calibration system available and so it is essential to understand how accurate the tests represent reality. This avoids unfruitful fine-tuning of the prediction system. Variability in testing can be assessed by evaluating repeatability:

Machey and Gauthier (1984) addressed the repeatability issue in a study of fourteen identical make and model test vehicles which were manufactured consecutively on the same production line in the same assembly plant in an attempt to achieve maximum possible uniformity. They concluded amongst other things that variability occurs from differences in methodologies across testing plants. HIC can vary 10%. Peak dynamic crush varied between 699 mm to 813 mm.

4.2 NHTSA Linear Stiffness Parameter

In a response to NHTSA report entitled: “Updated Review of Potential Test Procedures for FMVSS No 208”, DaimlerChrysler referred to NHTSA’s definition of vehicle stiffness as “simplistic” and that it does not address locally high accelerations. The Agency (NHTSA) agreed that the measure is simplistic but argued that it provided an insightful measure. Owings (2000)

Whether the Agency intended for the stiffness parameter to be extended to a mass-spring analogy is unclear from the literature. Nevertheless, such an extension is logical and perhaps even obvious.

The NHTSA stiffness metric k can be derived from the law of conservation of energy. At zero velocity, just prior to rebound, all kinetic energy has been transformed to both mechanical work done and strain energy. In the mass-spring analogy, it is assumed that all kinetic energy is converted to strain energy, so that:

$$KINETIC ENERGY = STRAIN ENERGY$$

$$\frac{1}{2}M \cdot V^2 = \frac{1}{2} \cdot k \cdot X^2$$

Where k is spring stiffness of the mass-spring analogy, V is maximum velocity; X is the maximum displacement. Transposing reveals the well-published NHTSA Linear Stiffness Parameter equation:

$$k = M \cdot \frac{V^2}{X^2} \quad [4-1]$$

The metric is the so-called linear stiffness parameter where V is initial velocity; X is the maximum dynamic crush and M the whole vehicle mass. A text on vibration will provide transient equations for acceleration, velocity and position as follows:

$$A(t) = -V \cdot \sin(\omega \cdot t) \cdot \omega$$

$$V(t) = V \cdot \cos(\omega \cdot t)$$

$$X(t) = X \cdot \sin(\omega \cdot t)$$

$$\text{Where } \omega = \sqrt{\frac{k}{M}}$$

[4-2]

The equations in [4-2] are plotted with test data for Toyota Landcruiser ANCAP Test #B8057 to reveal the typical lack of fidelity in the acceleration.

Maximum velocity and maximum dynamic crush for Test #B8057 are given by:

$$V = 15.67 \frac{m}{s} \quad X = 0.719m$$

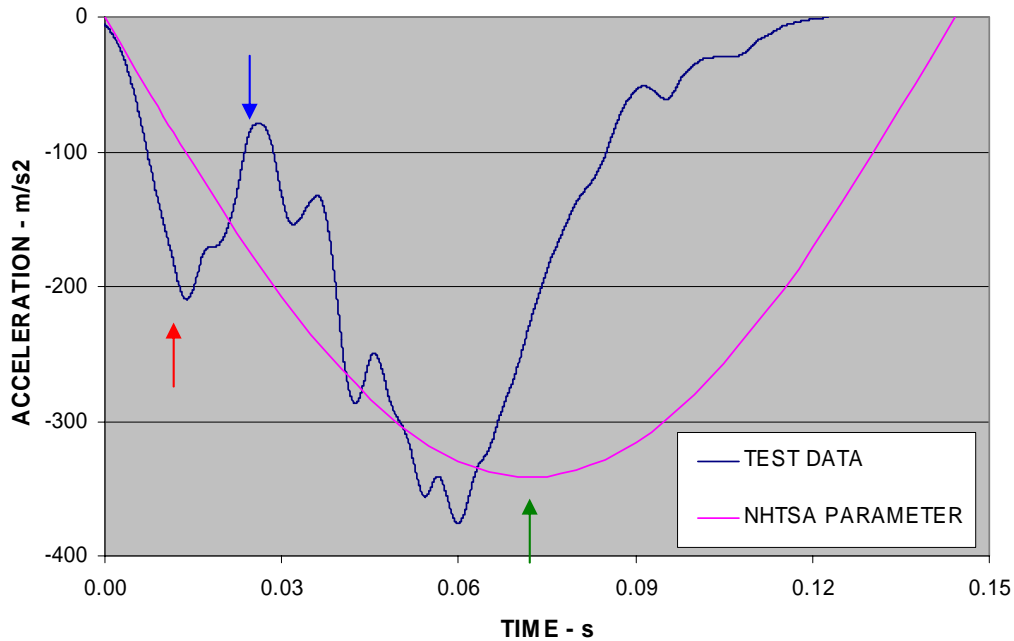


Figure 4-1: Comparison of acceleration test data from Toyota Landcruiser ANCAP Test #B8057 with equation derived from NHTSA linear stiffness parameter.

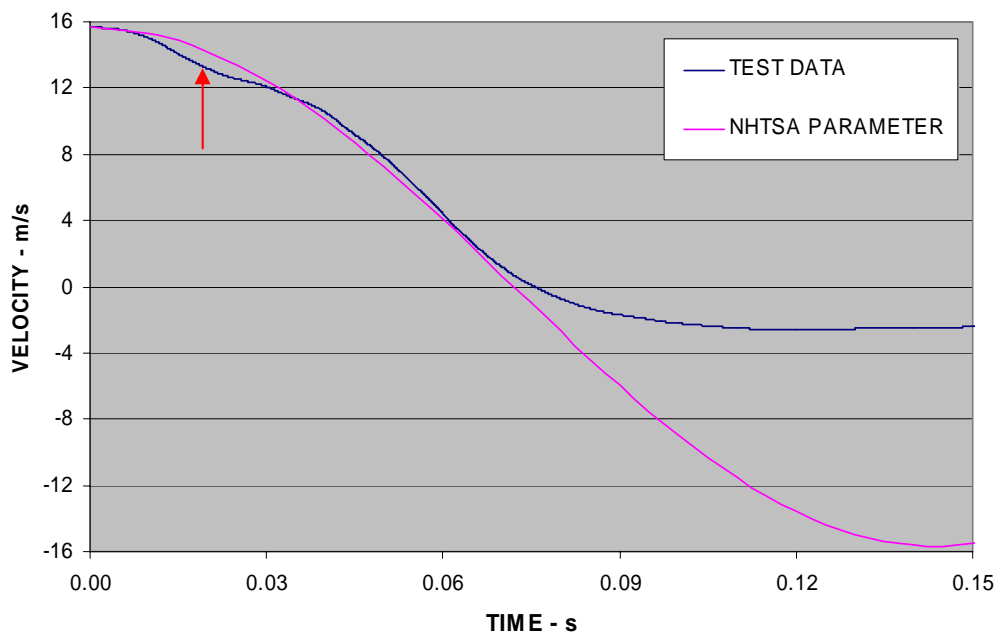


Figure 4-2: Comparison of velocity test data from Toyota Landcruiser ANCAP Test #B8057 with equation derived from NHTSA linear stiffness parameter.

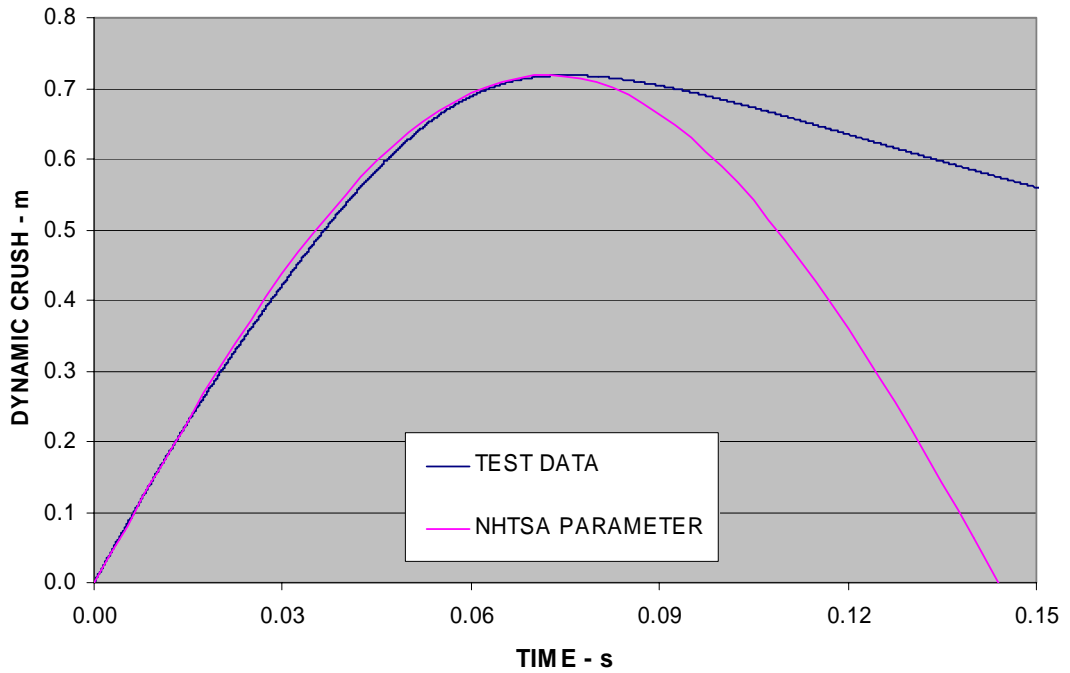


Figure 4-3: Comparison of positional test data from Toyota Landcruiser ANCAP Test #B8057 with equation derived from NHTSA linear stiffness parameter.

Figure 4-1 exhibits an initial acceleration peak at 0.015s at red arrow. This peak is responsible for the velocity trough at the red arrow in Figure 4-2. Neither the peak in Figure 4-1 nor the trough in Figure 4-2 has a corresponding expression in position Figure 4-3. This is caused by the inherent smoothing action of the integration procedure.

It is noteworthy that:

1. The initial peak and trough (red and blue arrows in Figure 4-1) are not reflected in the corresponding sine curve.
2. The peak of the sine curve (green arrow) occurs later than the peak of the test data.

Item 1 above would be reflected in the injury result as shown typically in the previous chapter. It therefore potentially poses a limitation on the use of the analogy for close body part proximities.

The mere lack of coincidence of the peaks observed as Item 2 above is by itself unimportant in a contact velocity – proximity study.

4.3 Using Reluctance as a Stiffness Metric

Clearer communication would follow if the crumple zone stiffness were described with its own specific terminology. Common stiffness descriptors, engineering stiffness (k) and circular frequency (ω) lead to unwarranted expectations in extrapolations. Circular frequency suffers from the additional handicap lacking immediately recognizable relevance. Reluctance on the other hand refers semantically to an unwillingness or resistance ostensibly to motion. It is accordingly more appropriate when applied to motion of the occupant cell.

Later there is need to distance associations with simple harmonic motion theory as the concept is extended to optimize injury fidelity rather than motion or structural stiffness. Reluctance so becomes a mere instrument of convenience offering improved communications.

The general usage of reluctance in industry is uncommon and confined to electrical and electronic engineering even though its full title is mechanical reluctance even in these disciplines. Adapting terms from other disciplines, however, is not uncommon and there is not always an exact equivalence. For example, the electrical ohm is derived by dividing voltage by current while the mechanical ohm is derived by dividing force by velocity. Kinsler and Frei (1962).

In testing the position of the reluctance terminology and its use in other disciplines, application is found in electrotechnology and mechatronics where it is considered a force that resists motion. It is generally an undesirable force that increases with speed of motion. A motor vehicle crash increases barrier force with increased initial impact velocity, so establishing a qualitative correspondence, at the least.

Mechanical reluctance as used in electrotechnology shows it as a force opposing motion caused by self-inductance of a coil. This is visualized in an application of a linear motor, as follows:

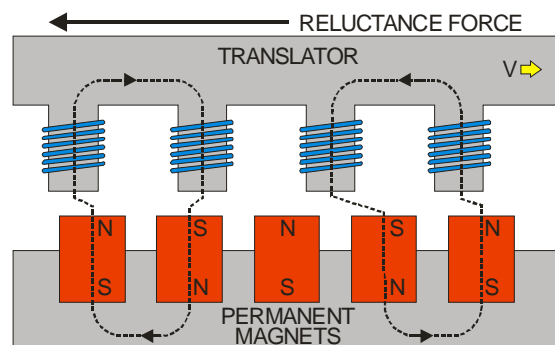


Figure 4-4: Sketch of linear motor redrawn from Otten, Vries et al. (1997)

The reluctance force on the translator is approximately sinusoidal with respect to position. (Amerongen (1998). This position changes linearly, the translator moving at constant velocity.

It will be shown here that the difference between mechanical reluctance as found in an electro-mechanical apparatus and the inertial force on a spring in a mass-spring oscillating system is merely the result of the method of application of motion. In the electro-mechanical model the application of motion is linear resulting in a sinusoidal force output. In the oscillating mass-spring system the position is sinusoidal, while the force is linear, as follows:

Considering Newton's 2nd law:

$$F = m*a \quad [4-3]$$

When Equation [4-3] is applied to simple harmonic motion, an expression for transient force follows:

$$F_{(t)} = m*a_{(t)}$$

$$F_{(t)} = m*(-V\sin(\omega t)*\omega) \quad [4-4]$$

$$F_{(t)} = -(m*V)\sin(\omega t)*\omega$$

Part 3 of Equation [4-4] permits convenient normalization on momentum ($m*V$) as graphed in Figure 4-5 for different circular frequencies. The selection of magnitude is arbitrary however, they happen to correspond with typical values used in later analyses.

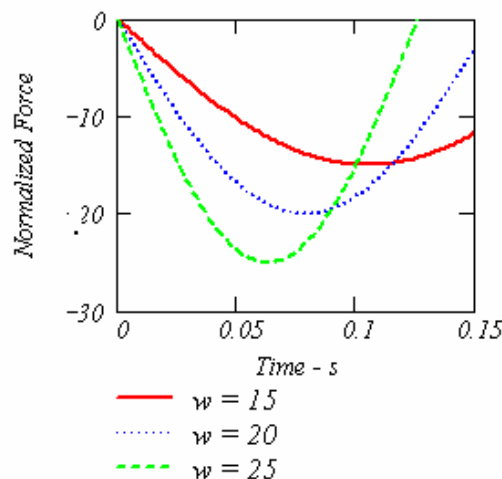


Figure 4-5: Normalized force for varying circular frequencies¹⁶.

¹⁶ ω is used for ω where graphing software lacks Greek typefacing facility.

Similarly, transient position is given by:

$$x(t) = X \sin(\omega t) \quad [4-5]$$

Equation [4-5] is graphed for normalized maximum displacement – X in Figure 4-6.

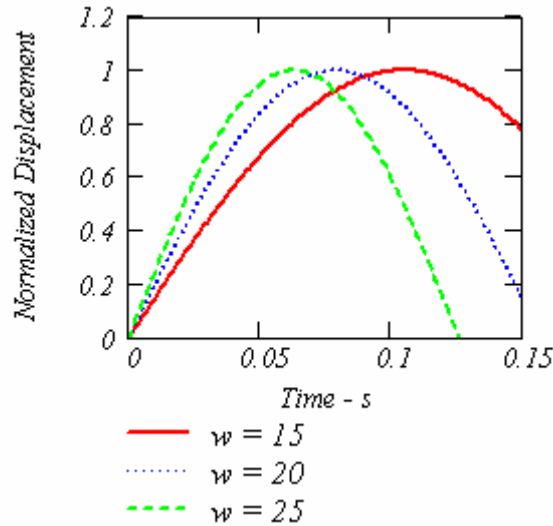


Figure 4-6: Normalized displacement for varying circular frequencies.

The momentum normalized inertial force is graphed against position parametrically in Figure 4-7 revealing the linearity of force in a sinusoidal system. It is the expected result given both force and displacement are sinusoidal. The minus sign is ignored to permit render in the first Cartesian quadrant.

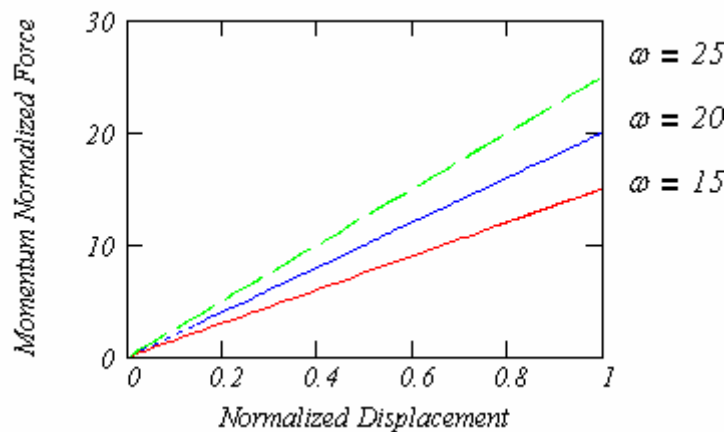


Figure 4-7: Parametric plot of normalized transient force vs. normalized transient displacement

The slope of line is given by the circular frequency ω . The table below summarizes the units of stiffness metrics:

Table 8: Comparison of reluctance units with NHTSA stiffness parameter units.

METRIC	EQUATION & UNITS
NHTSA PARAMETER	$M \cdot \frac{V^2}{X^2} = \blacksquare \frac{N}{m}$
IMPULSE RELUCTANCE	$\frac{M \cdot V}{X} = \blacksquare \frac{N \cdot s}{m}$
SPECIFIC RELUCTANCE	$\frac{V}{X} = \blacksquare \frac{N \cdot s}{kg \cdot m}$

Throughout this work specific reluctance is used, as follows:

$$Reluctance = \frac{V}{X} = \omega \quad [4-6]$$

4.4 Mass-Spring Analogy

Throughout this thesis, reference to and comparisons with, linear elastic springs is made. It is appropriate therefore to engage in a discussion on simple harmonic motion as a preamble to the velocity displacement interaction curve of the next section.

The NHTSA linear stiffness parameter is analogous to spring stiffness. It was extended previously to simple harmonic motion. However, some fundamental points apply to simple harmonic motion that may not apply to the example in Figure 4-1 thru to Figure 4-3

Mass cannot influence linear stiffness. Figure 4-8 illustrates this point by showing a spring without a mass of identical stiffness as the deflected spring under influence of the mass. (Removal of the marble restores the spring)

1. Initial velocity is independent of stiffness (in both cases).
2. Transient or initial velocity cannot influence stiffness



Figure 4-8: Mass on coil compression spring, showing one spring loaded and another identical spring unloaded to illustrate stiffness independence of mass.

There are circumstances when a linear spring behaves in a non-linear way, as follows:

1. When a spring bottoms out, acting like a solid, it has a secondary, very stiff, spring rate.
2. Surge conditions when coils touch locally as depicted in Figure 4-9.

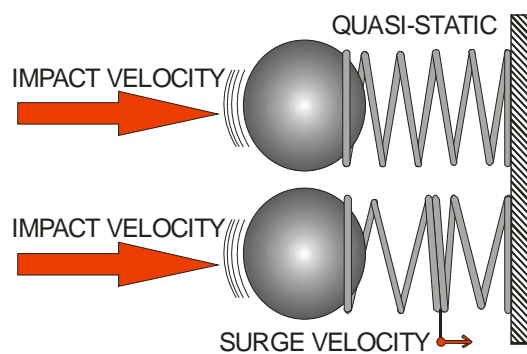


Figure 4-9: Visualization of surge velocity in linear elastic springs.

The application and implications of surge velocity to a crumple zone response is used here to point to subsequent work in this thesis on strain disturbance propagation.

The essential point for this work is that reluctance and the linear stiffness parameter are not spring stiffness but an abstract representation of the crumple zone for the impact velocity and mass in question. Any inference beyond these initial parameters in a causal framework is extending the analogy beyond its validity. This is especially the case when considering mass influence or velocity influence on stiffness, studied later in this thesis.

4.5 Fidelity of Linear Spring Analogy with Test Data

In this section it is reported how well the linear spring analogy represents transient velocity data for a number of vehicles.

The procedure involves determination of reluctances based on limits of test data for initial velocity (V) and maximum occupant cell displacement (X).

These reluctances are then compared with reluctances derived from curve-fitting using DataFit V8.0.32 software.

A number of vehicles were considered and one vehicle is presented in more detail to elaborate on methodology. The vehicle test data is sourced from ANCAP test #8055 for a Ford Falcon in a full frontal rigid barrier test.

Initial velocity is 15.8 m/s while dynamic crush or occupant cell displacement of 0.579 m was determined from test data by double integration of accelerometer readings. The resulting reluctance $\omega = 27.3$ was used to superimpose the appropriate curve on test data values in Figure 4-10.

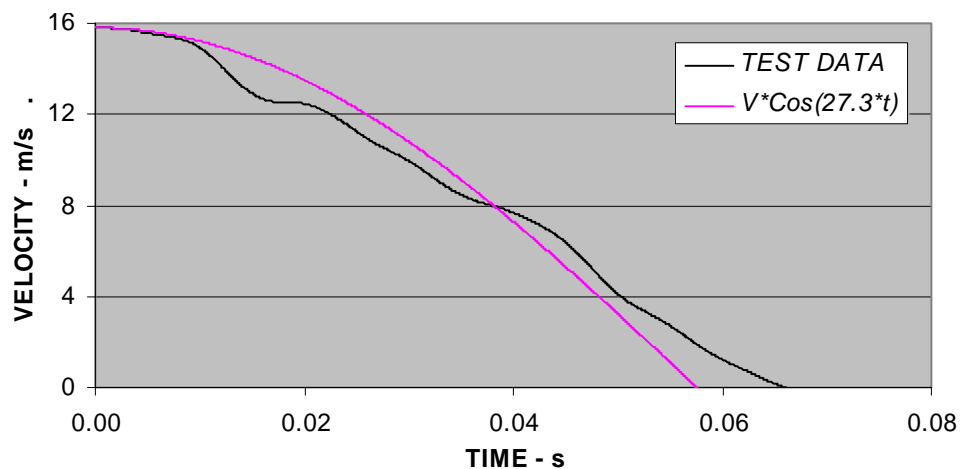


Figure 4-10: Falcon ANCAP test #8055 compared with cosine using reluctance derived from test limit conditions of initial velocity and dynamic crush.

Velocity data at each time step including the time step was submitted to the curve-fitting program to obtain a best-fit reluctance. The program predicted a better fit using a reluctance of $\omega = 25.8$ giving a coefficient of determination of $R^2 = 0.958$, meaning 95.8% of the test data is explained by the transient velocity equation below:

$$V_t = 15.8 \cdot \cos(\omega \cdot t) \quad [4-7]$$

Equation [4-8] is plotted with the original test data in Figure 4-11.

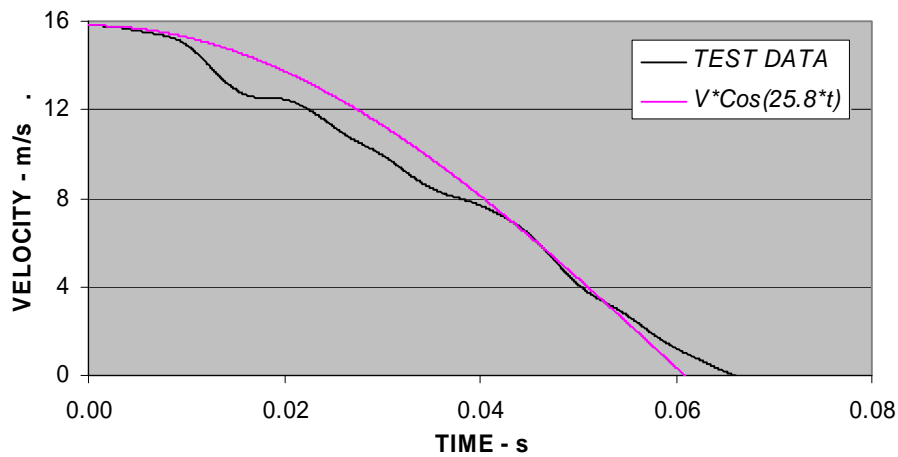


Figure 4-11: Falcon ANCAP test #8055 compared with cosine using reluctance derived from best-fit of data.

Ten more vehicles were similarly processed and the results posted to Table 9.

Table 9: Fidelity of reluctance to best sinusoidal fit of data

TEST No	DETAILS	LIMITS (TEST DATA)		RELUCTANCE ω		%GE IMPROVEMENT
		V	X	V/X	BEST FIT	
8055	1998 Falcon Forte AU	15.81	0.579	27.3	25.8	5.8%
7030	1997 Holden	15.72	0.805	19.5	19.1	2.1%
2543	1996 Holden	13.52	0.750	18.0	18.2	-1.1%
B9001	1998 Nissan 4WD	15.58	0.677	23.0	22.4	2.7%
B8057	1998 Toyota 4WD	15.67	0.753	20.8	20.6	1.0%
B9002	1998 Holden 4WD	15.67	0.589	26.6	25.5	4.3%
B8052	1998 Subaru 4WD	15.75	0.777	20.3	19.4	4.6%
V2836	1998 Honda Accord	13.25	0.597	22.2	21.2	4.7%
4248	2003 BMW 325i	15.48	0.546	28.3	25.9	9.3%
4266	2003 Toyota Corolla	15.53	0.658	23.6	23.3	1.3%
4273	2003 Mini Cooper	15.60	0.492	31.7	29.6	7.1%

In conclusion, there appears scope to improve reluctances used in representing test data.

4.6 Velocity-Displacement Interaction Curve.

This section is a contribution by the author and is reported in Brell and Veidt (2002d). The value of the velocity – displacement curve is found in its facility to monitor values both velocity and displacement simultaneously. It is also a convenience reference curve by which to compare test data. The curve also assists in the presentation of instantaneous stiffness and impedance.

At any point in time in the velocity decay of a mass in a linear spring system there is a corresponding mass position. Transient position and transient velocity can be shown on a single curve. The curve is an interaction curve, named the system curve reflecting the full complement of mass, stiffness, initial velocity and maximum displacement. Any point on the curve can be joined to the origin to make a parameter line the angle of which denotes proportion of elapsed time to total time.

The system curve is useful in comparing real data with an equivalent linear elastic spring. The system curve also forms the basis of the analysis of mass and velocity softening phenomena, to follow.

System curves for a single spring (e.g, as depicted in Figure 4-8) are concentric circles when velocity and displacement are normalized.

An example is shown in Figure 4-12. The velocity being the independent variable is shown as the x-axis because in the context of this thesis the system always commences with initial velocity. The parameter line increases in slope in a logical sense with time.

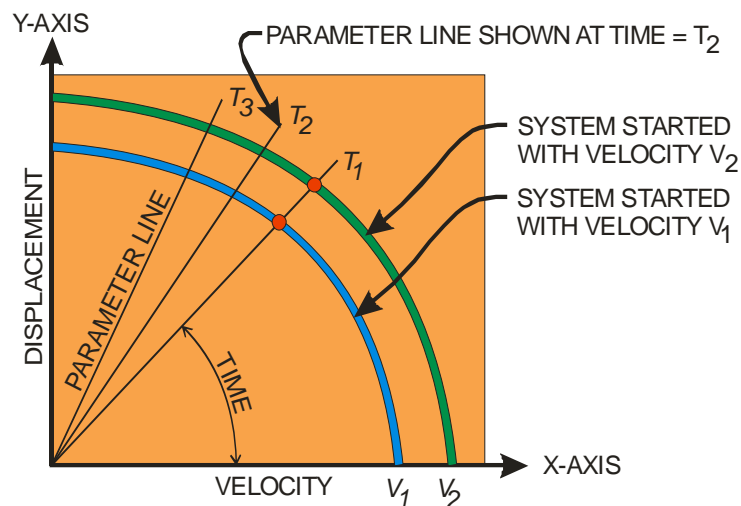


Figure 4-12: System curves drawn for two initial velocities for the same spring.

It is of value to show velocity decay and displacement concurrent with a system curve. To achieve this, Figure 4-12 must be rotated to appear in the 2nd Cartesian quadrant, as shown in Figure 4-13:

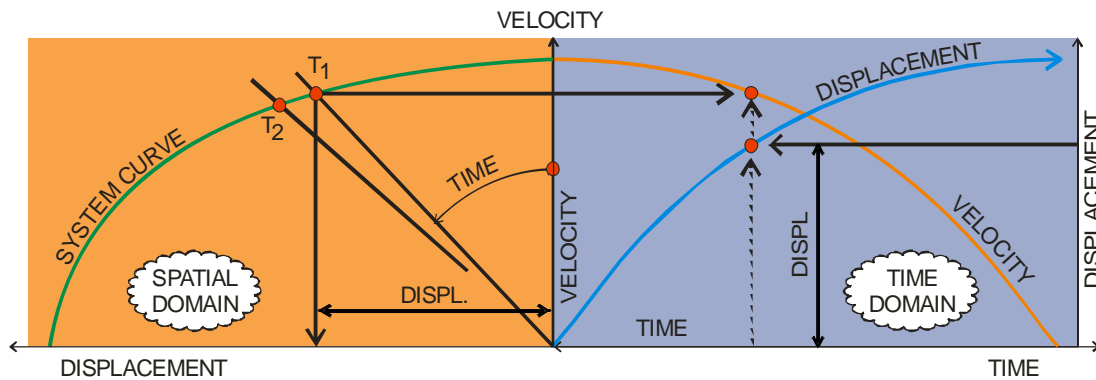
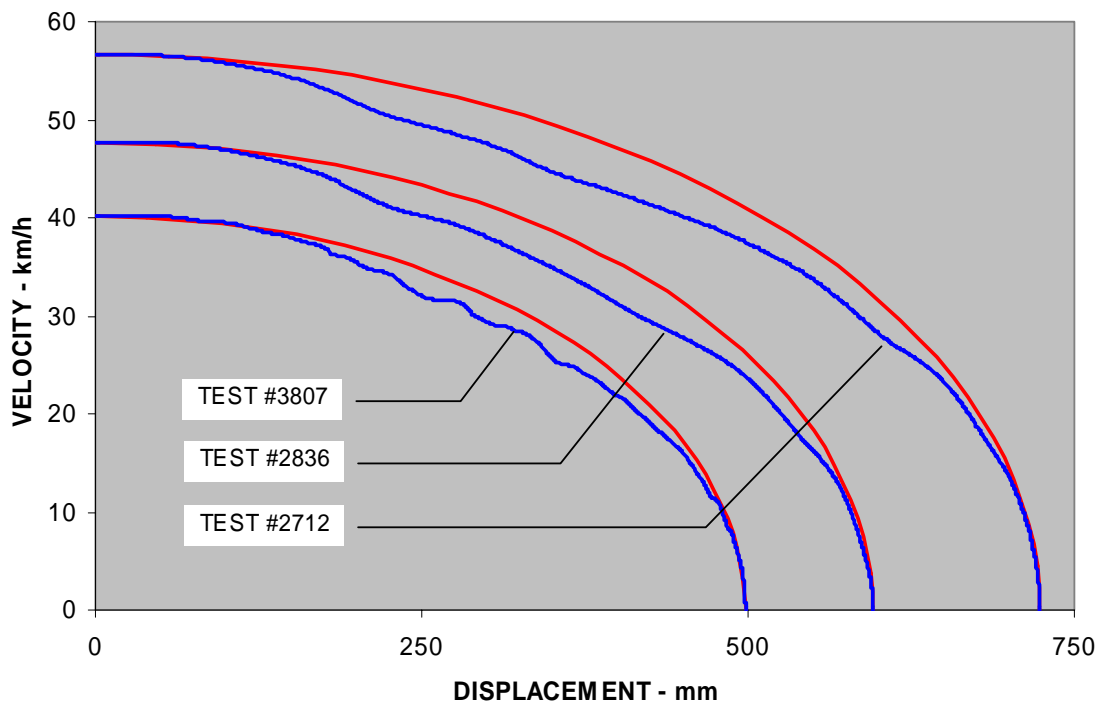


Figure 4-13: Elastic spring depicted in time and space illustrating the parametric nature of the system curve.

Interaction curves, called system curves here are drawn for the initial and final conditions of initial velocity and dynamic crush respectively for three crash tests of identical vehicles. The test data also provided velocity decay and displacement at each time step. These were recorded on the same graph shown in Figure 4-14 enabling the departure of test data from an equivalent linear elastic spring to be visually distinguished.



**Figure 4-14: Honda Accord system curves
(Red curves are equivalent linear elastic system curves)**

4.7 Progression of the Occupant Cell at the Micro Level.

4.7.1 Instantaneous Reluctance

Instantaneous reluctance is determined as for normal reluctance except that velocity (V_i) and displacement (X_i) are taken at an instant point in time, as follows:

$$\omega_i = \frac{V_i}{X_i} \quad [4-8]$$

It is not used here except to contradistinguish from instantaneous stiffness.

4.7.2 Instantaneous Stiffness

As the crash progresses, the rate of response of velocity change to change of displacement, varies. Instantaneous stiffness is a concept devised for this study to study this response and to introduce the specific impedance concept subsequently. Instantaneous stiffness is defined as the rate of velocity reduction compared to the rate of crush at a point in time, tangent with the normal to the centre of curvature of the system curve. Instantaneous stiffness, or instant stiffness, is determined by the slope of the system curve as shown in Figure 4-15 and as calculated below.

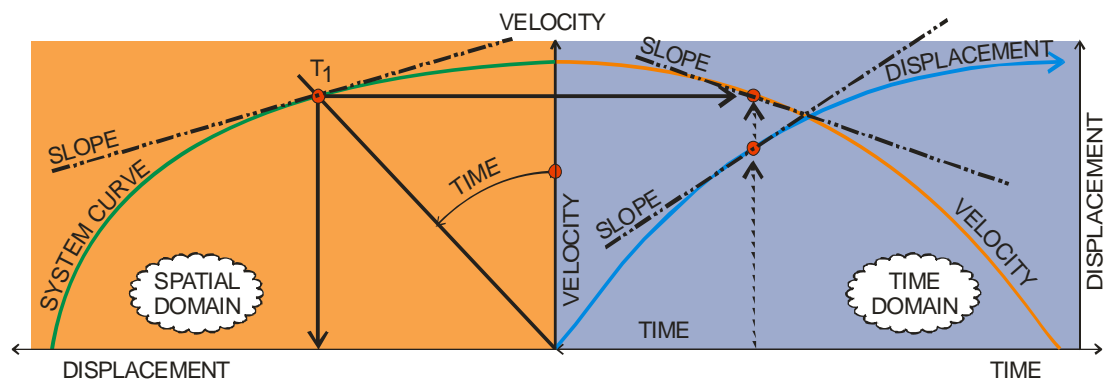


Figure 4-15: Slope in spatial domain reflecting slopes in transient domain.

$$\frac{dV}{dX} = \frac{\frac{dV}{dt}}{\frac{dX}{dt}} \quad [4-9]$$

Equation [4-9] when interpreted with real data and a system curve produces slopes as shown typically in Figure 4-16 but exaggerated for emphasis.

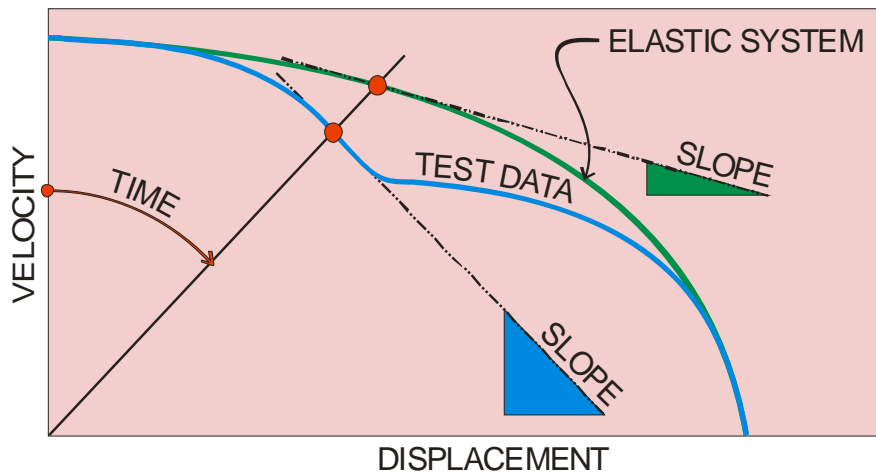


Figure 4-16: Instantaneous stiffness of system curve compared with test data.

Comparison in the transient domain is performed below but first needs adjustment of the reluctance value for cosine comparison of an equivalent linear elastic spring to permit coincidence of the time crossing of velocity curves at the x-axis. This permits convenient normalization for time. The cosine derived from peak velocity and peak occupant cell position can create different intersections with the x-axis. This is shown in Figure 4-17.

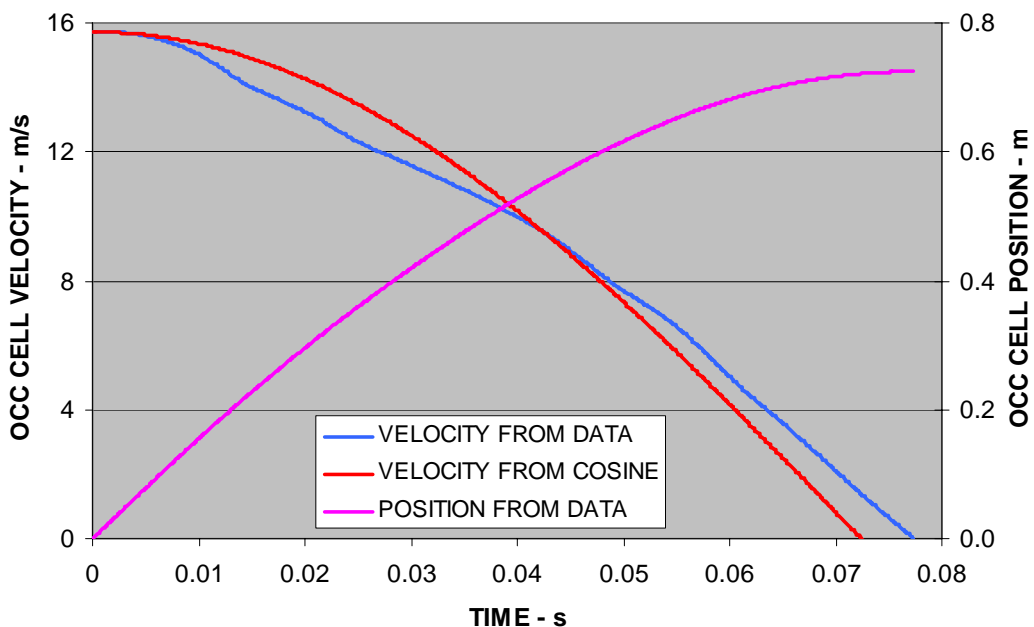


Figure 4-17: Velocity from cosine based on peak conditions.

The lack of coincidence with Figure 4-17 prevents effective time normalization and is shown adjusted in Figure 4-18.

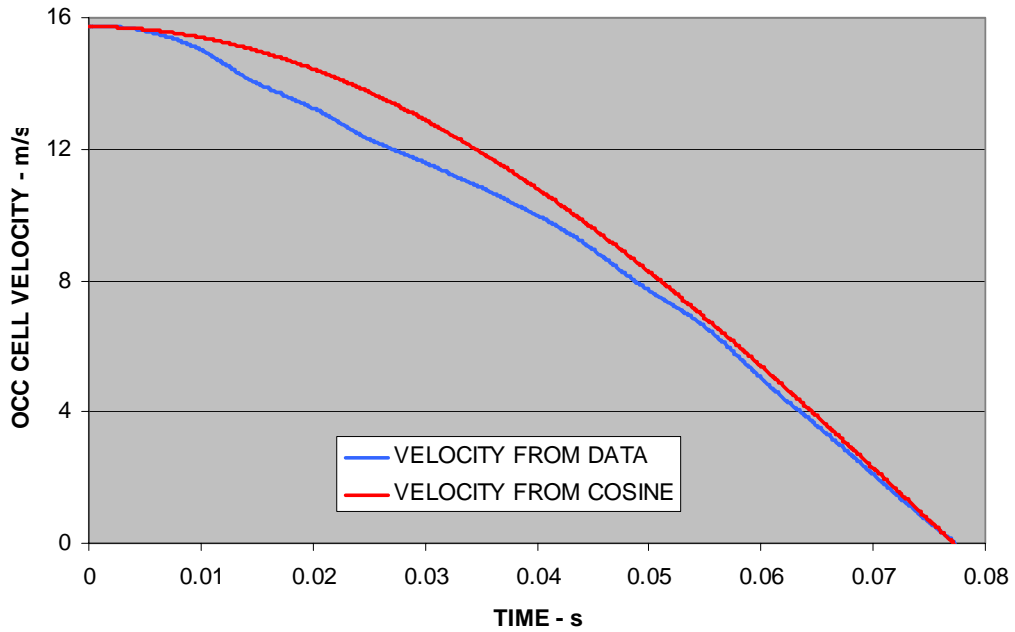


Figure 4-18: Velocity from cosine based on reluctance giving coincident intersection with the x-axis.

The time normalization for two Honda Accord full frontal rigid barrier tests is visualized in Figure 4-19. A third test was considered but omitted to minimize clutter. The results of the reluctance adjustments required for time normalization are posted to Table 10.

Table 10: 1998 Honda Accord full frontal rigid barrier test details

TEST NO	TEST SPEED (km/h)	VEHICLE MASS (kg)	V (m/s)	X (m)	ω (V/X)	ω (ADJ)
#2712	56.6	1595	15.72	0.725	21.7	20.32
#2836	47.7	1541	13.25	0.594	22.3	20.22
#3807	40.2	1556	11.17	0.499	22.4	21.2

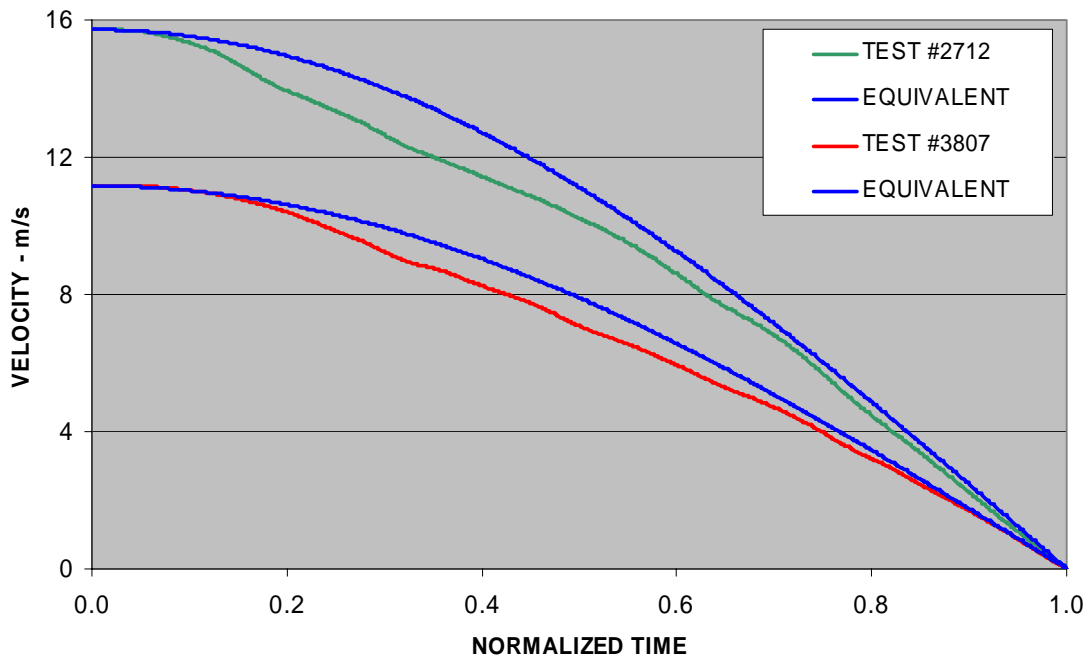


Figure 4-19: Test data for Honda Accord compared with time normalized cosine equivalents.

Equation [4-9] is used to calculate the instantaneous stiffness for the three Hondas described in Table 10 two of which are graphed in Figure 4-20. The adjusted reluctance values are used in the comparison of linear elastic spring equivalents in Figure 4-20.

Both the test data derived graph and its corresponding linear elastic spring equivalent show very high instant stiffness in Figure 4-20 as the occupant cell approaches full time (point of rebound). This may have implications in the formation of rebound. Strain rate materials would exhibit less effect and inertial material effects would be reduced, both on account of the reduced occupant cell velocity in the approach to the rebound point.

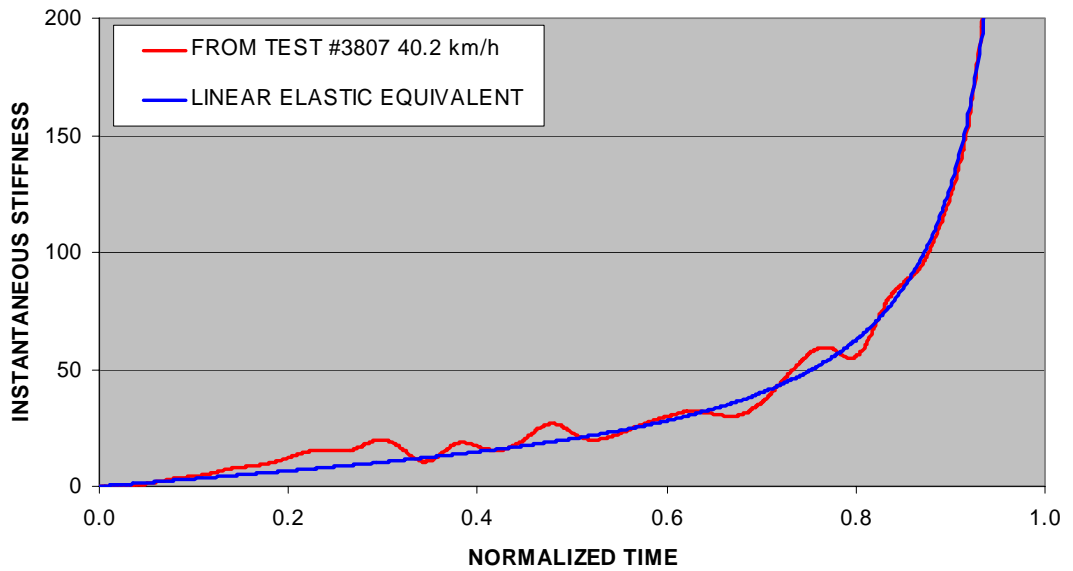
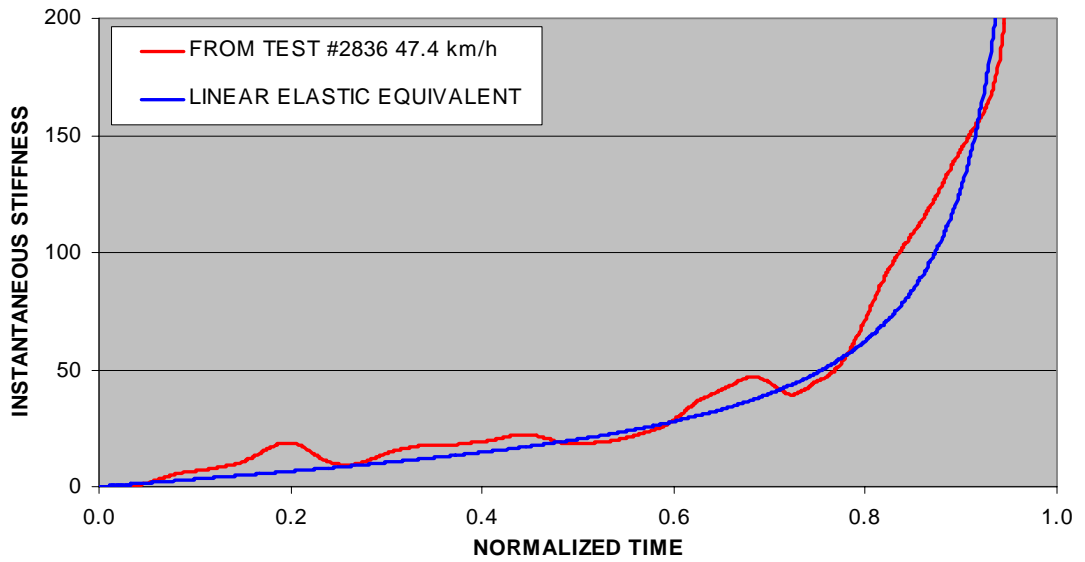
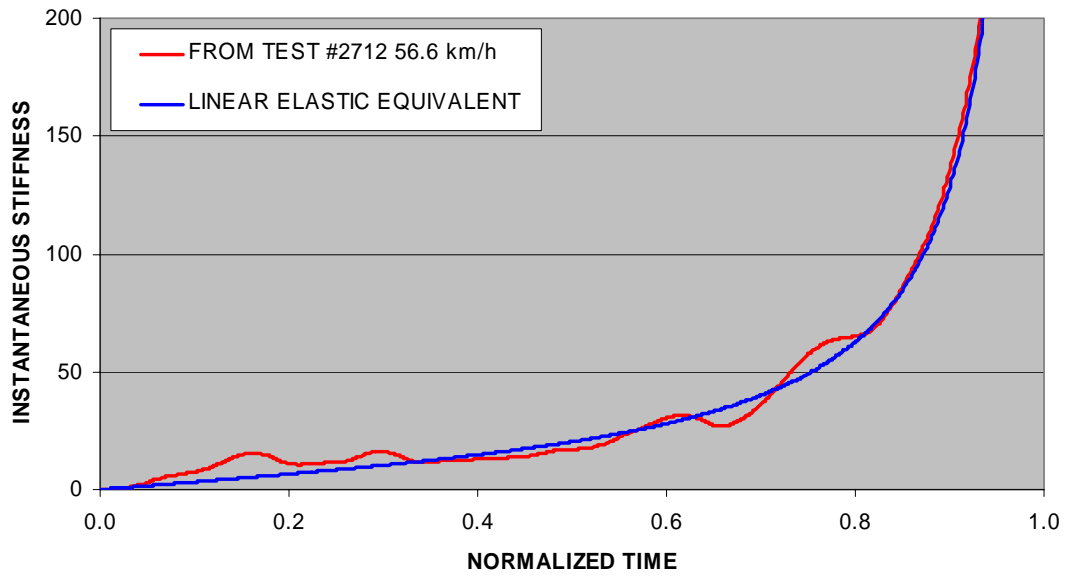


Figure 4-20: Instantaneous stiffness for Honda Accords compared with linear elastic spring equivalents on normalized time.

4.7.3 Specific Impedance

Specific impedance is a concept devised to permit study of the response of a crumple zone on a mm by mm basis. It is a contribution of this study and helps develop a model of rebound formation subsequently in this thesis.

Specific impedance is defined as the ratio of specific inertial force exerted by the occupant cell and its velocity at a point in the spatial progression towards zero velocity. Mechanical impedance can be expressed by the following (from Rothbart (1996) p5.34):

$$Z = \frac{F}{V} \quad [4-10]$$

Where F and V are inertial force and velocity of the occupant cell.

By the operation of Newton's second law, Equation [4-10] can be restated as:

$$Z = \frac{m \cdot \frac{d}{dt} V}{V} \quad [4-11]$$

Because the mass of the occupant cell is not conveniently available impedance is expressed per kilogram, hence the term specific impedance. If velocity is expressed as positional rate of change, specific impedance can be expressed as:

$$Z_s = \frac{\frac{d}{dt} V}{\frac{d}{dt} X} \quad [4-12]$$

Attention is drawn to the similarity of Equation [4-12] with Equation [4-9] leading to the following conclusion:

SPECIFIC IMPEDANCE IS THE SLOPE OF A TANGENT TO THE SYSTEM CURVE.

It should also be noted that specific impedance and instantaneous stiffness is the same entity. An arbitrary distinction between instantaneous stiffness and specific impedance is the former is assigned during normalized time while impedance is assigned at normalized position. The distinction is illustrated graphically below for Honda Test # 2712 using the adjusted reluctance from Table 10:

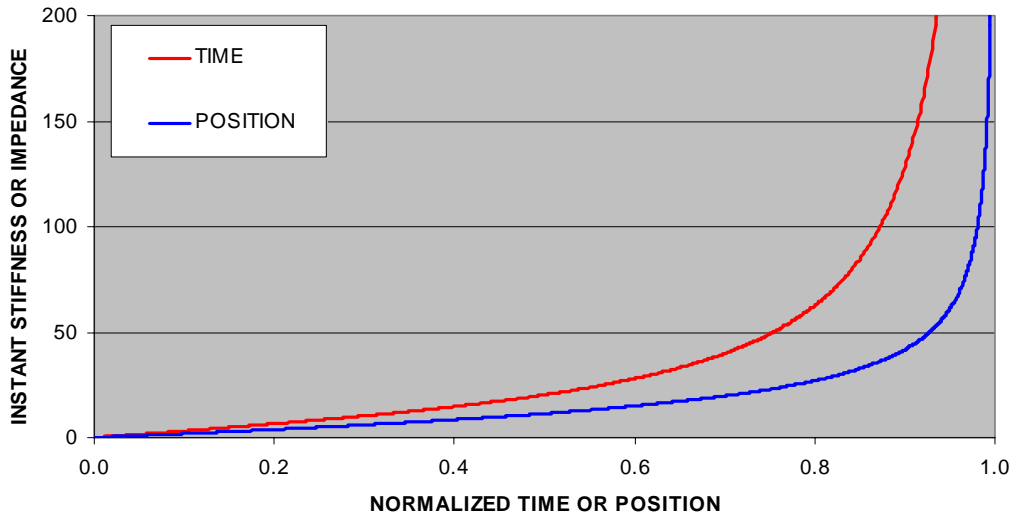


Figure 4-21: Comparison of time-based instant stiffness and position-based impedance.

The calculation of specific impedance for test data can be simplified by simplifying Equation [4-12], as follows:

$$Z_s = \frac{a_t}{v_t} \quad [4-13]$$

Where a_t and v_t are values for acceleration and velocity respectively at a common point in time.

Specific impedance is calculated using Equation [4-13] is used to calculate specific impedance for the three Hondas at each time increment. To comply with the specification set earlier for specific impedance, the plot is made at each normalized point of position. The results are graphed both test data and its linear equivalent in Figure 4-22.

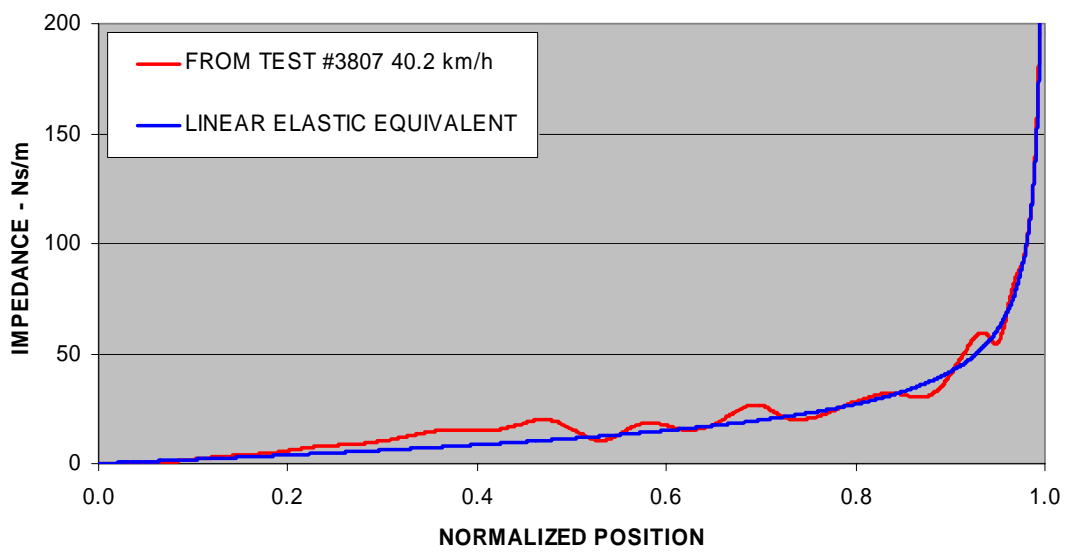
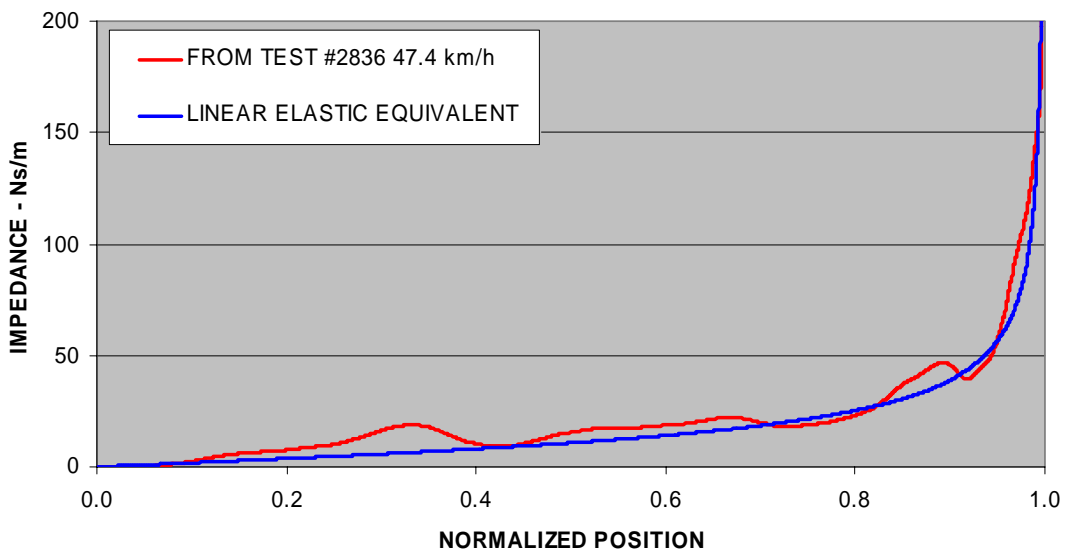
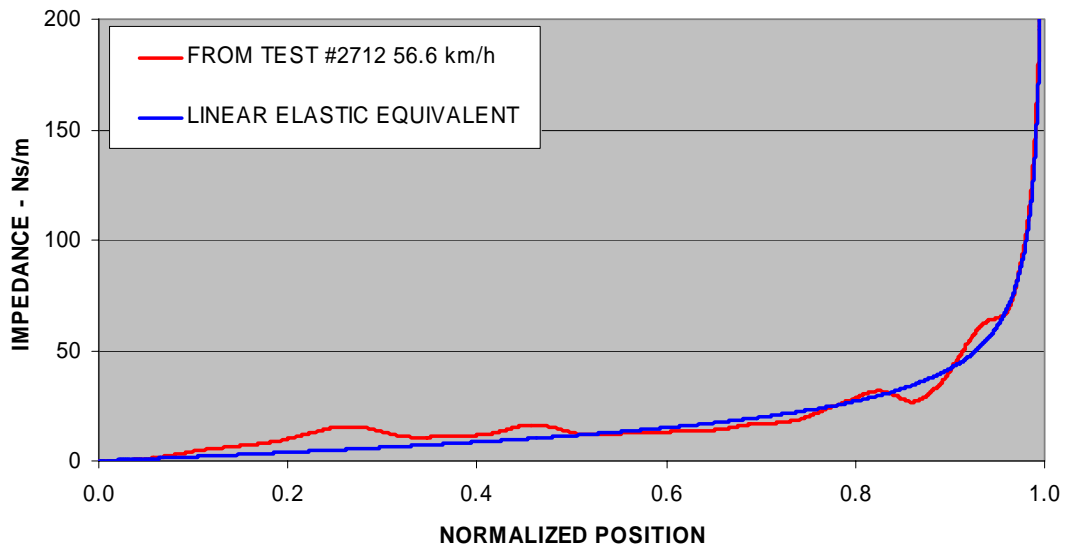


Figure 4-22: Impedance for Honda Accords compared with linear elastic spring equivalents on normalized positions.

Figure 4-22 indicates a rapid increase in force towards the end of stroke. A rebound mitigation device would show greatest effect during (say) the last 20% of crush stroke. The idea for such a device was presented in Brell, Thambiratnam et al. (2002c).

In order to gauge differences that might result from different initial impact velocities, the three linear elastic equivalent curves from Figure 4-22 are drawn on a single graph with the vertical scale increased to accentuate the differences.

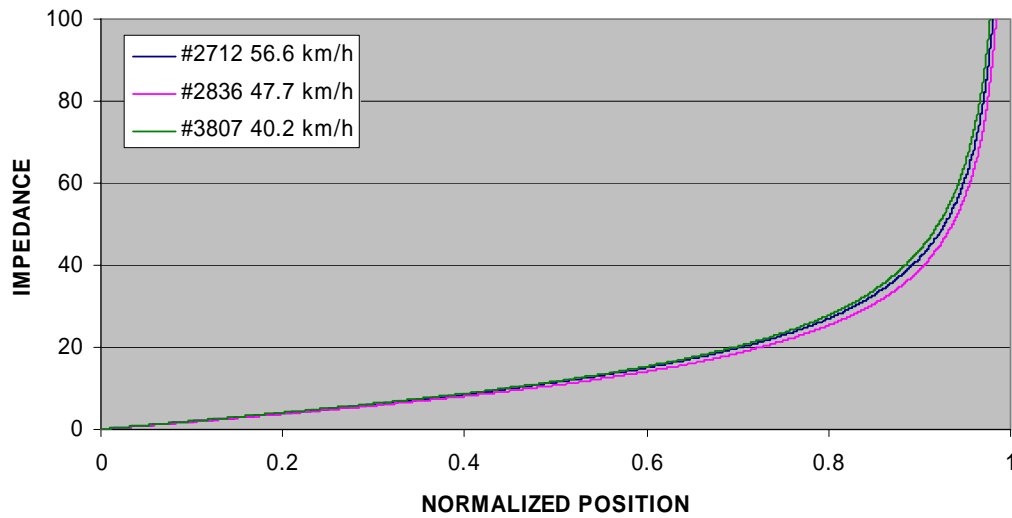


Figure 4-23: Impedance for Honda Accords linear elastic spring equivalents for normalized positions showing apparent absence of speed influence.

The lack of difference in Figure 4-23 for the three different initial impact velocities is of significant interest. However, the need for timely completion of the present project prevents the digression, given that the objective was to merely present the concept. The issue is raised as future research at the conclusion of this thesis.

4.8 Adding Rebound

This section considers using a system of cosine curves to represent test data beyond the ingoing phase.

Vehicle response has so far been represented only to the point of rebound. Rebound is an important part of vehicle response having significant implications in injury for small people and internal flying objects. The cosine function representing test data well for the ingoing phase will not represent rebound well. This is illustrated Figure 4-25.

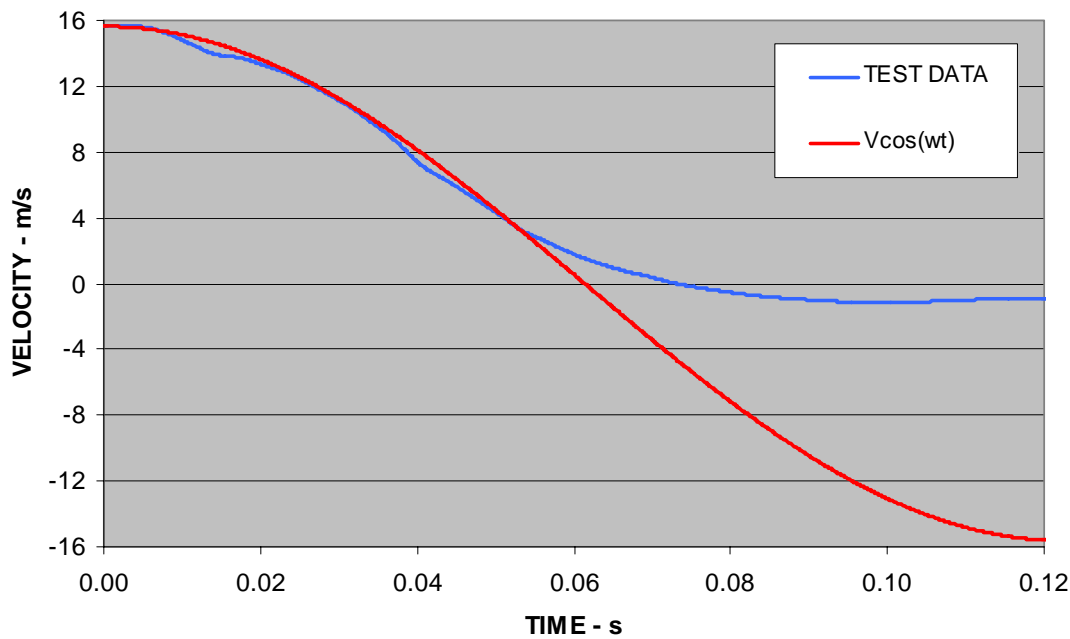


Figure 4-24: NCAP test data for 2005 Model Ford Escape Test #4952 with cosine reluctance based on limit conditions ($V = 15.6 \text{ m/s}$ & $X = 0.611 \text{ m}$)

Rebound can be represented by another cosine curve phased to coincide with the ingoing curve at the point of rebound. This point is where both curves cross the x-axis shown in Figure 4-25. The dotted curve can be determined by letting c be the coefficient of restitution and ω be reluctance of the main cosine curve in Figure 4-25, using the following equation for rebound velocity:

$$R_v = c \cdot V_i \cdot \sin \left[\frac{\omega}{c} \cdot t + \pi \left(1 - \frac{1}{2 \cdot c} \right) \right] \quad [4-14]$$

Where V_i is the initial impact velocity.

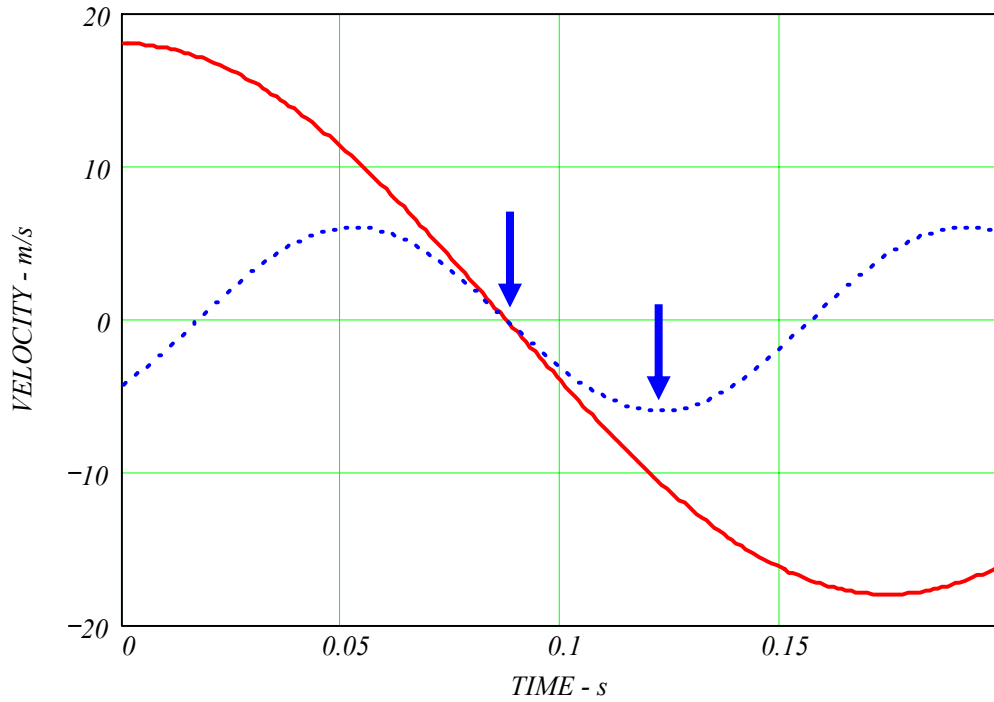


Figure 4-25: Rebound cosine curve added to ingoing cosine curve.

Rebound is only valid between the arrows in Figure 4-25. This can be a limitation for proximities which have the coupling phase extend past the later arrow. Moreover, if the rebound is low, the range between the arrows is small. An example of this is shown in Figure 4-26.

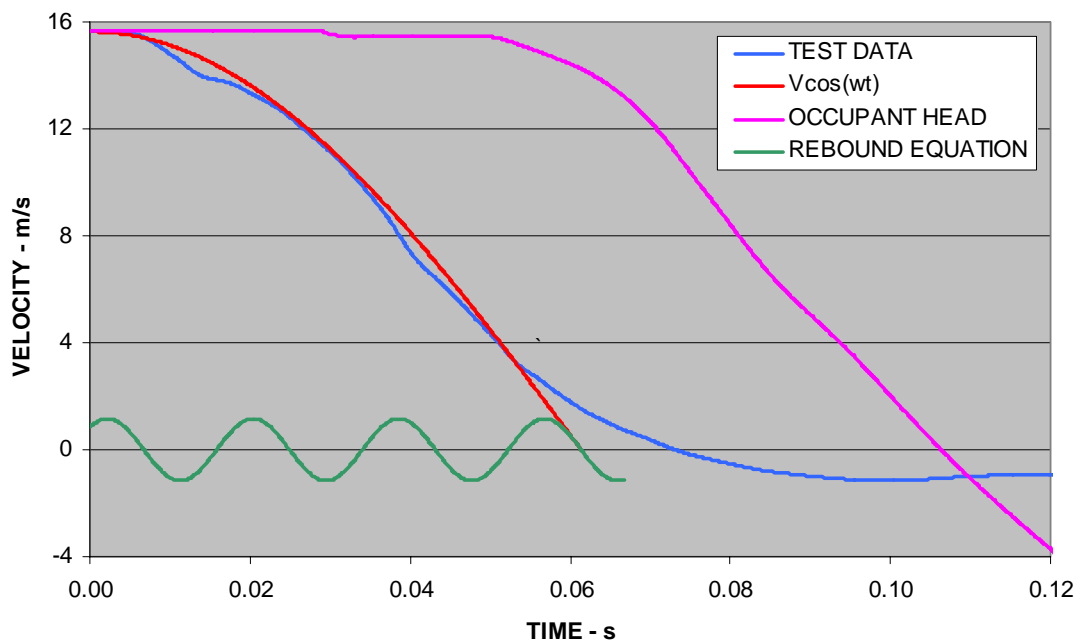


Figure 4-26: NCAP Test #4952 Ford Escape with rebound equation and occupant head velocity from test data.

The use of phased cosines to represent rebound in conjunction with small rebound velocities and large body part proximities cannot be recommended because it is incapable of encompassing a significant and common range of proximities found in occupant positions.

The value of presenting this facet in representing vehicle response lies in the completeness of the overall presentation of the cosine method of representing vehicle velocity decay.

4.9 Conclusion

Vehicle response to frontal impact was considered in this chapter from the micro perspective of the instantaneous to the mesoscopic view of the occupant cell progression. The qualitative defence of the idea that vehicle motion could be presented by an empirical model without a causal nexus is an important contribution to support the prime model to follow in subsequent chapters. The logical progression of this idea to injury so that a pseudo stiffness is deemed to represent vehicle motion to produce a fidelity injury result is a further contribution.

These concepts were applied to the familiar cosine functions that govern the motion of a mass-spring oscillator in analogy as a precursor to presentation of the prime model for this thesis. The presentation sequence progresses from the well-known cosine function to the lesser-known prime model of subsequent chapters.

System curves as well as the concept of instantaneous stiffness as applied to a crumple zone are contributions by the author. So too, is the concept of specific impedance, as well as the identification of its role as the slope of a tangent to the system curve. The discovery of almost identical normalized impedance curves for a vehicle at different initial impact speeds is a further contribution and has potential implication in a “universal” stiffness metric for each vehicle model.

These contributions have implications in explaining the formation of rebound and underpin recommended future research in this area.

5. VEHICLE RESPONSE TO VARYING CONDITIONS

5.1 Introduction

In this section feasibility is demonstrated predicting vehicle response for different crash conditions viz. velocity and mass. Spectrum stiffness is introduced in this section using the industry standard Crash3 algorithm.

Spectrum stiffness is a view on stiffness for a given vehicle across a range of conditions such as varying velocity and/or mass.

A crash test can only give results for a single set of conditions. Yet in real motor vehicle crashes these conditions can vary substantially. The motivation for this chapter is to extend the usefulness of crash tests to other conditions.

5.2 Spectrum Stiffness

In the literature, stiffness concepts are applied on a vehicle basis for a single set of crash conditions. This reflects the knowledge of a crash as a highly non-linear event. The idea that a vehicle might have predictable responses across a range of conditions including vehicle loading reflecting occupancy & luggage etc., is a contribution of this study and termed spectrum stiffness.

Spectrum stiffness is defined as a view on crumple zone response to impacts over a variety of conditions. The spectrum stiffness concept permits overall analysis and comparison of crumple zone performance with respect to injury when linked to injury.

Spectrum stiffness predicts reluctance which, in turn, predicts vehicle response at the micro level. There are two aspects to spectrum stiffness:

1. Vehicle speed.
 - Given a single crash test data set, can crash conditions be predicted for other crash velocities?
2. Vehicle mass.
 - Can factory set tare facilitate statutory compliance in a crash test?
 - Given a single crash test data set, can crash conditions be predicted for other vehicle loading conditions?

The scope for prediction requirement is nominally $\pm 15\%$ of test data. In this range linear extrapolation along the Crash3 algorithm displays sufficient accuracy to make the comparative points required. The extrapolation accuracy issue is further considered later in this chapter.

5.3 Spectrum of Initial Velocities

A crash velocity can vary according to the speed of travel generally limited to 110km/h. Crash velocity can be much greater if there is an aggressivity mismatch. Aggressivity is increased by higher stiffness in one vehicle and/or lack of proper geometric engagement of the crumple zones. The effective closing speed under such conditions can increase substantially. Then there are circumstances where the driver and the collision partner each or both exceed the statutory speed limit. This gives review of the wide spread of the spectrum of impact velocities. The focus here is on velocities that can be verified with available test data. Such speeds have been shown to represent the majority of crashes.

A simple velocity spectrum stiffness graph is presented. The three crash tests listed in Table 9 are graphed below in definition of a spectrum stiffness graph.

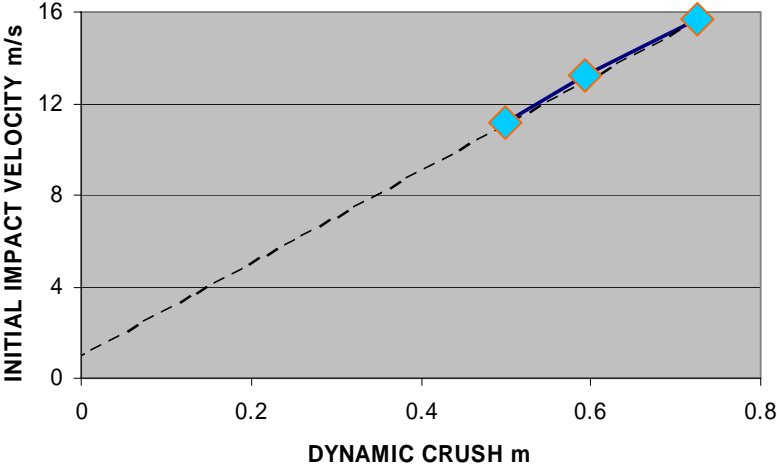


Figure 5-1: Three Hondas in full frontal rigid barrier crash tests graphed initial impact velocity vs. dynamic crush in spectrum setting. Dashed line projects to y-intercept.

Attention is drawn to the extended dotted line in Figure 5-1 to highlight the linear relationship.

Campbell (1974) first proposed a linear relationship between velocity and crush. The accident reconstruction industry has for many years used this linear relationship between initial impact velocity and crush, as follows:

$$V = B0 + B1 * CR \quad [5-1]$$

Where V is Barrier impact speed, $B0$ is “Zero Crush” speed, $B1$ is Slope of the speed-crush relationship graph and CR is Average residual crush to the front of the vehicle.

Equation [5-1] is the so-called Crash3 algorithm which has been found to reasonably represent observed crash test results. It is generally used in reverse. i.e. predicting initial velocity from crush. The equation tends to underestimate in very low speed impacts and over estimates in very high speed impacts, notes Bellion (2002). This gives insight not only into the boundary constraints associated with the Crash3 algorithm but also to the methods proposed here.

Strother, Woolley et al. (1986) and Woolley (2001) noted saturation of force at higher velocities. It is postulated the saturation is as a result of inertial stress a subject considered more fully in a subsequent section.

Changes in reluctance with velocity is further considered and calculated for a number of data points from Figure 5-1 and posted to Figure 5-2.

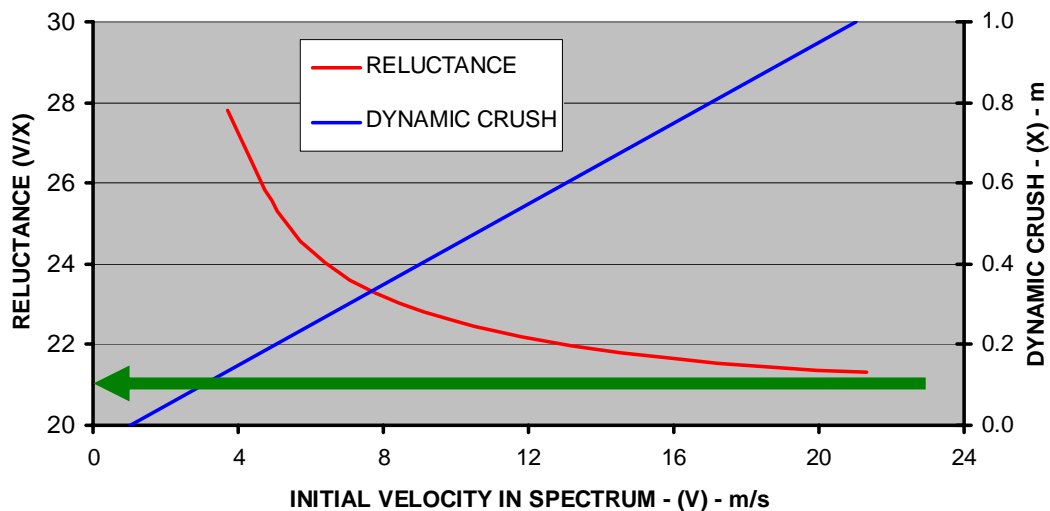


Figure 5-2: Reluctances calculated for 1998 Honda Accord for a range of initial velocities.

Figure 5-2 shows reluctances to be asymptotic to a nominal reluctance value of $\omega = 21$ (green arrow in Figure 5-2) confirming the saturation found by the other researchers.

5.3.1 Predicting Reluctance – Variations in Velocity.

If the values in the Crash3 algorithms are known then the full spectrum of reluctances for the variations in velocity can be predicted. However, in this section only a single point defined by initial velocity and dynamic crush is known from test data. The following hypothesis is tested by this section as a contribution by the author:

Velocity – Crush can be extrapolated from a single data point along an origin ray.

The procedure involves the three Honda tests shown in Figure 5-1. An extrapolation window of $\pm 10\%$ of crush is considered for deviation from the Crash3 line. The general idea is embodied in Figure 5-3 where the extrapolation window is drawn for one side only to reduce presentation clutter.

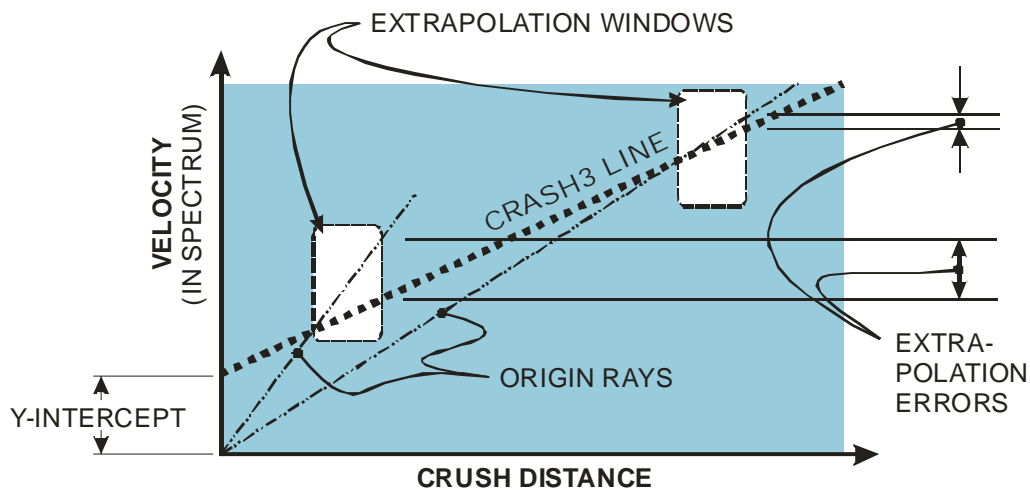


Figure 5-3: Extrapolation errors using origin rays on Crash3 line.

A study of Figure 5-3 leads to the conclusion that the error is less at the higher velocity-crush data points than at the lower points. A quantitative picture for the three Honda tests will now be developed.

The extrapolation window is conveniently sized so that the increase along the Crash3 line is 1.0 m/s. The extrapolation error then represents a decimal fraction of the increase. (E.g. an extrapolation error of 0.106 m/s becomes an error of 10.6%). The errors so calculated are maximum since there is usually a y -intercept in the Crash3 approach.

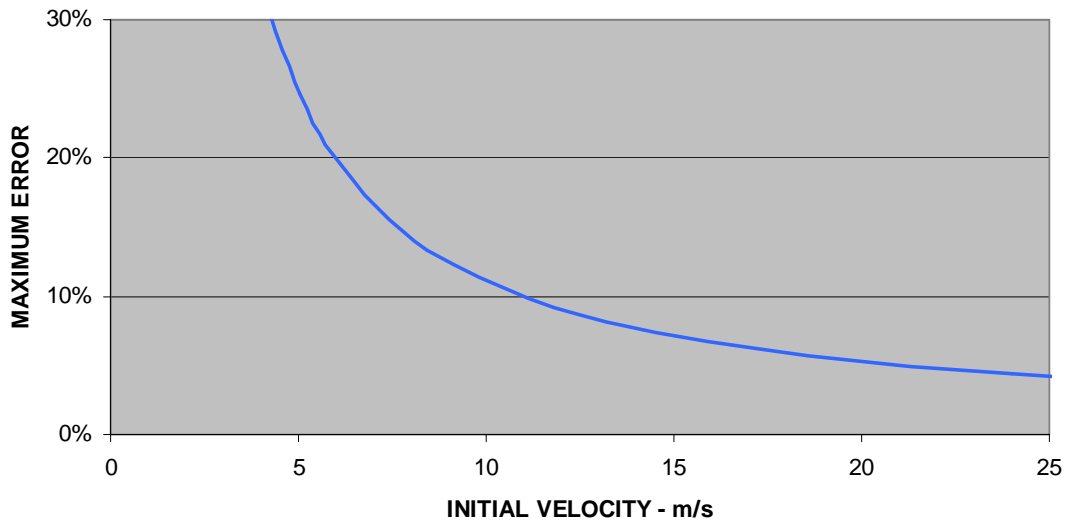


Figure 5-4: Maximum prediction error from extrapolation of a single data point for 1998 Honda Accord.

Figure 5-4 is to be read, for example, at 15 m/s initial velocity, a prediction up or down can incur an error no greater than 7% over the Crash3 prediction. Accuracy can be improved by knowledge of the y-intercept for the particular vehicle. The y-intercept corresponds with the so-called no-damage velocity, alluding to a maximum impact where no crush is recorded. The US legislated minimum required bumper strength (impact speed where no damage is incurred) is 4.0 km/h. The Insurance Institute for Highway Safety tests vehicle bumpers at 8 km/h.

Predicting velocity – crush from a single data point along an origin ray is a reasonably accurate procedure above 12 m/s. Significantly better accuracy is achieved if the minimum legislated (or preferably tested) bumper strength is taken into account. This has implications for the compliance/NCAP crash testing regime where one test could be eliminated or used for other purposes.

The value of this section lies in the comparison of the method of varying reluctance for the cosine function method of representing vehicle motion to the elegance of the prime model. The cosine function requires extrapolation; the prime model has a constant reluctance for all velocities in the range nominated for this study.

5.4 Vehicle Mass Variation

5.4.1 Introduction

When preparing for a crash test considerable care is taken to ensure that vehicle mass prior to the crash is according to the specification. Yet, in the everyday use of a motor vehicle mass is varied routinely. Some variations are minor yet others vary on a trip basis, as follows:

1. Body fluids; fuel, oil, radiator water & windscreen water.
2. Tyres; baldy tyres weigh less and spare wheel can be carried or left behind.
3. Occupancy; varies from small driver only to full complement of obese passengers.
4. Luggage; varies from an empty boot to overloading the vehicle carrying capacity.

The view that vehicle mass somehow affects effective structural stiffness is widely held. Yet, no study could be found that varies the mass of test vehicles prior to impact. No causal mechanisms appear reported in the open literature to support the positions above.

That test data including mass variations is sparse was observed by Evans (2001a).

Singh, Welcher et al. (2003) considered the effects of mass on vehicle speed change and found “no clear pattern in weight difference” and suggested the sample size may have been too small, adding that it was likely that 342 pounds (155 kg) mass addition may have been insufficient to highlight differences in a vehicle to vehicle crash.

Ross and Wenzel (2001), Van-Auken and Zellner (2002) & Kahane (2003) approach the vehicle mass issue from a demographic perspective and specifically the momentum aggressivity associated with an increase in mass. Evans (2004a) phrases the question succinctly: “Am I safer if I put bricks in my trunk?” He then proceeds to answer the question demographically.

There appears a clear knowledge gap in the literature on the effects of mass increase on:

1. Response of the vehicle crumple zone.
2. Relationship of injury risk to altered crumple zone response.

The Evans (2004a) question will be addressed to consider these as follows:

1. Study of two crash tests of identical vehicles with significant variations in test mass.
2. Simulation of a vehicle with a range of mass variations.

5.4.2 Simulation

The simulations presented here are multiply connected mass-spring models of the occupant compartment and interspersed components. Use of the simulation software is a contribution by the author only to the extent of validation of the prime model. The need for the simulation modelling derives from the dearth of crash tests with varying mass.

To produce such models for simulation requires system identification, a technique from a branch of applied mathematics (Kim and Arora (2001b)). Fortunately, the task is made simple by a computer program supplied by NHTSA called SISAME¹⁷. The version used for modelling in this study was SISAME2 last revised 13/8/03. Extraction was achieved by SISAMEM1 a program that correlates the dynamic factors from two identical vehicles crashed at different speeds.

Model extraction proceeds by optimizing masses against barrier forces captured by load cells. Vehicle motion captured by accelerometers is calibrated against optical records of the crash event. The program then calculates spring stiffness to nominated connecting springs. (Mentzer (2002) Figure 5-5 shows a model with four masses as named and nine connecting springs shown as zigzags.

The model submitted for simulation and presented here is a Ford Explorer four-wheel drive. The 1995 Explorer full frontal model is based on NHTSA full frontal VTB Test #2256 (47.3 km/h).

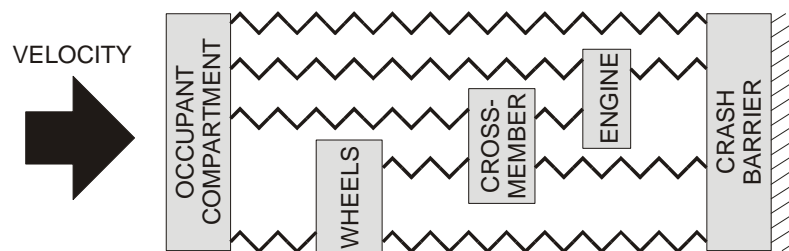


Figure 5-5: Schematic of one dimensional lumped parameter model.

The masses were varied subtracting 75 kg for the driver-only situation and up to 300 kg addition to reflect additional passengers and luggage.

The SISAME programs are well documented Mentzer (2002) Accordingly, only one input file for a simulation run is posted to conserve space. The file contents are found in Table 11. Output from the simulations are posted to Table 12 and Figure 5-6.

¹⁷ Acronym for Structural Impact Simulation and Model Extraction.

Table 11: Input file for simulation of 1996 Ford Explorer 47.3 km/h

<p>SISAME Input File Run Information RunID=ExplorerFF Title=1995 Ford Explorer Full Frontal Multiple-Event Model DelTOut=.0001 FinTOut=.125 Model Information ModID=ExplorerFF DimSys=Metric VehID=Explorer Make=Ford Model=Explorer Year=1995 Wt=2506 ImVel=47.31 MassID=OccComp Descr=Occupant Compartment Wt=2006 MassID=Engine Descr=Engine Wt=322 MassID=Wheels Descr=Front Wheels/Suspension Wt=178 SprID=Occ-Bar NegMass=OccComp PosMass=ExplorerFF.Barrier StaType=SI SU=50409.61 ST=0 X= 0 34.73684 69.47368 104.2105 138.9474 173.6842 208.4211 243.1579 277.8947 312.6316 347.3684 382.1053 416.8421 451.5789 486.3158 521.0526 555.7895 590.5263 625.2632 660 F= 0 0 16824.11 57842.71 117793.1 176802.9 211328.5 228910.1 231365.9 228825.7 254994.3 227570.8 144609.9 185235.2 184670.1 231385.1 124854.6 147804.2 254686.9 88309.57 DyuType=AM MSIp=.2050192 MMax=1.879926 SprID=Radiator NegMass=Engine PosMass=ExplorerFF.Barrier StaType=SI SU=1855.664 ST=0 X= 0 35.71429 71.42857 107.1429 142.8571 178.5714 214.2857 250 285.7143 321.4286 357.1429 392.8571 428.5714 464.2857 500 F= 0 0 0 2215.602 20727.8 30533.85 34221.52 34223.91 43059.94 67819.73 107783.9 133942.9 133942.9 133942.9 133942.9 DyuType=AM MSIp=.1227566 MMax=1.070995 SprID=Wheels-Bar NegMass=Wheels PosMass=ExplorerFF.Barrier StaType=SI SU=12652.27 ST=0 X= 0 37.85714 75.71429 113.5714 151.4286 189.2857 227.1429 265 302.8571 340.7143 378.5714 416.4286 454.2857 492.1429 530 F= 0 8649.091 14557.02 25030.86 41248.23 41248.23 41248.23 41248.23 41248.23 41685.02 41685.02 43926.6 43926.6 43926.6 133666.8 DyuType=AM MSIp=.03135248 MMax=2.7228</p>	<p>SprID=Firewall NegMass=OccComp PosMass=Engine StaType=SI SU=3217.021 ST=0 XSIk=0 X= 0 12.85714 25.71429 38.57143 51.42857 64.28571 77.14286 90 102.8571 115.7143 128.5714 141.4286 154.2857 167.1429 180 F= 0 0 0 0 472.1028 10700.43 17742.19 27986.8 38412.47 43280.81 43280.84 43280.84 43280.84 43280.84 63015.42 DyuType=AM MSIp=.1495215 MMax=7.879599 SprID=Occ-Wheels NegMass=OccComp PosMass=Wheels StaType=SI SU=282849.3 ST=6097.507 XSIk=1.543342 X= 0 10.71429 21.42857 32.14286 42.85714 53.57143 64.28571 75 85.71429 96.42857 107.1429 117.8571 128.5714 139.2857 150 F= 0 0 0 0 0 0 0 2283.026 2283.026 2283.026 2283.026 2283.026 2283.026 2283.026 2283.026 DyuType=AM MSIp=.2246327 MMax=4.989014 SprID=Wheels-Eng NegMass=Wheels PosMass=Engine StaType=SI SU=3285136 ST=1037.35 XSIk=1.322101 X= 0 3.571429 7.142857 10.71429 14.28571 17.85714 21.42857 25 28.57143 32.14286 35.71429 39.28571 42.85714 46.42857 50 F= 0 1.173263 2.346525 3.519788 4.69305 5.866313 7.039575 8.212837 9.386098 10.55936 11.73262 12.90588 12.90588 12.90588 12.90588 DyuType=AM MSIp=0 MMax=1 Output Information OutClass=MassTS Qty=AVD Mass=*</p>
--	---

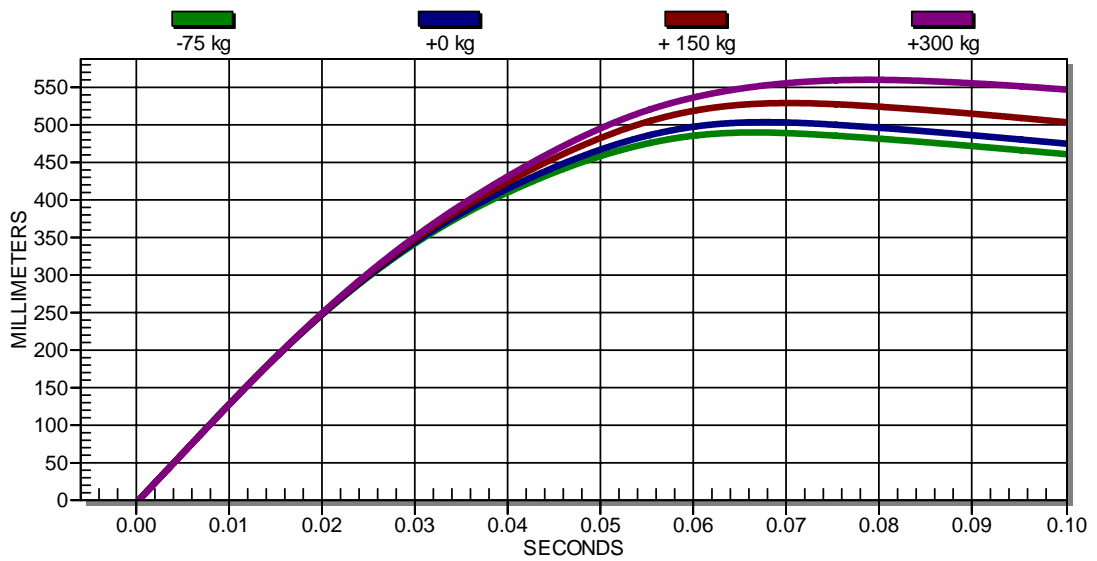


Figure 5-6 Transient position for occupant cell mass variations on Ford Explorer Test #2256 at test speed 47.3 km/h.

Table 12: Results of simulations of Ford Explorer Test #2256 with varying masses.

ADDED MASS (kg)	V (m/s)	X (m)	VEH MASS (kg)	OCC CELL MASS (kg)	RELUCTANCE $\omega = V/X$
-75	13.1	0.492	2131	1631	26.6
0	13.1	0.510	2206	1706	25.7
150	13.1	0.531	2356	1856	24.7
300	13.1	0.565	2506	2006	23.2

The reluctance data in Table 11 are graphed in Figure 5-7 for more convenient perusal. There is a clear indication of mass softening (reduction in effective stiffness). This is contrary to the findings of Sugimoto, Kadotani et al. (1998) who wrote:

“As vehicle weight increases, the stiffness of the vehicle front increases”

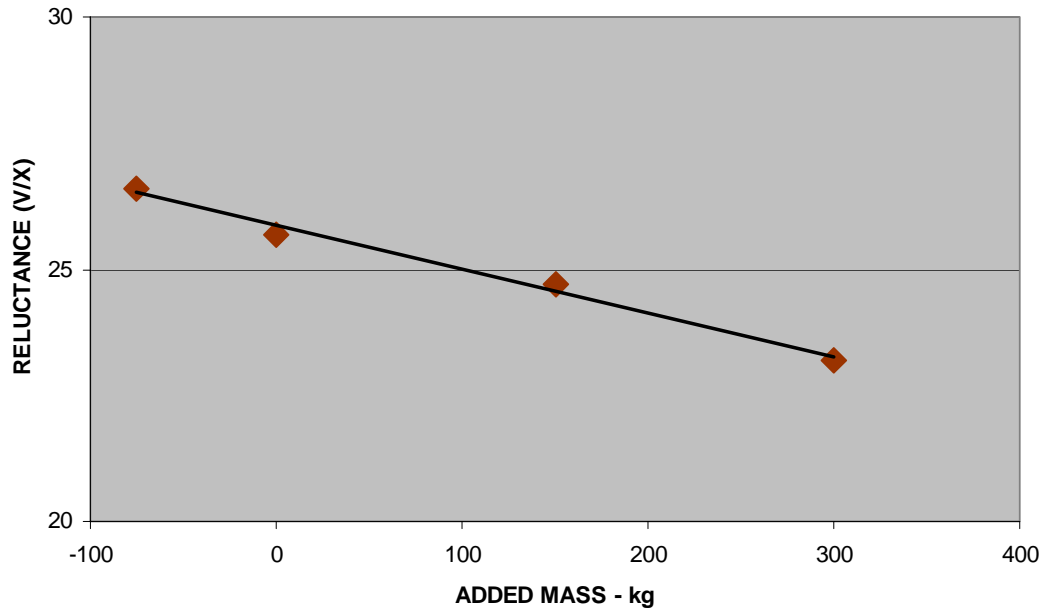


Figure 5-7 Reluctance change for occupant cell mass variations on Ford Explorer Test #2256 at test speed 47.3 km/h. (Data points trended)

Figure 5-7 shows a general reduction in reluctance with increase in mass. To show that the Ford Explorer is not an isolated case four more vehicles were simulated each at two different velocities for mass variations from -75 kg thru to +300 kg.

The results of these 32 simulations are graphed in Figure 5-8 for more concise overview.

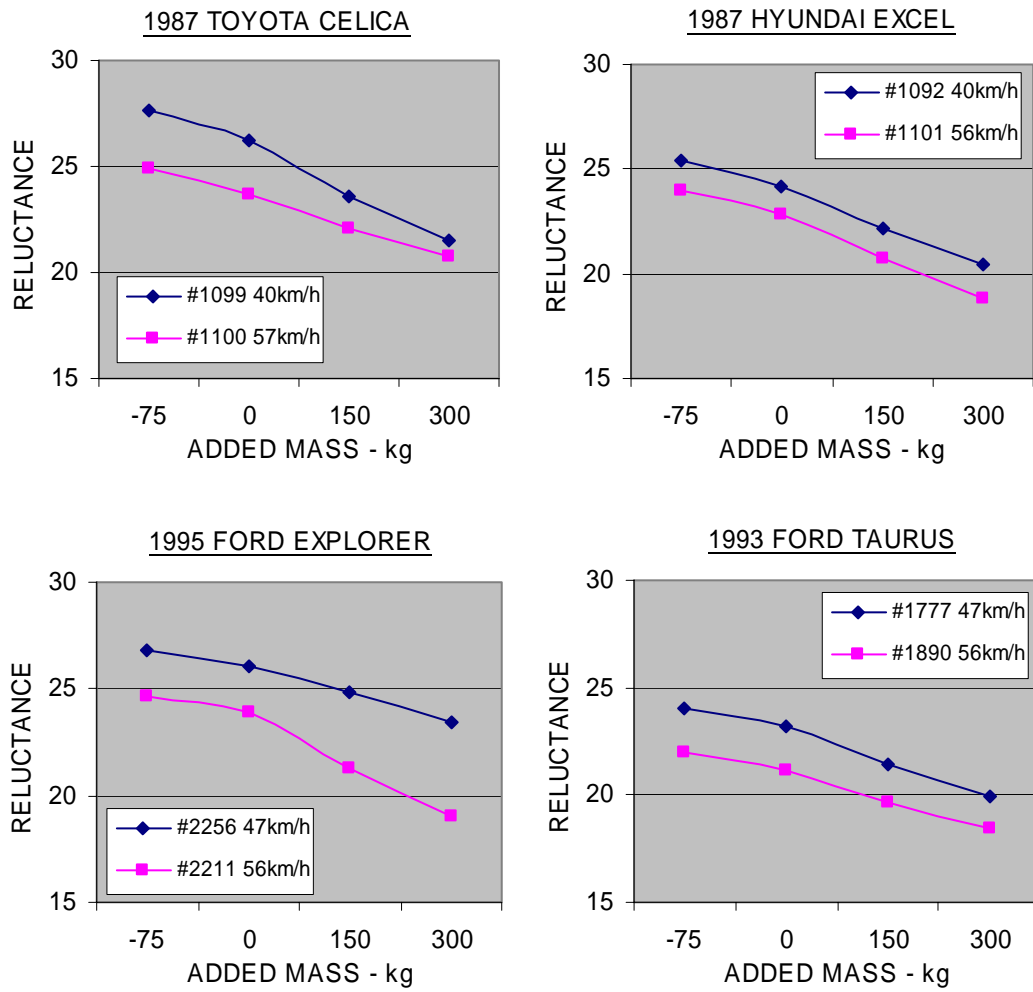


Figure 5-8: Reluctances for mass changes in simulation of eight crash tests.

The reduction in reluctances for increase in occupant cell mass evident in the foregoing is termed here mass softening being a reduction in spectrum stiffness on account of mass increase.

5.4.3 Mass Softening in Real Tests

The mass-softening phenomenon is a contribution of this study. The terminology is sourced from a similar phenomenon reported by Varat, Husher et al. (2001) describing departure from straight-line velocity-crush curves. Mass softening attests to a reduction in reluctance with an increase in vehicle mass.

The vehicle test data was sourced from a utility vehicle which had the engine replaced with an electric motor. Lead acid batteries were carried in the cargo area accounting for the extra mass.

The test vehicle was a 1980 Model Ford Courier Pick-up Truck being conventional (bell housing, gearbox, tail shaft and differential) except for the engine which was replaced by an electric motor for Test #279. The test report remarked that no structural modifications were evident. The weight distribution was checked front to rear and was approximately equal. The upper picture in Figure 5-9 was a production vehicle, Test #290.



Figure 5-9: Photographs of 1980 Ford Courier after 48 km/h rigid barrier impact. Upper vehicle weight 1427 kg – lower vehicle weight 1982 kg.

Values for dynamic crush were extracted from signals recorded from accelerometers sited on the floorpans by double integration and posted to Table 13.

Table 13: Effect of mass on reluctance in 1980 Ford Courier.

TEST	ENERGY SOURCE	VEHICLE MASS	VELOCITY (V)	DYNAMIC CRUSH (X)	RELUCTANCE (V/X)	IMPACT ENERGY (J)
#290	PETROL	1427 kg	13.2 m/s	0.483 m	27.3	124320
#279	ELECTRIC	1982 kg	13.5 m/s	0.637 m	21.2	180610

An increase in impact energy of about 50% can be associated with a decrease in reluctance. Because the velocities are very similar, it can be concluded that the additional mass (39%) has reduced the stiffness of the 1980 Ford Courier pick-up truck as measured by the reluctance metric by 22%.

5.4.4 Implications of Mass Softening

To see the effect of mass softening on injury, a displacement-time trace from the mass simulation is selected. The two traces for study from Figure 5-8 are Test #1092 plus 300kg and minus 75kg. The corresponding velocity – time traces are extracted and entered into a computerized spreadsheet where the proximity and contact velocity were calculated.

Figure 5-10 gives a clear message that vehicle mass increase results in reduced injury risk. The improvement in injury risk on account of increased mass has implications in the crash testing regime for statutory compliance. A marginal performer in the crash test laboratory can be made to comply simply by adding mass in the design of the corresponding production vehicles. This is seen as a disincentive to reduce vehicle mass in the National Fleet.

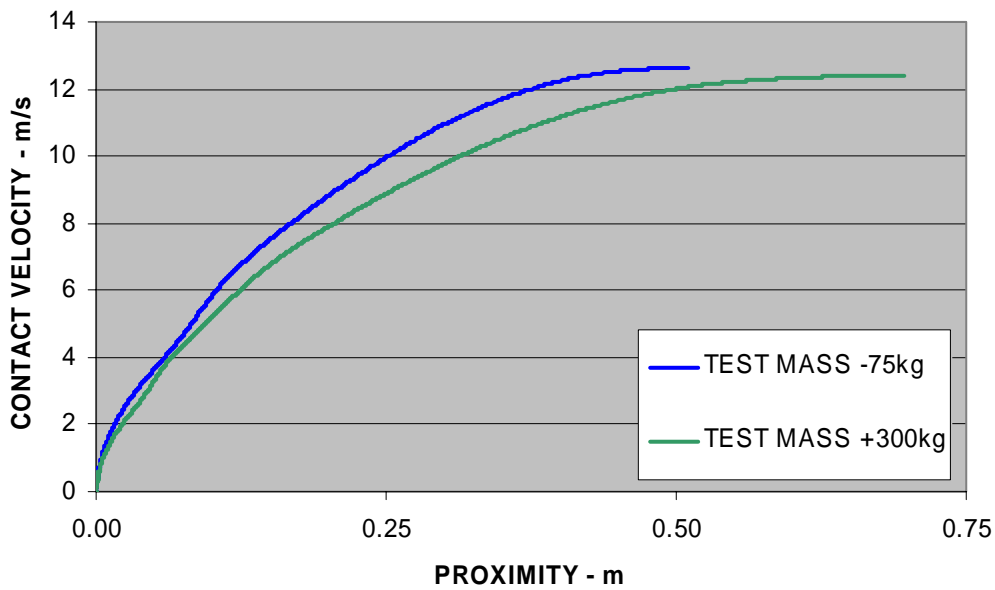


Figure 5-10: Injury risk for 1987 Hyundai Excel GLS Test #1092 40 km/h with 75kg deleted from test mass compared with 300kg added to test mass

5.4.5 Predicting Reluctance – Variations in Mass

It was shown earlier that reluctance varies with vehicle mass. To assess injury effects from variations in reluctance at conditions other than test conditions, it becomes necessary to predict the changes in reluctance according to the change in vehicle mass.

The hypothesis to be tested in this section is as follows:

Reluctance can be extrapolated from a single data point along an origin ray for mass variation.

The prediction system is visualized as shown in Figure 5-11 where two identical springs with different masses attached are initiated with velocity – V_i .

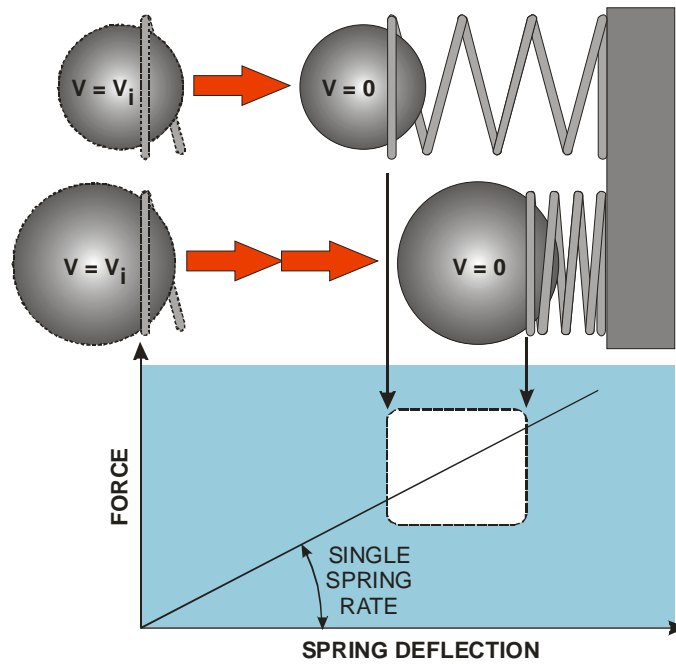


Figure 5-11: Visualization of linear elastic system under mass variation.

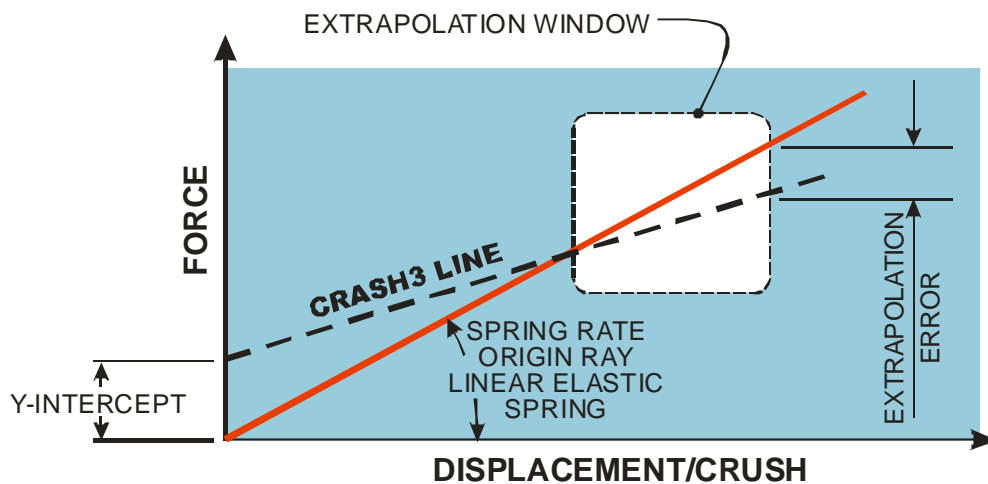


Figure 5-12: Extrapolation errors using linear elastic spring stiffness ray showing Crash3 line for reference.

The extrapolation error against the Crash3 system is visualized Figure 5-12. The hypothesis is to be tested against simulated and test data. The procedure has three main steps which are performed in Table 14:

1. Determine reluctance for the known data set.
2. Determine the linear stiffness parameter for the known data set.
3. Using the above stiffness parameter, calculate the reluctance using the new mass

Combining Equation [4-1] for the NHTSA linear stiffness parameter with Equation [4-6] defining reluctance produces Equation [5-2]:

$$\frac{V}{X} = \omega = \sqrt{\frac{k}{M}} \quad [5-2]$$

Equation [5-2] is transposed in Table 14 to facilitate determination of the linear stiffness parameter, as shown in Table 14. The reference mass is +300kg.

Table 14: Ford Explorer Test #2256 prediction of reluctance for lower vehicle mass.

ADDED MASS	VEHICLE MASS <i>M</i>	<i>ω</i> (V/X)	LINEAR STIFFNESS PARAMETER $k = \omega^2 \cdot M$	PREDICTED RELUCTANCE $\omega = \sqrt{\frac{k}{M}}$	ERROR
+300kg	2506 kg	23.4	1,372,185	-	
-75 kg	2131 kg	26.7		25.4	4.9%

The predicted reluctance of $\omega = 25.4$ compares well with the original calculated reluctance of $\omega = 26.7$ showing an error of 4.9% given the overall precision of the process discussed earlier.

To ensure the result in Table 14 is not isolated more vehicles were considered. The test results of the two Ford Couriers as well as all of the simulated results used to derive Figure 5-8 were calculated and posted to Table 15.

Table 15: Prediction of reluctance using occupant cell mass.

MAKE	TEST NO	VELOCITY m/s	CRUSH m	OCC CELL MASS kg	RELUCTANCE	STIFFNESS PARAMETER (k)	PREDICTED RELUCTANCE	ERROR %
COURIER	#290	13.2	0.483	678*	27.3		26.4	3.4%
	#279	13.5	0.637	1053*	21.2	4.7E+05		
CELICA	M1099	11.2	0.404	677	27.7		26.8	3.2%
		11.2	0.52	1052	21.5	4.9E+05		
	M1100	15.8	0.636	677	24.8		25.8	3.8%
		15.8	0.764	1052	20.7	4.5E+05		
EXCEL	M1092	11.0	0.434	776	25.3		24.8	2.3%
		11.0	0.541	1151	20.3	4.8E+05		
	M1101	15.6	0.648	776	24.1		23.0	4.6%
		15.6	0.827	1151	18.9	4.1E+05		
EXPLORER	M2256	13.1	0.490	1631	26.7		25.9	3.0%
		13.1	0.560	2006	23.4	1.1E+06		
	M2211	15.6	0.633	1631	24.6		21.1	14.3%
		15.6	0.819	2006	19.0	7.3E+05		
TAURUS	M1777	13.1	0.545	1128	24.0		23.0	4.2%
		13.1	0.657	1503	19.9	6.0E+05		
	M1890	15.6	0.712	1128	21.9		21.2	3.1%
		15.6	0.848	1503	18.4	5.1E+05		
*INCLUDES AN ESTIMATED ALLOWANCE FOR FRONT END								

Good prediction accuracy was achieved for all vehicles except the Ford Explorer at the higher velocity satisfying the hypothesis stated at the outset. The significant departure of this one simulation compared to all other results remains for future study.

5.5 Conclusion

This chapter introduces the idea of spectrum stiffness, being a single variable that describes response of the vehicle to different initial impact velocities. This contribution is introductory to later presentation of the prime model.

The concept of mass softening is introduced in this chapter. A study by the author of two identical vehicles but carrying different mass is presented showing that the additional mass reduces stiffness. Because of a lack of test data from crash tests where mass is varied on identical vehicles, a multiple mass-spring model is applied to a number of vehicles varying the mass.

These simulations by the author confirmed the mass-softening phenomenon. As a further contribution, a contact velocity and proximity study confirmed that additional mass reduces injury. This has implications in crash testing compliance where a marginal performer can simply increase vehicle mass to achieve the prescribed IARV's¹⁸.

Methodology was offered as a contribution of this study to calculate variations in reluctance according to variations in vehicle mass.

¹⁸ Injury Assessment Reference Values.

6. ACHIEVING AN INJURY REPRESENTATIVE PULSE

6.1 Introduction

The previous section was concerned with achieving an accurate representation of the response of the occupant cell to the crash forces. The implicit assumption was that if fidelity with test data existed then injury fidelity would follow. Indeed, in a perfect world where perfect fidelity was achievable the assumption would hold. An early force peak in the crash pulse may average with a later trough and appear a reasonable fit overall. However, when considered in terms of proximity and contact velocity, an early peak can influence injury for the remainder of the crash sequence. This insight underpins this section's contribution by the author.

By comparison with an analysis from previous section it will be shown that an accurate representation of the vehicle motion data may not necessarily reflect an accurate representation of injury data.

The previous work maintained a crude parallel with simple harmonic motion using a linear spring analogy. This served well as basic models were developed. As the need for better mathematical models is developed the link to simple harmonic motion becomes remote and unnecessary. Using the term reluctance in place of circular frequency facilitates this transition.

This section explores the idea of a notional pulse created to represent injury data. The emphasis then is on fidelity with injury-interpreted test data. Pseudo-reluctance is thereby determined. A notional reluctance that is sourced from injury-interpreted test data to improve injury accuracy is a product of this study.

Cosine equations for transient velocity were shown earlier to be suitable for optimization to improve fidelity with test data up to the rebound point. Since the coupling phase of typical body part proximities reaches well beyond the rebound point an alternate to the cosine equations is presented here.

6.2 Injury Fidelity Compared with Vehicle Motion Fidelity

Cosine equations and results used previously are to be used here in comparison. What was regarded as an optimum fit will be shown to be a poor fit when injury is considered. This has the effect of emphasizing the need for fidelity to injury rather than fidelity to vehicle motion. The equations used are defined by Figure 6-1.

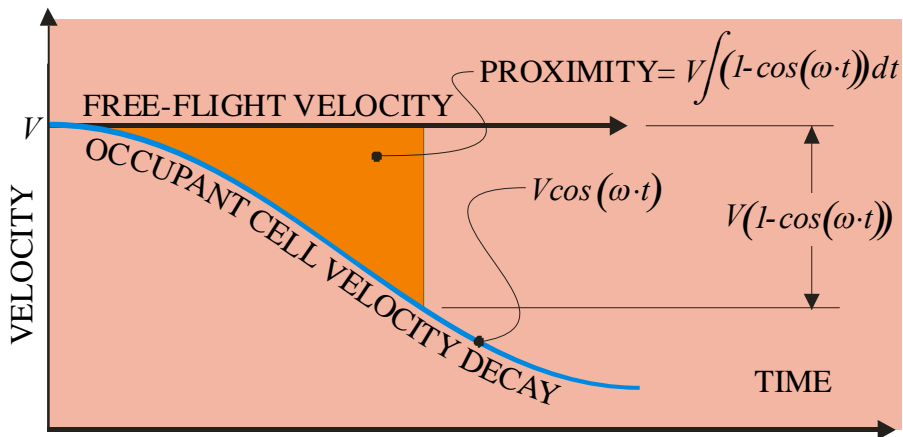


Figure 6-1: Definition of cosine-based injury equations.

The NHTA linear stiffness parameter was used to represent vehicle velocity decay in Figure 4-10 in an earlier chapter. An improved representation of vehicle velocity decay was offered by determining a best-fit reluctance in Figure 4-11. The improvement was achieved by reducing the reluctance from $\omega = 27.3$ for the linear stiffness parameter to $\omega = 25.8$ for the best-fit option. The injury results in terms of contact velocities for varying proximities are graphed respectively in Figure 6-2 and Figure 6-3.

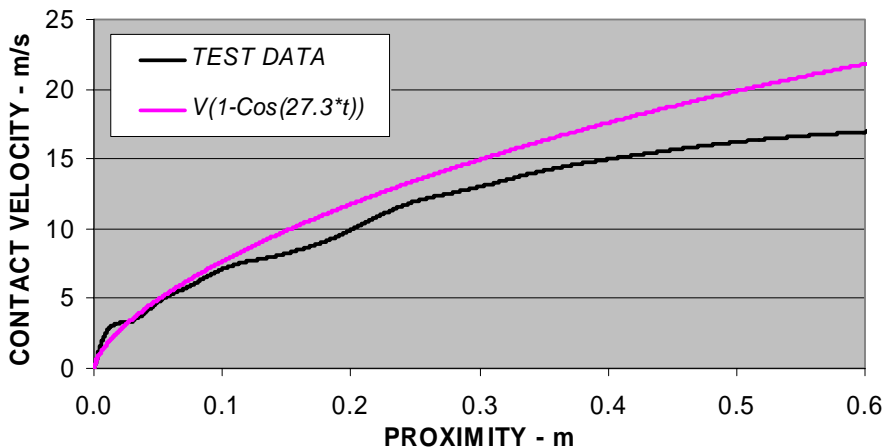


Figure 6-2: Comparison of contact velocities from test data of Falcon ANCAP #8055 using reluctance from NHTSA linear spring parameter.

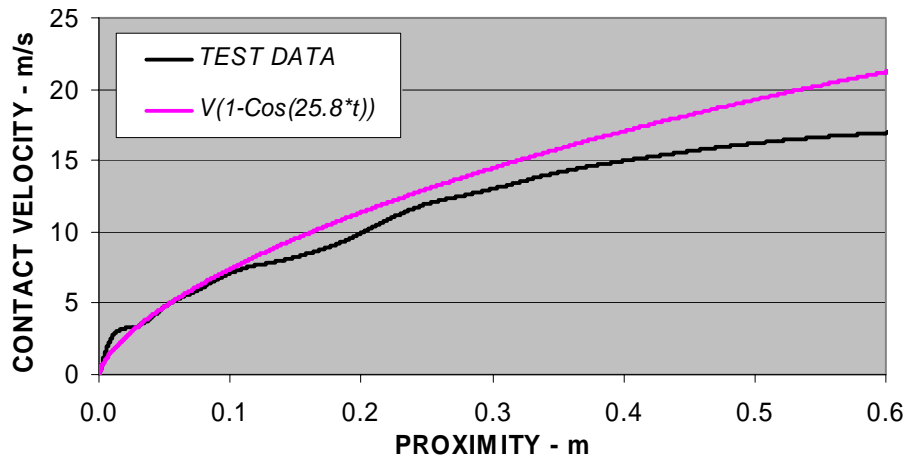


Figure 6-3: Comparison of contact velocities from test data of Falcon ANCAP #8055 using reluctance from best-fit improvement.

No significant improvement in injury result was evident between normal ($\omega = 27.3$) and the reluctance from the curve-fit ($\omega = 25.8$) thought to improve the result. This emphasizes the importance of reluctance values focussing on injury representation.

6.2.1 Optimized Reluctance for a Proximity Range

The distribution of proximity of a body part to internal impact point is a statistical distribution. The need for accuracy of reluctance may diminish in importance the greater (or smaller) the proximity is from the mean of the distribution. If better accuracy can be achieved over the representative range of the distribution, overall statistical error is minimized.

This idea is explored in this section by varying the reluctance to suit a statistical proximity distribution. The proximity probability distribution from knee-to-dash study in taxis Brell, Thambiratnam et al. (2002c) is used as an example of focussing accuracy needs to a predetermined width of proximity.

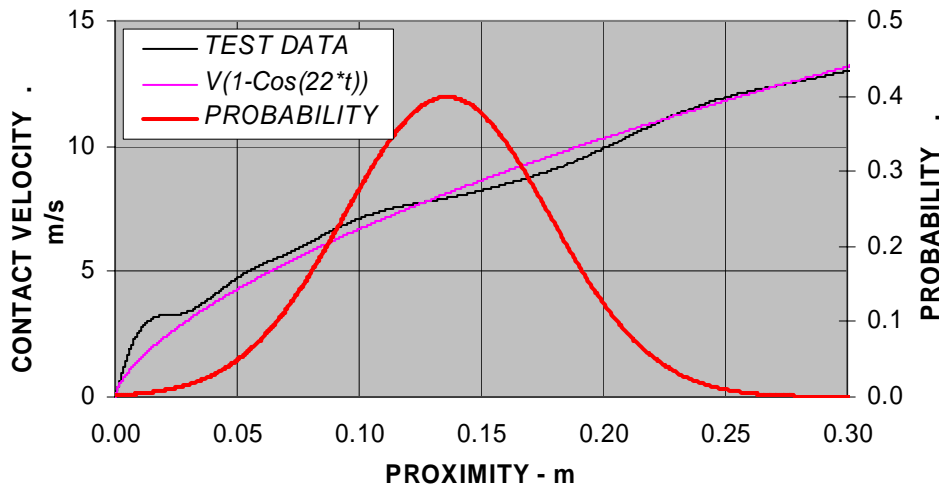


Figure 6-4: Comparison of contact velocity from test data of Falcon ANCAP #8055 with optimized reluctance to suit statistical distribution.

A reluctance of $\omega = 22$ gave a good correspondence with test data over the statistical range of proximities required, as shown by Figure 6-4.

This emphasizes the value of removal of the conceptual link with crumple zone structural stiffness to replacement by an optimal reluctance with no link to the physical but representing the test data better.

6.2.2 Haversine

The improvement in contact velocity fidelity in Figure 6-3 was over a narrow range of proximities. The cosine equations have been found not to be capable of representing injury data over a wide range of proximities and not beyond rebound. The phased haversine or, for convenience, just haversine will be developed here for suitability to represent injury risk as measured by contact velocity over the full range of proximities.

It is noted that Varat and Husher (2000) experimenting with different pulse shapes, square, triangular, sine and haversine found the haversine explained a crash pulse well. The study fell short of demonstrating fidelity with contact velocity or use as a predictive tool, leaving scope for this study to consider the haversine further as original work.

Whilst in most impact analyses the Heaviside function, Spiegel (1968) or the DuHamel integral, Rao (1986), are used, there is a plethora of choice of mathematical models available in curve-fitting facilities if adherence to the physics of the process is not needed. The pinnacle of fidelity is typically achieved by polynomials. Lim (1972) proposed a functional

relationship to exist in an 11th order polynomial for the collapse history of the test vehicle. Velocity and acceleration histories were obtained by differentiating the collapse history and velocity history respectively. Interpolation required a power curve technique.

The haversine is chosen for its simplicity and adaptability to velocity and vehicle mass variation. In addition, the resultant injury risk is able to be expressed in relation to occupant position mathematically eliminating the time parameter.

The first stage in the adaptation of the haversine to injury is to represent vehicle motion. The expression in Equation [6-1] is a versine according to Abramowitz (1972), followed Equation [6-2], a haversine, being half of the versine, as follows:

$$ver(t) = 1 - \cos(\omega \cdot t) \quad [6-1]$$

$$hav(t) = \frac{1}{2} \cdot (1 - \cos(\omega \cdot t)) \quad [6-2]$$

Equations [6-1] & [6-2] are plotted along with a cosine curve to enable convenient distinction.

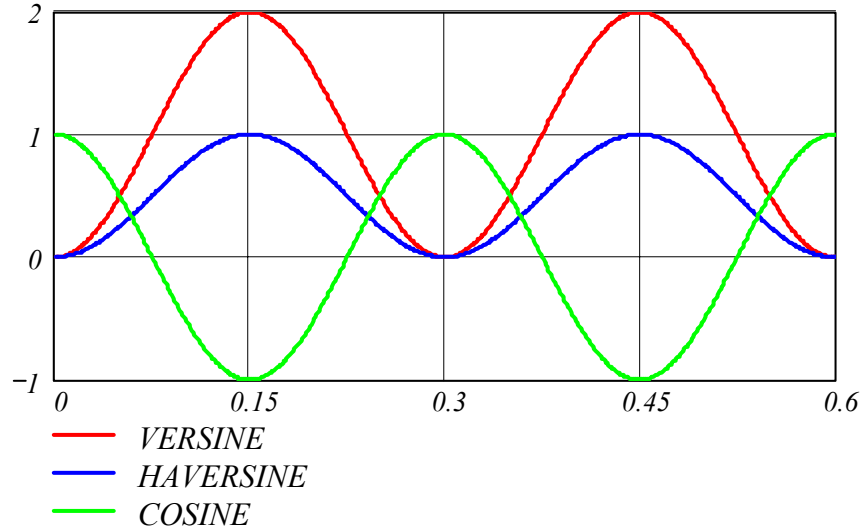


Figure 6-5: Plot of versine, haversine & cosine.

The versine and haversine are phased displaced to bring into more focus the potential of the haversine to represent velocity decay of the vehicle.

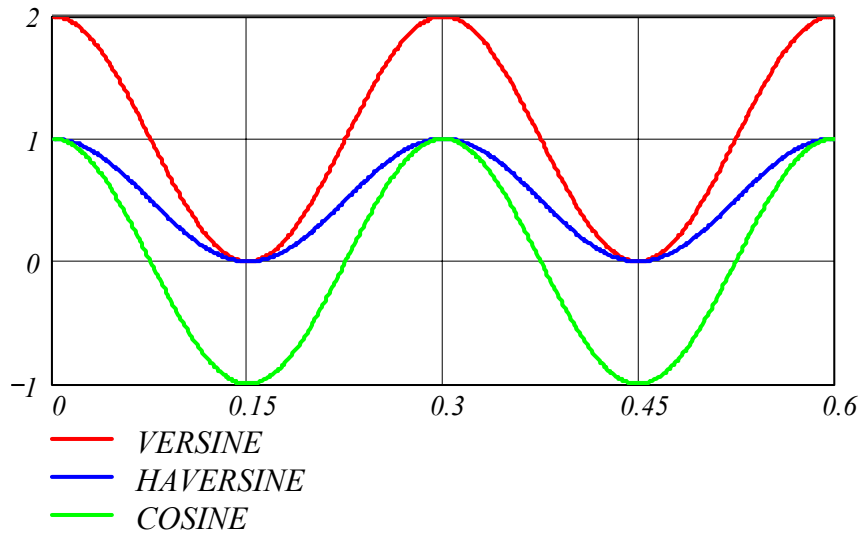


Figure 6-6: Plot of cosine and phase-displaced versine & haversine.

To demonstrate the versatility of the haversine, a nominal rebound value (c) is added in addition to the phase displacement (π) in Equation [6-3] to represent normalized velocity decay (V_D) of the vehicle. A plot of Equation [6-3] appears in Figure 6-7

$$V_D = (1 + c) \cdot \frac{1 - \cos(\omega \cdot t + \pi)}{2} - c \quad [6-3]$$

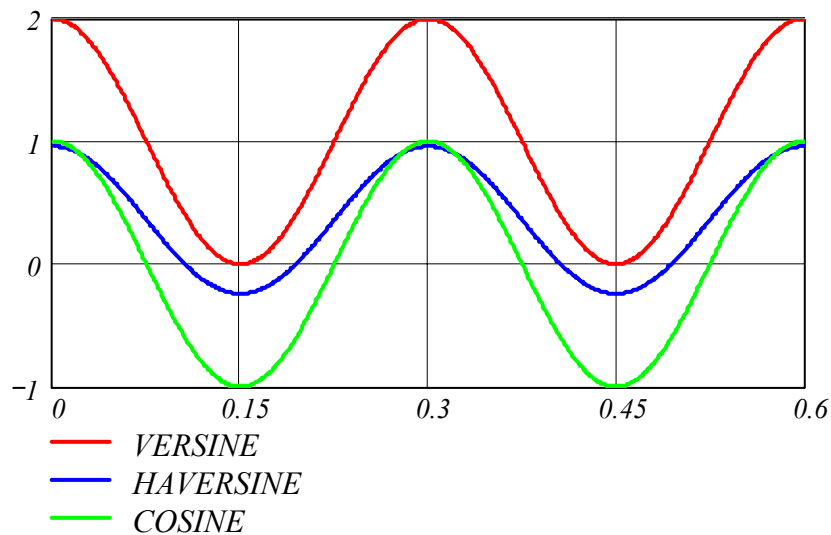


Figure 6-7: Plot of phased displaced haversine with rebound added.

An overview of the performance of the haversine is achieved by comparing system curves with test data. The system curves from Figure 4-14 for Honda Accord #2712 are re-graphed together with a haversine representation of the test data in Figure 6-8.

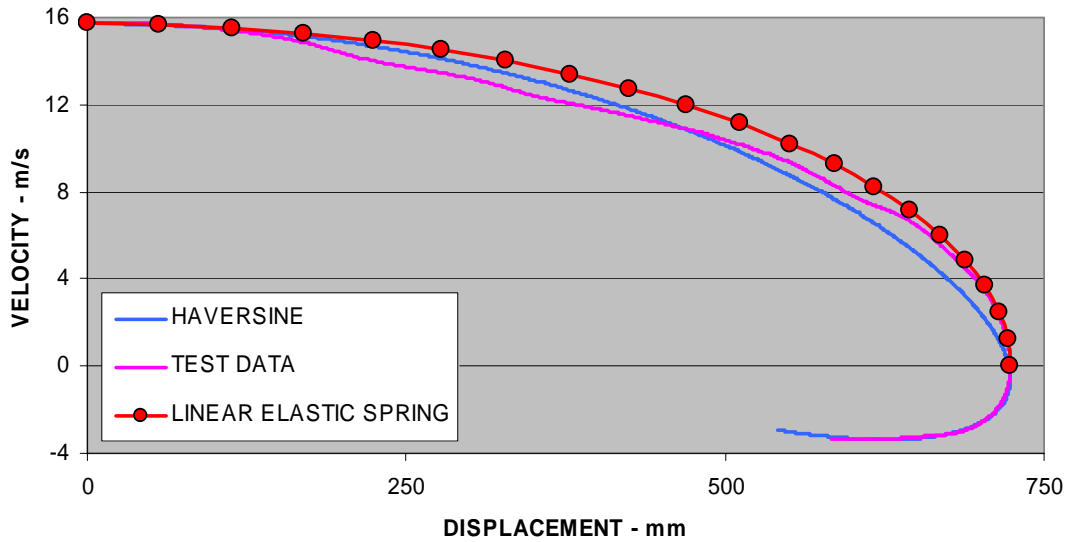


Figure 6-8: Linear elastic spring and haversine system curves compared with test data system curve for Honda Accord Test #2712

It should be noted that the haversine curve follows the data into the rebound zone. This feature makes the haversine useful.

An expression for proximity and contact velocity will now be developed with the aid of sketch as shown in Figure 6-9.

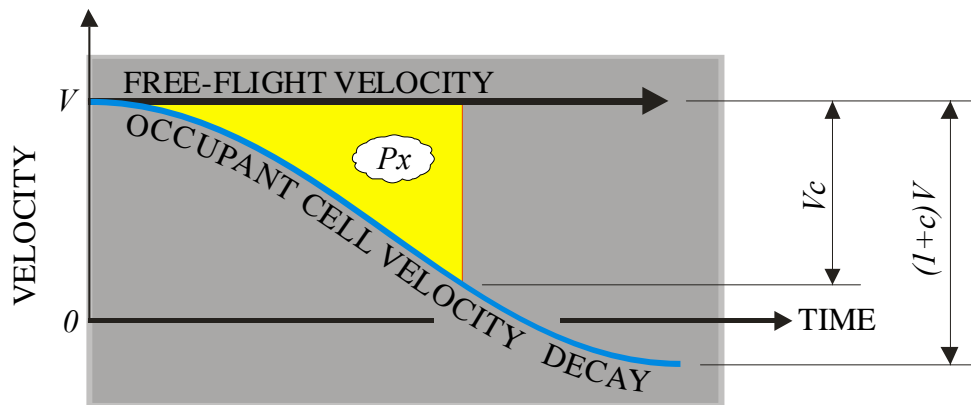


Figure 6-9: Derivation sketch of injury haversine equations.

Normalized contact velocity (V_c) can be found by subtracting a simplified Equation [6-3] from 1.0, as shown in Equation [6-4]:

First simplifying by applying:

$$\frac{1 - \cos(\omega \cdot t + \pi)}{2} = \cos^2\left(\frac{\omega \cdot t}{2}\right)$$

$$V_C = 1 - \left[(1 + c) \cdot \cos^2 \left(\frac{\omega \cdot t}{2} \right) - c \right] \quad [6-4]$$

By operation of a well-known trigonometric identity, Equation [6-4] simplifies further to:

$$V_C = (c + 1) \cdot \sin^2 \left(\frac{\omega}{2} \cdot t \right) \quad [6-5]$$

Normalized proximity is represented by the area between the free-flight velocity curve and the occupant cell velocity decay curve, as follows:

$$P_x = \int (c + 1) \cdot \sin^2 \left(\frac{\omega}{2} \cdot t \right) dt \quad [6-6]$$

Carrying out the integration and simplifying gives:

$$P_x = \left(t - \frac{\sin(\omega \cdot t)}{\omega} \right) \cdot \frac{(1 + c)}{2} \quad [6-7]$$

Equations [6-5] and [6-7] can be plotted parametrically to reveal the general shape of the haversine injury curve. This appears in Figure 6-10 where coefficient of restitution (rebound) is assigned a value of $c = 0.2$ and reluctance value of $\omega = 20$.

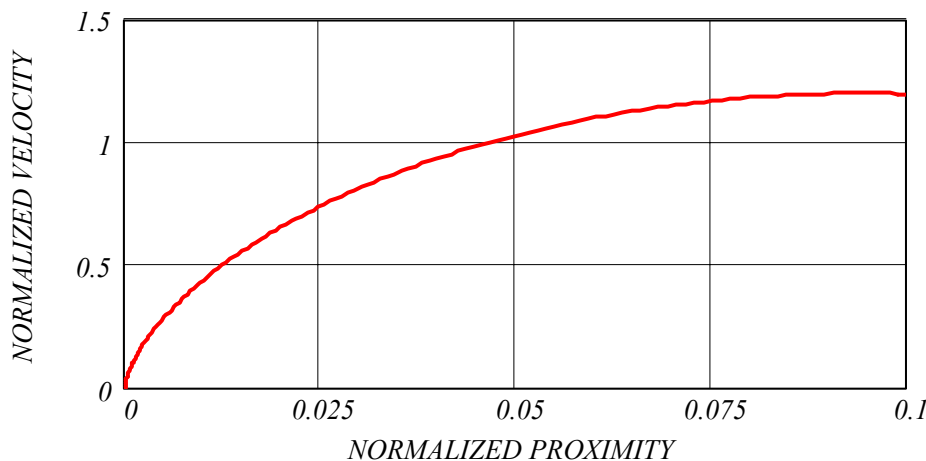


Figure 6-10: Typical parametric plot of normalized velocity and proximity.

The Falcon and Holden tests from the previous section are compared to see how the haversine performs reporting injury in a proximity study. Figure 6-11 and Figure 6-12 refer.

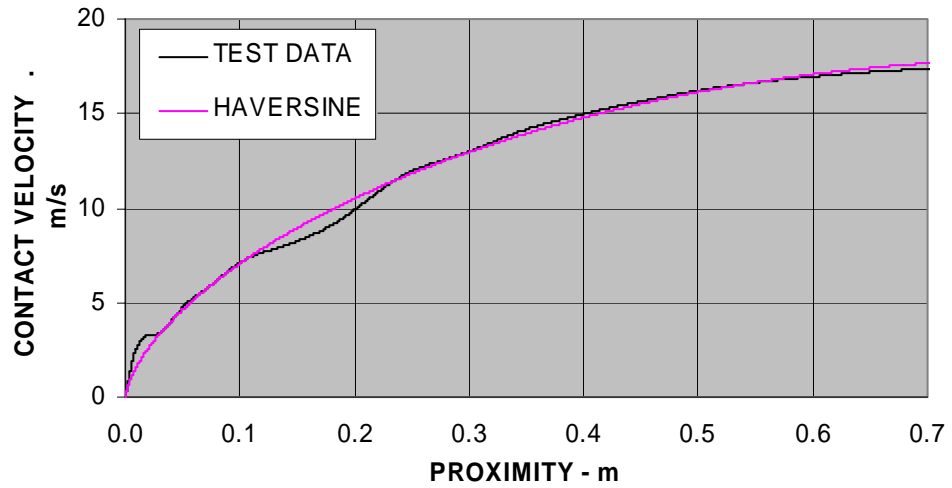


Figure 6-11: Contact velocity – proximity study for Falcon Test #8055.

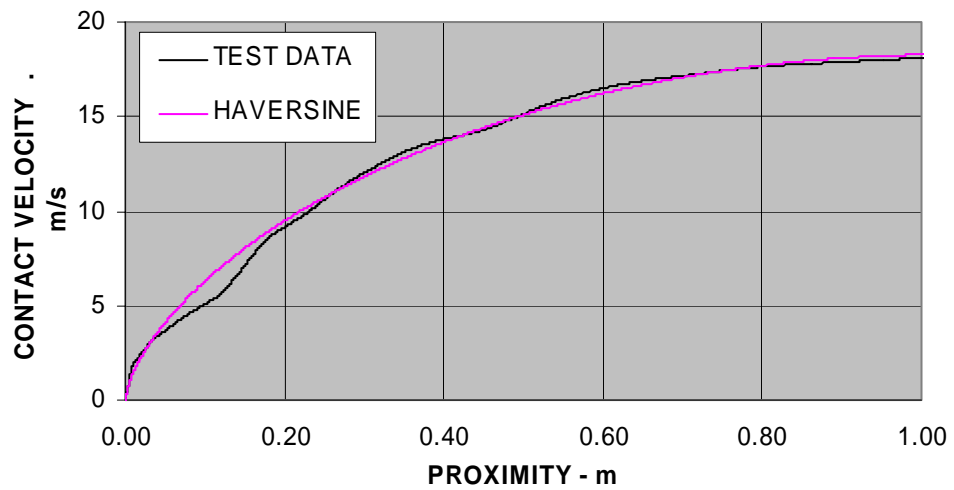


Figure 6-12: Contact velocity proximity study for Holden #7030 using haversine.

A similar quality result is evident as for the Falcon in the prior haversine comparison. Figure 6-12 shows a good range of proximity to 1.0 m with good representation from 200 mm upwards.

6.3 Conclusion

The central idea explored in this chapter is abandonment of the nexus of an equation with the physics of the process. This idea is well-precedented in the literature, for example, the Prandl¹⁹ Membrane analogy where torsion is represented by the volume under the membrane and shear stress is represented by the slope of a tangent to the membrane at its fixing point. Timoshenko and Goodier (1951). There is no physical nexus between membranes and shear stress.

Extension of this idea gave rise to the notion of pseudo-reluctance in cosine equations optimized to produce fidelity for a given range of statistical likely proximities, a contribution by the author.

Moving even further from the physics enabled an equation for injury risk based on a haversine. This equation showed good fidelity with test data for the full range of proximities. The haversine is the prime model for this thesis. It is introduced in this chapter as a parametric set of equations, to be refined in the next chapter.

Because of the haversine's adaptability to represent conditions other than crash conditions, the application of the curve shape to crash pulse data is more than just a curve-fitting exercise.

¹⁹ Ludwig Prandtl (1875-1953)

7. INJURY PREDICTION MODEL DEVELOPMENT

7.1 Introduction

This chapter marks the culmination of testing the following hypothesis:

A single crash test contains information that can be used to predict vehicle response accounting for different crash conditions such as vehicle mass and initial velocity and thus can be used to predict the effect on occupant injury risk for varying occupant positions within a vehicle

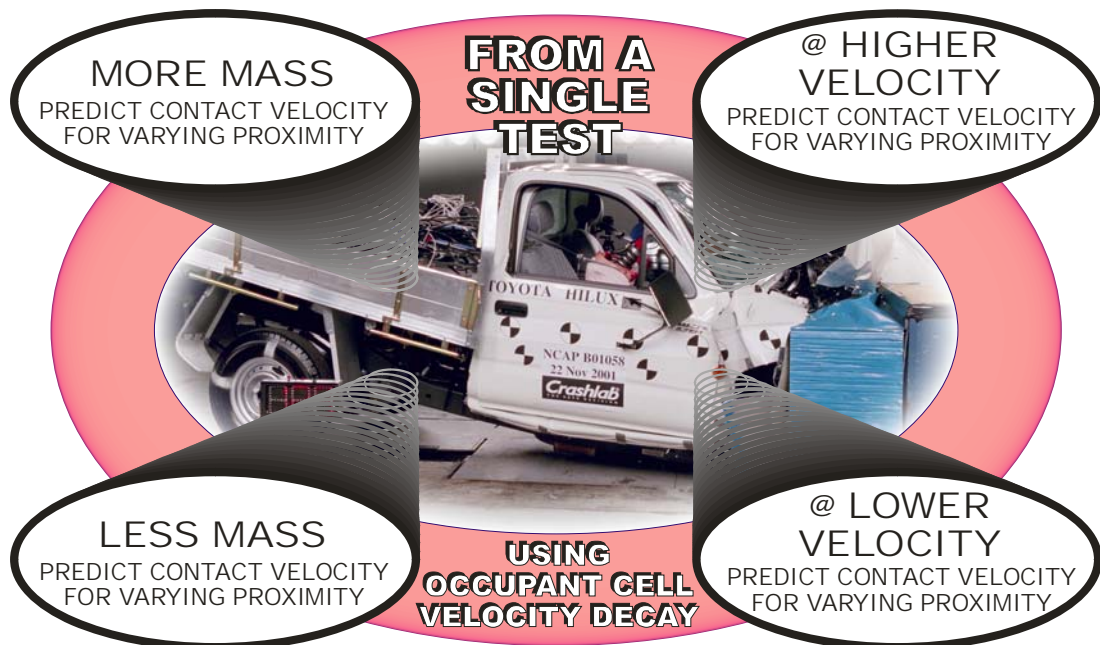


Figure 7-1: Visualization of hypothesis to be tested.

The requirement for the model to be developed here is to predict injury risk as defined, from a single crash test extrapolating to account for velocity and mass variations. The model is based on the haversine equation phased and repositioned to suit the need. Although the haversine was introduced earlier, it was presented parametrically. The parametric equations are solved in this chapter as a contribution.

It was shown earlier that good prediction of vehicle response does not necessarily equate with good prediction of injury risk.

Joksch (2000) uses the variable x to represent weight ratio of collision pairs in a fleet wide study. This merely accounts for momentum conservation rather than a stiffness change due to mass. The regression coefficients giving overall risk included dynamic and static stiffness. The effects of these coefficients were regarded as too remote to use on a vehicle by vehicle basis.

Ross and Wenzel (2001) also studied the fleet at large and emphasized that their mass-dependence result are mass-size dependencies, size being somewhat correlated to crush distance, following and quoting Evans and Frick (1992) who notes that mass and size are highly correlated.

Evans (2004a) asks the previously reported question: “Am I safer if I put bricks in my trunk?” confirming there are kinematic part-answers. Lamenting the lack of identifiable vehicle loading data in the National database, he proceeded to extract vehicle occupancy to vary mass in another fleet study. He concluded that adding a passenger reduces a driver’s frontal crash fatality risk by 7.5%. Although the improvement was at the expense of the other driver, his reference to single vehicle accidents clearly confirms his view that additional mass in a vehicle reduces injury severity.

The present chapter builds on Dr. Evans’ view. This work is distinguished by its focus on single vehicle behaviour (with respect to injury) rather than set in fleet demography and avoiding the potential obfuscation of momentum effects in a two-car collision.

Typically, test conditions fix vehicle mass, yet a typical suburban car will range from driver only loading to five or six occupants with luggage.

By varying the velocity or mass, a greater range of injury scenarios can be considered rather than just test conditions. This enhances the value of each crash test.

That an injury improvement at one crash velocity may reflect as an improvement at other speeds is an assumption which has not been fully disserted in the literature. It will be considered here by viewing the whole spectrum of velocities and normal vehicle loading.

A motor vehicle is a holistic compromise which should reflect the statistical significance of the causal factors involved. For example, if all occupants always sat a long way from the internal impact surface, all focus would need to be on rebound. In the other extreme, if all occupants sat touching the internal impact surface, preoccupation with vehicle deceleration would yield results. Clearly, the pole positions in the examples offer opportunity for optimization.

The procedure for prediction of response across the spectrum of conditions involves extraction of reluctance and coefficient of restitution from a single crash. Coefficient of restitution is covered more fully in the chapters dealing with rebound.

To permit earliest possible presentation of model development, the results of these chapters are pre-empted permitting a rebound velocity to be proportionally determined from initial velocity.

Two examples are provided making use of the model developed in this chapter. One example compares a production vehicle with the unique \$22USM ULSAB vehicle. The other example considers the enhanced injury ramifications of an hypothetical pillow interspersed between a girls chest and her seatbelt.

7.1.1 Injury Reluctance

Injury reluctance metric involves substitution of a reluctance value in the equations to minimize error in representing injury. This was introduced in an earlier chapter during introduction of the haversine method of representing injury. The haversine in the earlier chapter was presented parametrically. Equations will be developed in this section in X-Y Cartesian format eliminating the parameter as a contribution by the author. Equations [6.4] and [6-7] for contact velocity and proximity are repeated from the earlier chapter and rewritten to reflect present terminology needs. Reluctance is represented by Ω . Removing the fraction $\frac{1}{2}$ improves the flow of mathematics, reluctance being assigned to suit. The symbol V represents ingoing plus rebound to improve tractability. Equation [6-5] for contact velocity at a point in time becomes:

$$v = V \sin^2(\Omega \cdot t) \quad [7-1]$$

Similarly, proximity at a point in time becomes:

$$x = \frac{V}{2} \cdot \left(t - \frac{\sin(2 \cdot \Omega \cdot t)}{2 \cdot \Omega} \right) \quad [7-2]$$

Equation [7-3] is transposed for t :

$$t = \frac{1}{\Omega} \cdot \text{asin} \left(\sqrt{\frac{v}{V}} \right) \quad [7-3]$$

Equation [7-3] is substituted into Equation [7-2] to become:

$$x = \frac{V}{2 \cdot \Omega} \cdot \left(\operatorname{asin} \left(\sqrt{\frac{v}{V}} \right) - \frac{\sin \left(2 \cdot \operatorname{asin} \left(\sqrt{\frac{v}{V}} \right) \right)}{2} \right) \quad [7-4]$$

Where V is the absolute velocity differential between initial impact velocity and rebound velocity and v is the body part contact velocity at the time that x , the proximity, is achieved. Ω is the reluctance which best describes occupant cell motion with respect to injury.

Equation [7-5] can now be graphed to show the effect of increasing reluctance on injury.

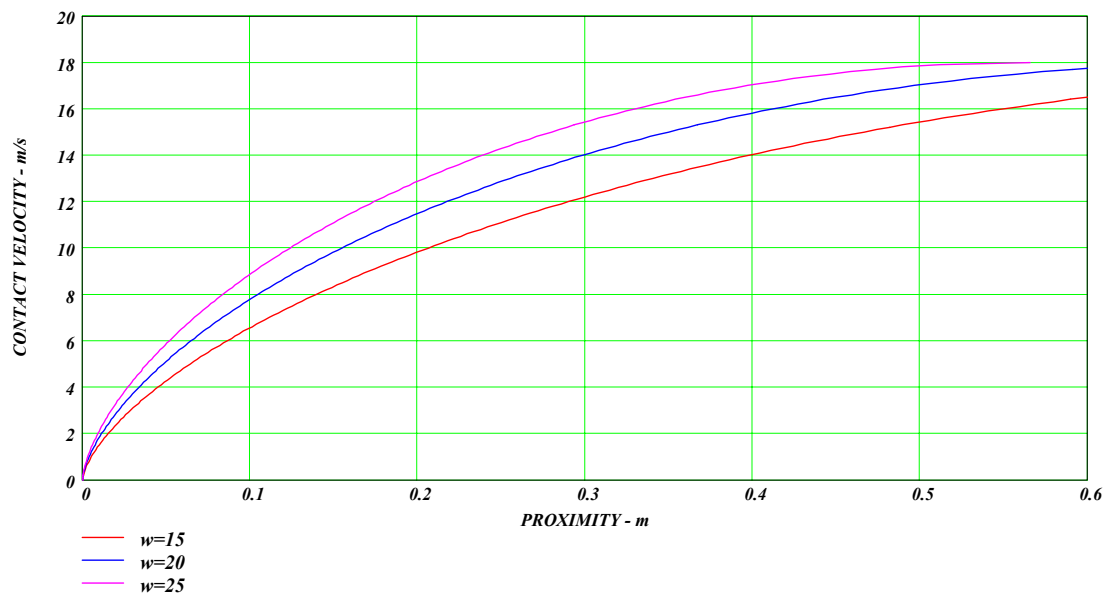


**Figure 7-2: Comparison of contact velocity at various proximities.
 (Initial impact velocity including rebound = 18 m/s)
 (Reluctances (Ω) shown as $w = 15$, $w = 20$ and $w = 25$)**

Figure 7-2 shows the effect of increased reluctance manifesting in increased injury. For example, for a reluctance (Ω) of $w = 15$ a 0.3 m body part proximity will incur a contact velocity of just over 12 m/s while the stiffer $w = 20$ will cause 14 m/s contact velocity.

7.1.2 Prediction for Different Velocity

Equation [7-4] fidelity with test data is shown in Figure 7-3. In this Figure, the data was arranged in a spreadsheet allowing the reluctance to be varied until representation of the data was visibly optimum.

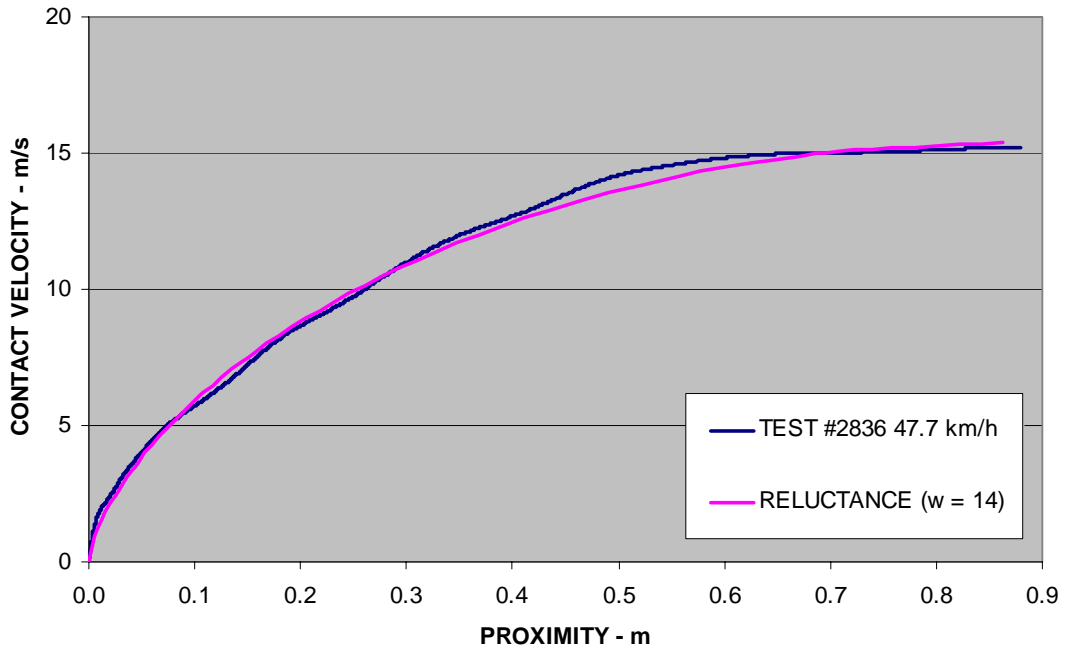


Figure 7-3: Determination of injury reluctance for Honda Accord Test #2836 by trial and error.

In order to determine the variance between contact velocities determined by the haversine equation and the test data it was necessary first to fit the test data to a representative curve. This was necessary due to the nature of solution of Equation [7-5]. The equation was recognized by the author to be a cycloid for which a known solution is available for the y -value as the independent variable. A 10th order polynomial was used explaining in excess of 99.95% of variance. This permitted variance determination with the haversine equation.

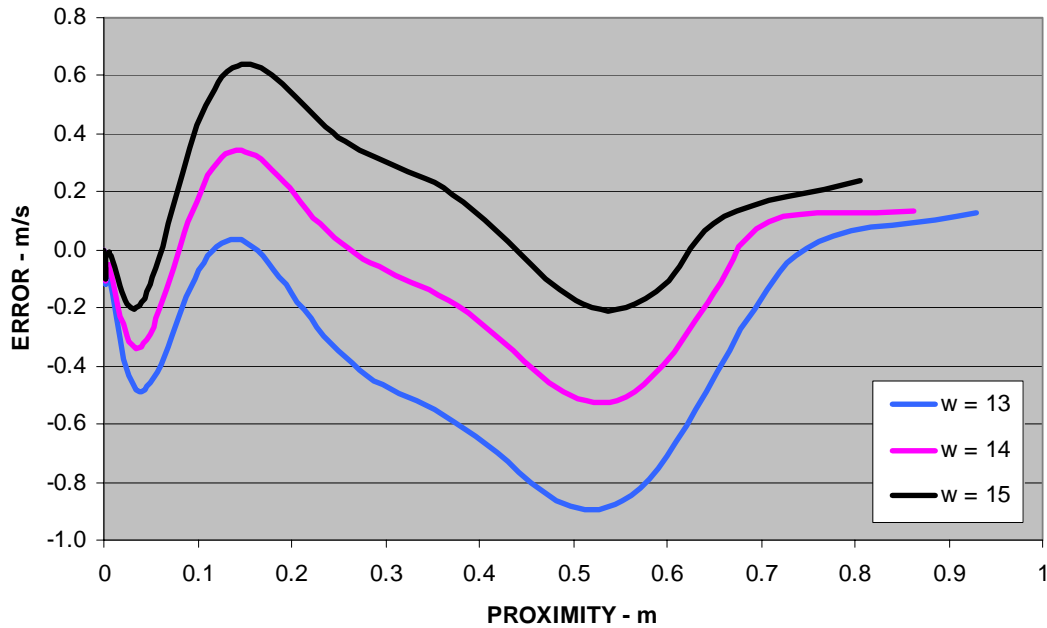


Figure 7-4: Error incurred by use of different reluctances (Ω) shown as $w=13$ to $w=15$.

The range of error varies little with reluctance and is considered later with the range of errors in the predicted situation. Figure 7-4 shows that an increase in reluctance can overstates injury. This has implications in certain types of reporting where categorical overstatement or understatement is a necessary approach. For example, in a criminal trial it would be necessary to show understatement so as to provide proof to a “beyond-doubt” quality. In a trial defence situation it may be of benefit to overstate to prove impossibility.

The reluctance determined by Figure 7-3 is used in Equation [7-4] here to predict injury at a higher initial impact velocity. Comparison is made with test data to evaluate prediction efficacy in Figure 7-5.

It should be noted that the accuracy is to some extent artificial since it uses rebound velocity from the actual test to be predicted. The value of this is to isolate a potential source of error that might confound the purposes of examining the potential of the haversine.

Predicting rebound is considered more fully later in the thesis in the context of fleet demography. Rebound as a proportion of initial velocity is used later in this paragraph for prediction purposes.

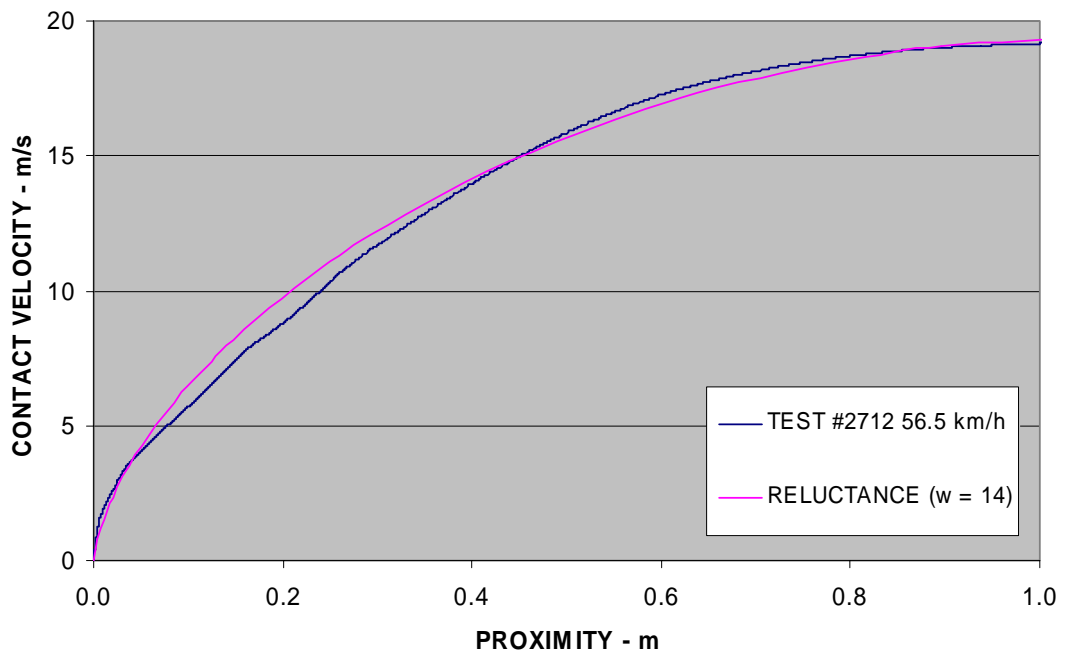


Figure 7-5: Prediction of injury and comparison with test data from Honda Accord Test #2712.

Table 16: Range of variation from test data summarizing Figure 7-6

Ω	BASE #2836 47.7 km/h			PREDICTED #2712 56.5 km/h		
	HIGH	LOW	RANGE	HIGH	LOW	RANGE
w=13	0.04	-0.89	0.93	0.72	-0.87	1.59
w=14	0.34	-0.53	0.87	1.09	-0.41	1.49
w=15	0.64	-0.20	0.84	1.45	0.01	1.45

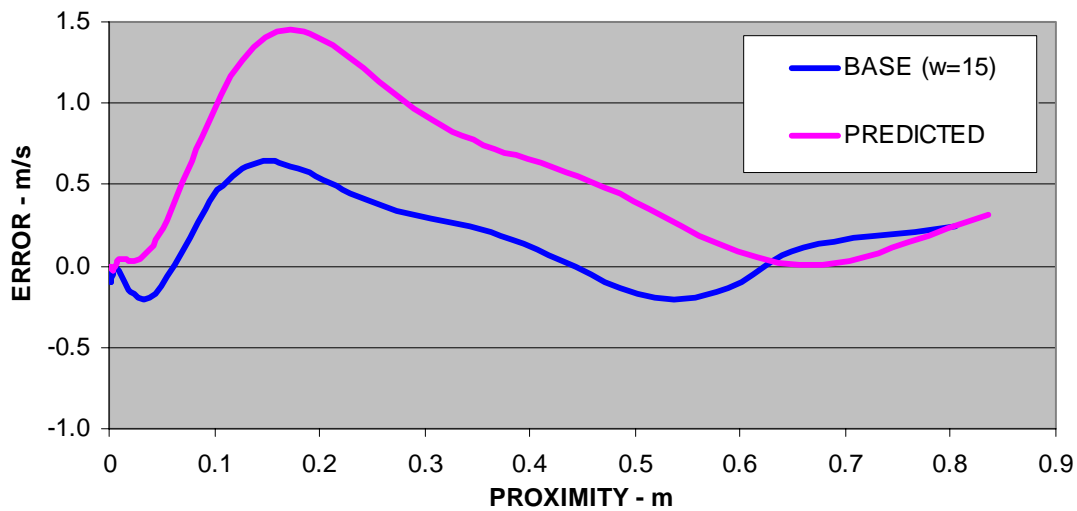
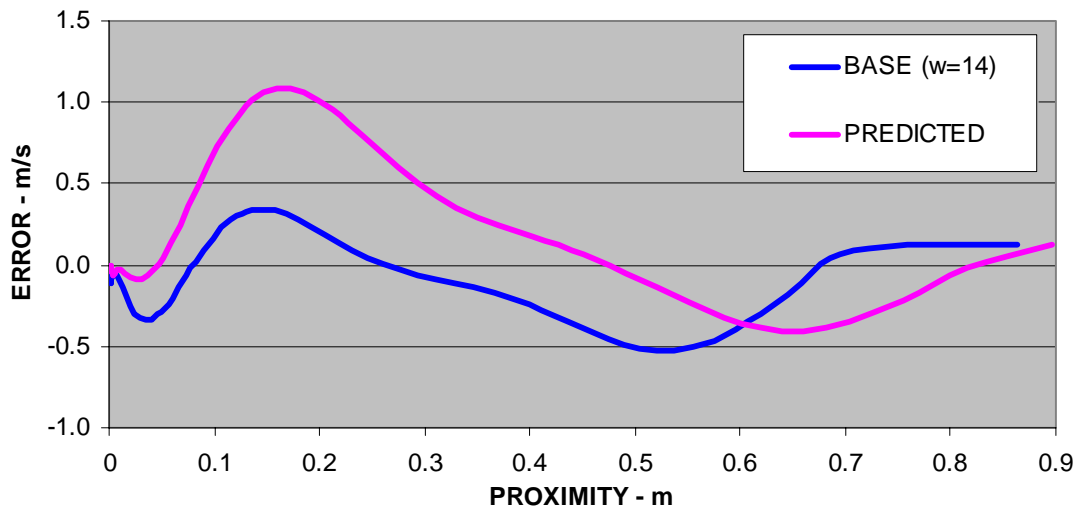
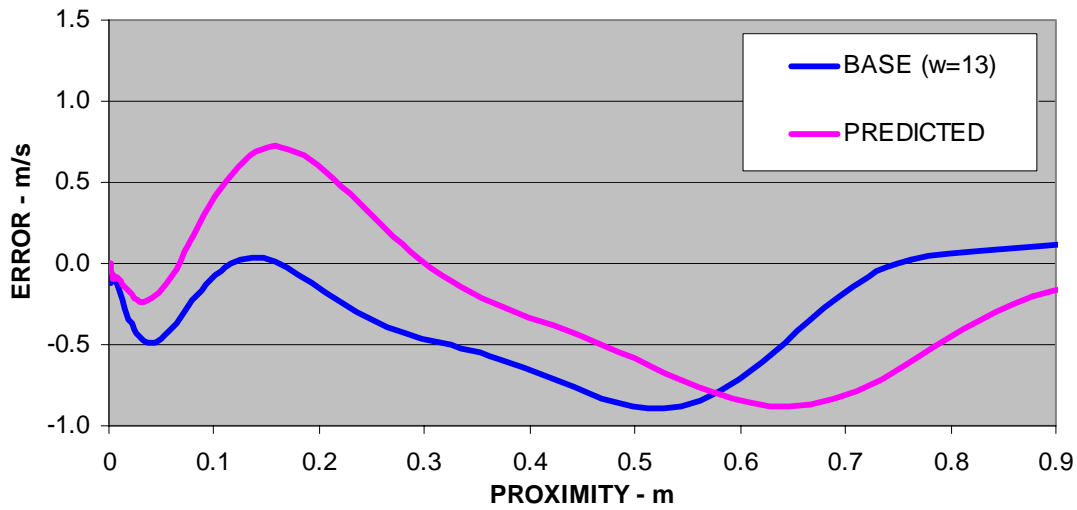


Figure 7-6: Variation from test data trying different reluctance values.

7.1.3 Accounting for Rebound

Rebound is shown later to be well represented as a fixed proportion of initial velocity. Accounting for rebound in prediction here is performed according to the following two steps:

1. Determine coefficient of restitution from base initial velocity and rebound velocity.
2. Apply coefficient of restitution so determined to initial velocity of prediction vehicle.

It is calculated in this way in the example to follow. Equation [7-4] is to be modified to account for rebound. First, by definition, coefficient of restitution is given by

$$c = \frac{R_v}{V_i} \quad [7-5]$$

Where R_v and V_i are rebound and initial velocity respectively. Absolute velocity differential V as defined previously is given by:

$$V = V_i + R_v \quad [7-6]$$

Equation [7-6] is modified by including Equation [7-5], as follows:

$$V = V_i + c \cdot V_i$$

$$V = (1 + c) \cdot V_i \quad [7-7]$$

Equation [7-7] can now be inserted into Equation [7-4] to provide the injury prediction model for this thesis accounting for both initial velocity variations and rebound velocity, as follows:

$$Px(v) = \frac{(1 + c) \cdot V_i}{\Omega} \cdot \left[\operatorname{asin} \left[\sqrt{\frac{v}{(1 + c) \cdot V_i}} \right] - \frac{1}{2} \cdot \operatorname{asin} \left[2 \cdot \operatorname{asin} \left[\sqrt{\frac{v}{(1 + c) \cdot V_i}} \right] \right] \right] \quad [7-8]$$

Where $Px(v)$ is proximity with contact velocity v as the independent variable.

To account for rebound, the coefficient of restitution is calculated from the test data of the base model. In the example below the test data shows an initial velocity of 15.6 m/s and a rebound velocity of 2.3 m/s for a 1990 Ford Taurus NCAP Test #1385. The coefficient of restitution is calculated by the above equation to be 0.147. Injury reluctance is determined at $\omega = 14$ by trial and error until the curve calculated by Equation [7-8] matches the injury curve derived from test data. The result is graphed below:

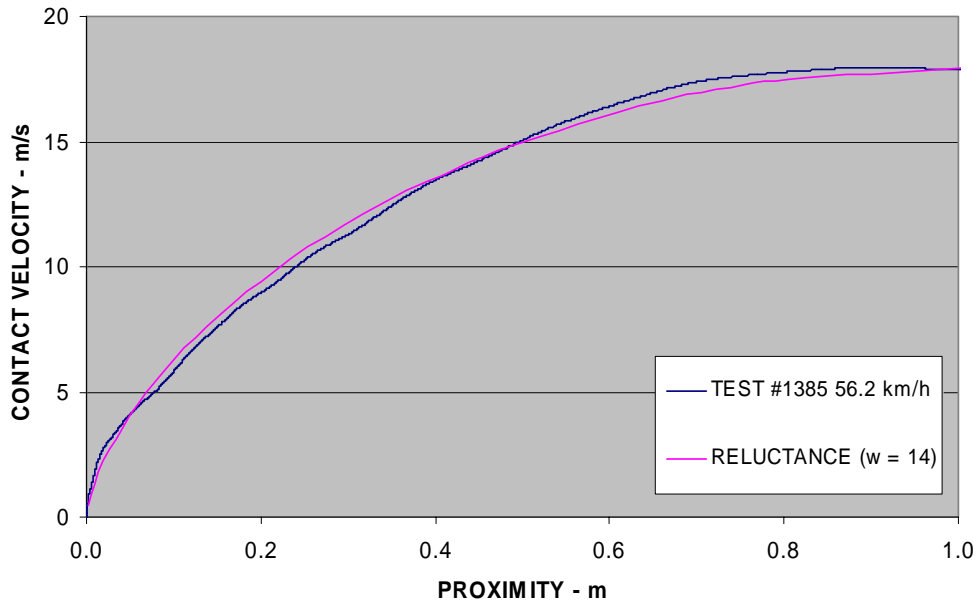


Figure 7-7: 1990 Ford Taurus injury test data used to derive reluctance.

Using the same injury reluctance and the same coefficient of restitution, Equation [7-8] is recalculated to suit a lower velocity test of the same model vehicle, being a statutory compliance test, Test #1403. The results are graphed below:

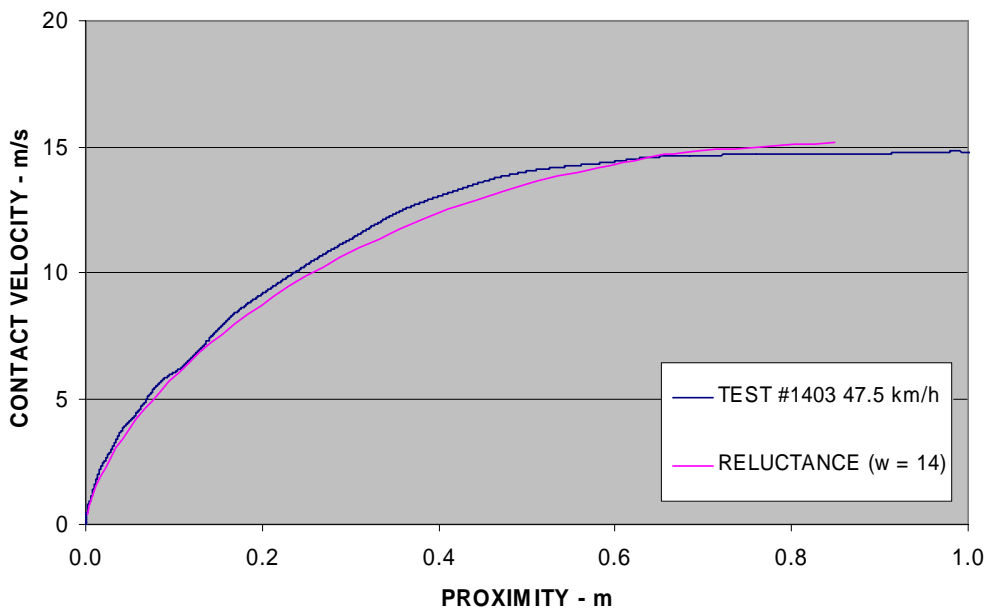


Figure 7-8: 1990 Ford Taurus injury values predicted from Test # 1385 and compared with test data from Test #1403.

Apart from the minor aberration around 400mm proximity, the prediction result is regarded as satisfactory, reporting contact velocities for a range of proximity to 800 mm.

7.1.4 Accounting for Vehicle Load Variations.

A passenger vehicle travelling on the road will have at least a driver and possibly four passenger and luggage. The working range of vehicle lading is thus estimated to vary from 75 kg less to 300 kg more than the usual test conditions comprising driver and passenger.

Vehicle mass affects injury profiles significantly. To predict the effect of mass variation on injury values, simulation results from SISAME simulations are used to check the result. The procedure to predict reluctance is as detailed in Paragraph 5.4.5.

In a typical prediction environment, the occupant cell mass would not be conveniently available. However, vehicle mass can be more easily determined. Accordingly, this analysis proceeds using vehicle mass.

Varying loading conditions are accounted for by varying the injury reluctance using the mass spring model as presented earlier. The reference (+300kg) and predicted vehicles are shown in Figure 7-9.

Table 17: Prediction of injury reluctance for lower vehicle mass.

VEHICLE BASIS	ADDED MASS	VEHICLE MASS M	CONSTANT STIFFNESS PARAMETER $k = \omega^2 \cdot M$	RELUCTANCE $\omega = \sqrt{\frac{k}{M}}$
REFERENCE	+300kg	1547 kg	334291 (1547 kg)	14.7
PREDICTION	-75 kg	1172 kg	334291 (1547 kg)	$\Omega = 16.9$

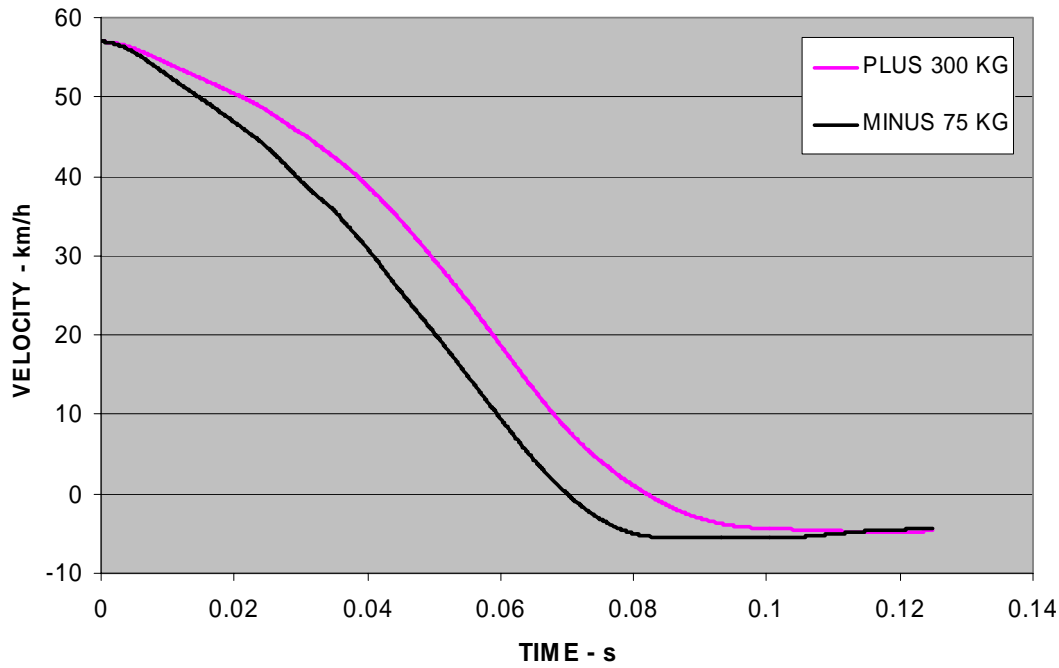


Figure 7-9: Simulated velocity decay curves for 1987 Toyota Celica from Test #1100 adding 300 kg and subtracting 75 kg from test mass.

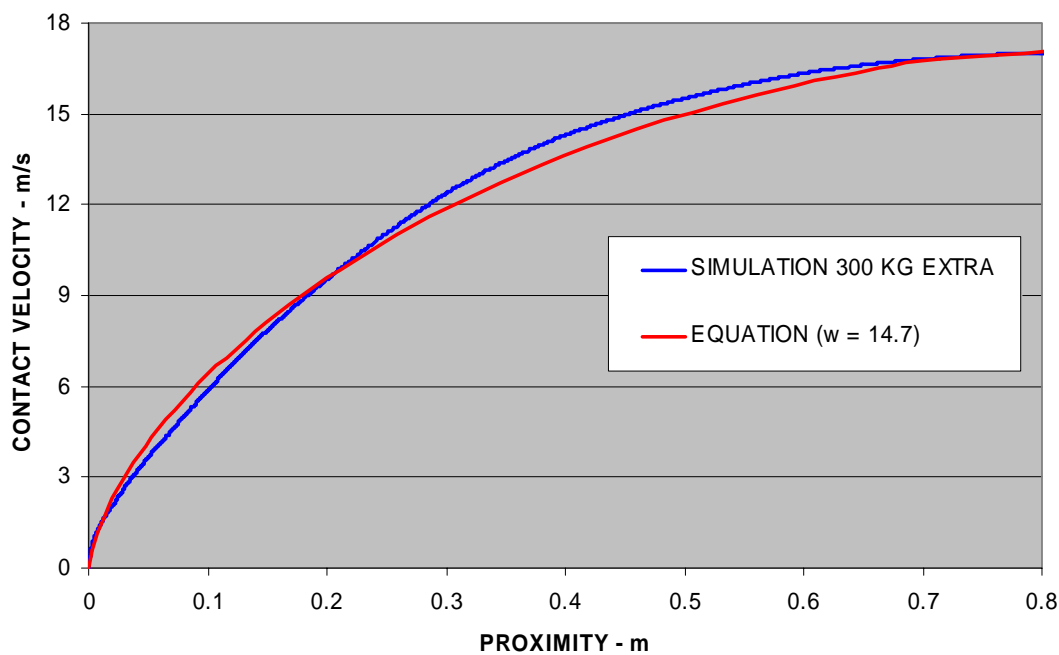


Figure 7-10: Injury values for simulated and mathematical models.

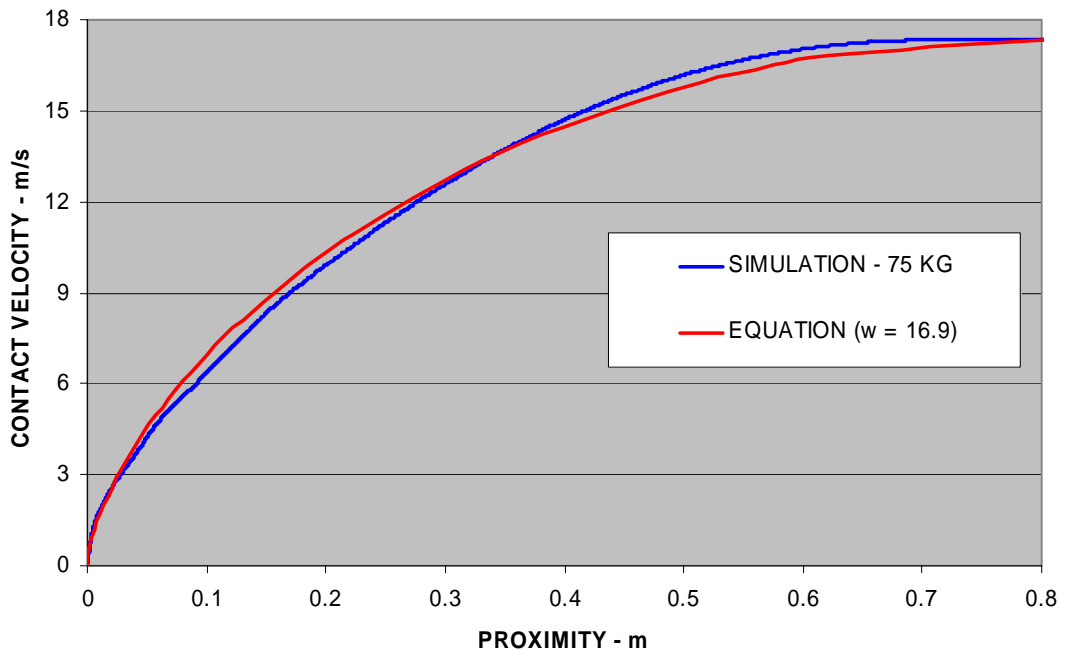


Figure 7-11: Predicted injury values from mathematical model.

Figure 7-11 shows a good prediction of injury values for variation in vehicle loading. Subject to further testing, there is now available a technique which enables mass variation to be taken into account when considering crumple zone performance expressed as injury risk.

7.2 Conclusion

An empirical mathematical model to predict injury from occupant cell response to frontal impact has been presented. The model was shown to predict injury risk over the full spectrum of proximities of body parts to internal impact surfaces, varying crash velocity and vehicle mass. The model answers the study hypothesis in the affirmative in this chapter. The remaining chapters are added in general support of the broader aims and objectives set earlier.

The performance of a crumple zone over a range of conditions can now be assessed by a single value for injury reluctance coupled with a single value for coefficient of restitution, both being available from a single crash test. Practical examples follow this conclusion.

The capability to predict over a wide range of conditions has implications for the following:

1. Compliance legislation.
2. Fitment of appurtenances e.g. bull bars and winches.
3. Accident repair.
4. Litigation support.

These items will be discussed in more detail below.

7.2.1 Compliance Legislation

It will be shown later that the practice of specifying maximum anthropomorphic dummy injury assessment reference values (IARV's) as achievement targets have been unsuccessful in bringing about real improvements. The legislation addresses peripheral issues in prescribing for remote causal factors while there are uncontrolled more direct causal factors at work.

Injury reluctance with coefficient of restitution are factors that go to the immediate causes implicated in injury reduction. Prescription of minimum values for these will provide quantitative and irrefutable gauging of performance and so set a pattern of real improvement.

7.2.2 Fitment of Appurtenances

Frontal protection bars were originally designed to prevent immobilization in the event of animal strike at remote location. They are now prolific in suburban streets protecting the owner from errant shopping trolleys at best. It is believed (by the owners) that they also improve crashworthiness. A definitive study has not been found by the author that links bull

bars to improved crashworthiness without increased aggressivity against the collision partner.

In a user-pays society an objective standard is needed to levy a charge on those road users who impose additional injury risk on others by the voluntary fitment of frontal (and rear) appurtenances. Maximum injury reluctance and maximum coefficient of restitution can provide such an objective standard to empower legislation.

Manufacturers of the appurtenances can show objectively the performance of their product.

7.2.3 Accident Repair

Front rails comprising the crumple zone are key elements in the crashworthiness response of the vehicle. Repair of these and other structural members by welding and splicing may affect the strain hardening initiated during manufacture. Splicing may strengthen undesirably. Crashworthiness performance after repair may therefore be impaired. Little is known in the repair industry about the crashworthiness of accident repair. (Dixon (2002)

A simple but objective standard of crash performance after repairs such as is provided by injury reluctance and coefficient of restitution may encourage the industry to develop a code of practice for accident repair.

7.2.4 Litigation Support

The enhanced injury doctrine dates back to a court case in 1968 where severe injuries were sustained by the plaintiff Larsen from steering intrusion in a 1963 Chevrolet Corvair. The court supported the idea that the injuries were enhanced on account of defective design rejecting General Motor's argument that there was no duty to design a vehicle to be safer to occupy during a collision, the vehicle purpose being other than for crashing. The decision fell short of imposing a requirement to design a vehicle intended for crashing but limited itself to those injuries above and beyond injuries which would have occurred anyway. (Ricci, Leopold et al.)

There are technical difficulties in determining what normal injuries are and what constitutes an enhanced level of injury with respect to a crash pulse and bio-mechanical interaction. A crash may occur at any speed, yet crash tests are performed at set speeds. A crash may occur when a vehicle is driver-only occupied or full of passengers with luggage.

This is where the present model is helpful by accurately predicting injury risk at conditions extrapolated from test conditions.

7.3 Example 1 –Production Vehicle vs ULSAB Injury Performance.

7.3.1 Introduction

In a subsequent section the \$22USM Ultra Light Steel Auto Body (ULSAB) vehicle is considered more fully. Here it is compared with injury performance with a vehicle of similar mass. The work is a contribution by the author to show the value of the techniques presented earlier. No particular search was done to find a vehicle “better or worse” than the ULSAB, the choice being based on convenience. The comparison vehicle selected was a 2002 Model Nissan Altima.

7.3.2 Published Vehicle Acceleration

The ULSAB consortium published an acceleration curve P32 ULSAB (1998) in raster image format. To use the information in a spreadsheet required vectorization. This was performed and posted to Figure 7-12:

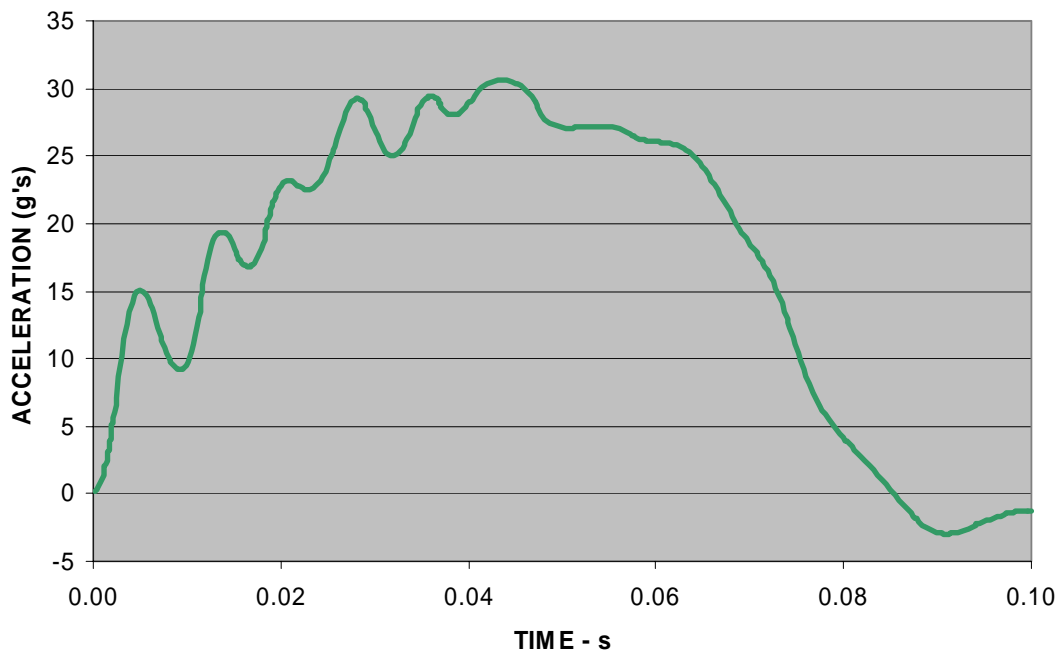


Figure 7-12: Vectorized copy of published ULSAB average car acceleration.

The accelerometer data for the comparison vehicle was sourced from an NCAP test NHTSA Test #4215. The left and right seat accelerometers readings were averaged and filtered to 60 Hz. then made positive to correspond with the ULSAB convention and graphed in Figure 7-13.

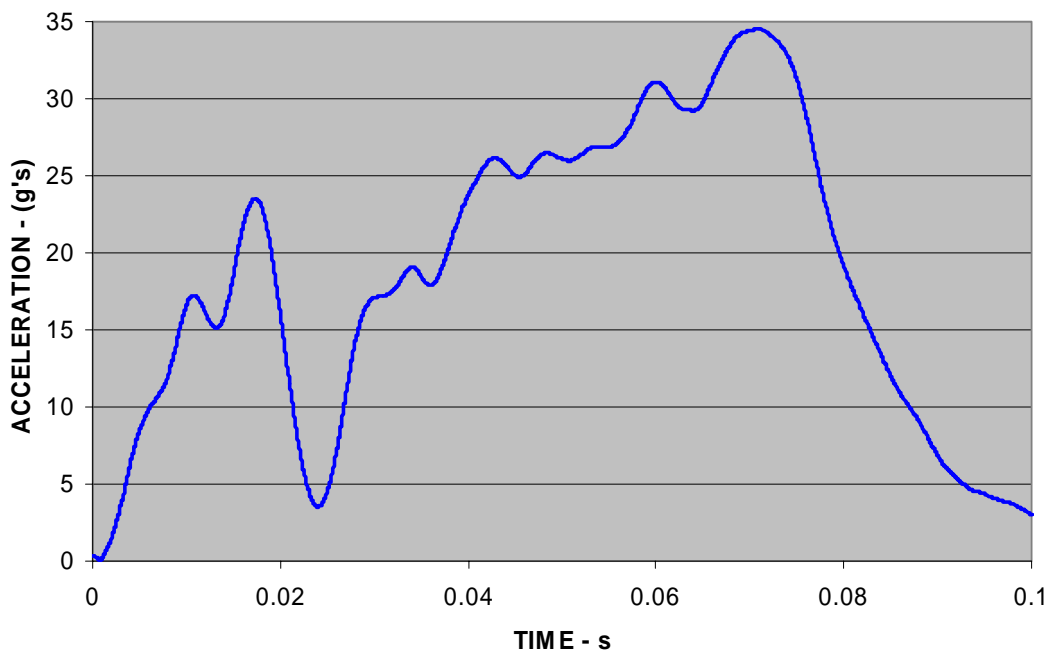


Figure 7-13: Accelerometer data for occupant cell Nissan NCAP Test #4215

The early fulgurant peak in Figure 7-13 and subsequent trough is significant and manifests in a levelling out of velocity decay at the 0.02 to 0.03 second zone. Also worthy of note is the high acceleration peak. The significance of such a peak was considered in Section 3.6 Optimum Pulse Shape on Page 3-68.

7.3.3 Velocity Decay of Comparison Vehicles

The acceleration data was time integrated and applied to initial velocity and subsequent velocities following the impulse-momentum arguments. The initial velocities varied from vehicle to vehicle as can be seen in Figure 7-14. This was not expected to affect comparisons of injury in the lower values of proximity as contact velocity was taken from the appropriate initial velocity.

The red arrow marks a velocity plateau. The plateau has the effect of improving injury risk. Brell, Thambiratnam et al. (2002c) showed the reduced injury effects of such a plateau. The effect of the velocity plateau resulting from the early force peak followed by the force trough is described below.

It is noteworthy that the pulse time (a metric sometimes used to assess crumple zone quality) is increased in the Nissan as compared with the ULSAB vehicle. By contrast, the rebound velocity is greater for the Nissan as compared with the ULSAB vehicle.

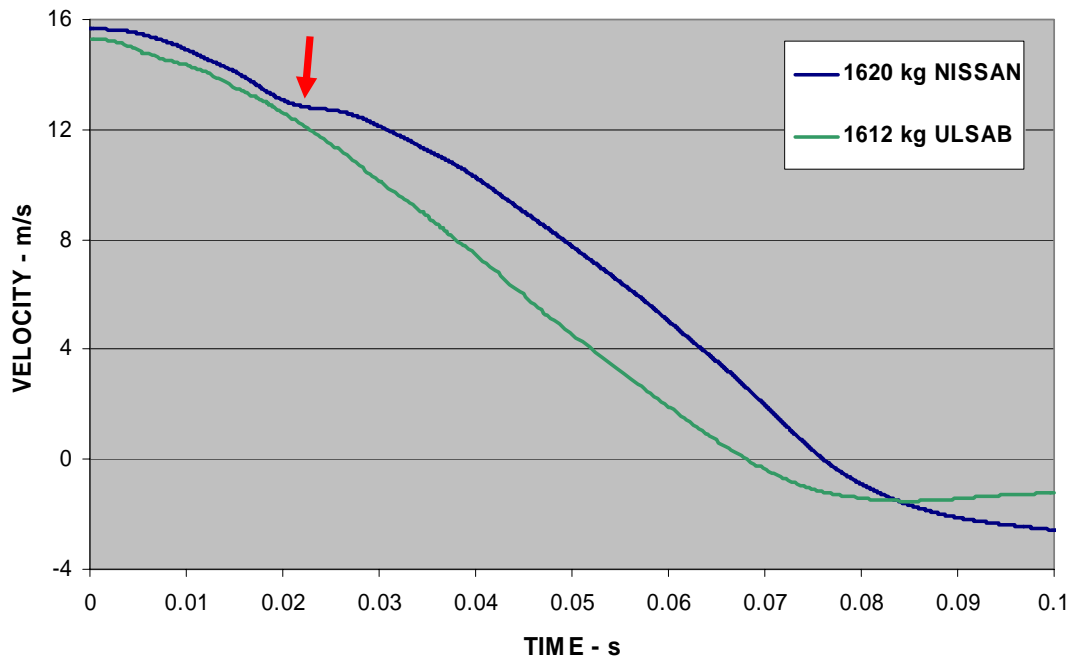


Figure 7-14: Velocity decay for ULSAB and Nissan vehicles.

7.3.4 Injury Risk Comparison

Generally as described in Chapter 1, the injury risk, contact velocity or body part velocity differential at point of internal impact was calculated for each time increment (50 microseconds for the Nissan). At the same time increment the additional area above the velocity curve was calculated and added to the previously calculated distance. Contact velocity and proximity could thus be graphed in parametric fashion with time the parameter. The results for both vehicles were graphed in Figure 7-15.

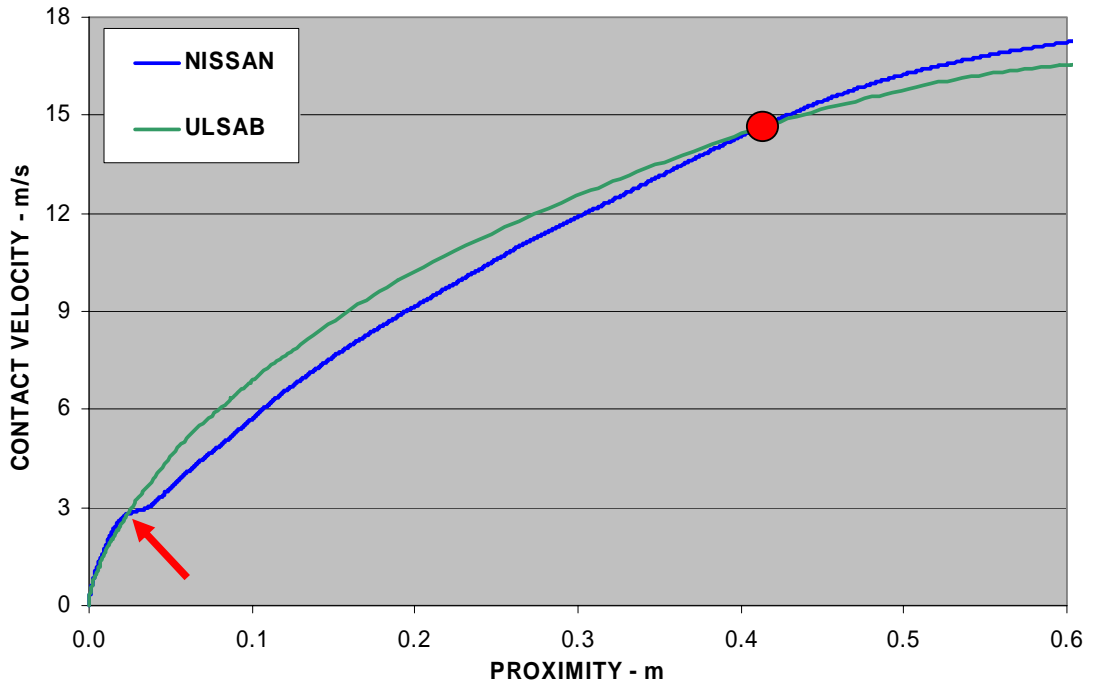


Figure 7-15: Injury risk comparison of ULSAB Vehicle with 2002 Nissan Altima.

The red arrow in Figure 7-15 marks the start of the plateau at the corresponding red arrow in Figure 7-14. It will be noted that the Nissan improves injury risk from the arrow to the red dot. The influence of rebound can be seen for proximities beyond the red dot.

7.3.5 Conclusion

The published acceleration profile of the ULSAB vehicle for NCAP crash testing velocities was compared with the NCAP test results of a similar sized vehicle. It was shown that a trough in the acceleration profile just after a fulgurant peak was responsible for significant improvement in injury risk in the comparison vehicle even though peak acceleration was higher than the ULSAB vehicle.

The comparison highlighted the need for early improvement in the crash pulse in the ULSAB vehicle as well as need for improvement in rebound velocity in the Nissan.

7.4 Example 2 – Safety Implications of Seatbelt Slack.

7.4.1 Introduction

An hypothetical example that utilizes all the concepts disserted earlier to summarize and emphasize the practical aspect of the work. The example is a contribution by the author. To reduce complexity and maintain relevance a preliminary expert position statement is proposed. The facts could be varied to reflect seatbelt slack with identical results. Two crash tests are used at two different impact speeds. One crash test is used for verification. The problem is considerably simplified for the purposes of illustration of the principles involved. A full assessment would include the coupling phase being affected by the cushion. The exercise distils to predicting injury from a lower velocity test to a higher velocity, comparing the contact velocity from the predicted case. The prediction is compared with the ‘real’ profile from the verification test for the purposes of this thesis.

7.4.2 Problem Statement

A litigant has sustained chest injury as a passenger in a 2001 Dodge Caravan. It is argued that a soft pillow between the chest and seatbelt placed there to defeat the steady (and annoying) tension of the inertia reel interfered with the design of the restraint system. The defence argued that such interference exacerbated the injury so potentially reducing compensation by principle of contributory responsibility. The passenger was 5th percentile female as shown before and after the crash in Figure 7-16.



Figure 7-16: Fifth percentile female in 2001 Dodge Caravan (pix mirrored to simulate Australian conditions).

Assume impact velocity was 56 km/h and collision partner impact interface was equivalent to rigid barrier impact.

Agreement has been reached that the pillow accounted for an additional slack of 100 mm changing the actual slack from 150 mm to 250 mm. The argument that the thickness of the pillow when crushed did not provide extra cushioning had been resolved. Occupant cell velocity profiles are determined below.

The profiles of the two vehicles are extracted from left and right accelerometer data readings. The data is checked for gross error and averaged. A smoothing filter takes out high frequency peaks and the signal is integrated with respect to time to arrive at velocity profiles. These are shown in Figure 7-17. The test data units in kilometres per hour are retained for Figure 7-17.

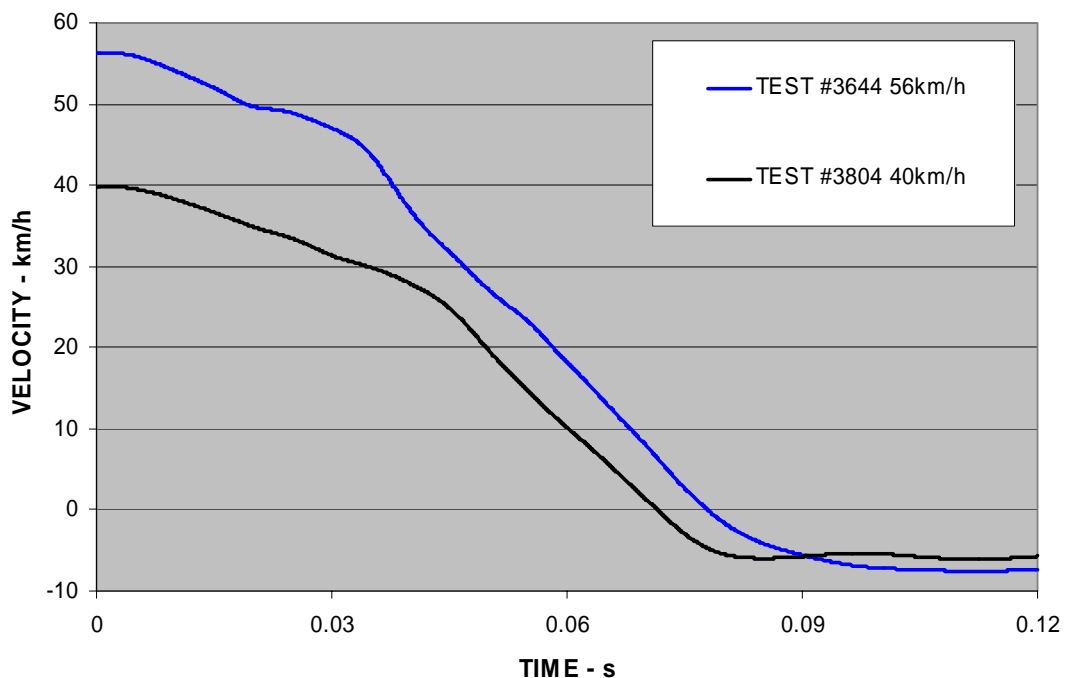


Figure 7-17: Velocity-time curves for 2001 Dodge Caravan.

7.4.3 Solution

Knowing that fidelity is needed in a specific area of proximity, injury optimized reluctance is chosen as the method of calculation.

The reluctance was varied manually in a spreadsheet to achieve a visually good fit for the proximity range needed. The best reluctance outcome ($\Omega = 16$) was graphed Figure 7-18.

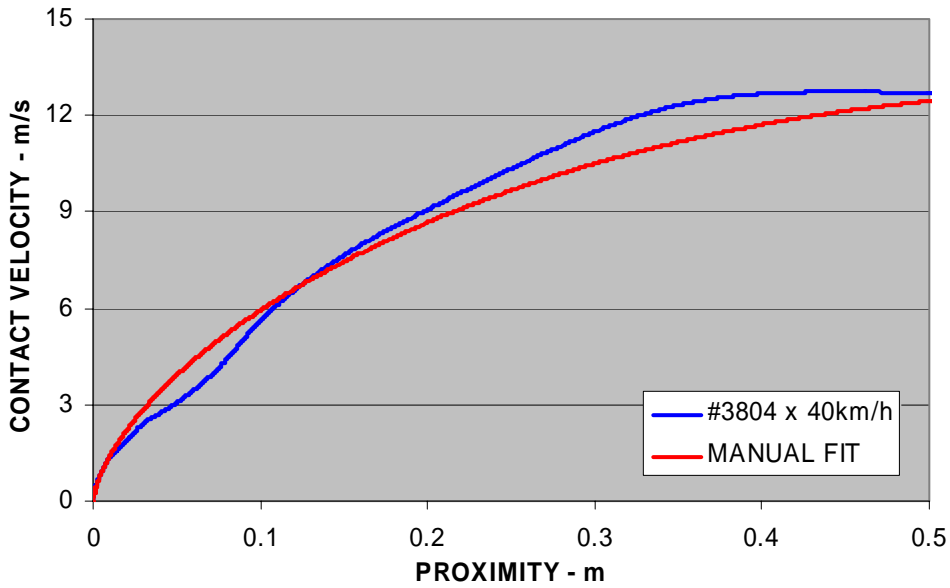


Figure 7-18: Manual-fit of 2001 Dodge Caravan crash test data (to suit maximum 0.25 m proximity).

The reluctance ($\Omega = 16$) determined for test velocity (40km/h) is to be used to predict at the incident velocity (56km/h). Coefficient of restitution is determined as per Paragraph 7.1.3, contact velocity calculated to Equation [7-8] and used to derive Figure 7-19. Test data is added to demonstrate the quality of prediction.

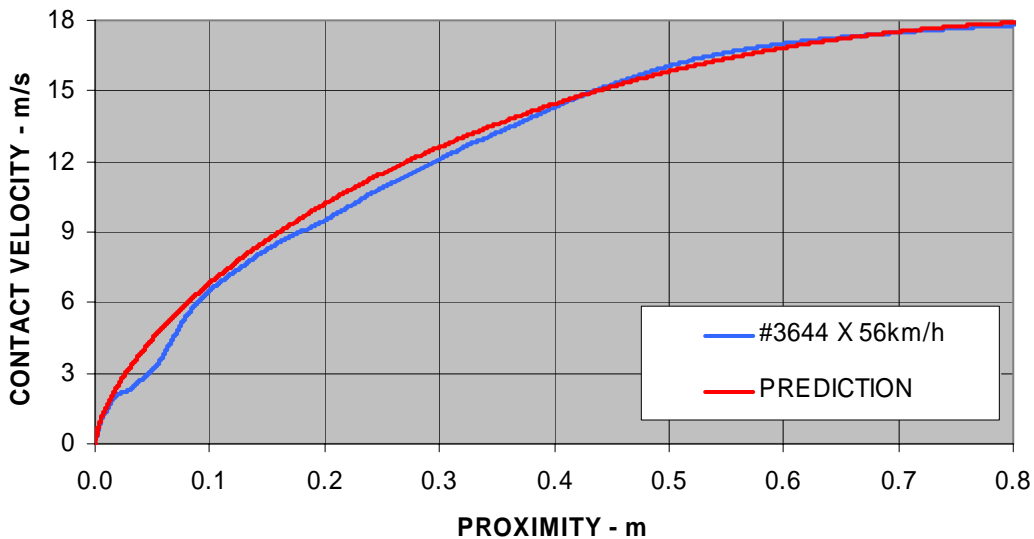


Figure 7-19: Predicted contact velocity compared with test data.

The scale is magnified in the appropriate area to facilitate reading in Figure 7-20.

7.4.4 Conclusion

The Interspersal of the pillow accounted for an additional slack of 100 mm changing the actual slack from 150 mm to 250 mm. Figure 7-20 was predicted from a vehicle test at 40 km/h for the incident speed of 56 km/h. Reading from Figure 7-20, the contact velocity increases from 8.7 m/s to 11.5 m/s.

Accordingly, interspersal of the pillow would have exacerbated the seatbelt injury.

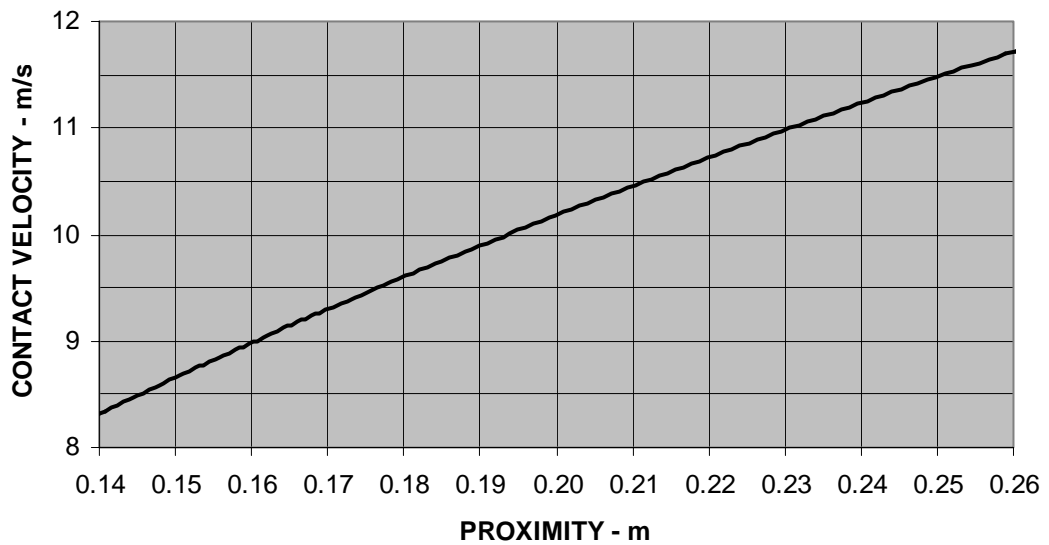


Figure 7-20: Predicted contact velocity for 2001 Dodge Caravan at 56 km/h (from 40 km/h)

BLANK

8. INERTIAL STRESS

8.1 Introduction

Frontal impact models in the literature typically assume that the crumple zone applies force to the occupant cell and that as a result of this force, the occupant cell retards. This paradigm is implicit in the mass-spring analogy as well as the lumped parameter model shown in Figure 5-5. One of the objectives of this chapter is to place this assumption into perspective with strain propagation. The assumption simplifies by ignoring energy absorption that might occur at right angles to the load path or ignoring the mechanism by which retardation of the occupant cell might occur from the rear of the vehicle where strain wave reflection can take place. The focus of this chapter is to provide a pointer to further simplified research into occupant cell motion that takes account strain progression. The work of others is presented because of the magnitude of effort involved in the present methods requiring weeks of continuous 'top-end' computer running.

Simple laboratory experiments are presented merely to support the knowledge of strain propagation. The quantitative details are minimized wherever possible as the subject matter is well-grounded in the prior art. Notwithstanding, the experiments gave insights not found in the literature.

This chapter also provides foundation to the chapter on vehicle rebound and is a contribution by the author. Since rebound is the result of strain energy storage, it helps to consider how the strain energy is dispersed during the progression of impact. Under impact loading, strain is not evenly distributed throughout the member immediately but localizes at the point of impact. Such localization does not affect the condition of the distal end of the member until the strain disturbance has reached the distal end. Such localization ignores slenderness considerations and can bring one end to plastic deformation while the other end remains unstressed. Equilibrium of forces under these conditions is provided by the inertia of the material, hence the title.

This chapter also considers inelastic strain, a predominant source of energy dissipation. Salience relates to wave motion, its initiation and prolongation.

The progression of the occupant cell towards the barrier when viewed positionally with respect to time appears smooth. The highs and lows of the accelerometer are absent in an optical trace (high speed film) and have no physical expression in a double integration representing transient displacement.

This section discusses the presence of the highs and lows in accelerometer data in terms of continuous strain progression, reflection and collision. The complexity and speed at which events take place it is not feasible to monitor strain progression as one might in a split Hopkinson apparatus. The motivation for this section is to take existing strain wave theory and present it in simple but innovative experiments and discuss how these relate to a crash event to understand better a crash and rebound formation.

A finite element analysis of a level of complexity needed to obtain strain progression is beyond the resources and intent of the present work. Rather, the results of an analysis performed by others are represented such that the salient events are highlighted. The interpretations are a contribution of the author.

The order of presentation is to establish the presence of wave motion in the accelerometer data, then present the finite element analysis. This is followed by reporting of a series of simple experiments concluding with their relevance to the finite element analysis. Load cell readings for a number of vehicles are examined local to the main crash load bearing members for evidence of force reduction with velocity decay.

A summary considers the implications of inertial stress on injury mitigation.

8.2 Strain Progression

Barrier force data shows the progression of impact commencing with a rising force. This accounts for the crushing of soft items like bumper and radiator. Then there is a rise in force when the vehicle structure properly engages. It takes time to strain the whole vehicle. The very earliest strain reflections returning from the rear of the vehicle account for 30 mm of progression of the occupant cell. (Using nominal values for celerity of 5000 m/s on a 5 m vehicle impacted at 15 m/s.)

A typical vehicle is made up of many components. Where parts join or terminate, reflection and superpositioning of a pulse onto another pulse occurs. As the crash progresses a chaotic cacophony of wave peaks and troughs reverberate throughout the structure. To give an indication of the response of a vehicle structure under crash impact a highly magnified series of accelerometer readings are presented. The close-up view is to encourage the perception that a motor vehicle structure quivers in response to impact.

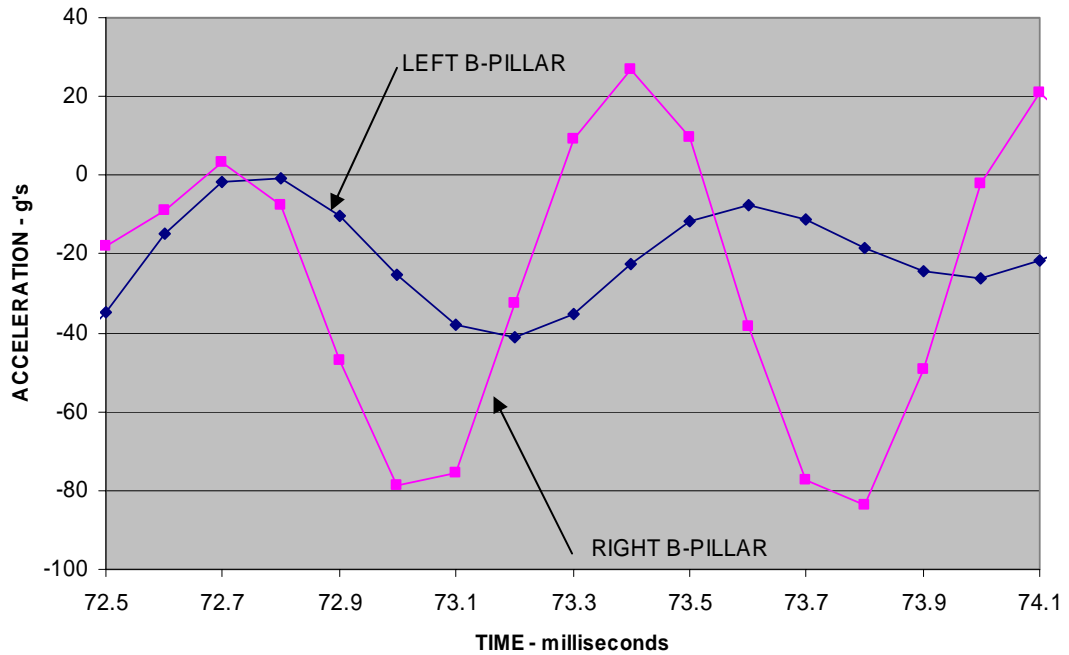


Figure 8-1: Typical accelerometer readings of left and right B-pillar undergoing crash-induced impulses.

At 72.7 milliseconds it can be seen in Figure 8-1 that left and right B-pillars are unloaded. Then in the space of 3 tenths of a millisecond the right B-pillar is accelerating 80 g's only to decelerate 100 g's in the next 4 tenths of a millisecond to await the next impulse.

A simple calculation (5000 m/s for .0001s) will show the wavelength of the pulses to be approximately 5 metres, a nominal car length. This means a pulse traverses the length of a car every millisecond sometimes in opposite directions and out of phase as shown in Figure 8-1

During the early traversal of the strain wave, reflection and redistribution of the waves cause concentration and localization. As the crash progresses, strain superposes over existing strain. Where material narrows or at a reflection point, stress is elevated. Concurrently, unloading occurs in other parts of the vehicle structure. (Jirásek (2002)

Reflection also takes place at the interface where plastic flow is occurring. Johnson (1972). The tertiary phases of the crash would thus see a shortened path for the elastic waves reflecting off the crushed front end.

Jones and Yu (1995) note that plastic strain energy density is concentrated near the impact point, supporting deformation localization under the dynamic conditions of impact.

8.3 Finite Element Analysis

The complexity and computational expense of a complete vehicle non-linear finite element analysis position such an undertaking beyond the intent of the present study. There is value however, in studying such an analysis by others for implications in inertial stress and stress propagation.

In 1992 the Clinton administration instigated a Partnership for a New Generation of Vehicles (PNGV) as a non-profit organization to encourage government and automobile manufactures in the research and development of new vehicles technologies that are safer, stronger, and lighter 3 times more fuel efficient. In early 1994, a consortium of 35 sheet steel producers from 18 countries set out to demonstrate a lightweight steel auto body structure that would meet a wide range of safety and performance targets.

In defence of its dominance against aluminium and composites, the steel industry presented its lightweight ULSAB²⁰ vehicle in 1998. The \$22USM vehicle continues to be a show piece for the industry holding pride of place in the 2004 “Great Designs In Steel” seminar. In its mission statement, AISI (2003) expects its “automotive team ... to make steel the material of choice for the fabrication and assembly of light vehicles (cars and light trucks) that will provide growth (volume and/or value) for steel companies” confirming that steel will continue to be dominant in the manufacture of cars.

The International Iron and Steel Institute supply photographs of the ULSAB car for downloading II&SI (2004). A collage (assembled by the author) of some of these photos is presented in Figure 8-2. To demonstrate legislative compliance with respect to crashworthiness of the USAB vehicle, a non-linear finite element analyses (FEA) were performed by Porsche Engineering with impact loading to represent different crash sequences. Of particular interest here is the NCAP full frontal rigid barrier test FEA. Each of these analyses was a significant undertaking with 178,386 elements (ULSAB (1998) used in the discretization of the vehicle. The software used was LS Dyna 3D explicit finite element analysis code, modelling all spot welds and laser welded areas.

The software Hallquist (1998) used is eminently capable of taking account of the usual geometric, boundary and material non-linearities as well as strain rate dependent plasticity and stress waves. Material constitutive models incorporating strain rate effects were provided by the Oak Ridge National Laboratory for the project. (Simunovic and Zacharia (1999)

²⁰ Acronym for Ultra Light Steel Auto Body

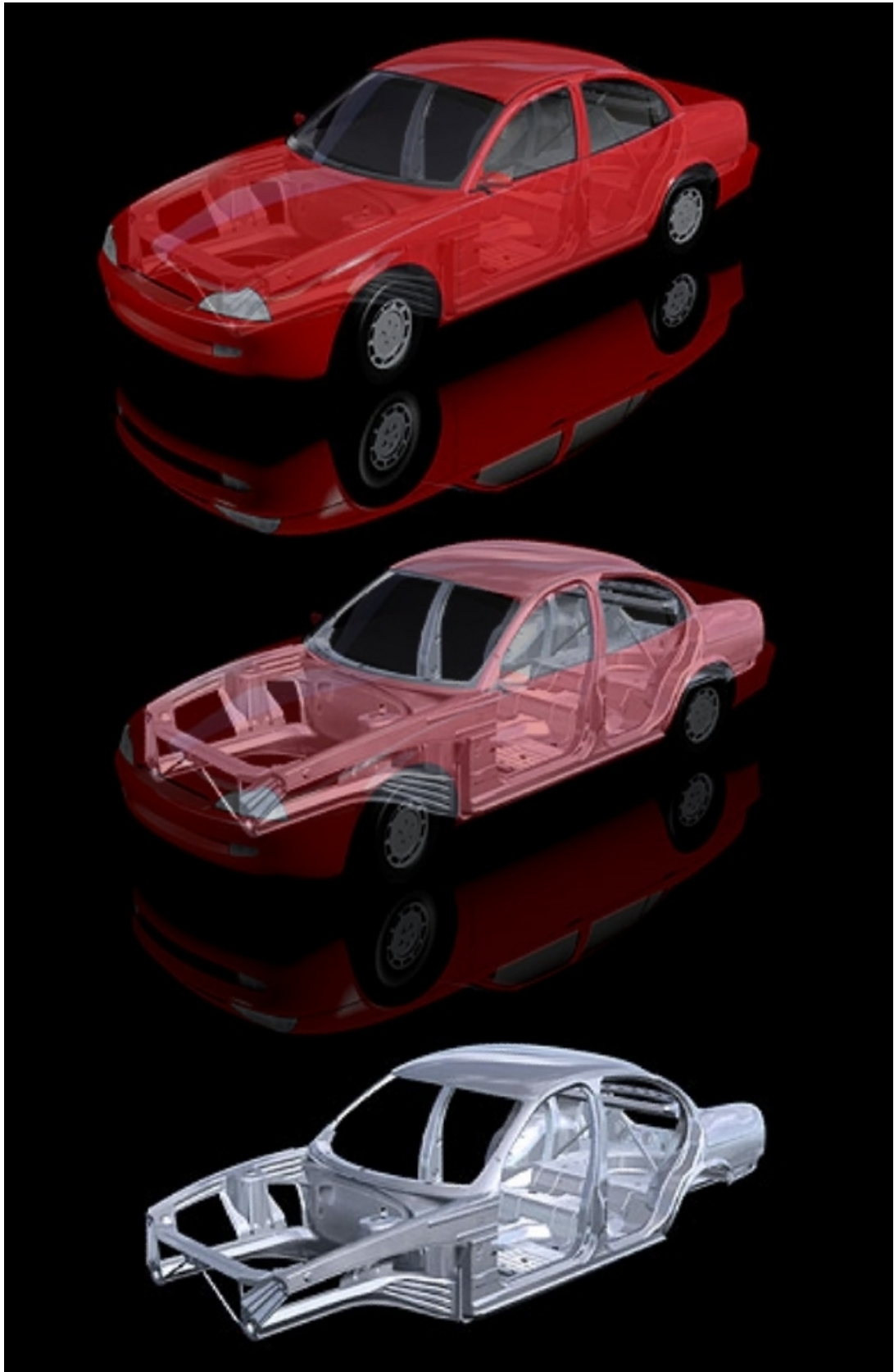


Figure 8-2: Progressive skeleton of ULSAB vehicle from cosmetic to structure.

The results of the finite element analysis were posted on the Porsche web site as a small animated GIF²¹ file. When decomposed into their time-sequenced still snapshots the raster images could be reprocessed. Three images were extracted, resampled and a Gaussian blur added to improve on the low resolution GIF rendering. In order to show relevance of each time-based snapshot, a cosine velocity decay curve is added showing the approximate occupant cell velocity at the time. The three images and the velocity decay are shown in a collage of sequences from ❶ to ❸ in Figure 8-4

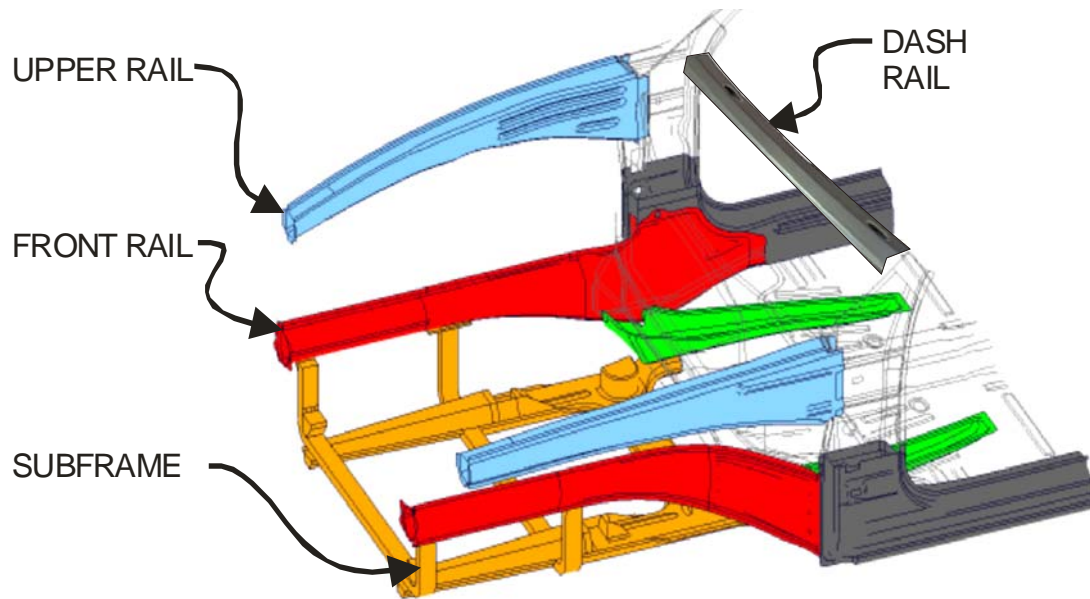


Figure 8-3: Terminology for ULSAB vehicle components.

The colour coding corresponds with peak loading as follows (ULSAB (1998)):

1. Front rail 120kN
2. Upper Rail 41kN
3. Subframe 49kN

²¹ CompuServe's GIF, or Graphics Interchange Format.

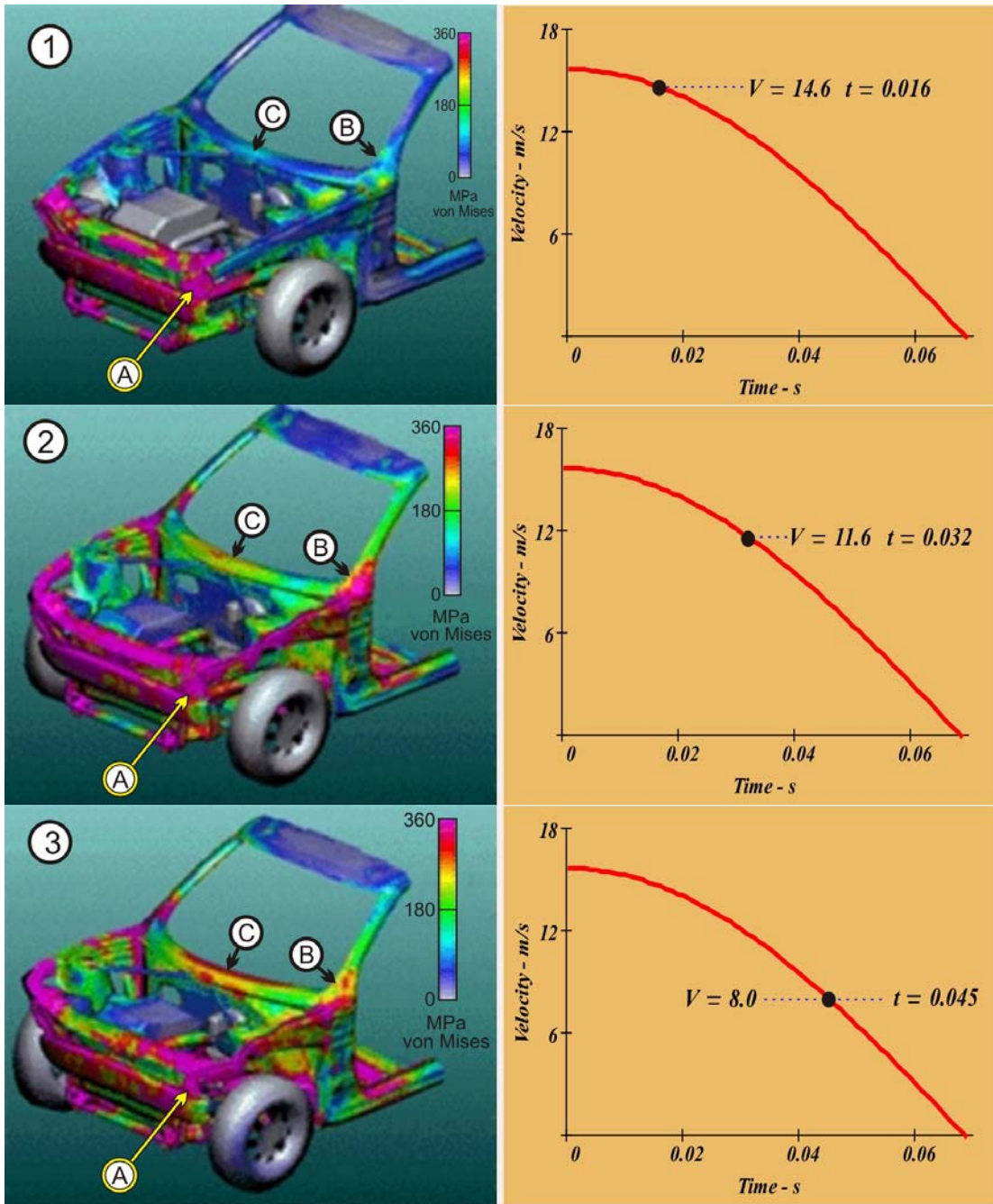


Figure 8-4: Non-linear finite element analysis of ULSAB vehicle under conditions of NCAP crash test showing also time-corresponding occupant cell velocity.

Two items are of particular interest, as follows:

1. The curved shape of the upper rail. In a quasi-static analysis a columnar end load would give rise uniform stress as well as bending stress. In the dynamic progression of the crash, buckling had not occurred in Sequence ① in Figure 8-4 even though the front section at ① was loaded to yielding at 350MPa von Mises Stress Criterion. First buckling of upper rails occurs at 0.021s as indicated in Table 18. This indicates localization of stresses to yield point at ① in the load path to the shock tower and ②.
2. Loading of the dash rail at ③. The progression of stress is to yielding by Sequence ③ even though this member is not in the direct load path. Given that the angle of the upper rail and A-pillar would predict a tensile force in the dash rail, a quasi-static analysis is unlikely to predict the degree of localization even if bending in the dash rail is included. It should be noted that stress begins to form already at 0.016s even though there is little or no stress indicated in the upper rail, the predominant source of force for this quasi-static analysis.

These two items give rise to the idealization as shown in Figure 8-5 and serve to introduce the next section where strain propagation by wave motion is discussed.

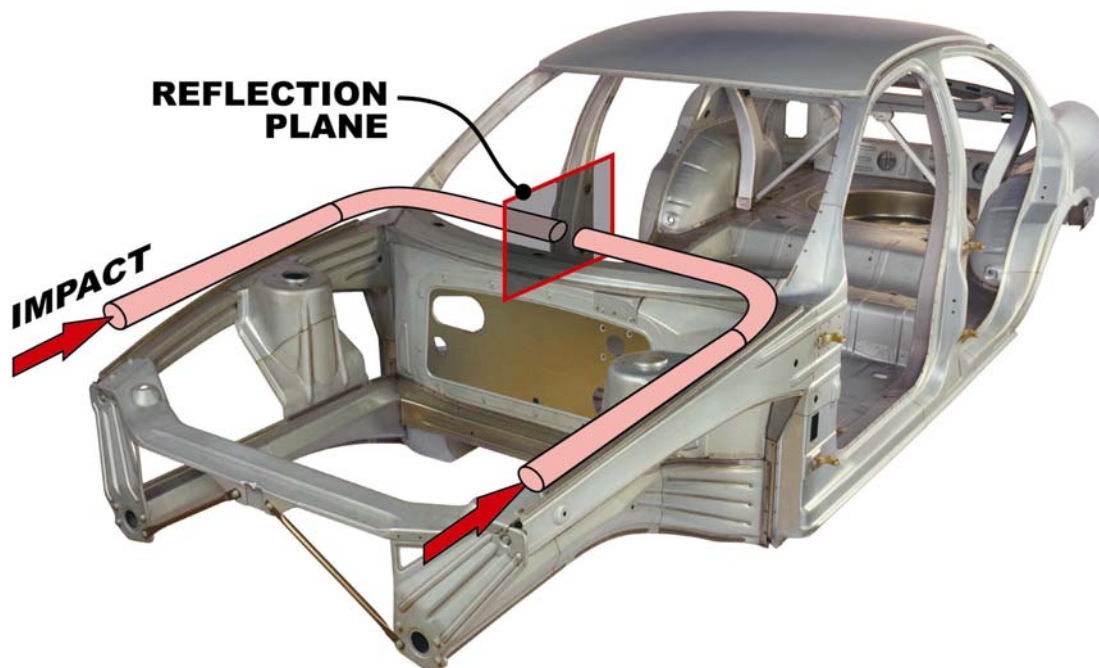


Figure 8-5: Idealization of impact load path replacing upper rail and dash rail with two impact bars and reflection plane.

Table 18: ULSAB vehicle millisecond event report (ULSAB (1998)).

This table is not available online. Please consult the hardcopy thesis from the QUT Library.

8.4 Impact Experiments

The motivation for this section is the idealization of the ULSAB vehicle finite element analysis depicted in Figure 8-5 as two bars with a reflection plane interspersed. This section will focus on wave progression in bars as proposed. The intention is not to offer a full treatise of the subject for two reasons, then first being beyond scope and secondly, it is adequately covered elsewhere. It is thought that in the context of physical experiments better understanding is created of the complex impact phenomenon of a crash.

The work is arranged presenting first elastic waves followed by inelastic or plastic waves. The work is a contribution by the author except where stated.

8.4.1 Elastic Waves from Collinear Impact

A hammer blow onto the end of a stationary bar initiates stress at the impact interface. This stress does not immediately distribute along the full length of the bar and cause free-body motion of the bar as a quasi-static analysis suggests, since time is needed for this stress to propagate. Stress simultaneously propagates along the striker (or hammer). The length of the striker, presumed the shorter of the two impacting bodies, governs the duration of the blow. This is shown in a Lagrange or characteristic diagram below:

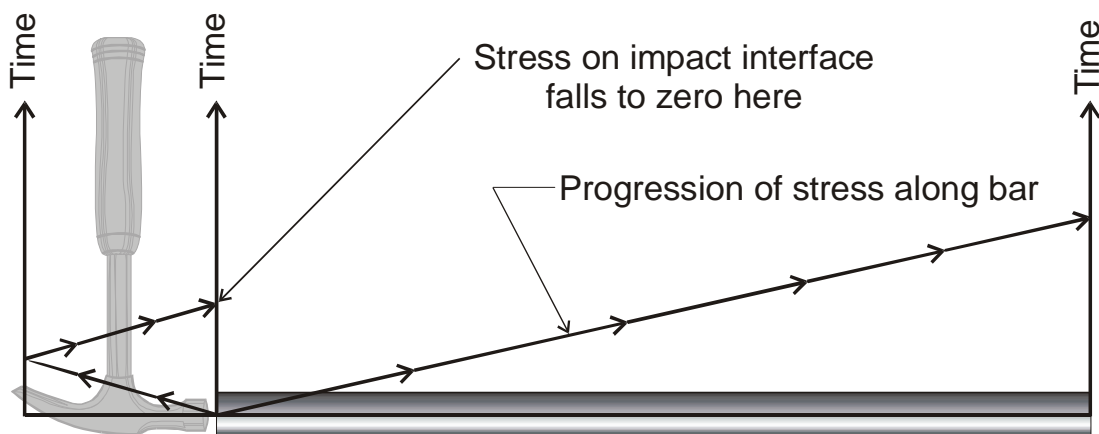


Figure 8-6: Lagrange Diagram showing pulse progression and separation point.

Since the bar is defined long and the striker is defined short, the pulse length is short compared to the fundamental mode of the bar. Note that a heavier blow does not increase the duration of blow but the magnitude of stress. This is envisaged as a stress pulse passing through the bar as shown below:

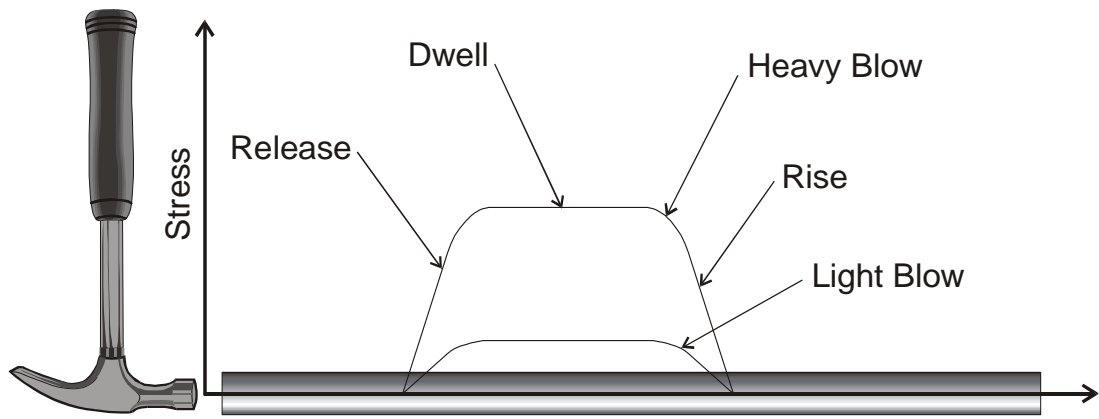


Figure 8-7: Stress Pulse in Bar

The stress created by the blow is not just a compressive stress in the direction of the longitudinal axis of the bar, but a tri-axial stress. This can be visualized in the exaggerated swelling of the stressed part of the bar below:

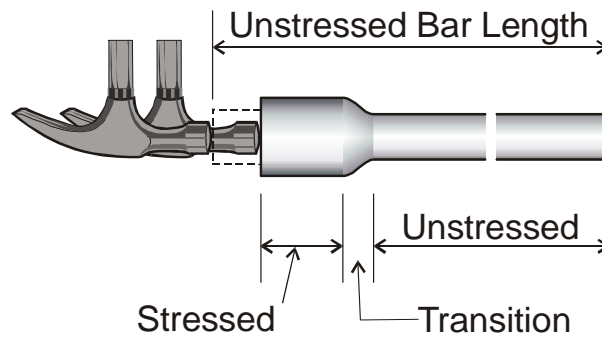


Figure 8-8: Exaggerated Effect of Impact

The exaggerated swelling draws attention to an increase of stress area and a corresponding decrease in stress. However, because the increase in area is small, it is ignored in the simplified analyses that abound in the literature e.g. Johnson (1972). Similarly, the uniaxial stress simplification ignores radial inertia Zukas, Nicholas et al. (1982). The general trapezoidal shape Figure 8-7 undergoes distortion as it progresses along the length of the bar where the pulse rise slows and the linear portion goes oscillatory. Johnson (1972) pp119

An end impact on an unconfined bar releases a wave of strain disturbances in the direction of impact for compressive impact (opposite wave direction to the direction of tensile impact). This is depicted in the figure below for compressive impact.

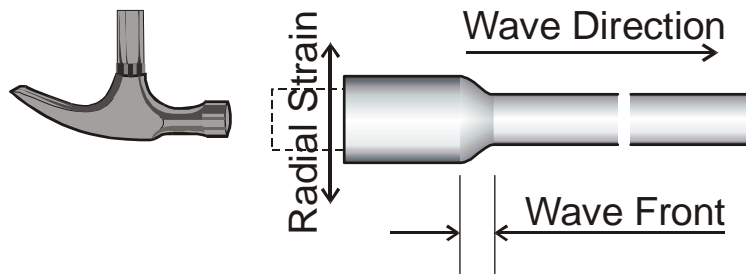


Figure 8-9: Wave Direction

Al-Mousawi and Harrison (1987) measured the varying strain in a bar at a position on the bar four bar diameters back from the impact interface. By varying the intensity of impact they showed that pulse length is independent of striker velocity. Their oscilloscope photograph is redrawn and annotated below emphasizing the three severities of impact by using three different shading intensities:

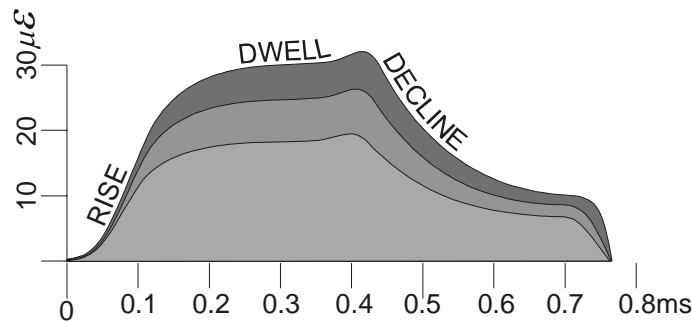


Figure 8-10: Pulse Length for Different Impact Severity

Since the graphs are in the time domain and since the measurement of strain is taken at a single point as the wave passes through this point one of the curves of Figure 8-10 is reversed and redrawn in space domain as if the bar were of infinite length. This aligns rise and decline in the direction of impact.

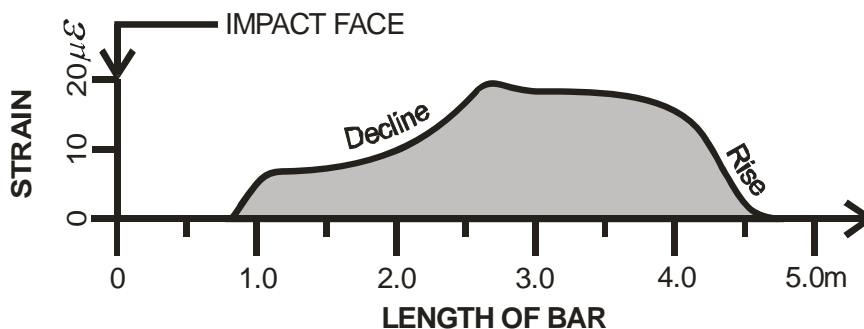


Figure 8-11: Wave Shape Visualization

The strain disturbance shaped nominally as shown in Figure 8-11 travels at celerity speed often referred to as acoustic speed nominally 5150m/s for steel and 5100 m/s for aluminium. (Table 1.1 p352 Johnson (1972). The “slug” of disturbed material has momentum.

8.4.2 In-line Momentum Trap

A simple momentum trap experiment gives physical appreciation of the progression of strain in a one-dimensional wave experiment on a long thin rod and a heavy steel bar on rollers. The relevance to motor vehicle crashes is that it demonstrates that the effects of impact are not immediately transmitted to all sections of the motor vehicle. Some strain disturbances may be trapped in sections of the vehicle and reflect in its own length.

More importantly, the experiment is a precursor to subsequent experiments.

The apparatus consisted of a long thin rod supported by two rollers and touching a short steel rectangular bar at the distal end, as shown in Figure 8-12.

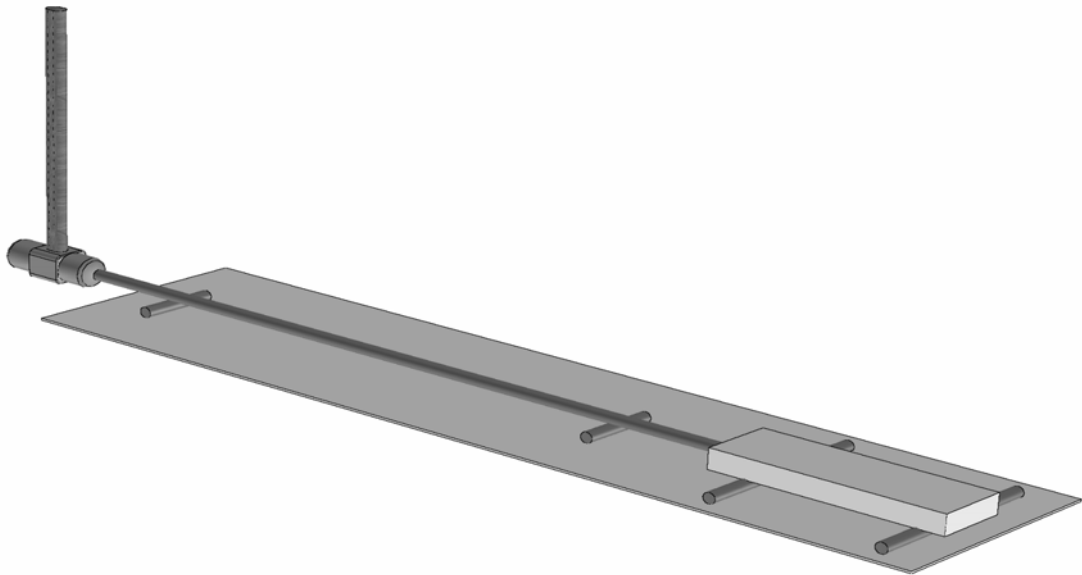


Figure 8-12: A Simple Momentum Trap Experiment

The rod was 8 mm diameter and 3 metres long. A light tap was all that was needed to cause the momentum trap, a 300 mm x 50 mm x 25 mm steel, to separate from the point of contact with the rod. The heavier the impact the further the trap would roll.

The delay between impact and action, although calculated at only 0.6 milliseconds was distinctly observable. It was noticed that when a bar was struck without the trap in place it would vibrate vehemently whereas with the trap operational, the bar would vibrate hardly at all indicating complete transference of kinetic energy from the hammer blow to motion in the heavy distal object.

8.4.3 Right-Angled Momentum Trap

The purpose of this experiment was to show that collinear impact can have consequences other than collinear. In the context of the ULSAB idealization in Figure 8-5, this experiment shows feasibility that a strain wave could travel a path as idealized.

A 3.0 metre long spring steel bar 8 mm diameter was bent 100 mm at one end by 90 degrees. It was placed in an apparatus as shown in Figure 8-13, so that the bar was free to move in the longitudinal direction and restrained laterally. The ends of the bar were rounded and the distal end was polished to minimize friction with the intended mating surface. The momentum trap from the previous experiment was used with the appropriate surface also polished. The trap was positioned on rollers similar to the previous experiment.

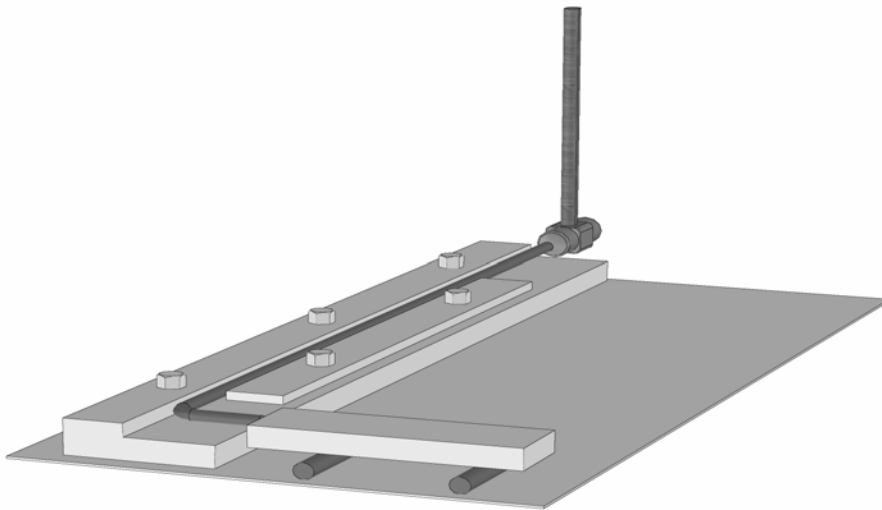


Figure 8-13: Sketch of Right-Angled Momentum Trap

Some care was taken to ensure that there was no ramp effect by setting the trap slightly less than at right-angles. Cigarette paper was used as a feeler gauge ensuring more clearance between bar end and impact face as the bar progressed away from the hammer end.

The distal bar end was then coated with marking to disclose the first contact point on the momentum trap. The apparatus was tested by moving the bar along its guide checking that contact was not made.

A light hammer blow caused the momentum trap to displace some 50 to 100 mm direction at right angles to the direction of bar travel. The blow required only wrist and slight forearm action. The point of distal end impact with momentum trap face was towards the end of the impact face indicating that motion of the bar had commenced prior to motion of the momentum trap. This is as a result of the elastic wave travelling the full length of momentum trap twice prior to contact separation.

8.4.4 Velocity of Strain Propagation

During collinear impact, two velocities are involved. One is the obvious closing velocity of the striker with the struck object. The other velocity is celerity being the speed at which the disturbance caused by the impact is transmitted. The object of this experiment was to determine the celerity of the bar used in the earlier experiment.

The apparatus consisted of a Polytec Model OVF502 Fiber Interferometer, an optically reflective target on the distal end of the struck bar and a Tectronix TDS420A oscilloscope to record the output. Real-time results were captured on a photograph of the oscilloscope screen appearing as Figure 8-14 showing transient velocity of the reflective target. The output was also recorded on a computer and graphed in Figure 8-15. Celerity was not recorded directly and is calculated below. It is noted the hammer blow velocity rose to a fulgurant peak very rapidly followed by a less rapid decay. Although eventually the progression and reflections ceased, there was little decay between one peak and the next over the time span considered. Of significance is the peak-to-peak measurement of 1.16 milliseconds to be used for wave speed calculations.

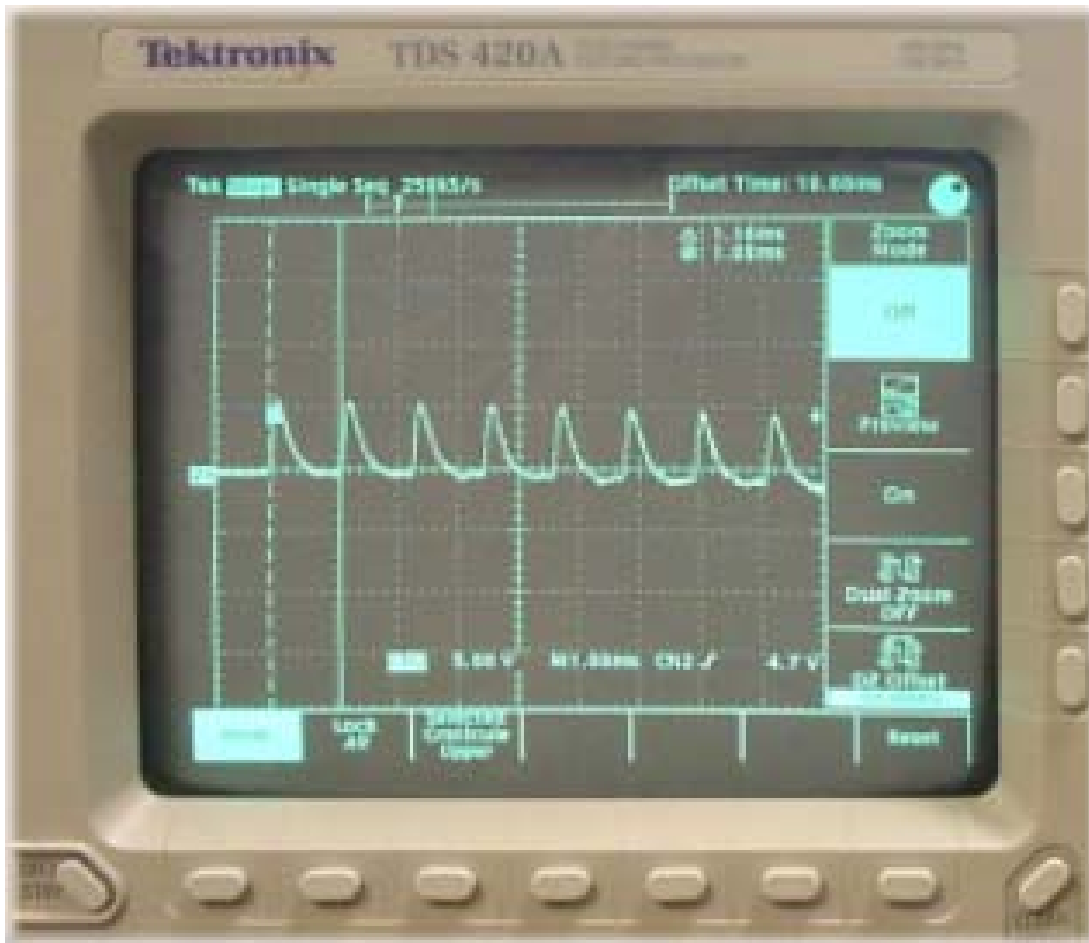


Figure 8-14: Photo of oscilloscope measuring real-time distal face velocity (mm/s)

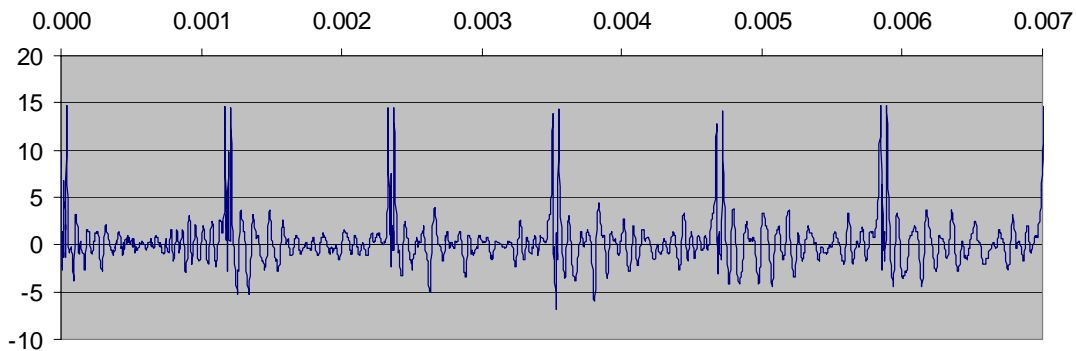


Figure 8-15: Interferometer output of distal end velocity (mm/s) against time (s)

The peak-to-peak time at 1.16 milliseconds, corresponds to a frequency of 862 hertz. The celerity for the 3.0 m long bar then calculates to 5172 m/s. (Celerity = 2 x Length x frequency). This value is close to the published value of 5150 m/s, the difference being accounted for by different physical properties of spring steel as against the mild steel values for the published data.

8.4.5 Directional Nature of Strain Disturbance.

The elastic behaviour of a liquid in a long containment pipe under collinear impact is approximately equivalent to an unconstrained solid bar. Swaffield and Boldy (1993) Impacting a liquid gives opportunity to show the directional nature of elastic waves.

To ensure that a high intensity wave was propagated through the liquid media, a pyrotechnic impactor described in Figure 8-16 was used. The apparatus consisted of a steel body housing two sliding shafts. One sliding shaft projected to the outside to permit impact with a hammer. This shaft also provided an opening for a 0.22" calibre bullet blank. The other sliding shaft, the striker piston, protruded a nubbin on its top face to initiate a rim-fire mechanism with the bullet shell on impact. Hammer impact caused the striker to project rapidly to the right of Figure 8-16 impacting the object inserted the distance of the step. On a long impact object, the striker piston length determines the duration of piston/object contact.

Although the experiment was designed to illustrate the directional nature of elastic waves, it also illustrated the radial component local to the impact site and reflection site.

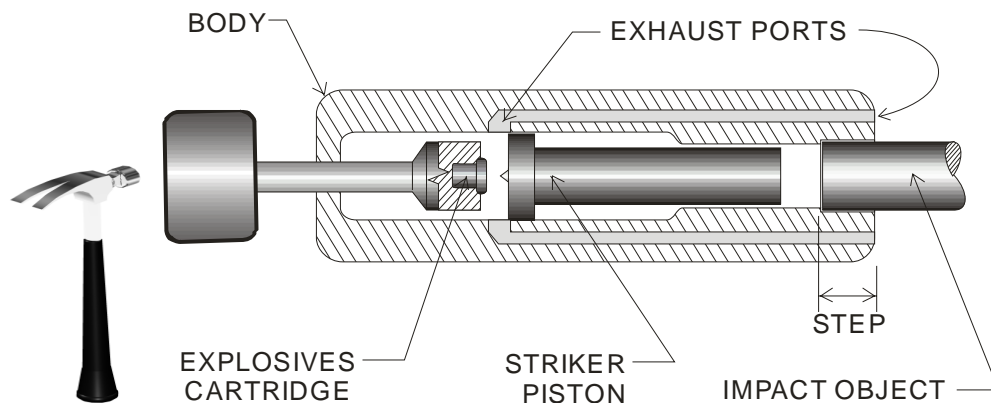


Figure 8-16: Schematic of impact gun prior to firing

The gun in Figure 8-16 was interspersed between the hammer and the impact object, shown as an arrow in Figure 8-17.

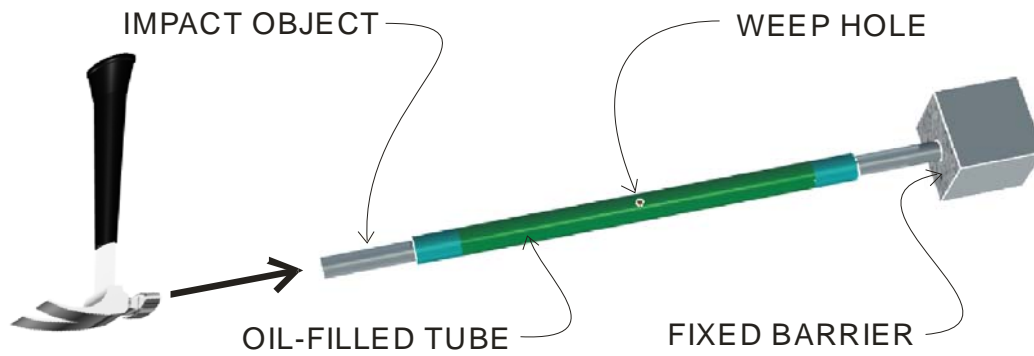


Figure 8-17: Apparatus for testing the directional nature of elastic waves.

The apparatus as shown in Figure 8-17 consisted of a 2.0 m long aluminium tube x 1.6 mm wall thickness, plugged at each end with 12.0 mm diameter steel pistons machined to fit accurately so as to minimize leakage of hydraulic oil. The pistons were able to freely translate each other's motion hydraulically. A central weep hole was added to disclose any hydraulic action. The weep hole was tested by restraining the motion of one piston while manually pushing in the other piston, causing oil to leak at the weep hole.

Disclosing wax on the impact end piston showed a piston displacement of approximately 10 mm as a result of the pyrotechnic impact.

The results showed a tube belling starting at each piston head diminishing within 3 to 4 diameter of the piston heads. No loss of hydraulic fluid occurred through the weep hole.

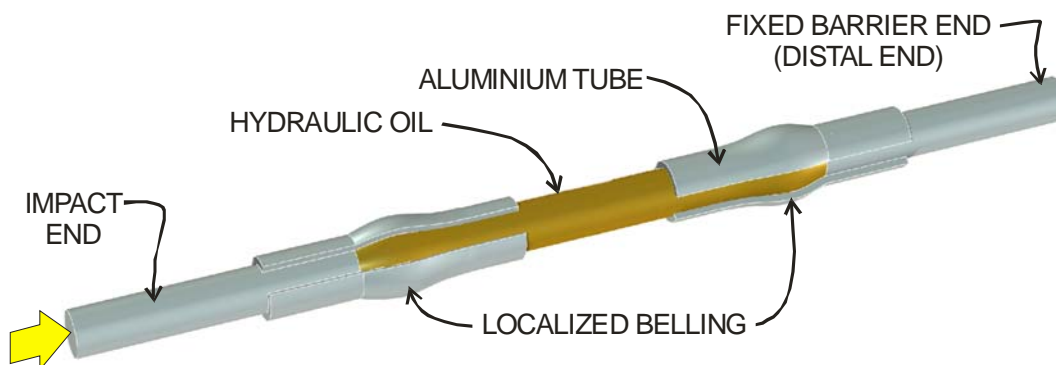


Figure 8-18: Cut-away section of apparatus showing tube belling at each end.

The test showed the following:

1. Radial wave motion is local to the initiation site and reflection site, confirming existing theory for solids.
2. Reflection of the longitudinal wave at the distal piston end created another radial wave.
3. The momentum of the longitudinal wave was sufficient to bell the distal end of approximately equal dimensions to the impact end.
4. Once the longitudinal wave was set in motion and passed the radial action, it contained no radial component, as evidenced by the lack of oil leakage.

The last point emphasizes the need to consider stress wave motion as a dynamic event rather than a tri-axial stress condition. This study also challenges the Poisson's ratio concept being applied to the dynamic condition remote from the impact site.

Further exploration of this phenomenon remains for future study.

8.4.6 Vectorial Nature of Strain Disturbance

The purpose of this experiment was to determine the effects of momentum change imposed on a longitudinal strain wave. Momentum change is achieved in this experiment by redirecting the momentum vector, given that no control over celerity or the mass of the strain affected "slug" of material is feasible.

The apparatus used consisted of two lead balls nominally 7.6 mm diameter and a bent aluminium tube with pistons fitted to each end. The piston in the longer leg was impacted by the pyrotechnic gun described by Figure 8-16.

One lead ball was interspersed in line with the impact direction to a fixed point and the other lead ball was between the head of the distal piston and a fixed point. The lead balls were attached with a pinhead quantity of methacrylate glue to maintain collinearity with impact direction. An angle bracket was attached to the tube to facilitate mounting the in-line lead ball. The apparatus in Figure 8-19 was laid flat on the table restrained by friction with the table and two reaction points at the lead balls. The system was tested ensuring the assembly was free to move sideways in response to hydraulic test action applied manually at the firing end (by pushing with finger).

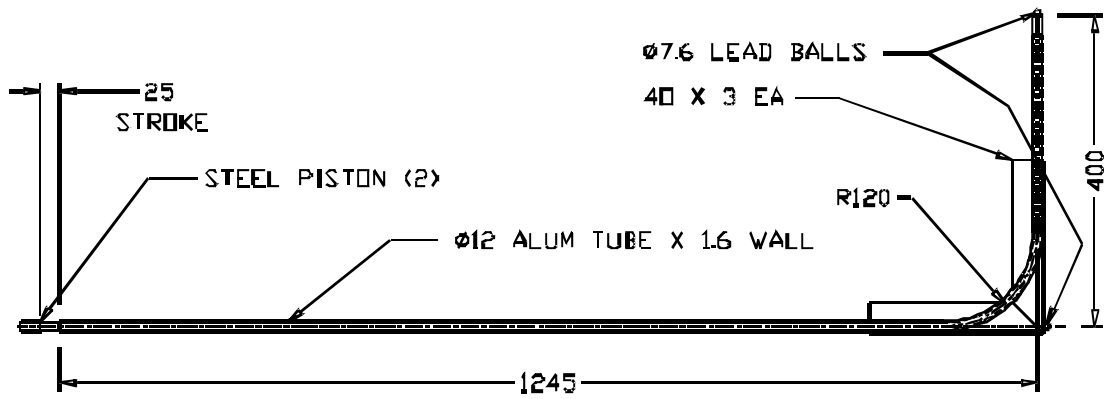


Figure 8-19: Plan view of oblique impact apparatus.

Two tests were performed; one with a side guide and one without a side guide. The test without a side guide ruled out any notion that the results were a response to hydraulic action.

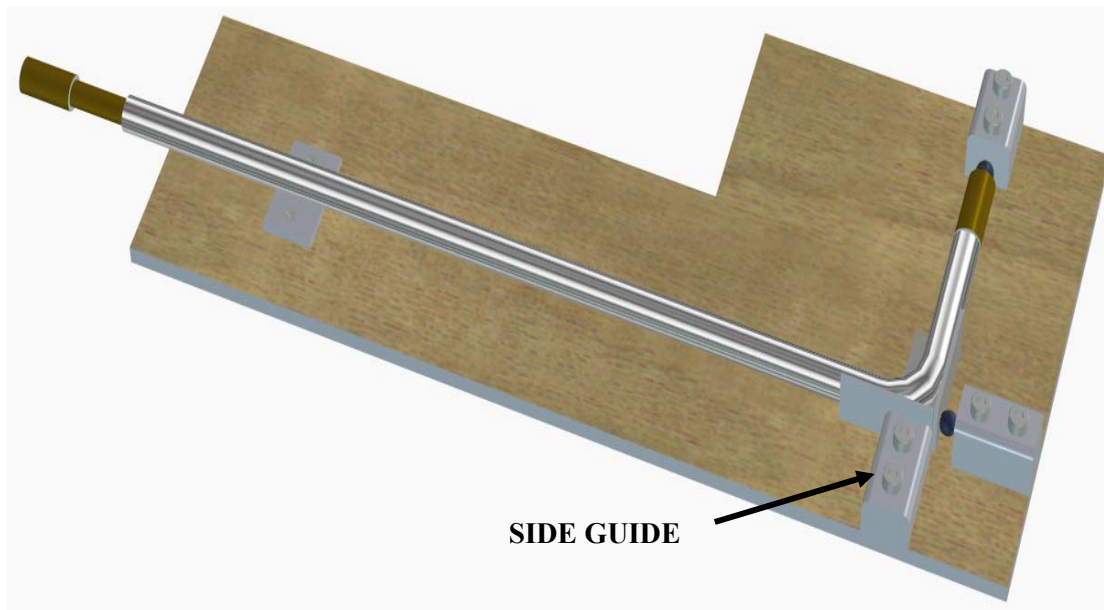


Figure 8-20: Schematic of oblique impact apparatus.

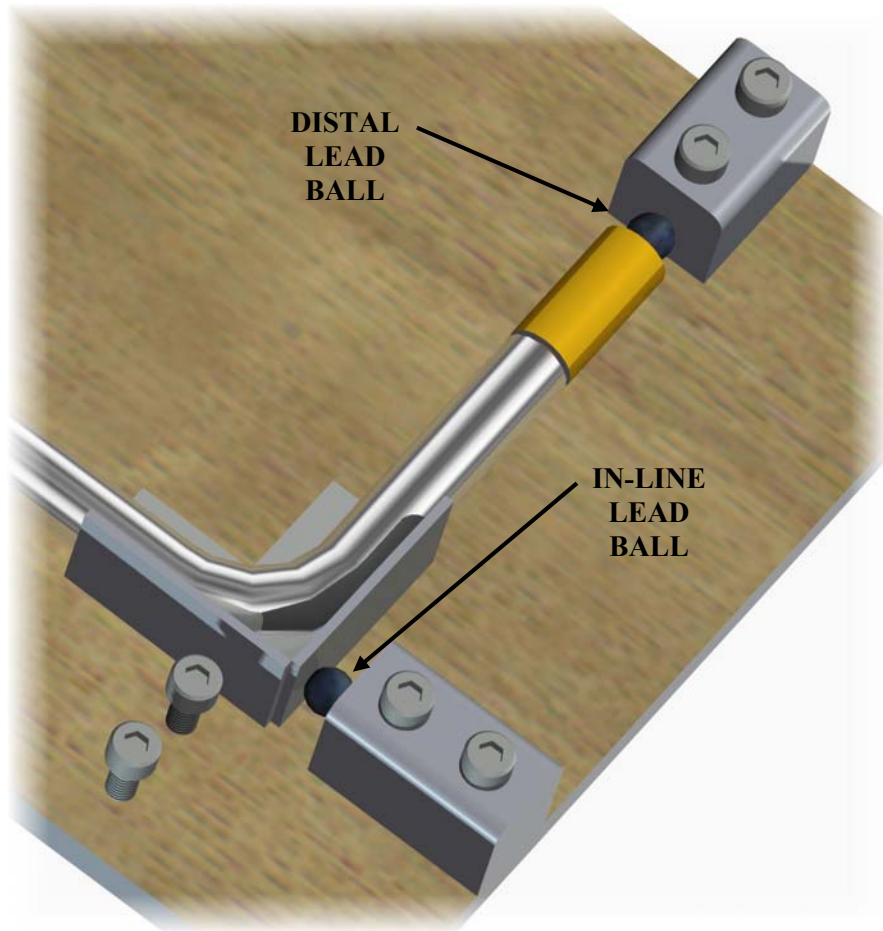


Figure 8-21: Schematic of oblique impact apparatus (with side-guide removed).

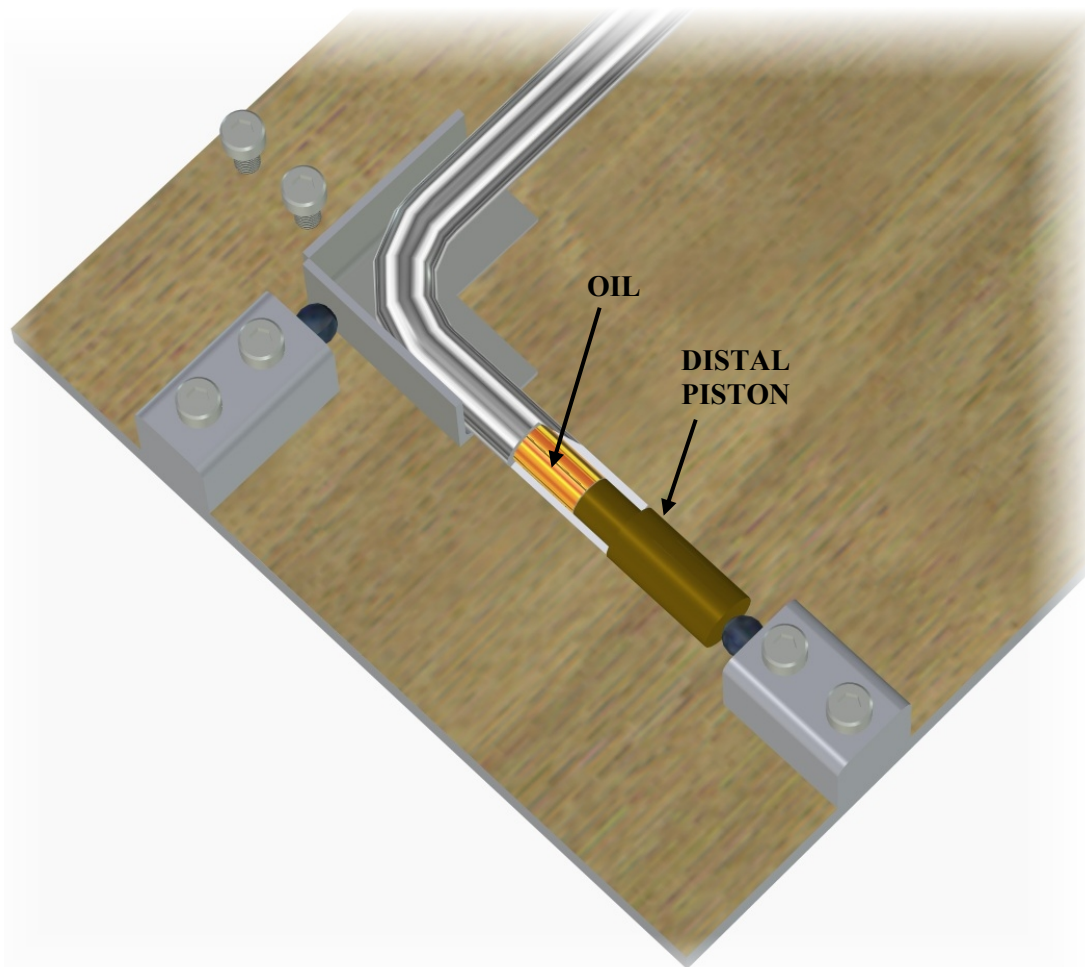


Figure 8-22: Schematic of oblique impact apparatus with tube cut-away at distal end showing distal piston and hydraulic oil.

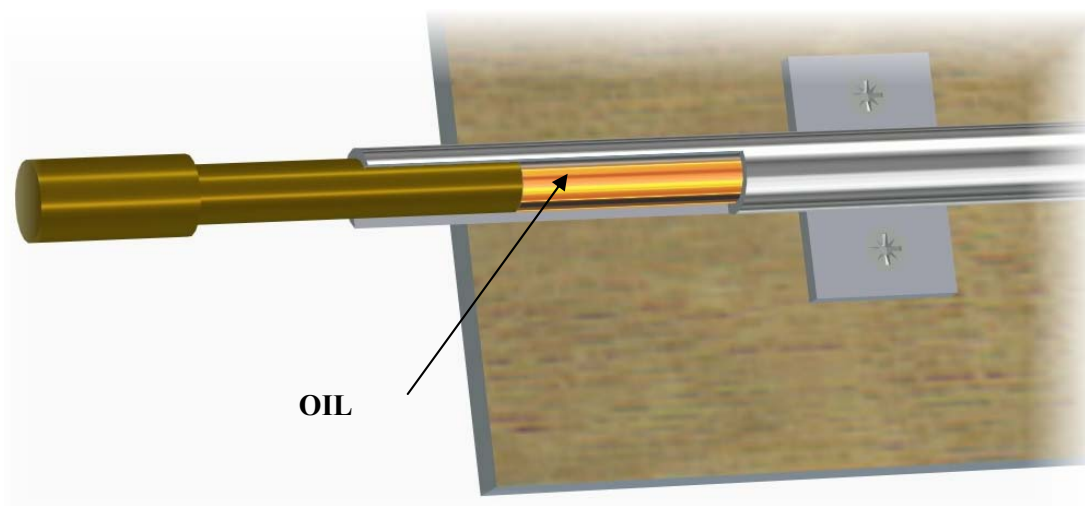


Figure 8-23: Schematic of oblique impact apparatus with tube cut-away at impact end showing piston and hydraulic oil as well as support glide plate minimizing interaction with table.

The test results are shown in the photographs in Figure 8-24 and Figure 8-25 and tabulated in Table 19.



**Figure 8-24: Photograph of lead ball after impact with side guide fitted.
(LHS is in-line ball, RHS is distal ball.)**



**Figure 8-25: Photograph of lead ball after impact with side guide removed.
(LHS is in-line ball, RHS is distal ball.)**

Table 19: Measurements of lead balls after impact.

SIDEWAYS RESTRAINT	IN-LINE BALL		DISTAL BALL		THICKNESS REDUCTION CHANGE
	BEFORE & AFTER	THICKNESS REDUCTION	BEFORE & AFTER	THICKNESS REDUCTION	
FIXED	7.6 / 5.5	2.1	7.6 / 3.9	3.7	1.6
FREE	7.6 / 4.2	3.4	7.6 / 4.2	3.4	0
CHANGE	-	1.3		0.3	

Discussion

The test results showed evidence of an impulsive force on the lead balls. The forces were approximately equal for the test where the side restraint was removed. Conservation of momentum, when applied to the results, shows that a wave momentum will split approximately 50:50 when re-routed through 90° . When an additional impulse was added to the system by way of side restraint, the distal ball received additional impulse, as evidenced by the reduced thickness. This additional impulse came at the expense of the in-line ball which showed reduced distortion.

The idea that reflection of the pulse may account for the difference in distortion between the two tests was considered. For this idea to be viable, the pulse would need to reflect from the distal piston to the bend and back again in a continuous loop. To test this, the wave length in metres of hydraulic fluid was estimated, as below:

The impact gun tup is made from hardened steel. Its length is 80 mm representing a pulse duration of 30 microseconds. This in turn represents merely 30 mm of length in the hydraulic oil having a nominal celerity of 1000 m/s. The strain in the hydraulic fluid then, travels in an affected length (“slug”) of 30 mm. The distance from the bend to the distal end was approximately 400 mm, being sufficient distance for the strain disturbance to pass without compounding or cancelling.

8.4.7 Inelastic Waves

This section is important because inelastic strain (plastic working) accounts for a great proportion of energy dissipation. To gain a visual appreciation of this proportion, Figure 8-26 is posted below. The areas under the curve are proportional to the appropriate energy.

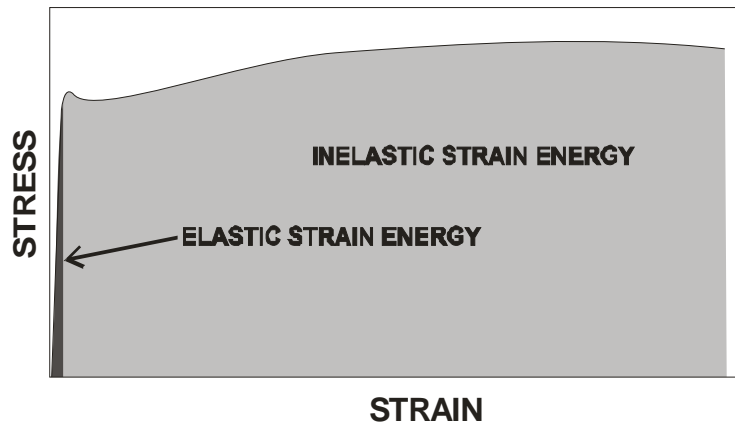


Figure 8-26: Stress-strain diagram for low-carbon steel showing mechanical work done (per unit volume) as areas under curves comparing elastic (dark grey) with inelastic energy (light grey) areas.

Initiation of plastic action is shown to occur in this section at abutments or where there is a discontinuity of strain propagation. This can have potentially good and bad implication for a crumple zone:

1. A poor transition between the chassis horns and occupant cell can give rise to local yielding prematurely and cause intrusion. For an example of improved distribution refer Figure 3-7 where a reinforcement strut is added splitting the strain disturbance. In addition the continuation of the chassis horns to well under the occupant cell in this figure is an example of good transition.
2. An intentional abutment or impedance change can initiate plastic working in a desired area and so improve overall energy absorption.

Referring now to Figure 8-4, between Sequence ❶ and Sequence ❷ in the stress in the length of upper rail was raised from negligible to 350MPa. Although intermediate snapshots are not provided, it can be assumed that yielding took place progressively in this member. Even though buckling of the upper rail took place at 0.21s the maximum stress was reached in the whole member by 0.031s. The buckling event did not ameliorate whole member stress

as might be expected from columnar collapse in a quasi-static analysis. The idea of a plastic wave holds appeal to explain these events.

Velocity above a threshold value causes yielding. Impact above this threshold value releases two waves, one elastic and the other inelastic or plastic wave according to Johnson (1972) and the findings of these experiments. In the classical theory, at a point in time after impact there is line of influence beyond which the material being impacted is unaffected. This is shown in Figure 8-27.

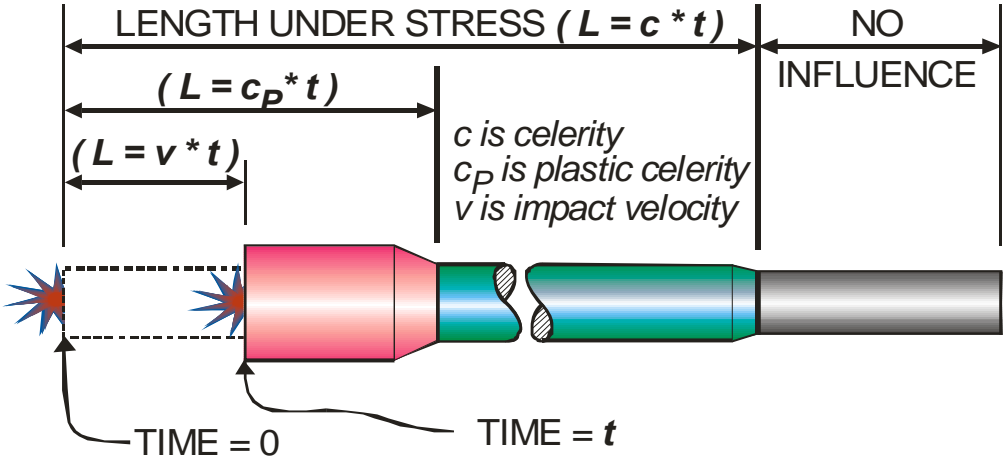


Figure 8-27: Collinear Impact of Long Bar

The green central section of Figure 8-27 is shown larger in diameter for visual effect. In the light of earlier findings where the weep hole did not weep, the notion that a strain disturbance causes lateral dimensional growth is in doubt.

Embodied in Figure 8-27 is the idea that impact can raise stress of a member to yielding while sections of this member are unaffected. This has implications in the crumple zone context. A high yield material will impose a greater force to the collision partner raising aggressivity. This is an undesirable consequence of using high-strength steel – a trend in the industry fuelled by weight reduction goals. A detailed study of aggressivity is beyond scope of this work.

The purpose of these experiments is to help understand and explain the complex phenomena of plastic localization and plastic yield progression in the longitudinal members of a crumple zone. The experiments involve 12 mm diameter aluminium rods impacted at one end with the pyrotechnic device of Figure 8-16.

Three different arrangements were used in the experiment:

1. A single rod shot into a capture box.
2. A single rod shot onto a solid abutment with no clearance prior to the shot.
3. A rod shot onto another rod with mating surfaces touching.

An apparatus was set up as shown in the figure below to fire a hardened striker at one end of bars 12.0-mm diameter of various lengths. The bars were from 2011-T3 Aluminium. A recess in the gun measuring 12.15 diameter had a shoulder 13.7 deep from the face of the body. The recess and the shoulder ensured good alignment for the rod with the body axis. The body was hand-held and the rod, if long, was supported and loosely guided by an inverted structural angle. The friction with the angle and the slight upward trajectory did not appear to affect the results.

A hammer blow onto where the icon is shown sets off the explosive cartridge in turn activating the striker piston. Care was taken to ensure the striker piston was well back away from the rod to ensure the hammer blow was not part of the impulse.

Into Capture Box

The first shot was onto a 2.75 metre long rod into a capture box. The diameters were measured at various positions from the firing end and recorded. The far end diameters remained unchanged dimensionally. The dimensions are not presented to retain brevity.

The sequence of events will now be considered with the aid of a location diagram. The classic location diagram is turned on its side to correspond with displacement – time curves used in prior sections of this work. It is not to be inferred that the curves are linear even though they are drawn that way for simplicity. Also, for simplicity, the loading diagram is taken as a step function with instant rise, flat dwell and instant decline.

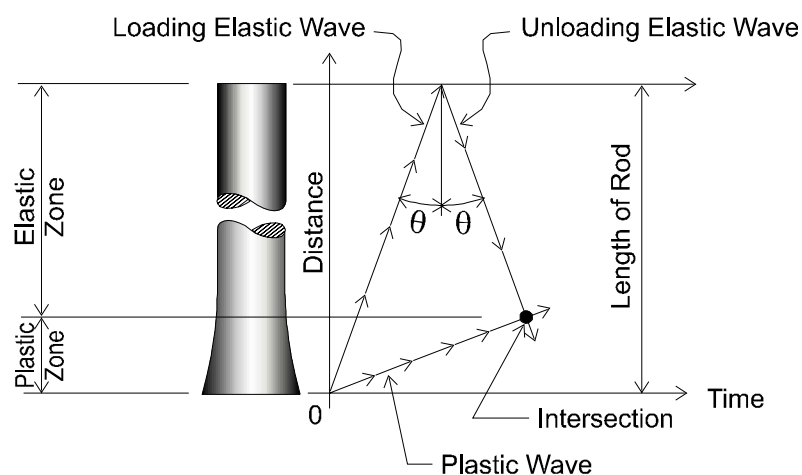


Figure 8-28: Unloading Elastic Wave – Lagrange Diagram

Classic theory states that upon impact, two waves are released. One is an elastic wave and the other, a much slower wave, is a plastic wave. When the elastic wave has travelled the

full length of the rod, it reverses and unloads the rod stress as a tensile wave to satisfy boundary conditions.

Where the tensile unloading elastic wave meets the compressive plastic wave, the plastic wave is cancelled out. The muted elastic wave trapped in the rod continues back and forth until its energy is expended. The vibratory energy could be felt by gently touching the rod after the shot had been fired.

Onto Abutment

The pyrotechnic gun was loaded with more 12.0 diameter rods and fired into a heavy abutment made of steel. Alignment was more critical as the slightest misalignment caused the rod to bend at the abutment end notably in the plastic zone.

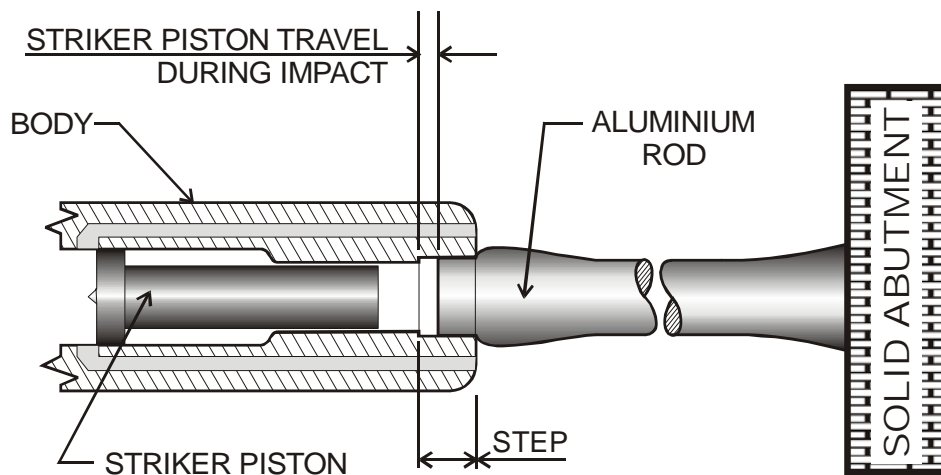


Figure 8-29: Schematic of Shot after Firing at Abutment

It was noticed that all shots onto the abutment were characterized by the following:

1. Bulging immediately past the mouth of the gun.
2. Cylindrical section of rod expanded and got stuck in the mouth of the gun.
3. Flaring at the abutment end.

The events are explained by reference to the rotated location diagram below:

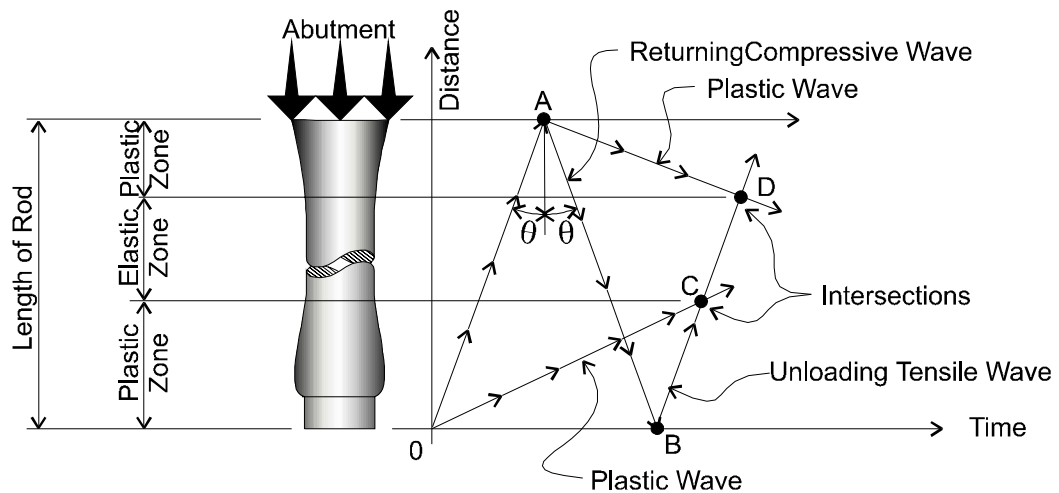


Figure 8-30: Location Diagram of Shot onto Abutment

At impact of the striker with the rod end, the two waves are released at $time = 0$ as in the previous diagram. This time instead of an unloading tensile wave returning from the distant end, two compressive waves return from the abutment from A. One is elastic and the other is plastic. The elastic wave becomes an unloading tensile wave at B where it unloads the plastic wave, which had been travelling from the beginning, at C. The result is a plastic zone that is longer than the previously described shot.

The unloading tensile elastic wave continues and unloads at D the compressive plastic wave initiated at A. With both plastic waves unloaded the elastic wave travels back and forth until its energy is spent.

The crumple zone implications are that there is propensity for initiation of plastic deformation where large change of section/mass occurs. There may be scope in the design of crumple zone members where such initiation increases the overall energy absorption.

Onto Mating Rod

The gun was set up as previous with a 1.77 metre rod in the recess. Another rod also 1.77 metres long were butted at the distal end ensuring that the butting faces were square and flat.

The shot was fired and measurements taken. It was found that the distal bar was distorted at the mating face only similar to the first shot (into the capture box). There was clear separation between the two bars after the shot indicating momentum transfer. The events are described by reference to the location diagram below:

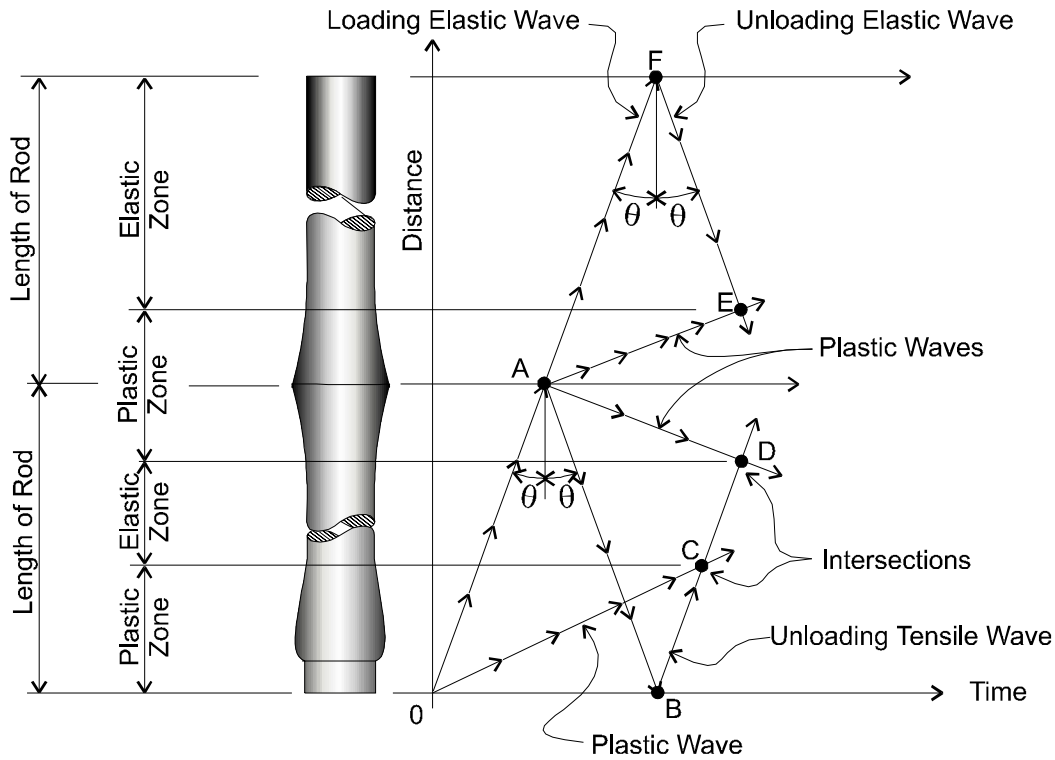


Figure 8-31: Location Diagram for Collinear Rods

The lower part is identical to the previous diagram and the upper part is identical to the first diagram with the plastic waves unloaded at C, D and E by unloading tensile waves initiated at B and F.

There may be scope in the design of crumple zone members to include a discontinuity in the axial force direction without affecting bending strength or torsional rigidity. Such a discontinuity may result in increased energy absorption. There may be scope to add a number of abutments judiciously placed ahead and behind the cross-member to improve energy absorption.

8.5 Evidence in Vehicle Reluctance

Varat, Husher et al. (2001) proposed velocity softening as a reduction of stiffness with increase in impact velocity. No theory or explanation of the cause for the phenomenon was offered. Varat, Husher et al. (2001) use the terminology as departure from straight-line velocity-crush curves. The distinction is abandoned for this chapter.

Reluctance, the ratio of impact velocity over dynamic crush, is used to introduce and demonstrate a natural propensity for softening with velocity even on a straight-line velocity-crush curve. To make the point, the straight-line velocity-crush curve for the Honda tests from Figure 5-1 is used to calculate the reluctances over the full range of velocities linearly extrapolated above and below the test velocities and is the subject of the graph in Figure 8-32.

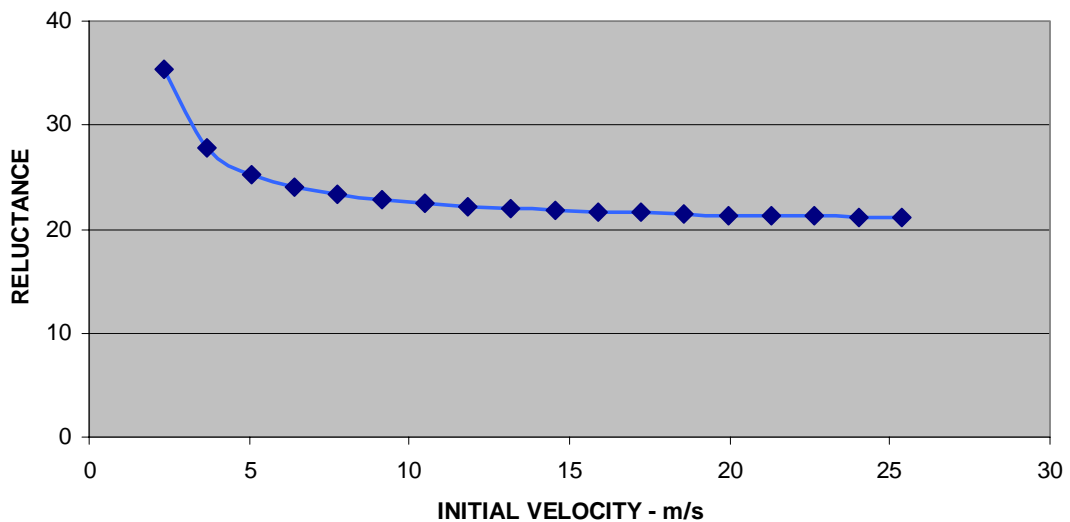


Figure 8-32: Reluctances for Honda tests #2712, #2836 & # 3807 for linearly extrapolated velocities over and under test velocities (from Figure 5-1).

The purpose of Figure 8-32 is to emphasise that the Crash3 y-intercept (shown in Figure 8-32 as the x-intercept because of rotation of the graph) heavily influences the early reluctances. Rephrasing, a higher Crash3 y-intercept will create higher reluctances until the asymptotic plateau controls.

Accordingly, it can be concluded that the threshold “no-damage” velocity of the Crash3 algorithm is an important overall indicator of crumple zone performance.

The asymptotic nature of the reluctance curve shows the influence of inertial stress agreeing with the findings of Emori (1970) who suggested that the elastic component in high speed crashes is small and can be ignored.

8.6 Evidence at the Component Level

“The main energy management components, such as longitudinal rails that provide the major portion of the energy absorption, undergo large plastic deformations. The work hardening effect and strain rate sensitivity of the material, as well as dynamic instability of the rails *are* (italic by author) considered in their design.” AISI (2002) The front rails often referred to as the horns, of the crumple zone carry the main crash load. (Refer Figure 8-3 for typical comparative forces). Giess and Tomasz (1998) refers to these as Key Structural Components in optimizing energy absorption arguing that overall energy absorption is improved by focussing on the main components. A similar rationale is used in this contribution.

The horns are columns poised in the direction of the crash and attach to the occupant cell at the firewall. The resistance to longitudinal impact is achieved by cross-sectional area and some bending strength to allow for the ‘dog-leg’ shaping that clears the cross-member. It was shown earlier that under dynamic conditions, the bending strength of the dog leg is somewhat irrelevant at least for a time due to localization. Columnar collapse occurs well into the crash sequence. A typical horn cross-section is shown Figure 8-33, although there are many variations across vehicle models. What is significant about this vehicle weighing only 1158 kg is the quite large aspect ratio of the horns. The value of this will receive further consideration later.

By plotting the force in the horns and velocity decay of the occupant cell simultaneously, a link between occupant cell velocity decay and force reduction in the horns is to be demonstrated here.

The procedure is to isolate the readings of load cells in the barrier which approximately correspond with force in the horns and determine a crude trend with velocity. A number of vehicles have been investigated from the mini type vehicle to truck size. The trend line is drawn in each case to reflect velocity and force decay above occupant cell velocity of 6 m/s. This velocity was calculated as the minimum velocity yielding stress. With strain rate effects, strain hardening during manufacture and the general trend for higher strength steels, it is likely to be exceeded in practice. Scaling of Y-axes affects the slope of the trend line. The essential finding is the direction of slope rather than actual slope. A conscious effort was made to scale for visual effect. Other vehicles are added in this study to ensure the Echo is not an isolated case.

This study has determined that there is an unloading of barrier force after a fulgurant peak in the general vicinity of the chassis horns of a vehicle. This finding is significant because it is contrary to expectations which would insist that force in the horns should continue to increase while velocity in the occupant cell remains as per the mass-spring paradigm. Elastic

strain propagation by wave motion has been used here to attempt to explain this very complex event, concluding that the local barrier readings have similarities with a long homogenous bar impacting a rigid anvil as published by Lensky in the USSR in 1949 and reported by Johnson (1972) p219. The relevance of earlier work presented on impacted elastic media experiments is thereby supported.

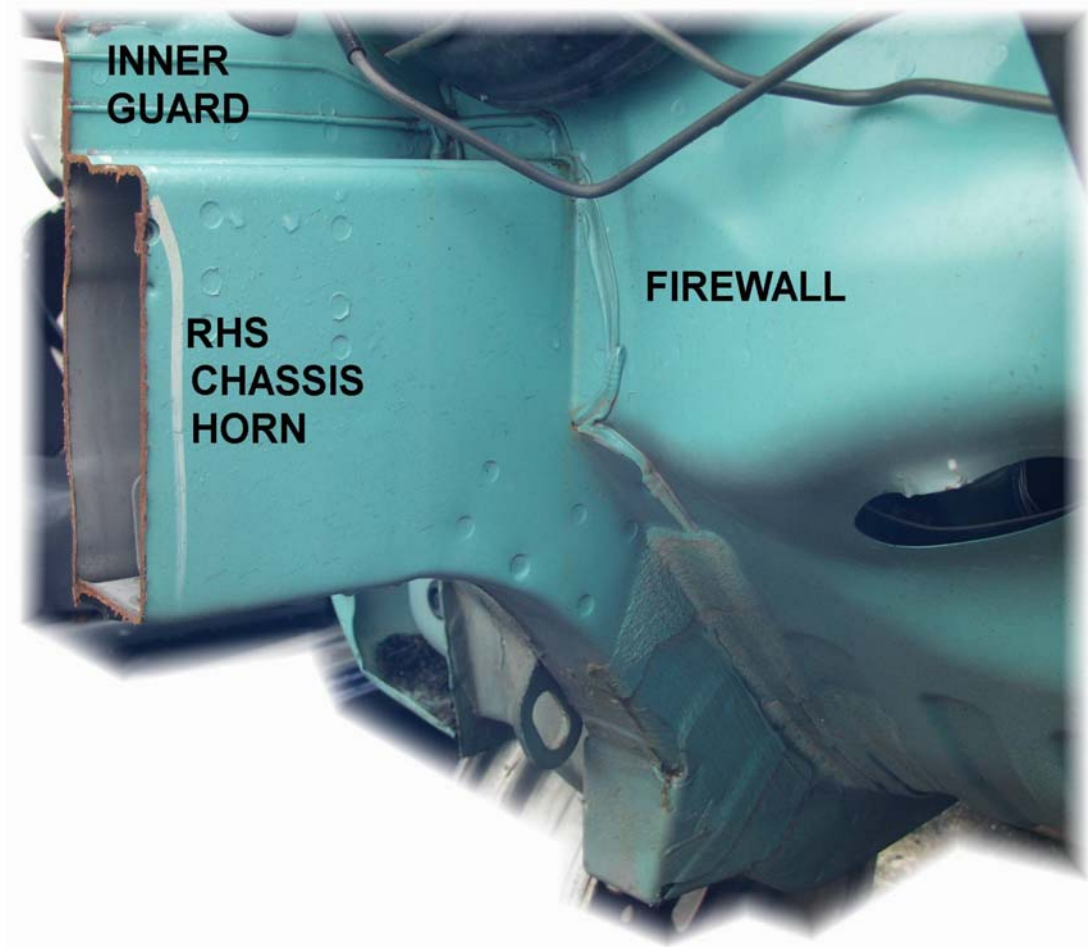


Figure 8-33: Chassis horn for Toyota Echo shown cut away.

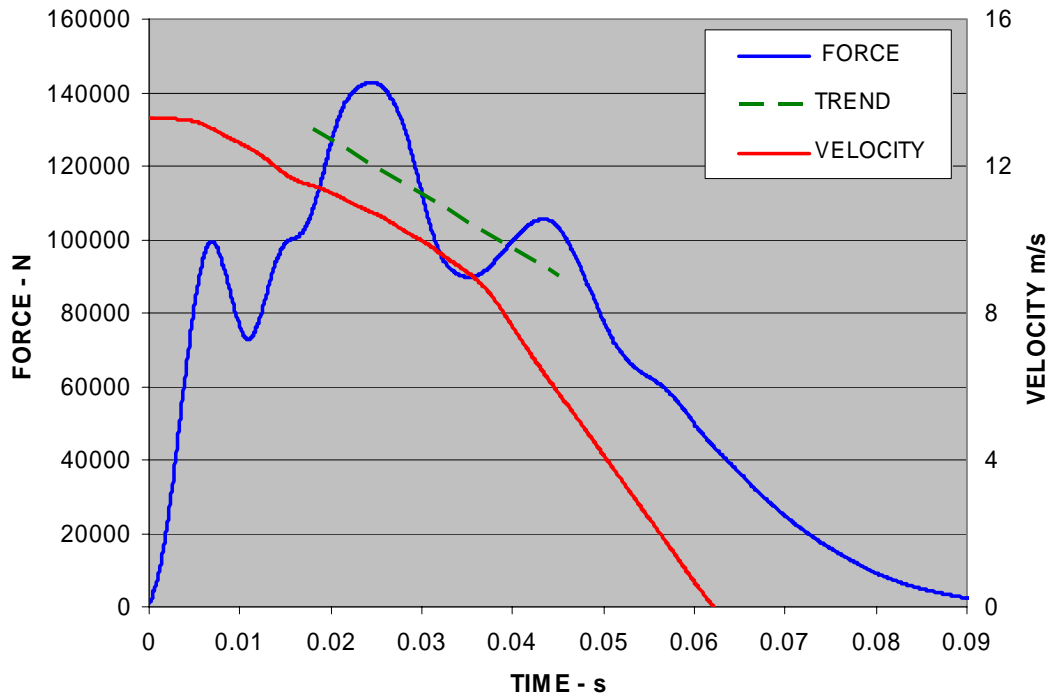


Figure 8-34: Combined left and right load cell force in barrier approximately in-line with chassis horns showing velocity of occupant cell and approximate trend of velocity and force decay for Model 2001 Toyota Echo Test #3806.

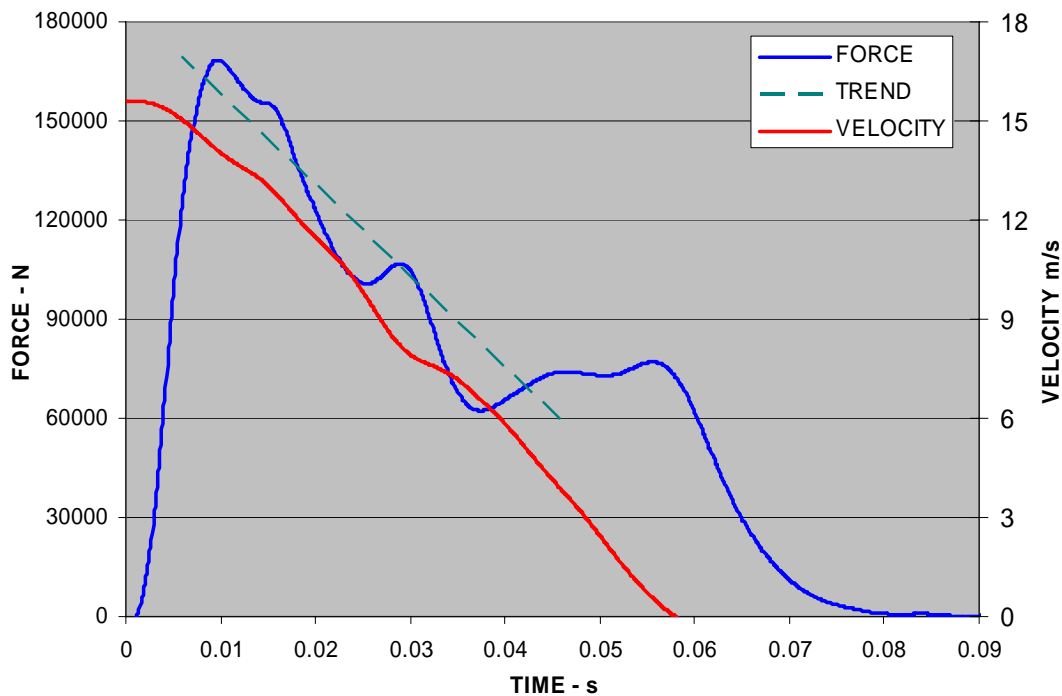


Figure 8-35: Combined left and right load cell force in barrier approximately in-line with chassis horns showing velocity of occupant cell and approximate trend of velocity and force decay for Model 2003 Mini Cooper Test #4273.

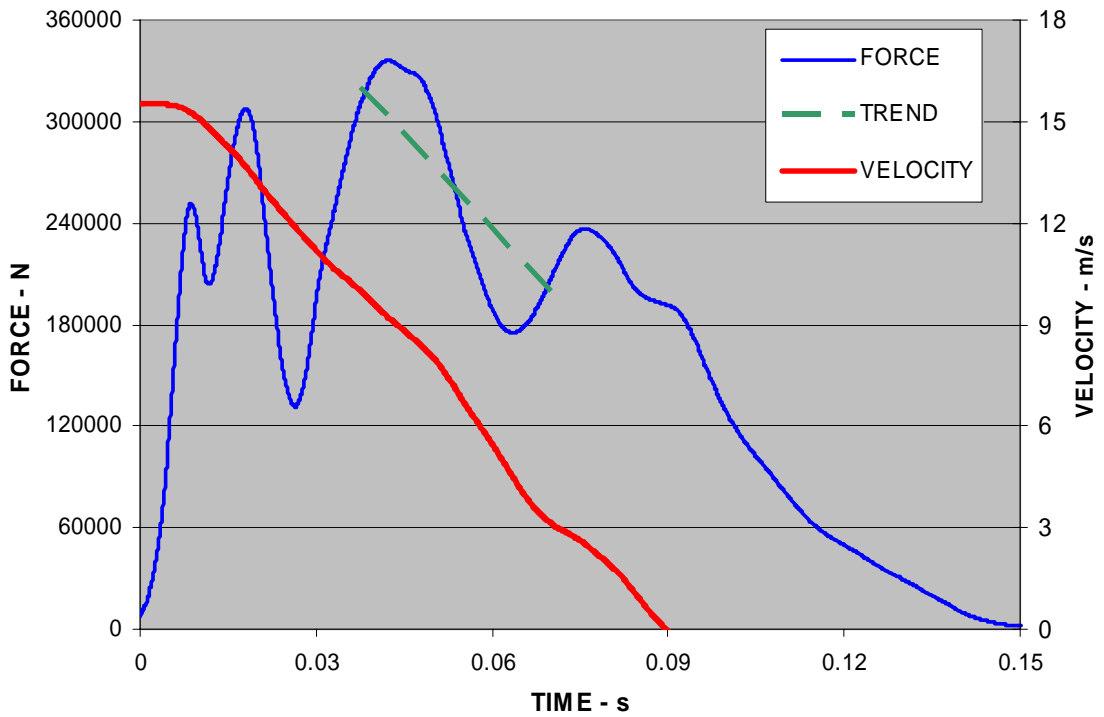


Figure 8-36: Combined left and right load cell force in barrier approximately in-line with chassis horns showing velocity of occupant cell and approximate trend of velocity and force decay for Model 2003 Chevrolet Silverado Test #4472.

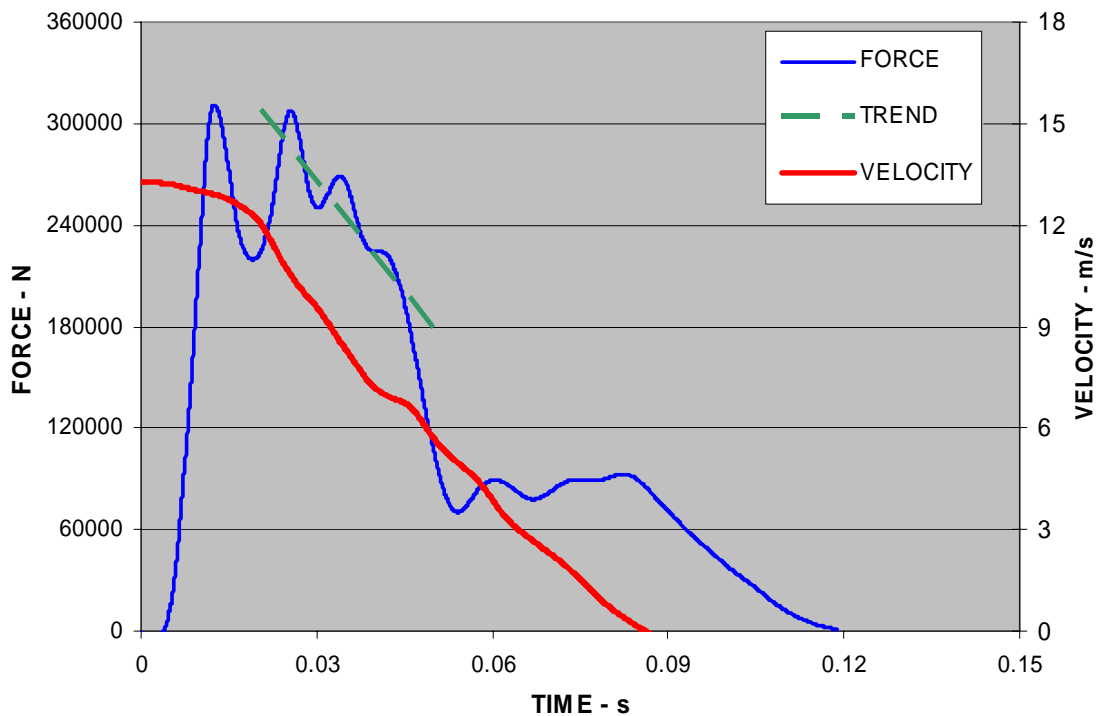


Figure 8-37: Combined left and right load cell force in barrier approximately in-line with chassis horns showing velocity of occupant cell and approximate trend of velocity and force decay for Model 2001 Ford F150 Test #3902.

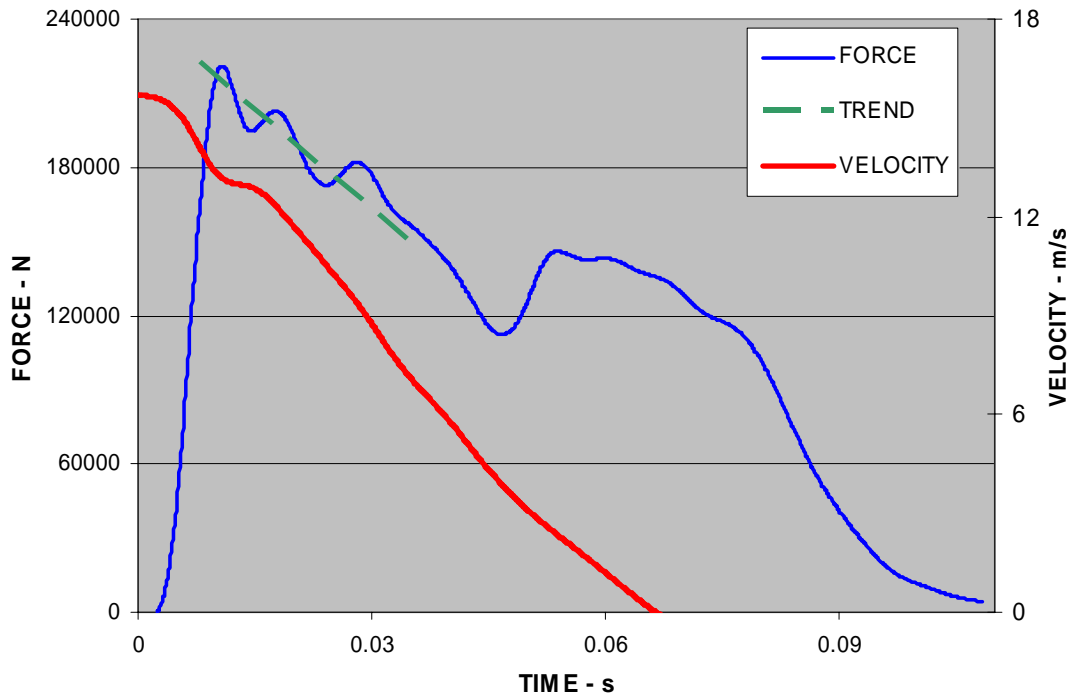


Figure 8-38: Combined left and right load cell force in barrier approximately in-line with chassis horns showing velocity of occupant cell and approximate trend of velocity and force decay for Model 2002 Isuzu Rodeo Test #4241.

The chassis horns do not interact directly with the barrier, but distribute across the bumper and supporting structure. They also interact with the structural connection to the cross-member and engine mounts. All of the assembly ahead of engine mounts respond to engine kinetic energy. This interaction helps explain the initial fulgurant peak in the load-time graphs above. Once the local interaction is largely complete the horns begin to respond to impact velocity. The response is one of unloading with reduction of velocity. It takes approximately 2 milliseconds for an elastic pulse to travel the length of a vehicle and return in homogenous steel. A plastic wave would travel the length of a crumple zone in 3 milliseconds under ideal conditions.

Design Implications

The two load cells selected for this study incur a significant portion of the overall impulse. How the horns respond to this impulse is important. The initial fulgurant peaks mimic the requirements of Motozawa, Tsuruta et al. (2003a) to produce a desirable crash pulse. The initial peak and trough that follows is also desirable from an injury perspective as shown by Brell, Veidt et al. (2001b). To achieve the configuration requires high strength material ahead of engine mounts and low strength material behind the engine mounts. Bending

strength is better achieved by high aspect ratios to maintain the lowest cross-sectional. A high aspect ratio is also of benefit in under bonnet packaging.

The Toyota Echo in Figure 8-33 takes advantage of aspect ratio and packaging compactness.

8.7 Summary

In this section it has been shown by accelerometer readings and finite element analysis that there is a progression of strain in the structure of the crashing vehicle causing localization of stress. Material yielding occurs first at the front of the vehicle. Yielding also occurs at right angles to the crash load path. This has been explained by a series of simplified experiments. This has implications for the design of connections of chassis horns to occupant cell, allowing lateral yielding to add to energy dissipation.

Material yielding has been linked to vehicle velocity decay in parallel with force decay of the main structural members for a number of real vehicle crash tests. This is important to support the velocity stress model of rebound formation in the next chapter.

Since material yielding occurs in response to velocity impact, low yield strength promises early onset of yielding, thereby maximizing energy absorption. However low material yield strength also increases the need for a longer crumple zone providing opportunity for optimization trade-offs.

High early acceleration peaks are desirable for injury mitigation. These peaks can be achieved by high yield strength. By virtue of the localization mechanism shown, potentially add a high early acceleration peak to the collision partner as well.

By using low material yield strength coupled with high aspect ratios for chassis members between shock towers and occupant cell, occupant cell deceleration can be minimized later in the crash sequence when body part coupling is taking place. The deceleration profile expected from such a combination in concert with yielding localization is expected to mimic the desirable U-shape proposed by Motozawa, Tsuruta et al. (2003a) and Motozawa and Kamei (2000b) and so reduce injury severity.

The existence of inertial stress has been demonstrated providing a theoretical foundation to the velocity stress model in the next chapter as well as a practical base to the understanding of stress formation by strain propagation.

BLANK

9. VEHICLE REBOUND

9.1 Introduction

Rebound of an occupant cell from a barrier and by implication from any other collision partner is implicated in increased injury risk for the larger proximities, small child, no restraint, internal loose objects, etc. The contact velocity under these circumstances is the original vehicle velocity plus rebound velocity. Rebound also affects the quality of ride-down, exposing the body part to increased deceleration. Accordingly, the issue of rebound is important. The work is a contribution by the author.

The effect of velocity and mass in the theoretical formation of rebound is considered in this section. Rebound is also considered later on a phenomenological basis later where it is found to be in fixed proportion to initial impact velocity. It is this finding and earlier evidence of inertial stress that motivates the two theoretical models.

In this section two models are presented to explain the behaviour of an occupant cell in response to impact with respect to rebound at the instantaneous level. The proportional model postulates that plastic action ceases at a fixed percentage of crash stroke irrespective of velocity. The other model recognizes a threshold of force, the absolute value of which is determined by the dynamic plasticity of the material of construction of the front end crumple zone. This model is represented by the inertial stress model. Inertial and velocity stress terminology is used synonymously. Both models are visualized below:

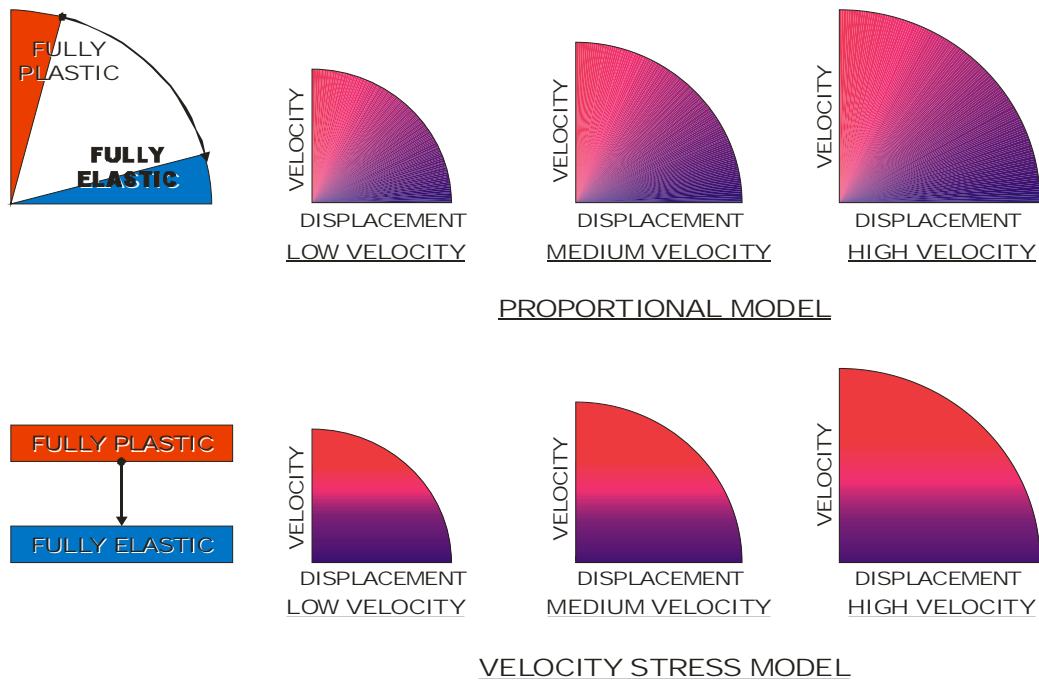


Figure 9-1: Theoretical models to explain formation of rebound.

In Figure 9-1 each quadrant represents a crash at low, medium and high velocity. The curved portion of the three quadrants of each model schematically represents the locus of time taken for the crash; the longer the $\frac{1}{4}$ circumference, the longer the time. In the proportional model then, the midway between plastic and elastic is approximately 45° . In the inertial stress model, the onset of pure elastic action is determined by the yield stress of the material.

The theoretical models rely on the assumption that a linear elastic spring system curve (as shown in the six velocity-displacement curves in Figure 9-1) is reasonably representative of the ingoing phase of the crash. A further simplification is that heavy items (engine, cross-member, etc.) interactions with occupant cell can be ignored. The assumption is summarized by all capacitive energy being formed during the ingoing phase and all capacity energy being discharged during rebound and prior to separation.

The correspondence of the system curves between linear elastic and test data has been presented in Figure 4-14. In this section, the rate of exchange of kinetic energy is compared with a linear elastic springs. Instantaneous reluctance and rate of instantaneous reluctance (abbreviated instant rate) are presented to demonstrate some validity for the two models.

The rebound prediction model presented later is phenomenologically based. The work presented here attempts to links the model causally.

The motivation of this section is to study support for either theoretical model in rebound formation taking into account, mass effects and/or velocity effects in crumple zone stiffness.

To demonstrate the existence of velocity effects, a study of a non-linear finite element analysis of the Ultra Light Steel Automobile Body (ULSAB) is presented. Although the analysis was performed by others, the presentation and conclusions drawn from the analysis output in support of the inertial stress perspective are by the author of this thesis.

The velocity perspective is further supported by presentation of a series of practical experiments which were performed by the author of this thesis to study the progression of strain disturbance in elastic media. A reader who is well-versed in the area of stress wave propagation can easily skip the section without loss of continuity. Even though the purpose of the experiments was to confirm existing theory, they are novel and provide new insight into the phenomena.

Stiffness of crumple zone at the instantaneous level is first considered with the expectation that effects of either the proportional or the inertial stress model may independently manifest. This level is considered for different initial impact velocities in barrier crash test data. Stiffness at the instantaneous level is also considered for variations in occupant cell mass keeping velocity constant in a simulation involving a multiple mass-spring model.

9.2 How Mass and Velocity Affects Models

At maximum dynamic crush, when the occupant cell is stopped, just prior to rebounding from the barrier, all kinetic energy is accounted for by either mechanical work done or stored energy in the form of elastic strain. A portion of elastic strain is recovered in the form of rebounding kinetic energy, rebound. In this idealization, the influence of heavy objects such as engine and wheelset bouncing out from the barrier and interacting out of phase with the occupant cell is ignored. The simplification assumes that these items are motion-still at the point of rebound. At the point of rebound all strain energy is assumed to have been formed. The rebound forming events are visualized below to occur only just prior to rebound. There may not be complete support for this idealization in a real crumple event; however, there is value in exploring the two theoretical models.

The proportional model is expected to predict a rebound increases with increase in velocity or mass while the inertial stress model is expected to predict a nominal fixed rebound irrespective of velocity increase. This is visualized by showing the system curves with velocity decay curves in time concurrently on the same graph, the technique having been presented earlier.

Pure plastic action is separated from pure elastic action by a single line, as idealized for the two models in Figure 9-2 and Figure 9-3 showing velocity increases.

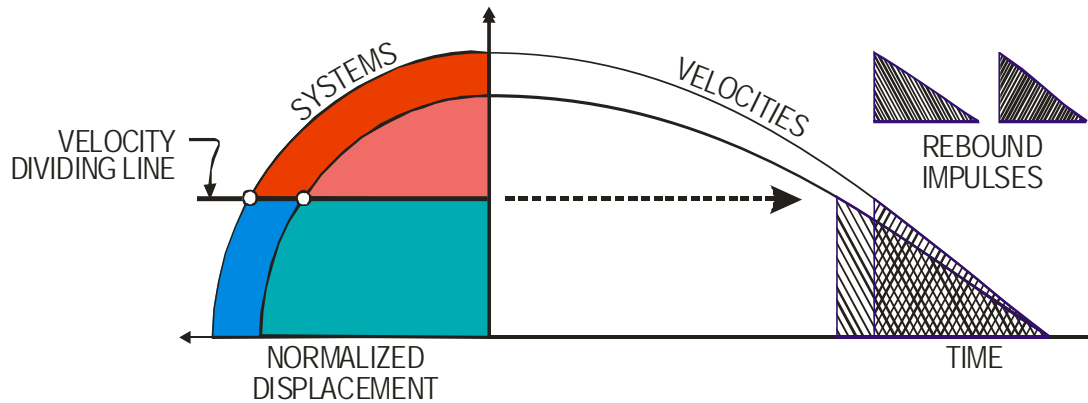


Figure 9-2: Inertial stress model showing reduction in rebound impulse with increase in velocity

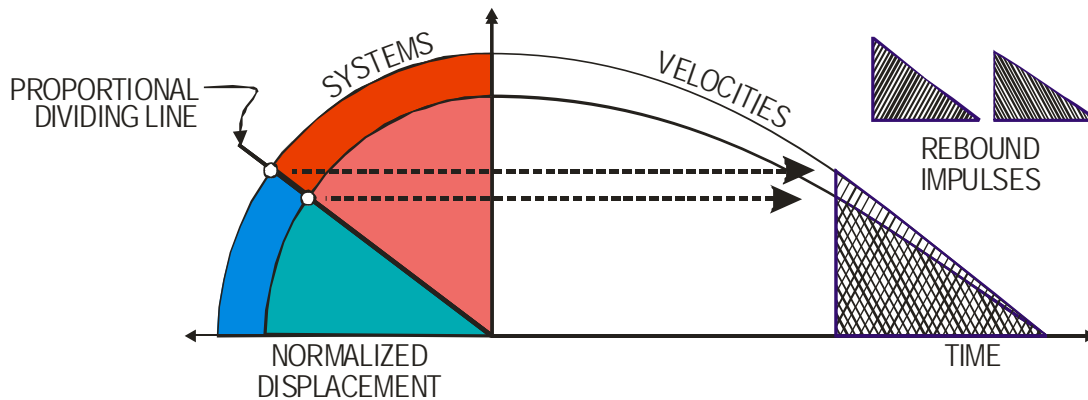


Figure 9-3: Proportional model showing increase in rebound impulse with increase in velocity.

Test data velocity decay curves may not necessarily coincide in time in a real crumple event, so adding to the degree of idealization. Notwithstanding, it is significant that one model predicts an increase in impulse with the other predicts a decrease.

Figure 9-4 and Figure 9-5 where the red shadings represent plastic working and blue shadings represent elastic working show the idealized differences in rebound formation for changes in velocity and changes in mass of occupant cell.

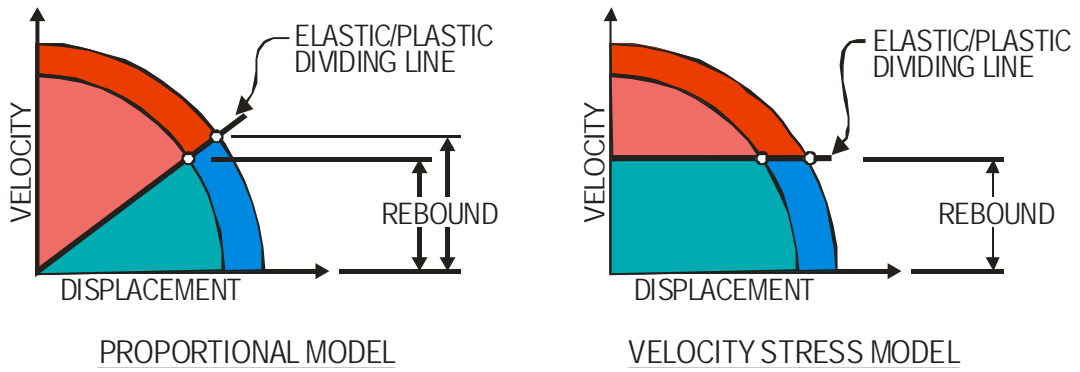


Figure 9-4: Models for rebound formation under conditions of increased velocity.

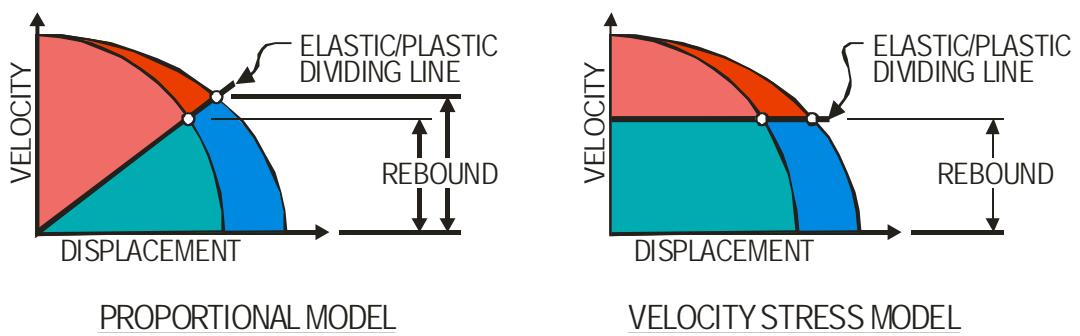


Figure 9-5: Models for rebound formation under conditions of increased mass.

The proportional model predicts rebound to commence at a higher velocity than would be the case for the inertial stress model. The additional rebound velocity is depicted for increased mass and increased velocity in Figure 9-6

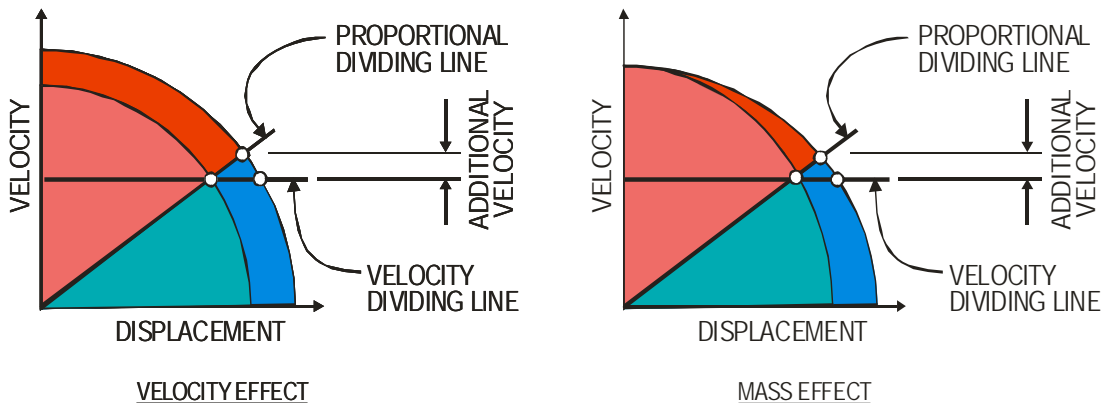


Figure 9-6: Increased rebound velocity prediction for mass and velocity effects.

The positions of the proportional and velocity dividing lines have been set in Figure 9-4 thru Figure 9-6 generally centrally for presentation convenience. When the two dividing lines are set higher on the normalized models it denotes one or both the following:

1. The initial velocities are lower (initial velocity is closer to yielding velocity).
2. The crumple zone material has higher yield strength.

The opposite applies to the converse. To illustrate this further, a fraction of initial velocity is introduced, q , to represent the quantitative relationship between the normalized idealized plastic/elastic dividing line and normalized initial velocity.

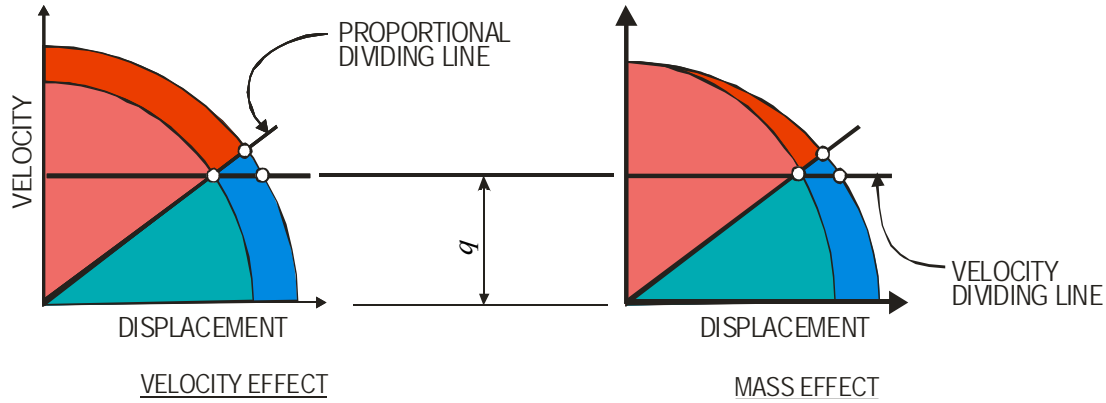


Figure 9-7: Fraction of normalized velocity concept.

To illustrate the fraction concept further high and low velocity conditions are shown in and high and low mass are shown in .

The additional rebound velocity shown in Figure 9-6 varies with the height of the dividing lines. The difference between the models becomes more 'noticeable' under certain circumstances. Effect discernment sensitivity is considered in Figure 9-8

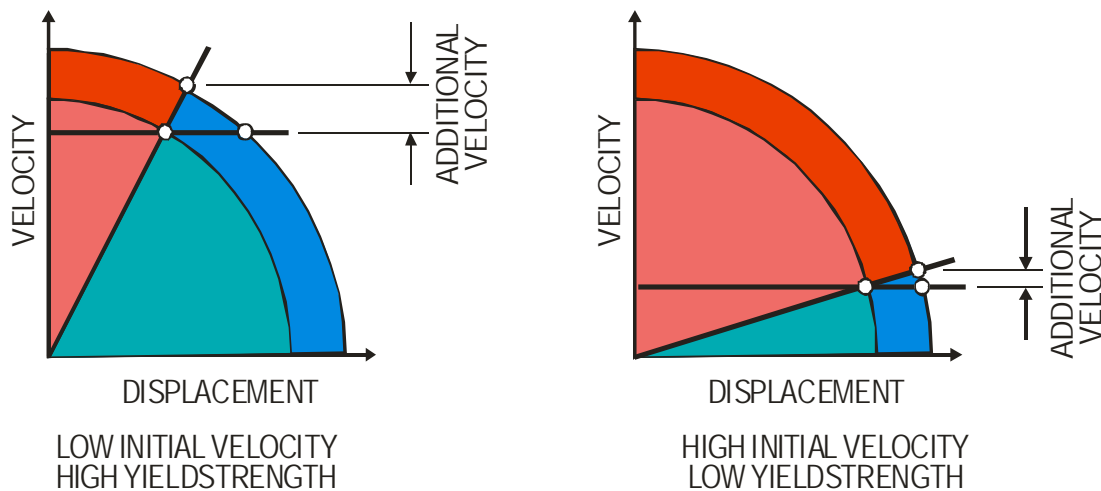


Figure 9-8: Discernment sensitivity of controlling effect varying velocity.

The proportional model then is expected to be more discernible in the data of low initial velocities and/or high material yield strength (high value of q). Conversely, if the data

reflects high initial velocities and/or low yield strength (low value of q), distinction between the two models fades.

This is not entirely the case when velocity is varied with an increase in occupant cell mass, to be demonstrated below.

Figure 9-9 represents a normalized velocity and normalized displacement system curve. Mass is added to increase the crush (normalized displacement) by an amount represented by E producing the outer ellipse. It is mathematically convenient to replace q with θ . High angles of θ represent low initial velocity (or high material yield strength), while low angles of θ represent high initial velocity (or low material yield strength). V_θ represents the increase of rebound velocity of the proportional model over the inertial stress model.

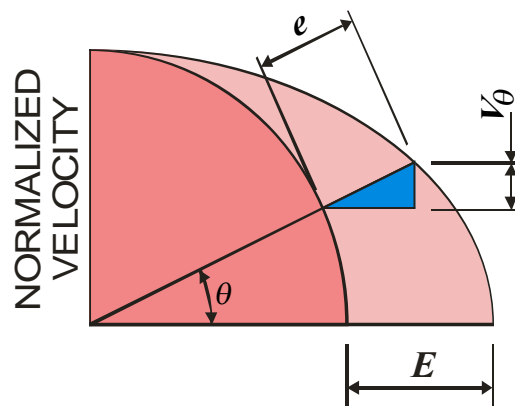


Figure 9-9: Mass influence sensitivity on rebound formation.

The length of e varies with θ as follows:

$$e = E \cdot \cos(\theta) \quad [9-1]$$

Increase in rebound velocity, V_θ varies with e as follows:

$$V_\theta = e \cdot \sin(\theta) \quad [9-2]$$

Combining Equations [9-1] and [9-2]:

$$V_\theta = E \cdot \cos(\theta) \cdot \sin(\theta) \quad [9-3]$$

Equation [9-3] is normalized on E and θ to give an expression for normalized rebound velocity in terms of position from θ representing a horizontal line to l representing a vertical line as graphed in Figure 9-10. It is semantically convenient to refer to the velocity fraction as high velocity fraction requiring merely reversal of the symmetrical curve.

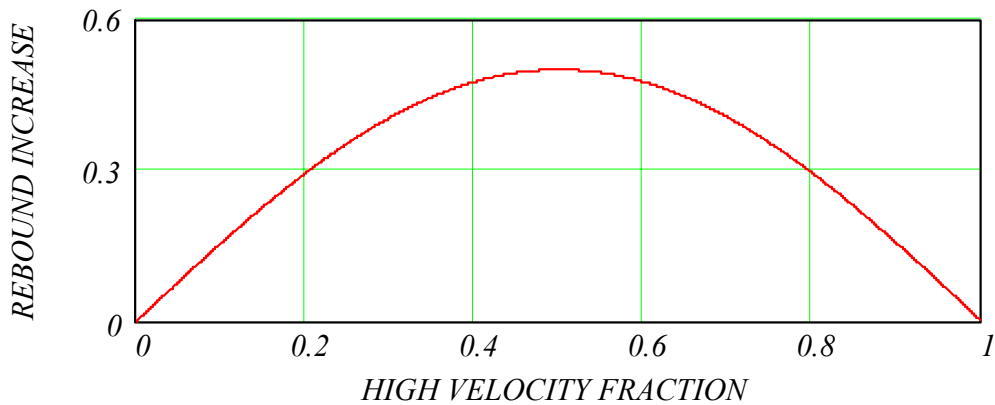


Figure 9-10: Mass effect comparing proportional model rebound increase over inertial stress model varying velocity fraction (0 denotes low velocity and 1 denotes high velocity crashes)

In the light of Figure 9-10 it is not expected to distinguish test data to a great extent for any influence that might result from additional mass on rebound at the upper and lower velocities.

9.3 Conclusion

Two theoretical models were presented to explain rebound formation in the crash prior to rebounding from the barrier. The proportional model supported earlier findings of high impedance in the last stages of the crash stroke. The inertial stress model predicted a constant rebound governed by the dynamic yield stress of the material of construction.

The inertial model was shown to be well founded in inertial stress coverage in the previous chapter while the proportional model is supported by test data in the next chapter. The value of presenting the inertial model is to balance the strong pull of theory and test data agreement in ascribing cause. In essence both models contribute to cause of rebound formation. Accordingly, both models need to be considered in an endeavour to reduce rebound. This makes both models important even though the proportional model is used in this study.

Optimization studies working with the proportional model might lead to late-sequenced relief devices alleviating high forces while the inertial model may lead to high aspect ratio horn sections coupled with low yield strength steel.

Accordingly both models are recommended for further study.

10. REBOUND IN THE FLEET

10.1 Introduction

In many papers comprising the literature rebound is disserted as structural restitution. Rebound is similarly considered here as structural restoration or discharge of capacitive energy built up during the ingoing phase. The correlation of rebound with initial impact velocities as a fixed proportion is represented by the proportional theoretical model of the previous section. It is pursued here in fleet data as represented in crash data recorded twenty years apart. The work is a presentation by the author.

The literature positions on coefficient of restitution are diverse. Wood (2000) in modelling the crumple zone as a collapsing tube found that “the magnitude of the rebound velocity is proportional to the forces on the body at the instant of maximum dynamic displacement ...” supporting an earlier assumption that all rebound is formed prior to rebound. Howard, Bomar et al. (1993) studied low speed impact (below 13 km/h) and found coefficients of restitution averaging 0.3.

Monson and Germane (1999) cite Marquardt (1974) that the coefficient of restitution (CofR) will never exceed 0.1. Emori (1970) recommends a CofR of 0 (fully plastic) for high speed impact. In partial support Strother (1985) found CofR significant up to speeds of 48 km/h (13.3 m/s). This was confirmed by the findings of Tamny (1992). Kerkhoff, Husher et al. (1993) found a descending linear function of velocity from 0.1 at 15 mph to 0.03 at 50 mph.

An almost opposite position to Marquardt (1974) was found when data for 161 vehicles in Smith and Tsongos (1986) was curve-fitted (by the author) to a power curve allowing extrapolation to emphasize the contradiction point.

This is shown in Figure 10-1. The values below 3.5 m/s appear to partially support Howard, Bomar et al. (1993) even though the Smith and Tsongos (1986) study is seven years older.

The diversity in the findings motivates this chapter to develop confidence in a constant proportional value for rebound for the range of velocities considered in this thesis.

This image is not available online. Please consult the hardcopy thesis available from the QUT Library.

Figure 10-1: Coefficient of restitution for 161 vehicles from Smith and Tsongos (1986) data.

No particular allowance appeared considered in the Smith and Tsongos (1986) study for the influence of vehicle mass in rebound. Other studies mentioned did not consider mass as a variable.

10.2 Mass Influence on Rebound

By way of introduction, one of the vehicles simulated to show mass softening is considered here for mass effect on rebound.

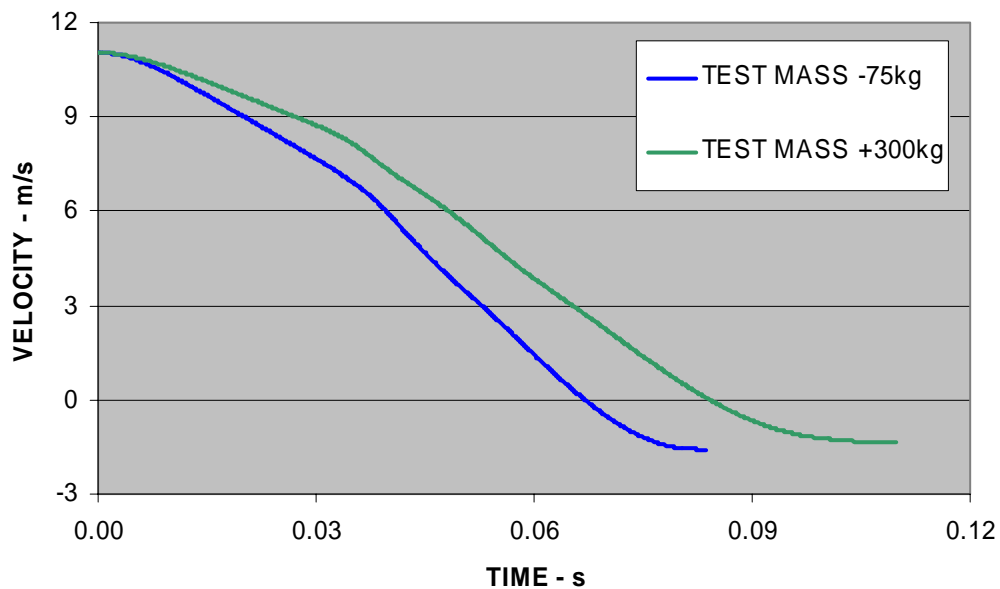


Figure 10-2: 1987 Hyundai Excel GLS Test #1092 40 km/h with 75kg deleted from test mass compared with 300kg added to test mass to compare rebound.

Figure 10-2 shows a slight decrease in rebound on account of a mass increase of 375kg.

The decrease in stiffness on account of mass increase was discussed in an earlier section.

To consider what aggregate effect vehicle mass variations may have, 73 ANCAP vehicles were studied. They were selected from the earliest tests and the most recent to achieve the following:

1. Determine the effect of mass on coefficient of restitution.
2. Gauge any improvement either absolutely or by trend.

Beyond the obvious motivation was an expectation to eliminate a variable (mass) from considerations in the light of findings depicted by Figure 10-2. The results were plotted and trended by a linear regression in Figure 10-3.

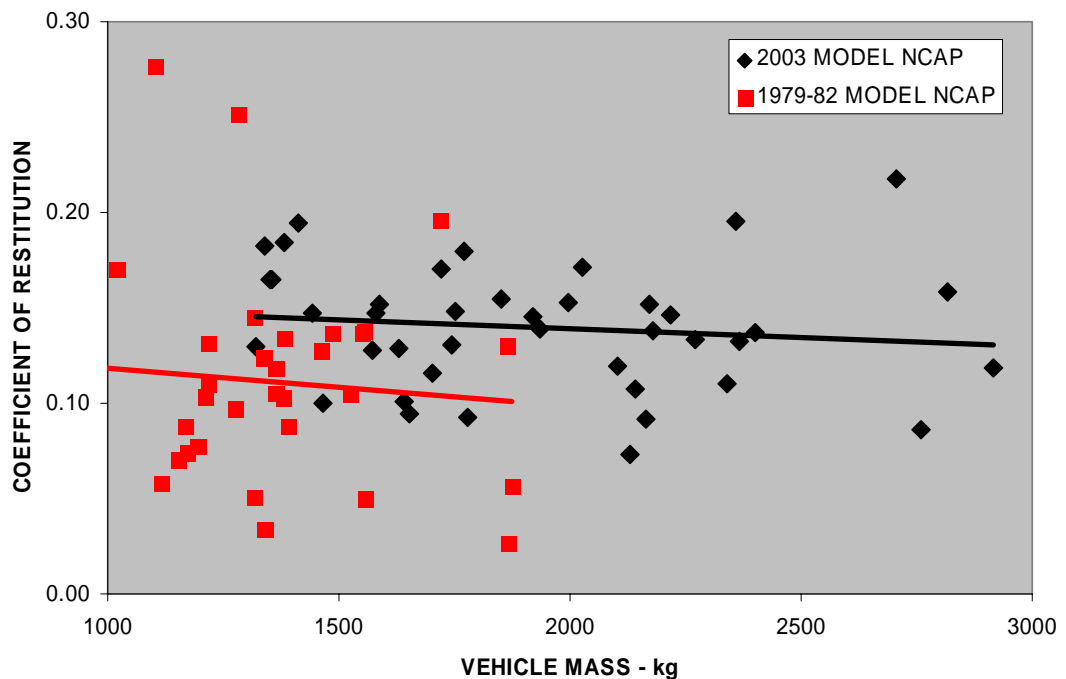


Figure 10-3: Comparison of coefficient of restitution of older to new NCAP cars (N=41 for 2003 models & N=32 for early models) linear regression lines to highlight trends.

It was concluded from Figure 10-3 that coefficient of restitution correlation trend with vehicle mass is unremarkable at the velocity considered and consistent with expectations resulting from Figure 10-2.

The two trend lines show an increase in the coefficient over the time periods. This runs counter to consumer expectations demanding improved passive safety.

10.3 Specific Energy Absorption

A portion of the initial kinetic energy is converted to heat sound and mainly mechanical work done. Some of it is merely stored and manifests by accelerating the vehicle in the opposite direction – rebound. A kinetic energy balance can be easily derived from test data, ascribing the difference between kinetic energy inbound to outbound to absorption. Specific

energy absorption is the ratio of absorbed energy to vehicle mass. It is expressed in units of Joules/kg. A similar treatment of this important measure was not found in the literature in respect of rebound. The presentation is a contribution by the author.

The presentation to follow is a perspective of the National fleet. It is not a statistical sample of the fleet because it is based on crash tests performed in response to legislation compliance for a particular vehicle model. To draw fleet wide conclusions, a distribution of such a vehicle model in the fleet would be needed. No attempt is made to draw such conclusions as this would widen the scope of the study unacceptably. Nevertheless, the study shows that no improvement in rebound reduction is evident sampling the 20 year period of compliance testing.

Nineteen vehicles were tested in 1983 against a rigid fixed barrier at nominal compliance speeds (30mph - 48km/h). Test weights and rebound velocities were extracted from the test reports and posted to Table 18.

Specific energy absorption (*sEA*) is derived from the kinetic energy equation omitting the mass component, as follows:

$$sEA := \frac{1}{2}(V^2 - R_v^2) \quad [10-1]$$

Where R_v is the rebound velocity and V the initial impact velocity.

As well, the average and standard deviation of the data was calculated and posted to

Eighteen modern vehicles models ranging from 1997 to 2000 year models were similarly treated except that rebound data was extracted from double integration of accelerometer test data. Table 21 refers.

The average specific Energy Absorption (*sEA*) derived from the data was 84.9 Joules/kg of vehicle mass for both studies. The standard deviation for the 1983 study was calculated at 1.2 J/kg while the modern study was 2.6 J/kg. The distribution across vehicles for the 1983 study was tighter about the mean while the modern study shows a greater variance from the mean. The implications of the greater variance in the modern study beyond the ostensible difference that the best vehicle performs significantly better than the worst, is beyond the intent of the study.

Table 20: Specific energy absorption for 1983 sample of cars.

TEST #	VEHICLE	MASS	TEST VELOCITY		REBOUND		
		kg	km/h	m/s	km/h	m/s	sEA
646	MITSUBISHI TREDIA	1001	47.5	13.2	2.9	0.8	86.7
647	MITSUBISHI CORDIA	998	47.0	13.1	3.3	0.9	84.8
648	AMC EAGLE	1456	47.1	13.1	6.1	1.7	84.2
649	RENAULT ALLIANCE	899	47.0	13.1	8.7	2.4	82.4
650	MAZDA 626	1047	47.2	13.1	8.1	2.2	83.4
651	TOYOTA TERCEL	995	47.0	13.1	3.6	1.0	84.7
652	FORD LTD	1339	47.1	13.1	5.0	1.4	84.7
653	DODGE 600	1236	47.1	13.1	6.7	1.9	84.0
654	NISSAN PULSAR	831	47.2	13.1	6.8	1.9	84.2
655	CHEV S10 BLAZER	1339	47.2	13.1	4.7	1.3	84.9
656	MITSUB MIGHTY MAX	1117	47.2	13.1	5.6	1.6	84.9
660	FORD THUNDERBIRD	1442	47.3	13.1	7.2	2.0	84.4
670	FORD BRONCO	1474	47.4	13.2	5.1	1.4	85.8
671	TOYOTA CAMRY	1090	47.0	13.1	5.7	1.6	84.0
657	FORD TEMPO	1118	47.4	13.2	4.6	1.3	85.7
672	CHEV CAVALIER	1166	47.5	13.2	3.1	0.9	86.7
673	NISAN STANZA	1045	47.5	13.2	6.8	1.9	85.2
658	FORD MUSTANG	1398	47.6	13.2	3.5	1.0	86.8
659	CHEV CELEBRITY	1248	47.6	13.2	5.6	1.6	86.1
AVERAGE sEA							84.9
STANDARD DEVN							1.2

Table 21: Specific energy absorption for modern cars.

TEST #	VEHICLE	MAS S	TEST VELOCITY		REBOUND		
		kg	km/h	m/s	km/h	m/s	sEA
2437	1997 FORD F150 PICKUP	2136	47.2	13.1	3.4	0.9	85.4
2462	1997 LINCOLN MARK	1921	46.5	12.9	3.4	0.9	83.0
2463	1997 CHRYSLER SEBRING	1717	47.2	13.1	5.2	1.4	84.9
2467	1997 FORD EXPEDITION	2513	47.2	13.1	5.5	1.5	84.8
2468	1997 SATURN SL1	1251	47.3	13.1	6.9	1.9	84.5
2469	1997 MITSUBISHI GALANT	1483	47.2	13.1	6.7	1.9	84.2
2489	1997 PONTIAC GRAND AM	1565	47.3	13.1	7.6	2.1	84.1
2497	1997 CADILLAC ELDORADO	1968	49.0	13.6	2.7	0.8	92.3
2498	1997 FORD E150 VAN	2474	46.8	13.0	5.5	1.5	83.3
2558	1997 CHEVROLET S-10	1880	47.2	13.1	5.1	1.4	84.9
2773	1998 PLYMOUTH VOYAGER	1870	47.0	13.1	5.9	1.6	83.9
2813	1998 NISSAN ALTIMA	1551	47.4	13.2	10.0	2.8	82.8
2830	1998 JEEP GRAND CHERK.	2024	46.7	13.0	5.7	1.6	82.9
2831	1998 BUICK CENTURY	1749	48.1	13.4	4.4	1.2	88.5
2833	1998 FORD ESCORT	1293	47.6	13.2	8.9	2.5	84.4
2895	1998 CHEVROLET VENTURE	2028	46.7	13.0	9.7	2.7	80.5
3346	2000 JEEP CHEROKEE	1873	47.8	13.3	6.8	1.9	86.4
3352	2000 CHEVROLET ASTRO	2367	48.0	13.3	6.6	1.8	87.2
AVERAGE sEA							84.9
STANDARD DEVN							2.6

To explore the concept of *sEA* further, another comparison was made but at a higher nominal test speed. The comparison was between the very first NCAP tests and the most recent. The expectations in making the comparisons were that the *sEA* value should be significantly higher for the modern NCAP tests as against cars 20 years older. The comparisons are posted to Table 22 and Table 23.

Table 22: Specific energy absorption values for oldest NCAP tests.

TEST #	VEHICLE	MASS	TEST VELOCITY		REBOUND		
		kg	km/h	m/s	km/h	m/s	<i>sEA</i>
216	1980 HONDA PRELUDE	1154	56.2	15.6	4.0	1.1	121.2
221	1980 EAGLE MPV	1868	56.2	15.6	1.5	0.4	121.8
263	1979 FORD FIESTA	991	56.2	15.6	1.8	0.5	121.7
271	1980 FORD THUNDERBIRD	1716	56.8	15.8	11.2	3.1	119.7
289	1980 SUBARU WAGON	1337	56.2	15.6	7.0	1.9	120.0
407	1982 FORD ESCORT	1168	56.5	15.7	5.0	1.4	122.2
418	1982 VOLVO DL	1521	56.2	15.6	5.9	1.6	120.5
444	1982 DODGE OMNI	1211	56.7	15.8	5.9	1.6	122.7
445	1982 VW SCIROCCO	1216	56.5	15.7	6.2	1.7	121.7
446	1982 SAAB 900	1461	56.8	15.8	7.3	2.0	122.4
448	1982 PLYMOUTH RELIANT	1273	56.0	15.6	5.5	1.5	119.8
450	1982 CHEV CAMARO	1555	57.0	15.8	7.9	2.2	123.0
451	1982 CHEV CELEBRITY	1485	56.3	15.6	7.7	2.1	120.0
452	1982 FORD ESCORT	1172	55.5	15.4	4.1	1.1	118.2
453	1982 DODGE 400	1381	56.3	15.6	7.6	2.1	120.1
454	1982 TOYOTA CELICA	1388	55.8	15.5	4.9	1.4	119.2
455	1982 HONDA ACCORD	1195	56.0	15.6	4.3	1.2	120.3
462	1982 NISSAN STANZA	1218	55.7	15.5	7.3	2.0	117.6
463	1982 RENAULT FUEGO	1316	56.3	15.6	2.9	0.8	122.0
464	1982 NISSAN SENTRA	1114	56.7	15.8	3.3	0.9	123.6
465	1982 VW QUANTUM	1340	55.7	15.5	1.9	0.5	119.6
466	1981 CHEVROLET IMPALA	1864	56.8	15.8	7.4	2.1	122.4
467	1982 VOLVO DL	1550	56.2	15.6	7.7	2.1	119.6
468	1982 FORD LTD	1873	57.0	15.8	3.2	0.9	125.0
470	1982 MAZDA 626	1315	56.7	15.8	8.3	2.3	121.4
471	1982 FORD GRANADA	1556	55.7	15.5	2.8	0.8	119.4
477	1982 CHEV CITATION	1361	56.7	15.8	6.0	1.7	122.7
496	1982 TOYOTA CORONA	1379	56.0	15.6	5.8	1.6	119.7
522	1981 MAZDA GLC	1103	56.3	15.6	15.6	4.3	112.9
523	1982 CHEV CAVALIER	1284	56.3	15.6	14.2	3.9	114.5
550	1982 CHRYSLER LE BARON	1361	56.8	15.8	6.7	1.9	122.7
610	1982 RENAULT LE CAR	1018	56.2	15.6	9.6	2.7	118.3
AVERAGE <i>sEA</i>							120.5
STANDARD DEVN							2.5

Table 23: Specific energy absorption values for most recent NCAP tests.

TEST #	VEHICLE	MASS kg	TEST VELOCITY		REBOUND		
			km/h	m/s	km/h	m/s	sEA
4217	TOYOTA MATRIX	1411	55.9	15.5	10.9	3.0	116.1
4255	ACURA 3.2 TL	1771	55.8	15.5	10.0	2.8	116.1
4259	CADILLAC CTS	1851	56.7	15.7	8.8	2.4	120.8
4266	TOYOTA COROLLA	1350	55.9	15.5	9.2	2.6	117.3
4303	HONDA PILOT	2173	55.9	15.5	8.5	2.4	117.8
4419	TOYOTA COROLLA	1355	56.2	15.6	9.3	2.6	118.5
4435	FORD EXPEDITION	2758	56.5	15.7	4.8	1.3	122.3
4444	BMW Z4 ROADSTER	1630	57.0	15.8	7.3	2.0	123.2
4445	CHEVROLET CAVALIER	1382	55.9	15.5	10.3	2.9	116.6
4446	FORD ESCORT ZX2	1340	56.5	15.7	10.3	2.9	119.1
4457	HONDA ACCORD	1586	56.5	15.7	8.6	2.4	120.3
4459	TOYOTA TUNDRA	2217	55.9	15.5	8.2	2.3	117.9
4460	NISSAN FRONTIER	1998	55.6	15.4	8.5	2.4	116.4
4462	HONDA S2000	1465	57.0	15.8	5.7	1.6	124.0
4463	HONDA ODYSSEY	2178	56.8	15.8	7.9	2.2	122.1
4464	CHEV AVALANCHE	2917	56.6	15.7	6.7	1.9	121.9
4472	CHEV SILVERADO	2359	55.9	15.5	10.9	3.0	116.0
4473	HYUNDAI ACCENT	1322	55.8	15.5	7.2	2.0	118.3
4476	FORD CROWN	2128	56.8	15.8	4.2	1.2	123.8
4477	NISSAN 350Z	1723	55.7	15.5	9.5	2.6	116.0
4478	TOYOTA TACOMA	1918	55.6	15.4	8.1	2.2	116.8
4479	SUBARU FORESTER	1640	57.0	15.8	5.7	1.6	123.9
4483	MERCEDES E320	1935	56.7	15.7	7.9	2.2	121.4
4484	JAGUAR X-TYPE	1777	55.7	15.5	5.1	1.4	118.8
4485	HONDA ACCORD	1571	55.8	15.5	7.1	2.0	118.2
4486	TOYOTA AVALON	1752	56.7	15.7	8.4	2.3	121.1
4487	SATURN ION	1444	56.1	15.6	8.3	2.3	118.6
4488	MAZDA A6	1579	55.8	15.5	8.2	2.3	117.5
4491	MERCEDES C230	1704	56.3	15.6	6.5	1.8	120.7
4493	VOLVO XC 90	2166	56.5	15.7	5.2	1.4	122.1
4500	ISUZU RODEO	2102	56.7	15.7	6.8	1.9	122.0
4544	NISSAN MURANO	2028	56.1	15.6	9.6	2.7	117.7
4545	TOYOTA SEQUOIA	2339	56.5	15.7	6.2	1.7	121.6
4546	TOYOTA 4RUNNER	2140	56.2	15.6	6.1	1.7	120.3
4548	KIA SORENTO	2271	56.2	15.6	7.5	2.1	119.8
4549	CHEVROLET TAHOE	2706	56.3	15.6	12.3	3.4	116.6
4555	HONDA ELEMENT	1745	56.0	15.6	7.3	2.0	119.0
4559	MITSUB OUTLANDER	1652	56.3	15.6	5.3	1.5	121.2
4560	BMW X5	2400	55.8	15.5	7.7	2.1	118.0
4567	CHEV SUBURBAN	2816	56.3	15.6	8.9	2.5	119.4
4572	CHRYSLER PACIFICA	2367	56.7	15.7	7.5	2.1	121.6
					AVERAGE sEA		119.5
					STANDARD DEVN		2.4

The average specific energy absorption for the older NCAP cars at an average of 120.5 Joules/kg was greater than the 119.5 Joules/kg for the newer cars. This means there is less energy absorption in the modern cars. Consumer expectation would be that there should be more.

10.4 Velocity Influence on Rebound

Monson and Germane (1999) studied 53 legislation compliance crash tests at nominally 48 km/h and 70 NCAP tests at nominally 56km/h. They concluded that there is an increase with velocity in average coefficient of restitution from 0.139 to 0.152 compliance/NCAP respectively. Because these values were based on averages taken at the nominal test speeds, it was thought that there was risk of distortion on account of the narrow spread of velocity. Also a vehicle represented in NCAP may not have the exact vehicle model represented in the compliance testing list.

To eliminate some of the variables above, the presentation to follow uses three test speeds for each of the six models with a seventh model having only two tests but with velocities wide apart.

Table 24: Rigid barrier full frontal tests used to show velocity influence on restitution.

TEST NO	YEAR	VEH ID	INITIAL VELOCITY		REBOUND VELOCITY		SEA
			km/h	m/s	km/h	m/s	
3833	2001	FORD F150	39.91	11.1	5.26	1.5	60.4
3902			47.70	13.3	5.20	1.4	86.7
3494			56.02	15.6	5.37	1.5	120.0
4196	2002	ISUZU RODEO	39.91	11.1	5.90	1.6	60.1
4241			56.66	15.7	7.55	2.1	121.7
3805	2001	TOYOTA ECHO	40.02	11.1	7.21	2.0	59.8
3806			47.92	13.3	7.27	2.0	86.6
3537			56.60	15.7	7.11	2.0	121.6
4319	2001	HONDA ACCORD	40.30	11.2	7.53	2.1	60.5
3801			47.90	13.3	7.59	2.1	86.3
3611			56.31	15.6	8.56	2.4	119.5
3817	2001	FORD ESCAPE	40.08	11.1	4.62	1.3	61.2
3784			48.25	13.4	4.34	1.2	89.1
3593			56.39	15.7	4.31	1.2	122.0
3798	2001	CHEV IMPALA	39.95	11.1	6.88	1.9	59.7
3843			47.82	13.3	7.96	2.2	85.8
3471			56.20	15.6	7.25	2.0	119.8
3225	2000	FORD TAURUS	44.04	12.2	9.87	2.7	71.1
3224			48.31	13.4	8.09	2.2	87.5
3248			56.70	15.7	8.94	2.5	120.9

A quick overview of rebound velocity vs. initial velocity will disclose an apparently random correlation ranging from U-shape for the F150 and Taurus to increasing for the Rodeo and Honda. There appeared a clear trend with the *sEA* values. The *sEA* from Table 23 was graphed as a scatter graph and a linear regression line fitted. The fit was good, however a power series curve fitted better. The scatter graph is shown as Figure 10-4.

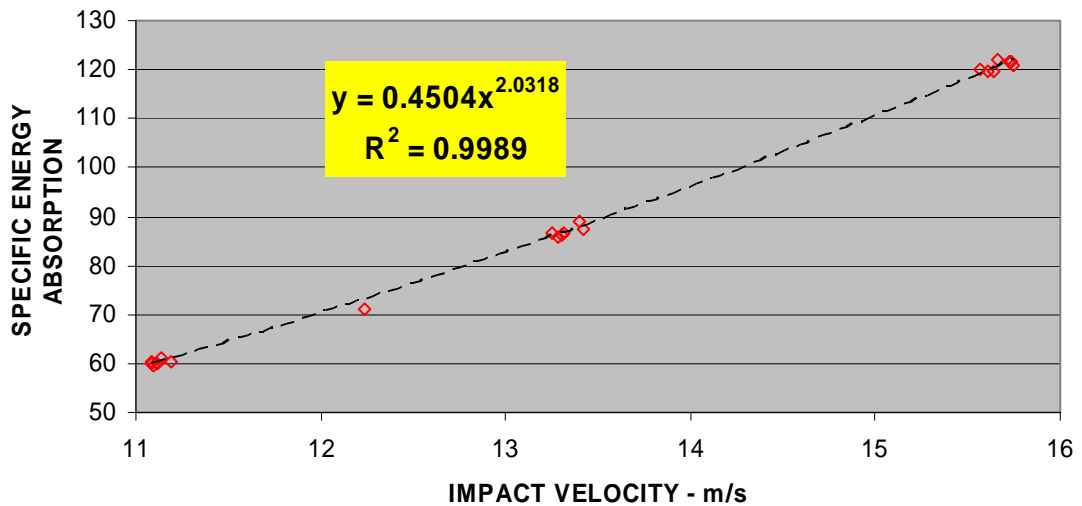


Figure 10-4: Best power curve-fit to data from Table 24.

The index in the fit equation was too close to ignore the appeal of a quadratic potentially having roots in the kinetic energy equation. The data was fitted to an $a \cdot x^2$ curve and the coefficient of determination compared.

The coefficient of determination (R^2) was found to be 0.9987 comparing favourably with the earlier best fit value of 0.9989. Accordingly, the following relationship was adopted as explaining the data very well:

$$sEA := 0.490 \cdot V^2 \quad [10-2]$$

When set equal to the specific energy definition equation, the following expression results:

$$\frac{1}{2}(V^2 - R_v^2) = 0.490 \cdot V^2 \quad [10-3]$$

Giving the following expression for rebound:

$$R_v := 0.141 \cdot V \quad [10-4]$$

From which the coefficient of restitution can be extracted:

$$CofR := 0.141 \quad [10-5]$$

The equation will now be used in a rebound comparison with the Monson and Germane (1999) values.

Table 25: Results of rebound equation compared with literature.

<u>Test Speed</u>	<u>Rebound Velocity</u> $R_v := 0.141 \cdot V$	<u>Rebound Velocity</u> <u>Monson and Germane</u> <u>(1999)</u>
48 km/h	1.88 m/s	1.85 m/s
56 km/h	2.19 m/s	2.36 m/s

The results of the study are similar to the values from the literature. When the individual $CofR$ is determined for each vehicle, a different result emerges. The average $CofR$ becomes 0.1338, highlighting the folly of averages. The results of individual vehicle velocities correlated to their specific energy absorption as shown in Table 24 is determined giving the coefficient a for the power equation (index 2) and the calculated $CofR$ are summarized to Table 26 together with the regression coefficient.

Table 26: Results of individual curve-fit of specific energy absorption and velocity giving individual vehicle coefficients of restitution.

VEH ID	a	CofR	R²
FORD F150	0.4918	0.1281	0.999976
ISUZU RODEO	0.4925	0.1225	0.999942
TOYOTA ECHO	0.4911	0.1334	0.999889
HONDA ACCORD	0.4888	0.1497	0.999827
FORD ESCAPE	0.4956	0.0938	0.999993
CHEV IMPALA	0.4890	0.1483	0.999814
FORD TAURUS	0.4871	0.1606	0.999659
AVERAGE CofR =		0.1338	

The very high regression coefficient (coefficient of determination – R^2) suggests that the power curve may have good predictive capabilities.

10.5 Rebound Prediction Example

To test the predictive capabilities of the above power curve system a late model vehicle was selected having available two full frontal rigid barrier crash test data at different crash velocities but not out of the selection above. The choice was for a 1998 Nissan Altima automatic front-wheel drive four door sedan at nominal speeds 56 km/h and 48 km/h. The accelerometer trace from a stable point within the vehicle was integrated and graphed comprising Figure 10-5:

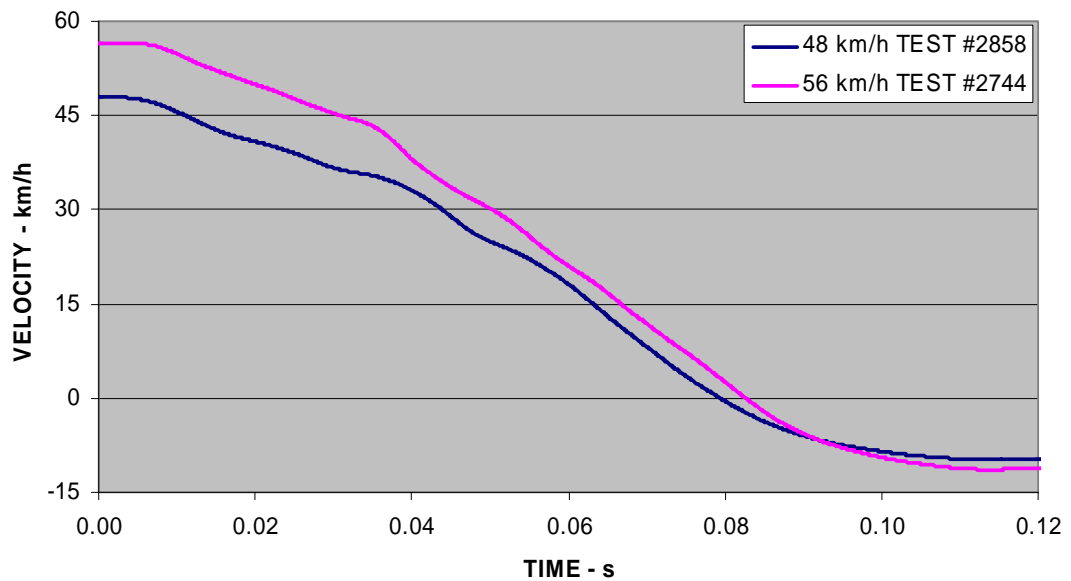


Figure 10-5: Velocity-time graph for 1998 Nissan Altima full frontal rigid barrier tests #2858 & #2744

Rebound velocities were read off the graph at 9.8 km/h and 11.4 km/h for #2858 and #2744 respectively. The higher rebound was predicted from the lower value and vice versa. A two-step process was involved in each case, as follows:

1. Determine the regression coefficient a from the test data.
2. Use the regression coefficient a to predict the rebound.

The relevant equations stem from setting specific energy absorption from the test and correlation equal, as follows:

$$sEA_{Test} = sEA_{Correlation}$$

$$\frac{1}{2}(V^2 - R_v^2) = a \cdot V^2 \quad [10-6]$$

Transposing to make regression coefficient a the dependant variable:

$$a = \frac{I}{2} \cdot \left(I - \frac{R_v^2}{V^2} \right) \quad [10-7]$$

Test values are assigned to Equation [10-7] and a value calculated and used in Equation [10-8]. In Step 2, Equation [10-6] is transposed to make rebound velocity R_v the dependant variable:

$$R_v = V \cdot \sqrt{I - 2 \cdot a} \quad [10-8]$$

Predicted rebound velocity is calculated using the regression coefficient a as previously determined. The results predicting both up and down as well as the error are tabled below:

Table 27: Predicted rebound values for 1998 Nissan Altima.

SOURCE TEST	INITIAL VELOCITY m/s		REBOUND m/s		ERROR %
	SOURCE	TARGET	ORIGINAL	PREDICTED	
2744	15.73	13.30	2.72	2.67	1.8
2858	13.30	15.73	3.16	3.22	1.9

The calculated errors of predicted rebound values compared to the test values of less than 2% is thought to be much lower than the accuracy demanded of the general process of crash testing and injury assessment. The method of prediction can accordingly be recommended subject to further testing.

10.6 Conclusion

It was shown in this section that vehicle mass is not a significant influencing factor in rebound. Specific energy absorption, meaning energy absorption per kilogram of vehicle mass, was shown to be a good predictor of rebound between nominally 40 km/h and 56 km/h. An average coefficient of restitution of 0.14 was presented showing excellent agreement with test data over a wide range of vehicle size and velocities. The average coefficient of restitution is also in general agreement with recently published literature values. Whilst it was shown that the averaging of the coefficient of restitution over a number

of vehicles is prone to error, prediction of individual vehicle rebound at other than test speeds was shown to be feasible with little error using the presented technique.

The crash testing regime demonstrating legislative compliance and the higher speed NCAP have failed to reduce rebound over 20 years of testing. Instead rebound has increased, contrary to consumer expectations.

10.7 Discussion

It appears from the work so far that rebound is linearly related to initial velocity and that the relation to rebound is contained in the information gained from a single crash test. This was one of the base objectives prescribed at the outset. The structural restitution of a crumple zone is a complex event. The diversity and sometimes conflicting findings in the literature suggest a discussion of factors influencing rebound is appropriate. The points of discussion are listed in summary below:

1. Heavy objects rebounding within crumple zone prior to separation.
2. Internal cold working causing work hardening.
3. Accelerometer reads elastic pulse – delay in registering events under bonnet.
4. Locked stresses being carried away after separation.
5. Occupant cell rebounding from heavy objects after separation.
6. Theoretical models.

1. Heavy objects rebounding within crumple zone prior to separation.

The heavy objects such as engine and cross-member do not become stationary once forward components have been crushed but behave not unlike a mass in a spring system of masses with different mode shapes of vibration. This phenomenon can be observed from high speed cinematography taken from the underside of the engine area. It is shown here by integrating accelerometer traces from the engine and occupant compartment. The resulting velocity-time curves comprise Figure 10-6 for a 2003 Model Toyota Matrix NCAP Test No 4217 suitably annotated to highlight the salient phenomenon.

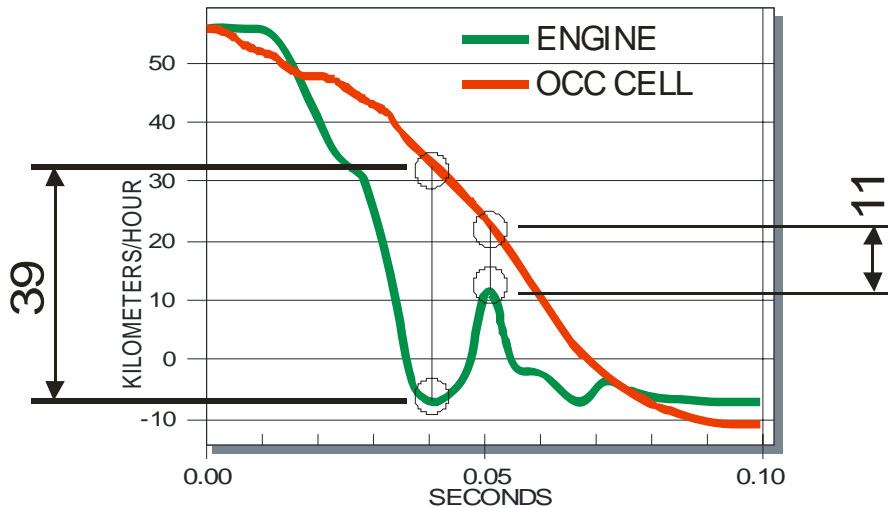


Figure 10-6: Velocity-time curves for 2003 Toyota Matrix highlighting rapid relative velocity change of engine to occupant cell from 39 km/h difference to 11 km/h difference in 10 milliseconds.

In the tight under-bonnet packaging of modern cars, it can be expected that the engine interacts with the firewall or through engine mounts and thus influence the occupant cell velocity profile. The effect on occupant cell velocity from the first highlight (0.04s) in Figure 10-6 to the second highlight (0.05s) would be beneficial as it would lengthen the occupant cell time to separation. Immediately beyond the second highlight is reverse, tending to shorten the time.

The jostling forward and back would pound away on internal members to lock in elastic stresses. The jostling would also plastically work the elements and dissipate energy to reduce rebound.

2. Internal cold working causing work hardening.

The jostling referred to above is relevant to all the heavy members in the crumple zone. Cold working of structural element can increase strain hardening. Strain hardening raises the yield point of the material. The higher the yield point of the material, the more strain energy is available for rebound.

3. Accelerometer reads elastic pulse – delay in registering events under bonnet.

The occupant cell stable point accelerometer is remote from the plastic workings of the crumple zone both physically and by time registering a delay to allow the elastic signal to arrive by way of a material strain disturbance. Other strain disturbances created earlier and

reflected also arrive simultaneously. The process can introduce errors. For this reason the data is often supported by cinematographic calibrations. Only accelerometer data was used for this study.

4. Locked stresses being carried away after separation.

Varat and Husher (2000) found over many tests that some dimensional crumple recovery took place well after separation. This would be of significant interest to Accident Reconstructionists who predict impact velocity from residual crush. In this work locked in stresses are treated as if they were plastic work done.

5. Occupant cell rebounding from heavy objects after separation.

The assumption that all kinetic energy is converted to either strain energy or mechanical work done at the point of rebound is a simplification. Rebound of individual objects is phased so that heavy objects may rebound out of phase and act in mitigation or exacerbation of occupant cell rebound after separation.

6. Explanatory Theories.

The two theoretical models were presented as if mutually exclusive one against the other. This was done for presentation convenience and clarity. Interaction between the two models was not considered and is recommended for further study.

BLANK

11. MASS & STIFFNESS TRENDS IN FLEET

11.1 Introduction

The objective for this section is to examine the mass and stiffness trends over time. These trends are a test of the efficacy of legislation governing crash testing procedures, amongst other things..

It would be difficult to obtain a statistical sample of unscheduled crashes that occurred under identical conditions. Fortunately, the crash testing regimes have produced test results at constant nominal velocity and conditions. However, to represent the fleet accurately requires weighting according to the frequency with which each test vehicle occurs in the fleet. This step has been omitted in this analysis owing to the need to bring the project to a timely completion. However, the representativeness issue is recommended for future study.

This chapter is a contribution by the author. Two sets of data are considered. The first is a study of 1622 crash tests sourced directly from the NHTSA database. The other data st was sourced from Hollowell, Gabler et al. (1999) because dynamic crush distance rather than static crush distance was used in this study. Dynamic crush distance is preferred for injury determinations. The NHTSA database sourced data is included because of the greater numbers of crashes available and because the tests are over a wider base of crash velocity than just the NCAP speeds.

The salient results of these tests are used in the present analysis and are tabled below showing the first four and the last four tests, curtailed for brevity.

Table 28: Table of 558 NCAP tests showing first and last four tests.

TEST	YEAR	MAKE & MODEL	VEHICLE MASS kg	TEST SPEED km/h	CRUSH m	STIFFNESS kN/m
5	80	CHEVROLET CITATION	1465	56.3	0.785	581.5
7	79	VOLKSWAGEN RABBIT	1179	56.0	0.719	551.9
27	79	TOYOTA CELICA	1372	56.0	0.767	564.3
33	79	PLYMOUTH CHAMP	1051	56.8	0.818	391.0
"	"	"	"	"	"	"
"	"	"	"	"	"	"
2550	97	DODGE DAKOTA	2015	56.6	0.602	1374.4
2551	97	BUICK LESABRE	1788	56.5	0.866	587.3
2552	97	CHEVROLET VENTURE	1946	56.8	0.760	838.7
2556	97	JEEP CHEROKEE	1839	56.2	0.632	1122.1

Table 29: Table of 1622 NHTSA tests showing first and last four tests.

TEST	YEAR	MAKE & MODEL	VEHICLE MASS kg	TEST SPEED km/h	CRUSH mm	STIFFNESS kN/m
72	78	CHEVROLET IMPALA	1997	56.8	511	581.5
103	78	SUBARU BRAT MPV	1300	47.6	541	551.9
128	78	TOYOTA CRESSIDA	1547	47.6	531	564.3
135	78	MAZDA RX	1496	48.3	588	391.0
"	"	"	"	"	"	"
"	"	"	"	"	"	"
2550	04	TOYOTA 4RUNNER	2277	56.17	580	1648
2551	05	CHRYSLER T & C	2229	56.49	602	1514
2552	05	FORD ESCAPE	1797	56.3	527	1582
2556	05	CHEVROLET EQUINOX	2015	56.3	657	1142

11.2 Errant Trends

To show the spread of data and to highlight the scope for drawing wrong conclusions from demographic data, the NCAP test data is plotted for vehicle mass and crush.

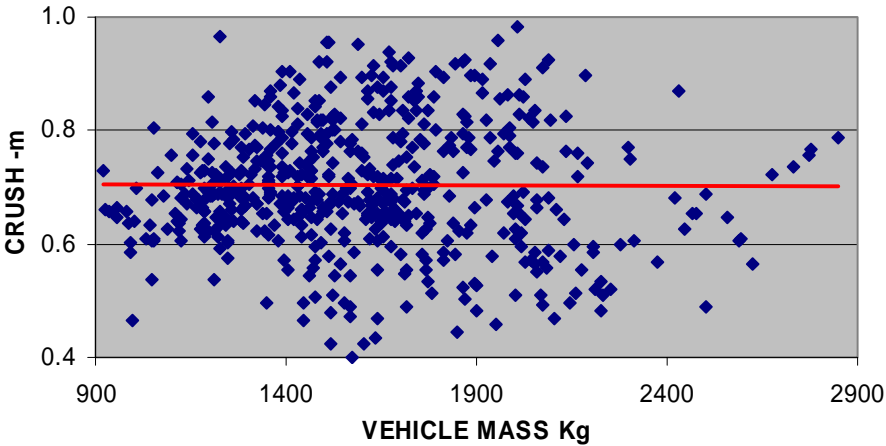


Figure 11-1: 558 NCAP tests mass-crush plot with trend line.

Superficially, Figure 11-1 suggests vehicle mass has no influence on crush. Intuitively, the greater the mass, the greater the crush expected. Moreover, intuition was confirmed by simulation and physical testing in a previous presentation for this thesis.

Similar scope for wrong conclusions flow from correlating the NHTSA linear stiffness parameter with vehicle mass

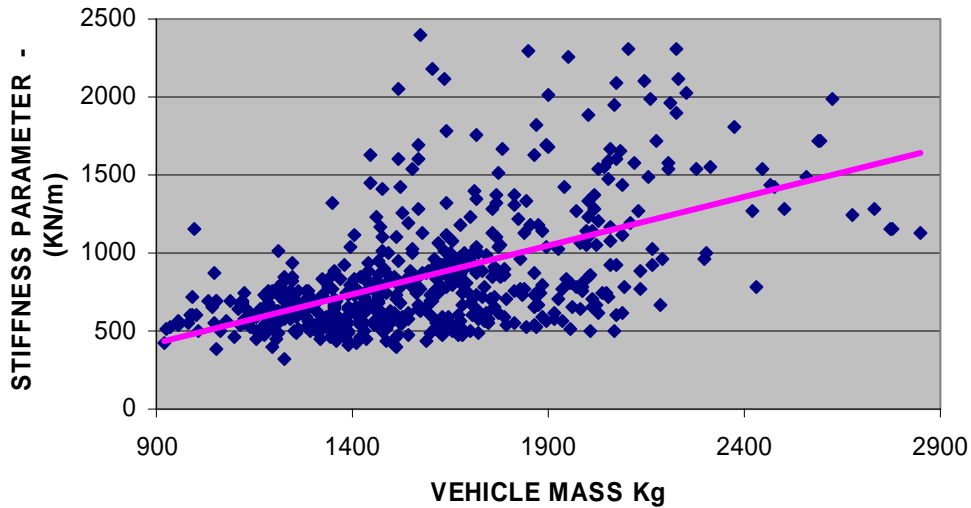


Figure 11-2: 558 NCAP tests mass-stiffness plot with trend line.

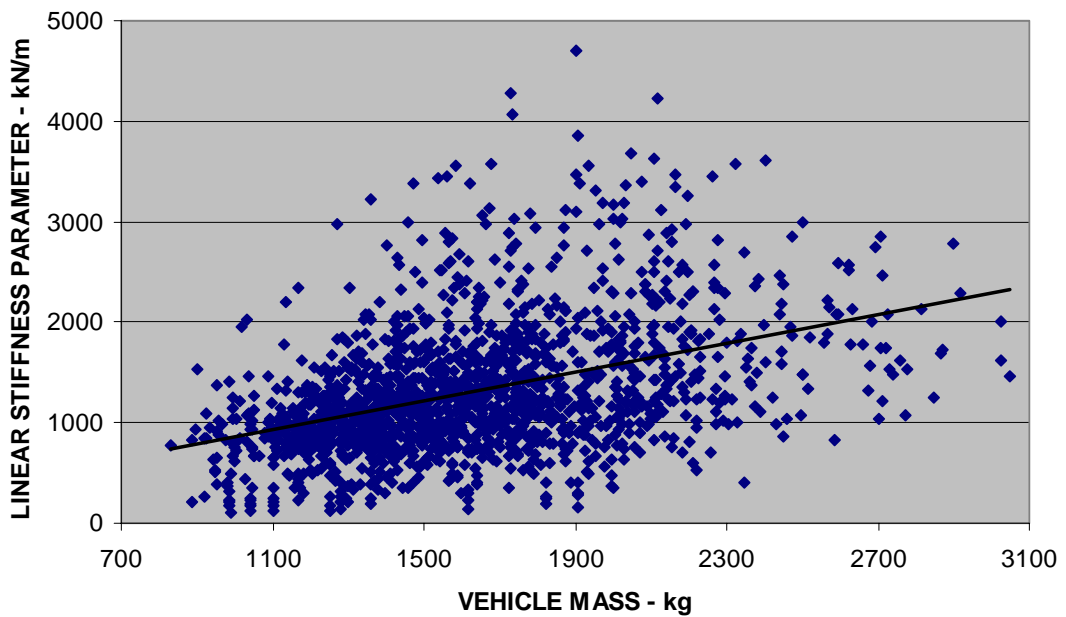


Figure 11-3: NHTSA crash tests mass-stiffness plots for 1622 vehicles.

Gabler and Hollowell (2000a) note that "... stiffness of a vehicle is also somewhat related to its mass". Similarly, the mass/stiffness relational view is also shared by Abdel-Aty (2002) who writes: "...stiffness correlates more or less with mass."

In the literature commentary related to Figure 11-2, the conclusion follows that increased vehicle mass increases stiffness. The contrary was shown in an earlier presentation showing that vehicle stiffness reduces with increase in mass.

Without a clear causal nexus between mass and stiffness, conclusions affecting structural vehicle stiffness do not necessarily follow from demographic considerations.

Such a nexus can be demonstrated, for example, a heavier car is likely to have heavier structural components to resist the demand of the higher stresses associated with the increased mass. If a car is considered as a simply supported beam then its bending moment is proportional to its span or wheelbase. It is not surprising to see a relationship between wheelbase and vehicle mass in fleet demography. This can be seen in Figure 11-4 which was converted to metric from Joksch, Massie et al. (1998) An increased chassis bending strength is likely to have real effect on structural stiffness in terms of axial crush loading strength.

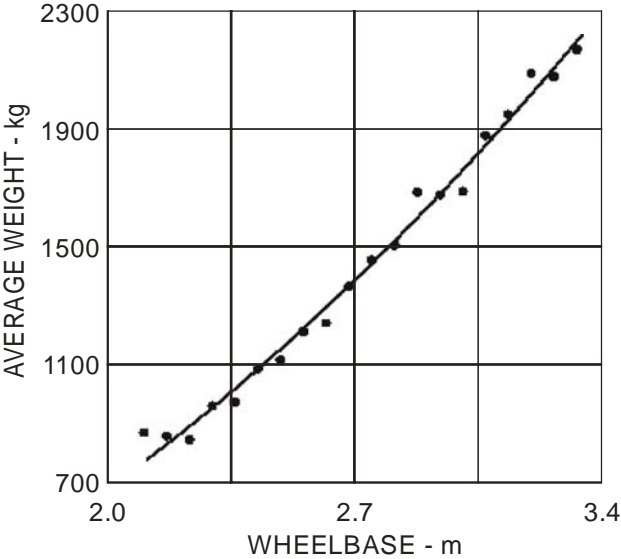


Figure 11-4: Demographic relationship of wheelbase and vehicle mass.

A simple procedure to show stiffness trend over time would be to average and plot the NCAP linear stiffness parameter data for the year of capture. This was done to produce Figure 11-5.

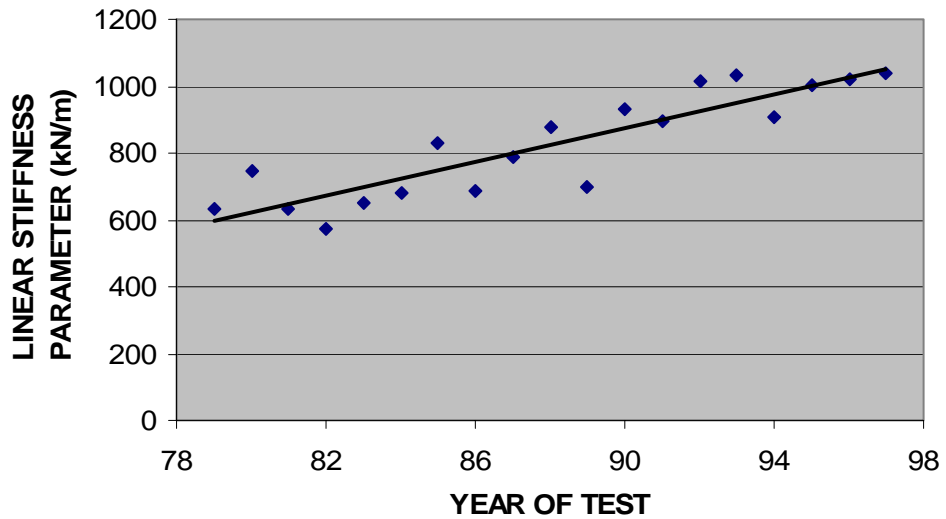


Figure 11-5: NCAP cars linear regression analysis of average linear stiffness in year of test.

Figure 11-5 indicates an increase in demographic stiffness. However, these results are sensitive to vehicle mass variations owing to the nature of the NHTSA linear stiffness parameter equation, Equation [4-1]. The linear correspondence between parameter k and mass M on opposite sides of the equation suggests that an increase in mass will have a proportionate increase in stiffness parameter. Figure 11-5 may thus merely reflect a mass increase in the fleet. This is highlighted by the changing trends in Figure 11-6. The yearly results are not averaged to show the spread. This is to visually support the changing slopes.

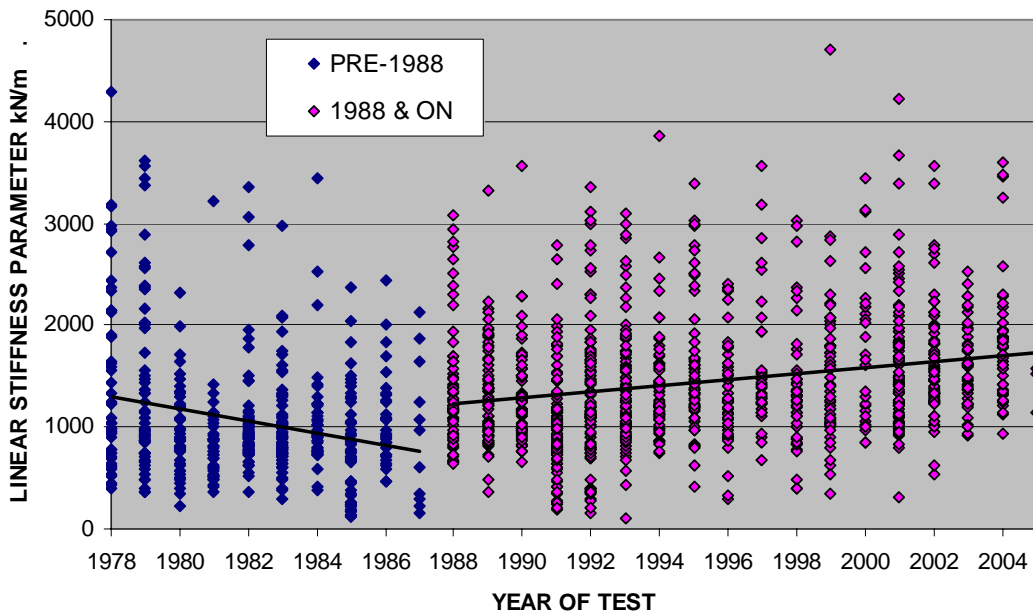


Figure 11-6: 1622 NHTSA test results for stiffness by year of test.

Figure 11-6 shows an apparent decrease in stiffness until the year 1988 from whence the trend increases to the year 2005 models.

11.3 Vehicle Mass Trend

The mass from the 558 NCAP tests was averaged by year of test and graphed in Figure 11-7 data and trended by linear regression.

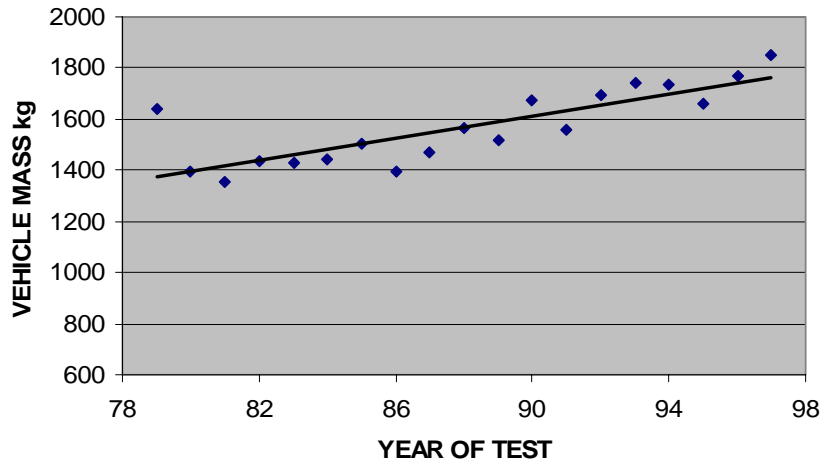


Figure 11-7: NCAP cars linear regression analysis of average vehicle mass in year of test.

The trend in Figure 11-7 showed 27 % total increase in vehicle mass over the 18 years.

To show the influence of mass in the linear stiffness metric data of Figure 11-6, the vehicle mass year by year for the 1622 vehicle tests are trended, but not averaged to visually support the trends.

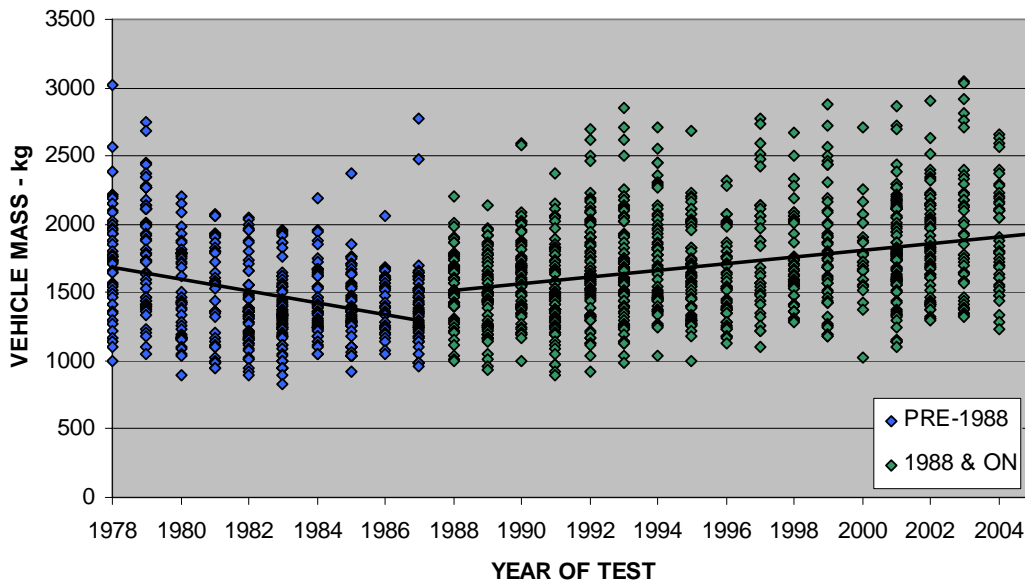


Figure 11-8: 1622 NHTSA test results for stiffness by year of test.

Figure 11-8 shows a trend pattern very similar to the stiffness trends of Figure 11-6, so implicating an erroneous mass influence in the linear stiffness parameter.

11.4 Demographic Reluctance Trend

Demographic reluctance is identical to the specific reluctance metric introduced in Equation [4-6]. Here it is applied to the fleet. It has the advantage over the linear stiffness parameter in that it eliminates the mass component which confounds fleet trends.

However, reluctance is indirectly affected by the increase in vehicle mass but only on account of the extra crush legacied by the extra mass. For example, if heavy vehicles are over-represented in a sample, the influence of the additional crush would manifest in a lower stiffness. Even so the reluctance metric gives useful insight into the stiffness evolution of the fleet.

The reluctances of the NCAP data were calculated and graphed without averaging to show spread in Figure 11-9. A linear regression was calculated and also graphed.

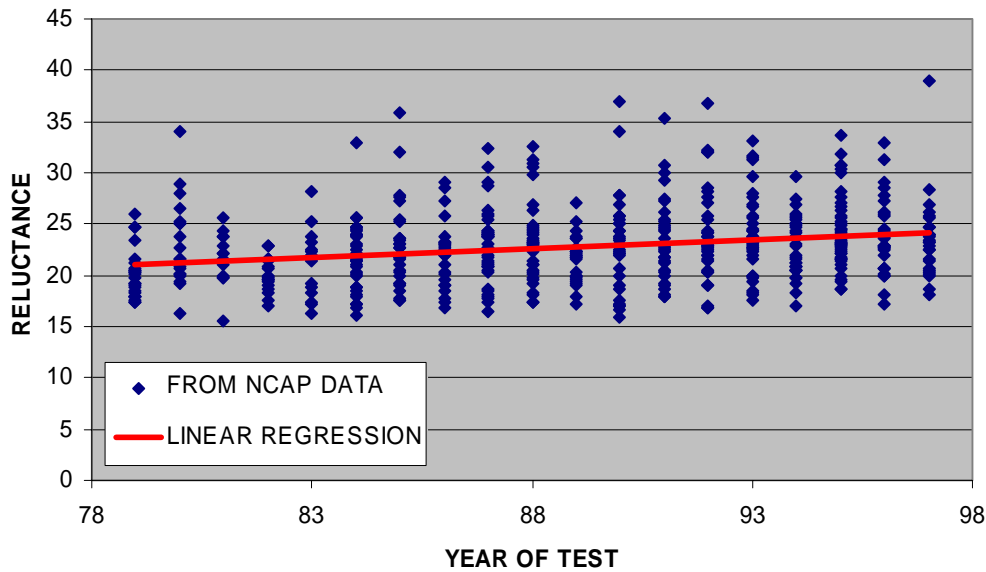


Figure 11-9: NCAP cars stiffness by reluctance metric.

Figure 11-9 shows an average increase in stiffness according to the reluctance metric from $\omega = 21.2$ to 23.7 . Because increased mass reduces stiffness, the year average stiffness values are not sensitive to this reduction. A compensatory adjustment for the mass trend increase (Figure 11-7) could be applied making the stiffness trend in Figure 11-9 greater. In the interests of understatement Figure 11-9 thus reflects a minimum increase.

A similar reluctance trend increase is shown Figure 11-8, noting the absence of trend slope change of stiffness evident in Figure 11-6. This further highlights the mass influence in the linear stiffness parameter.

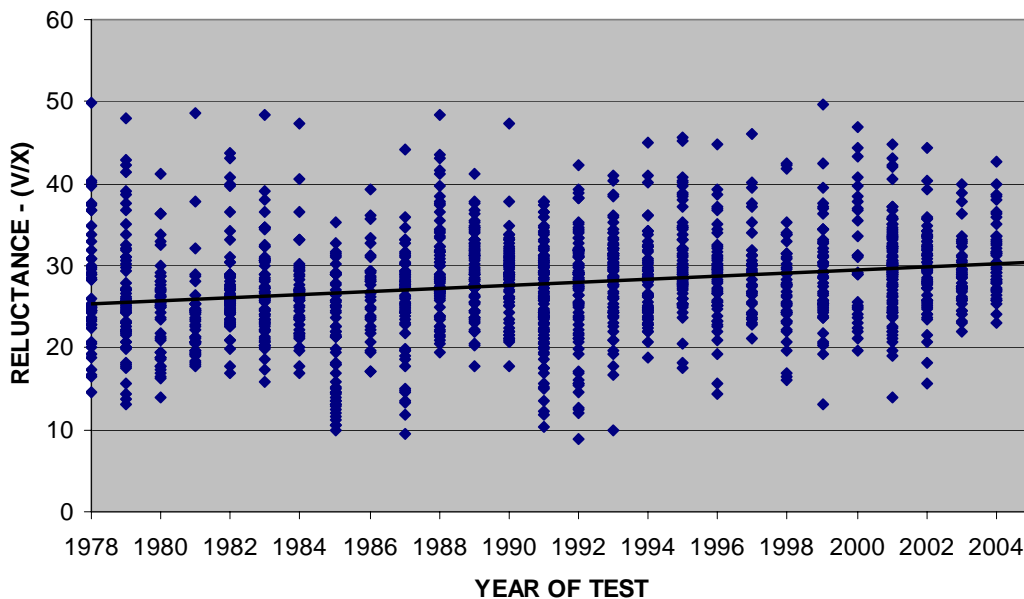


Figure 11-10: 1622 NHTSA test results for reluctance by year of test.

11.4.1 Injury Implications of Trend

The injury increase for reluctance increase from the year 1979 to the year 1997 of from $\omega = 21.2$ to $\omega = 23.7$ will be determined here. It should be noted that the study for the 1622 NHTSA test results are not used in injury determinations owing to the static crush data capture practices.

Rebound is to be estimated from Table 25 at $CofR = 0.141$. Since rebound is to be included in the analysis, the haversine equations are to be employed. In Section 7 the focus was predict from existing test data sets to other conditions. Here it is required to derive injury curves from reluctances derived from initial impact velocity and dynamic crush. The procedure for this was not covered in the earlier section to avoid distraction from the immediate objectives for the particular section. It is to be covered here where it is needed.

The procedure is essentially a conversion from ω to Ω . The former is cosine-based while the latter is haversine-based reluctance. The rationale for this comparison is based on the knowledge that the cosine curve is reasonably capable of representing injury but only to the point of rebound. It has the advantage of being calculable from fleet data. The haversine curve does not have this facility. Fortunately the haversine can be defined from two known points in time from the cosine equation, as follows:

1. At zero time both initial velocities are known.
2. At zero velocity the cosine time is known.

First the cosine equation is solved at $V=0$ to obtain an expression for time – t :

$$\begin{aligned} \cos(\omega \cdot t) &= 0 \\ t &= \frac{1}{2} \cdot \frac{\pi}{\omega} \end{aligned} \tag{11-1}$$

Then the expression for time is substituted into the haversine equation, also at $V=0$, as follows:

$$\begin{aligned} \left[(I + c) \cdot \cos^2(\Omega \cdot t) \right] - c &= 0 \\ \left[(I + c) \cdot \cos^2 \left[\Omega \cdot \left(\frac{1}{2} \cdot \frac{\pi}{\omega} \right) \right] \right] - c &= 0 \end{aligned} \tag{11-2}$$

Equation [9-2] is solved for Ω , as follows:

$$\Omega = \frac{2 \cdot \omega}{\pi} \cdot \arccos\left(\sqrt{\frac{c}{1+c}}\right) \quad [11-3]$$

Using a conservative coefficient of restitution of $c = 0.14$, reluctance values are inserted into Equation [11-3] yielding the following values for demographic reluctance:

$$\omega = 21.2 \quad \text{yields} \quad \Omega = 16.4 \blacksquare$$

$$\omega = 23.7 \quad \text{yields} \quad \Omega = 18.3 \blacksquare$$

Equation [7-1] & [7-2] for contact velocity (V_c) and proximity (P_x) are modified to show coefficient of restitution (c) and graphed parametrically the above to parameter t in Figure 11-11.

$$\begin{aligned} V_c &= V \cdot (1+c) \cdot \sin^2(\Omega \cdot t) \\ P_x &= \frac{V \cdot (c+1)}{2} \cdot \left(t - \frac{\sin(2 \cdot \Omega \cdot t)}{2 \cdot \Omega} \right) \end{aligned} \quad [11-4]$$

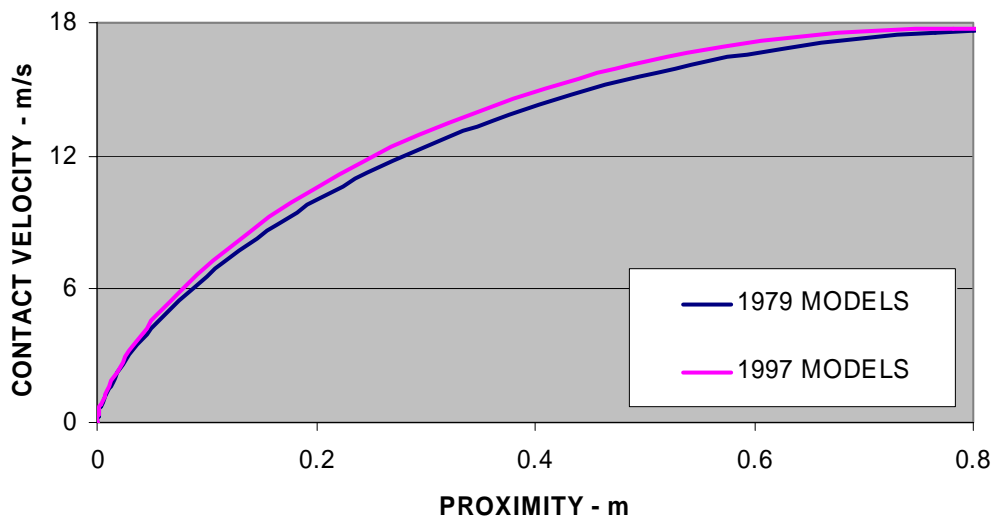


Figure 11-11: Injury risk for 1979 model cars compared with 1997 model cars.

Figure 11-11 shows an increase in injury risk in the more modern cars. What is significant is that an expected improvement is absent. Ross, Sicking et al. (1993b) recommend a maximum contact velocity of 5 m/s. It can be seen in Figure 11-11 that proximities above 70 mm would not comply. This highlights the need to reduce to improve crumple zone response generally and rebound specifically, in the fleet. Figure 11-11 also suggests that the recommendations of Ross, Sicking et al. (1993b) may be unrealistic when considered against typical proximity statistics.

12. CONCLUSION

12.1 The Essence

The research question whether a crash test result contains sufficient information to permit extrapolation to other velocities and vehicle load variations has been considered from two perspectives:

1. Fidelity to vehicle motion
2. Fidelity to injury risk as a result of vehicle motion.

If vehicle motion test data were perfectly represented by the model, the second perspective would follow with perfect fidelity to injury risk. Unfortunately, both the model and the test data it tries to emulate are imperfect. Given the choice between vehicle motion and injury risk fidelity, injury risk received the priority, so declaring the focus of this thesis. The distinction between stiffness representing vehicle motion and pseudo-stiffness representing injury risk was introduced in Section 6.2 and refined for the prime model in Section 6.2.2 parametrically and injury risk directly from occupant position in Section 7.1.1.

A mathematical model (prime model) was presented that was able to represent the crash data well in respect of injury risk for the crash data. The model was adaptable to predict injury risk for higher and lower initial impact velocities (with respect to test velocities). The model uses a haversine equation in its cosine form (\cos^2). The empowering kernel for the model was termed reluctance to emphasize the motion aspect rather than engineering stiffness or circular frequency. Once the reluctance was extracted from the crash test injury risk data it could be used to predict injury risk data for other impact velocities substantiated at the range of vehicle crash test speeds for full frontal rigid barrier test. (40-56 km/h).

Many crash tests are performed all over the World. These tests are expensive, each costing tens of thousands of dollars. The ability to predict vehicle response in the format of injury risk has the potential to reduce the number of crash tests performed and so offering considerable savings for the community. For example, an NCAP test at 56 km/h could predict injury test results to replace compliance tests normally performed at 48 km/h and vice versa.

Methodology was presented to vary the reluctance to reflect variations in vehicle loading to account for luggage and occupancy in Section 5.4. Responding to the dearth of crash data that varies vehicle mass, validation was achieved against simulated data, simulations being corroborated at two test speeds. In Section 5.4.3, corroboration was also achieved for two real crash tests of identical vehicles where one was modified to be battery powered, carrying

the extra load of lead acid batteries. It was found that additional mass reduces stiffness as measured by the reluctance metric and reduces injury risk as measured by contact velocity of body parts with the internals of the vehicle.

The ability to predict mass effect on injury has implications in litigation: “Did overloading exacerbate injuries?”

Reduction of injury resulting from increased vehicle mass can be used to make a marginal crashworthiness performers comply with the regulations. All that is required is to increase the mass of production vehicles to justify test mass.

Vehicle mass appeals to a pervasive “bigger is better” mindset in the community. This is fuelled by a perceptual and actual reduction in injury. Unfortunately this comes at the expense to the collision partner in a momentum mechanism. This benefit disappears if all vehicles increase in mass, a propensity supported by fleet statistics.

The overall result is an increase in aggregate vehicle mass of the National fleet. A study by the author is presented showing a steady annual increase amounting to 27% total over a period of 18 years of NCAP testing. This fleet mass increase is contrary to the stated position of the industry that sees benefit from reduced fleet fuel consumption and reduced vehicle costs resulting from vehicle mass reductions.

Rebound was identified as an important element of crashworthiness. The importance of rebound in injury in modern vehicles was shown to apply even for short proximity distances on account of soft internal impact surfaces. A common interaction between body part and internal impact surface showing a coupling phase well into rebound is shown in Figure 2-3. Increased vehicle mass showed little increase in rebound (Section 10.2) adding to the attractiveness of mass increase as a crash test compliance solution. A study by the author was presented (Section 10.3) showing no improvement in rebound using specific energy absorption in vehicles separated by 20 years of NCAP testing. There are no direct statutory requirements for limiting rebound.

A study was presented that showed rebound to be a fixed percentage of initial velocities for the particular vehicle under study. This helped in formulating the prime model to include rebound as well.

12.2 Summary of Contributions

To assess crashworthiness requires some form of injury criteria. The literature injury criteria specific to body parts were shown to be unsuitable for broad spectrum assessment of the crumple zone. Contact velocity as an injury criterion led to critical analysis of the literature “ride-down” concept where the body part velocity couples and equalizes with contact surface velocity and is thus safe from further injury. It was shown that ride-down occurs only on hard surface contact where multiple impacts are featured rather than be safe. Since hard surface impacts are rare in modern vehicles, study of the concept served to highlight that most body part coupling events span into the rebound zone. This recognition in turn highlighted the important role of rebound in injury causation.

Since rebound is implicated in most injury, a study of rebound causation was a logical progression. This proceeded first by evaluating the physical component’s contributions to rebound leading to two theoretical models of rebound formation. An impedance concept was developed from instantaneous stiffness showing an example of identical normalized impedance for a vehicle at different crash velocities. The implications of this are discussed in Section 12.3. The half-trumpet shape of the impedance curve favoured a proportional model while a study of inertial stress favoured the velocity stress model of rebound formation. It was concluded, subject to further research, that both models are active even though it was shown by a fleet-sampled study that a proportional model is better explained by crash test data. Efforts made to reduce rebound are thus not drawn by and not confined to the test-corroborated theory of rebound formation.

A knowledge gap was identified in injury variation attributable to changing vehicle mass. It was shown that increased vehicle mass could be used to make a marginal performer comply with legislation. Another fleet-sampled study showed that overall crumple zone performance had not improved over 18 years of crash testing due to increased stiffness. The study also showed that aggregate vehicle mass had increased substantially over the period. The implications of these findings are that legislative reform may offer scope for remedies.

In the study of rebound formation it was shown that energy absorption is feasible at right-angles to impact direction by elastic wave collision causing plastic deformation. The idea provides opportunity for designers to increase energy absorption by attention to design of structural abutments permitting elastic wave flow rather than reflection. It also emphasized that judicious placement of abutments and/or material impedance change could initiate plastic deformation and so increase the overall energy absorption.

The prospect of increased fleet stiffness being implicated in increased injury gave impetus to develop a mathematical model capable of predicting injury risk for variations in vehicle mass, impact velocity and proximity distance of body part to internal impact surfaces. Such a model offered potential benefits in reducing the number of expensive crash tests performed and scope to analyse each test more fully, extracting maximum benefit from the investment in crash testing.

The cosine velocity decay curve model followed logically from the NHTSA stiffness parameter in a simple harmonic motion analogy. However, breaking with the idea that the physics of the event needs to be reflected in the analogy, permitted optimization of the cosine curve to reflect injury risk more accurately. This showed that better representation of test data could be achieved. Even so, the lack of fidelity in the area of rebound in the cosine curve led to consideration of other mathematical models. It was found that the haversine could be phased and positioned to represent test data well including rebound. A reluctance stiffness metric was introduced capable of predicting velocity decay from a single crash test result at impact velocities other than test velocity. It was shown that the method of extrapolating for varying vehicle mass introduced for the cosine model could also be used for the haversine model. Thus the full spectrum of injury results could be determined for variations in vehicle mass, initial impact velocity variations both for varying proximity distances. This offers increased value to expensive crash tests and has the potential to eliminate some tests altogether or allocate the tests to other areas needing corroboration.

Since occupant position in the test vehicle in compliance crash tests are controlled by seating track mid-position, a vehicle with much legroom, is disadvantaged. A luxury vehicle boasting such a refinement could be shown to be a better performer than its compact counterpart by a proximity study using the haversine method. Design improvements affecting crumple zone structure may disclose a better performance at higher/lower (as appropriate) speed by analysis of the test data with haversine prediction of different speeds and vehicle mass. This may influence the choice of crumple zone refinements and assists in vehicle to vehicle comparisons as shown in the example in Section 7.3.

The methodology offered to extract haversine reluctance from initial velocity and dynamic crush facilitates analysis of the fleet across a spectrum of conditions and not simply at test condition. The knowledge of crumple zone response in these varying conditions improves the quality of aggressivity studies in vehicle to vehicle presently assigned with fixed stiffnesses.

The ability to predict injury for the varying conditions is a resource to the legal profession either to show or deny responsibility as appropriate, as shown in the example in Section 7.4.

12.3 Further Research

The overall scope of the research project encompassed by this thesis was necessarily broad. Accordingly, not all the potential avenues could be explored fully and still bring the work to a timely conclusion. Some areas which were thought to have good potential are discussed below.

The haversine showed great promise in predicting for a variety of injury-linked parameters. The number of test data sets examined has had to be limited to bring the work to a conclusion in a reasonable time frame. Thus it is recommended that many more test data sets be examined to increase confidence that the good results are indicative of the fleet.

It was shown that initial force peaks followed by troughs have a beneficial effect on injury. The haversine reluctance provides an overall injury profile. Thus it cannot provide the benefit bestowed by local force peaks and troughs. It is recommended to study the significance of such benefits missed by the overall haversine report.

High initial force peaks often coincide with columnar collapse of the chassis outstands from the occupant cell (horns). Failure initiators in the horns prevent gross columnar collapse but deny the occupant cell of the initial force peaks. These initiators are also an important precursor to greater energy absorption. Further research is recommended to determine if a balance can be achieved to accommodate these apparently conflicting priorities.

Increased vehicle mass reduces stiffness of the bullet vehicle and so reduces its aggressivity. However, the increased mass increases its aggressivity on account of momentum considerations. The net effect is recommended for study devising crash tests with varied vehicle mass.

The normalized impedances of one make of vehicle in crash tests at three different velocities were found to be almost identical. This may be indicative of a predictive constant. Further research is needed to determine whether the findings are isolated and whether the constant has predictive value.

The velocity stress model was shown to be implicated in the formation of rebound. Test data however, favoured the proportional model. More research is needed to determine why the velocity stress model is not ostensibly manifested in test data. The findings may bear significant fruit in the important quest for reduction of rebound.

This study was confined to full frontal rigid barrier crash tests. Further research is recommended to determine if the findings apply to other tests such as offset deformable barrier tests.

12.4 Recommendations

It was shown in this study that rebound is implicated not just in long proximities such as found in large cars and small people but in almost all injuries from contact with the softer modern materials used in vehicle interiors.

Recommending that rebound values be reported as part of NCAP procedures along with the star rating system.

Recommending that legislation be drafted limiting rebound to be a fixed maximum percentage of crash test velocity as part of the compliance program (say 5% by 2008).

It was shown that stiffness and mass are increasing in the fleet. Mass and stiffness are in inverse relationship with each other in relation to injury risk. Mass increase is societally undesirable from a momentum aggressivity viewpoint. Stiffness increase is undesirable from the injury risk position. There is much “breast-beating” in the industry on the virtues of modern high strength steel. Use of high strength steel will decrease mass but at the expense of increasing stiffness.

Recommending that legislation be drafted prescribing a maximum ratio of vehicle mass to crumple zone stiffness to prevent the use of vehicle mass to achieve compliance.

13. References

- Abdel-Aty, M. (2002). Vehicle Size and Safety, University of Central Florida - Center for Advanced Transportation Systems Simulation.
- Abramowitz, M. a. S., I. A. (Eds.). (1972). Handbook of Mathematical Functions with Formulas, Graphs, and Mathematical Tables. New York, Dover.
- AISI (2002). Automotive Steel Design Manual. Michigan, American Iron and Steel Institute & Auto/Steel Partnership.
- AISI (2003). An Investment in Steel's Future: 2002-2003 Progress Report, American Iron and Steel Institute.
- Al-Mousawi, M. and H. Harrison (1987). "Experimental Investigation of Transient Flexural Waves in Beams with Discontinuities of Cross Section." Experimental Mechanics 27(4): 404-413.
- Amerongen, J. v. (1998). Keynote Address - The Role of Control in Mechatronics. Symposium - Mechatronics In Control System Design at the Control 98 Conference, Swansea Wales, University of Wales.
- Atkinson, P., J. Benny, K. Sambatur, K. Gudipaty, V. Maripudi and T. Hill (1999). A parametric study of vehicle interior geometry, delta-V, and instrument panel stiffness on knee injury and upper body kinetic energy. 43rd Stapp Car Crash Conference, San Diego, California, USA, The Stapp Association, Ann Arbor, Michigan, USA.
- Autonews (2003). Ford 100 years. <http://www.autonews.com/page.cms?pageId=326>.
- Backaitis, S. H., M. E. Hicks, P. Prasad, T. Laituri and J. Nadeau (1995). Variability of Hybrid III Clearance Dimensions within the FMVSS 208 and NCAP Vehicle Test Fleets and the Effects of Clearance Dimensions on Dummy Impact Responses, SAE 952710.
- Barone, M. R., M. M. Kamal and J. A. Wolf (1981). Modern Automotive Structural Analysis. New York, Van Nostrand Reinhold Co.
- Bellion, P. (2002). Frontal Stiffness Co-efficients of Australian Passenger Cars. ICrash2002, Melbourne, Australia, Society of Engineers Australasia.
- Beuse, N. (2002). 5th vs. 50th Percentile Dummies in 56 kph (35 mph) Frontal Barrier Crashes, SAE Government/Industry Meeting.

- Bir, C. (2001). BME 7170 Experimental Methods in Impact Biomechanics. Detroit USA, Wayne State University.
- Brell, E., D. Thambiratnam and R. Troutbeck (2002c). On Quality of Crumple Zones. 10th Bi-Annual Postgraduate Conference, Brisbane, School of Civil Engineering Queensland University of Technology.
- Brell, E. and M. Veidt (2002d). A new analysis and visualization tool for vehicle crush data. ICrash2002, Melbourne, Australia, Society of Engineers Australasia.
- Brell, E., M. Veidt and B. Daniel (2001b). "Influence of Deceleration Profiles on Occupant Velocity Differential and Injury Potential." International Journal of Crashworthiness.
- Campbell, K. (1974). Energy Basis for Collision Severity. 3rd International SAE Conference on Occupant Protection 740565., Society of Automotive Engineers.
- Cavanaugh, J. (2000). BME 7160: Impact Biomechanics and Human Injury Tolerance. Detroit USA, Bioengineering Center Wayne State University.
- Chabert, L., S. Ghannouchi and C. Cavallero (1998). Geometrical Characterization Of A Seated Occupant Paper Number 98-S9-P-19. 16th Enhanced Safety of Vehicles (ESV).
- Choi, H.-Y. and I. Lee (1999). Advanced Finite Element Modeling of the Human Body for Occupant Safety Simulation. EURO-PAM'99.
- Chou, C. (2004). Fundamental Principles for Vehicle/Occupant System Analysis. Vehicle Crashworthiness and Occupant Protection. P. Prasad and J. Belwafa.
- Dale, B. (2003). "The Energy Within - Mechanism of Injury and the EMD." The National EMD Journal.
- Deshpande, B., T. Gunasekar, R. Morris, S. Parida, M. Rashidy and S. Summers (1999). "Methodology Development For Simulating Full Frontal And Offset Frontal Impacts Using Full Vehicle MADYMO Models." ASME.
- Deshpande, V. and N. Fleck (2000). "High strain rate compressive behaviour of aluminium alloy foams." International Journal of Crashworthiness 24 (3)(MAR 2000): 277-298.
- Dixon, P. (2002). Repair Industry in Australia. ICrash2002, Melbourne, Australia, Society of Engineers Australasia.
- Dubois, P., C. Chou, B. Fileta, T. Khalil, A. King, H. Makmood, H. Merz and J. Wismans (2004). Vehicle Crashworthiness and Occupant Protection.

- Emori, R. I. (1970). "Vehicle mechanics of intersection collision impact." SAE Paper 700177.
- Evans, L. (2001a). "Causal influence of car mass and size on driver fatality risk." American Journal of Public Health(91): 1076-81.
- Evans, L. (2004a). How to Make a Car Lighter and Safer. SAE World Congress Paper 2004-01-1172.
- Evans, L. (2004b). Airbag benefits, airbag costs. SAE World Congress Paper 2004-01-0840.
- Evans, L. and M. C. Frick (1992). "Car size or car mass -- which has greater influence on fatality risk?" American Journal of Public Health **82**: 1009-1112.
- Evans, L. A. (2003). "New Traffic Safety Vision for the United States." American Journal of Public Health. 93:1384-1386.
- Faidy, J.-P. (1995). The coupling phenomenon in the case of a frontal crash. 39th Stapp Car Crash Conference, San Diego USA, Society of Engineers SAE Paper 952709.
- Faith, N. (1997). Crash: The Limits of Car Safety. London, Macmillan.
- Ferguson, E., Johnson Amoako, M. Simpson, E. Stott. and J. Motha (2000). Report 102 - Road Crash Costs in Australia, Bureau of Transport & Regional Economics.
- Flyte, M. G. (1998). Frontal Impact Protection: Tailoring Safety System Performance By The Prediction Of Driver Size And Seated Position. 16th Enhanced Safety of Vehicles (ESV).
- Frei, P., R. Kaeser, M. Muser, P. Niederer and F. Walz (1999). Vehicle Structural Crashworthiness with respect to Compatibility in Collisions, University of Zurich.
- Gabler, H. C. and W. T. Hollowell (2000a). "The Crash Compatibility Of Cars And Light Trucks." Journal of Crash Prevention and Injury Control.
- Gadd, C. W. (1966). Use of a weighted-impulse criterion for estimating injury hazard. 10th Stapp Car Crash Conference, Holloman Air Force Base, New Mexico, USA.
- Giess, M. and J. Tomasf (1998). Improving Safety Performance In Frontal Collisions By Changing The Shape Of Structural Components. 16th ESV Paper Number 98-S1-O-07, NHTSA.
- Griffiths, M., M. Paine and J. Haley (1999.). Consumer crash tests: the elusive best practice. Symposium Worldwide Harmonization of Crash Test Programs, Cologne, Germany.

- Gurdjian, E. S. and H. R. Lissner (1964). The position and motions of the head at impact. Eighth Stapp Car Crash Conference, Detroit, Michigan, USA, Wayne State University, Detroit, Michigan, USA.
- Hallquist, J. O. (1998). LS-Dyna Theoretical Manual, Livermore Software Technology Corporation.
- Happee, R., R. v. Haaster, L. Michaelsen and R. Hoffmann (1998). Optimisation Of Vehicle Passive Safety For Occupants With Varying Anthropometry. 16th ESV Paper Number 98 S9-O-03.
- Hendler, E., J. O'Rourke, M. Schulman, M. Katzeff, L. Domzalski and S. Rodgers (1974). Effect of head and body position and muscular tensing on response to impact. 18th Stapp Car Crash Conference, Ann Arbor USA, Society of Engineers SAE Paper 741184.
- Hertz, E. (1997). The Effect of Decreases in Vehicle Weight on Injury Crash Rates, DOT HS-808 575, NHTSA.
- Hodgson, V. R. and L. M. Patrick (1968). Dynamic response of the human cadaver head compared to a simple mathematical model. 12th Stapp Car Crash Conference, Detroit, Michigan, USA, Society of Automotive Engineers, Inc., Warrendale, Pennsylvania, USA.
- Hodgson, V. R. and L. M. Thomas (1972). Effect of long-duration impact on head. 17th Stapp Car Crash Conference, Oklahoma City, Oklahoma, USA, Society of Automotive Engineers, Inc., Warrendale, Pennsylvania, USA.
- Hollowell, W. T., H. C. Gabler, S. L. Stucki, S. Summers and J. R. Hackney (1999). Updated Review Of Potential Test Procedures For FMVSS No. 208, NHTSA OFFICE OF VEHICLE SAFETY RESEARCH.
- Howard, R. P., J. Bomar and C. Bare (1993). "Vehicle restitution response in low velocity collisions." SAE Paper No 931842.
- Husher, S., M. Noble, M. Varat and F. Kerkhoff (1995). "An Analysis of ATD Seating Positions in NHTSA Frontal Crash Testing." SAE Paper 950890.
- Hyder, D. A. (2002). Road Accidents Take Costly Toll. GENEVA, Road Traffic Injury Research Network.
- Ignatovich, C. L., A. R. Diaz and C. A. Soto (2000). Strategies in Design for Enhanced Crashworthiness. 2000 NATO Meeting: Topology Optimization of Structures and Composite Continua,, Budapest, Hungary.

- II&SI (2004). ULSAB Image Library, International Iron & Steel Institute.
- Jawad, S. (2002). "Smart Structures for Frontal Collision Mitigation." SAE Paper 2002-01-0247.
- Jirásek, M. (2002). "Numerical modeling of strong discontinuities." Revue française de génie civil. Volume 6 -(6): 1133 à 1146.
- Johnson, W. (1972). Impact Strength of Materials. London, Edward Arnold.
- Joksch, H. C. (2000). Vehicle Design versus Aggressivity, U.S. Department of Transportation National Highway Traffic Safety Administration.
- Joksch, H. C., D. Massie and R. Pichler (1998). Vehicle Aggressivity: Fleet Characterization Using Traffic Collision Data. Ann Arbor, U.S. Department of Transportation National Highway Traffic Safety Administration.
- Jones, N. and J. Yu (1995). On the Inelastic Failure Criterion for Structures Subjected to Large Dynamic Loads. IUTAM Symposium Constitutive Relation in High/Very High Strain Rates, Noda Japan, Springer Verlag.
- Kahane, C. J. (2003). Vehicle Weight, Fatality Risk and Crash Compatibility of Model Year 1991-99 Passenger Cars and Light Trucks, NHTSA Technical Report DOT HS 809 662.
- Kallina, I., D. Scheunert and F. Zeidler (1999). "Main Aspects in Car Safety." Safety Science Monitor Special Edition Vol 3.
- Kamarajan, J., R. Rajagopalan and V. Gupta (1999). "Effects of Multiple Impacts on Head Injury Criteria." SAE Paper No 1999-01-0297.
- Kato, H. and R. Nakahama (1982). A study on the ride-down evaluation. 9th Enhanced Safety of Vehicles (ESV).
- Kerckhoff, J. F., S. E. Husher, M. S. Varat, A. M. Busenga and K. Hamilton (1993). An investigation into vehicle frontal impact stiffness, BEV and repeated testing for reconstruction. SAE International Congress and Exposition 930899.
- Kim, C.-H. and J. S. Arora (2001b). Nonlinear Dynamic System Identification for Automotive Crash Using Optimization: A Review. Iowa City, IA, Optimal Design Laboratory, College of Engineering, The University of Iowa.
- King, A. I., K. H. Yang and T. Khalil (2005). WSU Brain Injury Model. Detroit USA, Bioengineering Center Wayne State University.

- Kinsler, L. E. and A. R. Frei (1962). Fundamentals of Acoustics. New York, John Wiley & Sons.
- Kroell, C. K., M. E. Pope, D. C. Viano, C. Y. Warner and S. D. Allen (1981). Interrelationship of velocity and chest compression in blunt thoracic impact to swine. Paper No 811016. 25th Stapp Car Crash Conference, San Francisco, California, USA, Society of Automotive Engineers, Inc., Warrendale, Pennsylvania, USA.
- Kroell, C. K., D. C. Schneider and A. M. Nahum (1974). Impact tolerance and response of the human thorax. 18th Stapp Car Crash Conference, Ann Arbor, Michigan, USA, Society of Automotive Engineers, Inc., Warrendale, Pennsylvania, USA.
- Lau, I., J. Capp and J. Obermeyer (1991). A Comparison of Frontal and Side Impact: Crash Dynamics, Countermeasures and Subsystem Tests. 35th Stapp Car Crash Conference, San Diego, Society of Automotive Engineers SAE Paper 912896.
- Lim, G. G. (1972). Crash data analysis, SAE 720496.
- Machey, J. M. and C. L. Gauthier (1984). Results, analysis and conclusions of NHTSA's 35 mph frontal crash test repeatability program. SAE International Congress and Exposition, Detroit, Michigan, USA.
- Mahadevan, K., P. Liang and J. Fekete (2000). "Effect of Strain Rate in Full Vehicle Frontal Crash Analysis." SAE TECHNICAL PAPER SERIES 2000-01-0625.
- Makmood, H. and B. Fileta (2004). Design of Vehicle Structures for Crash Energy Management. Vehicle Crashworthiness and Occupant Protection. P. Prasad and J. Belwafa.
- Manary, M. A., C. A. C. Flannagan, M. P. Reed and L. W. Schneider (1998). Predicting Proximity Of Driver Head And Thorax To The Steering Wheel. 16th ESV Paper Number 98-S 1-O- 11.
- Marquardt, J. (1974). "Vehicle and Occupant Factors that Determine Occupant Injury." SAE Paper 740303.
- Marzougui, D., C.-D. Kan and N. E. Bedewi (1996). Development And Validation Of An NCAP Simulation Using Ls-Dyna3d, FHWA/NHTSA National Crash Analysis Center.
- McFeely, W. J., D. I. Bojrab, K. G. Davis and D. F. Hegyi (1998). Otologic Injuries Secondary to Airbag Deployment. American Academy of Otolaryngology--Head and Neck Surgery Foundation Annual Meeting, San Antonio, Texas.

- McHenry, R. R. and P. M. Miller (1970). "Automobile Structural Crashworthiness." Society of Automotive Engineers Paper 700412.
- McLean, A., B. Fildes, C. Kloeden, K. Digges, R. Anderson, V. Moore and D. Simpson (1997). Prevention of Head Injuries to Car Occupants - An Investigation of Interior Padding Options, NHMRC Road Accident Research Unit, University of Adelaide Monash University Accident Research Centre.
- Melvin, J. W., J. W. Lighthall and K. Ueno (1993). Brain Injury Biomechanics. Accidental Injury - Biomechanics and Prevention. A. M. Nahum and J. W. Melvin. New York, Springer Verlag.
- Mentzer, S. G. (2001). The SISAME2 Program: Structural Crash Model Extraction and Simulation. Virginia.
- Mentzer, S. G. (2002). The SISAME2 Program: Structural Crash Model Extraction and Simulation. Washington, National Highway and Traffic Safety Administration.
- Mineta, N. Y. and E. Martin (2002). Economic Impact of U.S. Motor Vehicle Crashes, US Transportation Dept.
- Monson, K. L. and G. J. Germane (1999). Determination and mechanisms of motor vehicle structural restitution for crash test data. Paper 1999-01-0097. SAE International Congress and Exposition, Detroit, Michigan, USA, Society of Automotive Engineers, Inc., Warrendale, Pennsylvania, USA.
- Mooi, H. and J. Huibers (1998). Simple and effective lumped mass models for determining kinetics and dynamics of car-to-car crashes. IJCrash '98, Dearborn USA, Woodhead.
- Moore, D. F. (1970). Minimization of occupant injury by optimum front-end design, SAE 700416.
- Motozawa, Y. and T. Kamei (2000a). "Controlling deceleration during a crash." Automotive Engineering International(June).
- Motozawa, Y. and T. Kamei (2000b). "A New Concept for Occupant Deceleration Control in a Crash." SAE TECHNICAL PAPER SERIES 2000-01-0881.
- Motozawa, Y., M. Tsuruta, Y. Kawamura and J. Noguchi (2003b). "A New Concept for Occupant Deceleration Control in a Crash - Part 2." SAE International Paper 2003-01-1228.
- Motozawa, Y., M. Tsuruta and Y. K. a. J. Noguchi (2003a). "A New Concept for Occupant Deceleration Control in a Crash - Part 2." SAE Paper 2003-01-1228.

- Nahum, A. M., A. W. Siegel and S. H. Brooks (1970). "Reduction of collision injuries: past, present, and future." Society of Automotive Engineers Paper 700895.
- Newman, J. A. (1980). Head Injury Criteria in automotive crash testing. 24th Stapp Car Crash Conference, Troy, Michigan, USA.
- Newman, J. A., N. Shewchenko and E. Welbourne (2000). A proposed New Biomechanical head injury assessment function - the maximum power index. 44th Stapp Car Crash Conference, Atlanta, Georgia, USA.
- NHTSA (1996). "The Third Report to Congress on the Effectiveness of Occupant Protection Systems and Their Use."
- NHTSA (1997). Actions to Reduce the Adverse Effects of Air Bags DEPOWERING FMVSS No. 208, National Highway Traffic Safety Administration - Office of Regulatory Analysis Plans and Policy.
- Otten, G., T. J. A. d. Vries, J. v. Amerongen, A. M. Rankers and M. Erik W. Gaal (1997). "Linear Motor Motion Control Using a Learning Feedforward Controller." IEEE/ASME TRANSACTIONS ON MECHATRONICS 2(3).
- Owings, R. P. (2000). Response to DaimlerChrysler Review of Test Procedures, US Dept of Transportation NHTSA.
- Park, B., J. Hackney, R. Morgan and H. Chan (1999). The NCAP Program: Has it led to Stiffer Light Trucks and Vans over the Years? SAE Congress 1999, Detroit, Society of Automotive Engineers.
- Parkin, S., G. Mackay and A. Cooper (1993). How Drivers Sit in Cars. 37th Annual Proceedings.
- Porter, P. (2002). Annual Review, Australian Transport Safety Bureau.
- Prasad, P. and H. Mertz (1985). "The Position of The U.S. Delegation to the ISO Working Group 6 on the Use of HIC in the Automotive Environment." SAE Paper 851246.
- Rao, S. S. (1986). Mechanical Vibrations, Addison Wesley.
- Ray, P. A., R. Sferco and R. Frampton (2001). Multiple impact crashes~Consequences for occupant protection measures. International IRCOBI Conference on the Biomechanics of Impact, Isle of Man, United Kingdom.
- Ricci, E. M., T. J. Leopold and B. Salzillo (2004). "The Minority Gets it Right." News & Events.

- Ridella, S. A. and D. C. Viano (1990). Determining tolerance to compression and viscous injury in frontal and lateral impacts. Paper No 902330. 34th Stapp Car Crash Conference, Orlando, Florida, USA, Society of Automotive Engineers, Inc., Warrendale, Pennsylvania, USA.
- Roberts, V. and C. Compton (1993). The relationship between deltaV and injury. 37th Stapp Car Crash Conference, San Antonio USA, Society of Automotive Engineers.
- Ross, H. E., D. L. Sicking, R. A. ZIMMER and J. D. MICHIE (1993a). Recommended Procedures for the Safety Performance Evaluation of Highway Features, National Cooperative Highway Research Program Report 350.
- Ross, H. E. J., D. L. Sicking, R. A. Zimmer, G. T.J. and J. D. Michie (1993b). NCHRP (National Cooperative Highway Research Program) Report 350 Recommended Procedures for the Safety Performance Evaluation of Highway Features, Transportation Research Board National Research Council.
- Ross, M. and T. Wenzel (2001). Losing Weight To Save Lives: A Review Of The Role Of Automobile Weight And Size In Traffic Fatalities. Washington DC, American Council for an Energy-Efficient Economy.
- Rothbart, H. A. (1996). Mechanical Design Handbook, McGraw-Hill.
- Rouhana, S. W. (1993). Biomechanics of Abdominal Trauma. Accidental Injury - Biomechanics and Prevention. A. M. Nahum and J. W. Melvin. New York, Springer Verlag.
- SAE-J885 (1986). Human Tolerance to Impact Conditions as Related to Motor Vehicle Design., Society of Automotive Engineers.
- Sala, D. M. and J. T. Wang (2003). Continuously Predicting Crash Severity. 18th ESV Paper Number 314, Japan, NHTSA.
- Santosa, S. (1999). Summary Report on Crush Response of Ultralight Structures. Mech Eng. Cambridge, Massachusetts Institute of Technology.
- Shojaati, M. (2003). Correlation between injury risk and impact severity. 3rd Swiss Transport Research Conference, Monte Verità / Ascona.
- Simunovic, S., J. Shaw and G. A. Aramayo (2000). "Material Modeling Effects on Impact Deformation of Ultralight Steel Auto Body." SAE 2000-01-2715.
- Simunovic, S. and T. Zacharia (1999). Steel Processing Properties and Their Effect on Impact Deformation of Lightweight Structures, Computer Science and Mathematics Division - Oak Ridge National Laboratory.

- Singace, A. A. (1999). "Axial crushing analysis of tubes deforming in the multi-lobe mode." International Journal of Mechanical Sciences **41**: 865–890.
- Singh, J., J. Welcher and J. Perry (2003). "Effects of Mass and Stiffness Ratio Variation on Vehicle Speed Change and Closing Speed Calculations." SAE Paper 2003-01-0890.
- Smith, K. (2000). Keynote Address – Road Safety: Past, Present and Future. Transportation 2000 International Conference, Gold Coast Qld., Australian Institute of Transport Management.
- Smith, R. A. and N. G. Tsongos (1986). "Crash phase accident reconstruction." SAE Paper 860209.
- Sparke, L. and J. Tomas (1994). Crash Pulse Optimisation for Minimum Injury Risk to Car Occupants’,. FISITA ‘94 Congress.
- Spiegel, M. (1968). Mathematical Handbook of Formulas and Tables. New York, McGraw Hill.
- Strother, C. (1985). "Velocity histories as an accident reconstruction tool." SAE Paper 850249.
- Strother, C. E., R. L. Woolley, M. B. James and C. Y. Warner (1986). Crush energy in accident reconstruction (Paper 860371). SAE International Congress and Exposition, Detroit, Michigan, USA, Society of Automotive Engineers, Inc., Warrendale, Pennsylvania, USA.
- Sugimoto, T., Y. Kadotani and S. Ohmura (1998). The Offset Crash Test - A Comparative Analysis of Test Methods Paper Number 98-S 1-0-08. 16th Enhanced Safety of Vehicles (ESV), NHTSA.
- Swaffield, J. A. and A. P. Boldy (1993). Pressure surge in pipe and duct systems. Avebury England, Aldershot.
- Tamny, S. (1992). "The linear elastic-plastic vehicle collision." SAE Paper 921073.
- Thompson, J. E. (1968). Total system approach to occupant response versus vehicle crush. 12th Stapp Car Crash Conference, Society of Automotive Engineers.
- Timoshenko, S. and J. Goodier (1951). Theory of Elasticity. New York, McGraw Hill.
- Troutbeck, R., T. Barker and D. Thambiratnam (2001). Roadside Barrier Design and Vehicle Occupant Safety T2000/0736, School of Civil Engineering, Queensland University of Technology.

- Turner, A. L. (1998). A Review Of Crash Severity Assessment Programs Applied To Retrospective Realworld Accident Studies. 16th Enhanced Safety of Vehicles (ESV) Paper Number 98-06-O-09.
- ULSAB (1998). UltraLight Steel Auto Body Final Report, American Iron and Steel Institute.
- Van-Auken, R. M. and J. W. Zellner (2002). An Assessment of the Effects of Vehicle Weight on Fatality Risk in Model 1985-98 Passenger Cars and Light Trucks. Volume II: Technical Report No DRI-TR-02-02, Dynamic Research, Inc.
- Varat, M. S. and S. E. Husher (2000). "Vehicle impact response analysis through the use of accelerometer data." SAE Paper No 2000-01-0850.
- Varat, M. S., S. E. Husher and J. F. Kerkhoff (2001). An Analysis of Trends of Vehicle Frontal Impact Stiffness.
- Vaughn, P. and D. Martin (2000). ULSAB-AVC will achieve advanced crash performance in anticipation of 2004 criteria., American Iron and Steel Institute.
- Verma, M. K., R. C. Lange and J. P. Lavelle (2003). "Relationship of Crash Test Procedures to Vehicle Compatibility." SAE Paper 2003-01-0900.
- Versace, J. (1971). A review of the severity index. 15th Stapp Car Crash Conference, San Diego, California, USA.
- Viano, D. (1988). Biomechanics of Head Injury - Toward a Theory Linking Head Dynamic Motion, Brain Tissue Deformation and Neural Trauma, SAE.
- Viano, D. C. and I. V. Lau (1990). " Biomechanics of impact injury." International trends in thoracic surgery -- surgical management of chest injuries, Chapter 2 Volume 7.
- Vilenius, A. and G. Ryan (1996). "Parameter estimation for head impacts and brain injury in crash reconstruction." International Journal of Crashworthiness 1(3).
- Wilson, R. A. (1969). Evaluating knee-to-instrument panel impact. 13th Stapp Car Crash Conference SAE 690801, Boston.
- Witteman, W. J. and R.F.C.Kriens (1999b). Numerical Optimization of Crash Pulses. EUROPAM '99 9th User Conference.
- Wood, D. (2000). "Structural Rebound Characteristics of the Car Population in Frontal Impacts." SAE TECHNICAL PAPER SERIES 2000-01-0461.

- Wood, D. P. (1992). Collision speed estimation using a single normalised crush depth-impact speed characteristic (Paper 920604). SAE International Congress and Exposition, Detroit, Michigan, USA, Society of Automotive Engineers, Inc., Warrendale, Pennsylvania, USA.
- Woolley, R. L. (2001). "Non-Linear Damage Analysis in Accident Reconstruction\". SAE Paper 2001-01-0504.
- Yang, R. J., C. H. Tho, C. C. Wu and J. Cheng (1999). A Numerical Study of Crash Optimization. DETC 99 ASME Design Engineering Technical Conferences, Las Vegas, Nevada.
- Zeidler, F., H. Schreier, A. Kief and J. Scheerer (1997). The significance of different severity parameters for product liability and car design. The 2nd International Conference on Accident Investigation, Interpretation and the Law, Brisbane, QUT.
- Zukas, J. A., T. Nicholas, H. F. Swift, L. B. Greszczuk and D. R. Curran (1982). Impact Dynamics. New York, John Wiley & Sons, Inc.